Role and Regulation of Tbx2 and Tbx3

Johannes Schmidt
Christ Church College, Oxford

Trinity Term 2015

Supervised by
Professor Colin Goding

This thesis is submitted to the Nuffield Department of Medicine, University of Oxford, in partial fulfilment of the requirements for the degree of Doctor of Philosophy.

Disclaimer

I declare that this submission is my own written work. To the best of my knowledge, it contains no material that has been written by another or previously submitted in the same or a different form as academic work, to this or any other university. The results presented herein derive from my own experiments.

Johannes Schmidt
Trinity Term 2015

Für Theresa.

Acknowledgements

I am hugely grateful to Professor Colin Goding for the opportunity to conduct my DPhil under his supervision, he was an invaluable source of ideas and encouragement. The Goding laboratory has been a very stimulating and friendly environment to work in and I am extremely thankful for all the help, inspiration, constructive criticism and consolation I received. Especially, I would like to thank Paola Falletta, Luis Sanchez and Rasmus Freter for their open ear for my science related questions and beyond; and Rob Siddaway, Richard Lisle and Hans Friedrichsen for the cheerful distractions making lab life more bearable when it was all going wrong. Mark Shipman was a tremendous help with the microscopes, and Dr Helen Lockstone's assistance with the microarray analyses was invaluable.

I am deeply indebted to Professor Colin Akerman, Dr Louise Kay, Agnes and Norbert Schlagheck, Nazim Hussain, Rebecca Merkley, and Andreas Tischbirek for their incredible support and empathy in my darkest moment to help me finding my way again. Equally, Anca and Benoit Hastoy have been amazing friends having always been there for me when necessary. A special mention has to go to Luke Lewis, thank you so much for broadening my horizon, I could not have asked for a better comrade during my time in Oxford. Besides, Lukas Alperowitz, Mikolaj Matloka, and Sebastian Behrens, even though living on the continent, never felt far away and I could always count on them. I am very fortunate and humbled to be able to call all of them friends.

Finally, my biggest thanks goes to my brother, Christoph, and my parents for putting up with all my crazy ideas and plans. Despite them not being life scientists, they were always interested in and supportive of my scientific endeavours.

Abstract

Role and regulation of Tbx2 and Tbx3

Johannes Schmidt, Christ Church College, D.Phil. Clinical Medicine, Trinity Term 2015

The T-box family of transcription factors plays a crucial role during embryonic development, especially in heart and limb formation. In the adult organism, two members of the family, TBX2 and TBX3, have been found to be overexpressed in several types of cancer associating them with tumour biology. However, little is known about their regulatory targets and subsequent function aside from their well-described role during development, that would give indications of their overall contribution to tumourigenesis. Here, an agnostic, genome-wide approach is chosen to reveal novel TBX2 and TBX3 regulated target genes in a human melanoma cell line, shedding further light on their regulatory activity. Furthermore, the regulation of the two T-box factors themselves by growth regulating pathways, dysregulated in cancer, is assessed. Both T-box factors are proposed to be involved in cancer homoeostasis, a process balancing nutrient supply and demand within the cancer cell to facilitate long-term proliferation without depletion of nutrients. Moreover, TBX2 and TBX3 are demonstrated to be regulated by the PI3K pathway mediated by PAX3, and that this regulation is implicated in the bypass of oncogene induced senescence.

Table of Contents

List of Figures

List of Tables

List of abbreviations

A	Adenine
AK	Aurora kinases
AMPK	5'-AMP-activated protein kinase
APS	Ammonium persulfate
APC	Anaphase-promoting complex
ATP	Adenosine triphosphate
BAD	BCL-2-associated agonist of cell death
BETA	Binding and Expression Target Analysis
BCL-2	B-cell lymphoma 2
β-gal	β-galactosidase
BIM	BCL-2 interacting mediator of cell death
bp	Base pair
C	Cytosine
CDK	Cyclin-dependent kinase
cDNA	Complementary DNA
ChIP	Chromatin Immunoprecipitation

ChIP-Seq	ChIP followed by sequencing
CKI	Cyclin-dependent kinase inhibitor
C-terminus	Carboxy terminus
CTLA4	Cytotoxic T-lymphocyte-associated protein 4
Da	Dalton
DAPI	4',6-diamidino-2-phenylindole
DMEM	Dulbecco's modified Eagle's medium
DMSO	Dimethyl sulfoxide
DNA	Deoxyribonucleic acid
Dox	Doxycycline
E2F2	E2F transcription factor 2
E.coli	Escherichia coli
ECM	Extracellular matrix
EDTA	Ethylenediaminetetraacetic acid
EEF2	Eukaryotic elongation factor 2
EEF2K	Eukaryotic elongation factor-2 kinase
EGF	Epidermal growth factor
EGR1	Early growth response protein 1
ELL	Eleven-nineteen Lys-rich leukaemia
EMSA	Electrophoretic mobility shift assay
EMT	Epithelial-mesenchymal transition
EPC	Endothelial progenitor cells

ER	Endoplasmic reticulum
ERK	Extracellular-signal-regulated kinases
EZH2	Enhancer of zeste homologue 2
FBS	Fetal bovine serum
FGF	Fibroblast growth factor
FoxO1	Forkhead box protein O1
FoxO3	Forkhead box protein O3
G	Guanine
GADD45A	Growth arrest and DNA-damage-inducible protein 45 α
GF	Growth factor
GFP	Green fluorescent protein
GK	Glycerol kinase
GMPR	Guanosine monophosphate reductase
GO	Gene ontology
GREAT	Genomic Regions Enrichment of Annotations Tool
Her2/neu	Human epidermal growth factor receptor 2
HGF	Hepatocyte growth factor
ICC	Immunocytochemical staining
IL-6	Interleukin 6
IL6R	Interleukin 6 receptor

kDa	Kilodalton
KEGG	Kyoto encyclopaedia of genes and genomes
KLF	Kruppel-like factors
LB	Luria-Bertani broth
LEF1	Lymphoid enhancer-binding factor 1
logFC	log-fold change
LTR	Long terminal repeats
MAPK	Mitogen-activated protein kinase
MC1R	Melanocortin 1 receptor
MEK	Mitogen-activated protein kinase kinase
MCL-1	Myeloid cell leukaemia 1
MDM2	Mouse double minute 2 homologue
MET	Mesenchymal-to-epithelial transition
MITF	Microphthalmia-associated transcription factor
MPF	Maturation-promoting factor
mTOR	Mammalian target of rapamycin
mTORC1	mTOR complex 1
mTORC2	mTOR complex 2
NICD	Notch intracellular domain
NLS	Nuclear localisation signal

PAX3	Paired box 3
PB	PiggyBAC
PBS	Phosphate buffered saline
PCA	Principal component analysis
PCR	Polymerase chain reaction
PDGF	Platelet-derived growth factor
PDK1	Phosphoinositide-dependent kinase-1
PHLPP	PH domain and leucine rich repeat protein phosphatase
PI	Propidium iodide
PI3K	Phosphatidylinositol-3-kinase
PIK3R1	Phosphatidylinositol 3-kinase regulatory subunit 1 (alpha)
PIP2	Phosphatidylinositol (4,5)-bisphosphate
PIP3	Phosphatidylinositol (3,4,5)-trisphosphate
PKB	Protein kinase B
PLGF	Placental growth factor
PMSF	Phenylmethylsulfonyl fluoride
PP2	Protein phosphatase 2
PRC2	Polycomb repressive complex 2
PRKAB1	5'-AMP-activated protein kinase subunit beta-1
PRKAB2	5'-AMP-activated protein kinase subunit beta-2
PSEN2	Presenilin-2
PSFM	Position specific frequency matrices
PTEN	Phosphatase and tensin homolog

PVDF	Polyvinylidene difluoride
qPCR	Quantitative polymerase chain reaction
Rb	Retinoblastoma protein
RNA	Ribonucleic acid
ROS	Reactive oxygen species
RPMI	Roswell Park Memorial Institute Medium-1640
rtTA	Reverse tetracycline transactivator
RT	Room temperature
RTK	Receptor tyrosine kinases
RYBP	RING1 and YY1-binding protein
S6K	Ribosomal S6 kinase
SASP	Senescence associated secretory phenotype
SGK	Serum/glucocorticoid-regulated kinase
shRNA	Short hairpin RNA
SIAH2	Seven in absentia homolog 2
siRNA	Short interfering RNA
SNAI2	Snail family zinc finger 2
SPRY2	Sprouty homolog 2 (Drosophila)
T	Thymine
TAZ	Transcriptional coactivator with PDZ-binding motif

TBE	Tris/borate/EDTA
Tbx2	T-box transcription factor 2
Tbx3	T-box transcription factor 3
TEMED	Tetramethylethylenediamine
tet-on	Tetracycline-controlled transcriptional activation
TF	Transcription factor
TGF	Transforming growth factor
TGF-β	Transforming growth factor β
TGF-β2	Transforming growth factor-β 2
TRE	Tetracycline response element
TSC1	Tuberous sclerosis 1
TSS	Transcription start site
UPR	unfolded protein response
USF1	Upstream stimulatory factor 1
USF2	Upstream stimulatory factor 2
UV	Ultraviolet
UVR	Ultraviolet radiation
VEGF	Vascular endothelial cell growth factor
VGF	VGF nerve growth factor inducible
VM	Vasculogenic mimicry
WB	Western blot

YAP	Yes-associated protein

Chapter 1

Introduction

1.1 Cancer

In an ever ageing society cancer is becoming a growing burden to health care today with expenditure of £5.8 billion in the UK alone in 2014 (NHS Networks). It is estimated, that in the UK half of the population born after 1960 will be diagnosed with some type of cancer during their lifetime, with still rising incidence rates. Improvements in health care and better treatment options led to at least 10 years survival of half of the diagnosed patients, denoting a doubling in survival rates over the last 40 years (Cancer Research UK, Cancer Stats). However, cancer is still responsible for more than 25% of all deaths in the UK, and an estimated 8.2 million people died from cancer worldwide in 2012 (Cancer Research UK), a number projected to rise to 13.1 million by 2030 (Ferlay et al., 2010).

The causes of cancer are multifaceted. There are more than 200 different types known today, but the underlying principle is the same, an uncontrolled growth of somatic cells. Despite the advancements of almost half a century of oncology research, still today the most common treatment for cancer is surgery, where feasible, combined with chemo- and/or radiotherapy. This crude approach can result in severe side effects and impairment of the patient's quality of life. With surgery, benign tissue encompassing the tumour is collaterally removed to ensure elimination of the entire tumour and avoid regrowth due to residual tumour cells at the site. Both, chemo- and radiotherapy, non-specifically target dividing cells irrespective of whether the dividing cell is benign or malignant. The rationale being that malignant, cancerous cells show a higher division rate compared to their benign counterparts and consequently will be more sensitive, while benign cells will also die but can be replenished by physiological stem cells. Thus, all three most

commonly applied treatment options considerably affect healthy tissue, a main reason for the observed side effects.

For more targeted and tailored therapies, an in-depth understanding of molecular cancer biology is necessary to dissect the molecular differences between a benign somatic cell and a malignant cancer cell.

1.1.1 Hallmarks of cancer

The transformation from a well-controlled somatic cell to a dysregulated cancerous cell is a multi-step process. It takes several mutations accumulated in a cell's DNA over time, to eventually end with a molecular set-up manifested in an uncontrolled, cancerous phenotype (Knudson, 1971, 1996; Tomlinson et al., 2001). In general, two different classes of genes have been described in the context of cancer, oncogenes and tumour suppressor genes (Hanahan and Weinberg, 2000). Oncogenes are genes with the potential to cause cancer when activated (Croce, 2008), whereas tumour suppressor genes protect a cell from cancer, causing tumour growth upon inactivation (Sherr, 2004). Consequently, many activating mutations in oncogenes and loss-of-function mutations in tumour suppressor genes are found in tumours (Sherr, 2004; Croce, 2008; Hanahan and Weinberg, 2000, 2011).

In their epochal review, Hanahan and Weinberg described in 2000 and its revised second edition in 2011 six key traits, so-called hallmarks, of cancerous cells governing the transformation from normal cells to cancer: 1) self-sufficiency in growth signals, 2) insensitivity to anti-growth signals, 3) evading apoptosis, 4) limitless replicative potential, 5) sustained angiogenesis, and 6) tissue invasion and metastasis (Figure 1.1) (Hanahan and Weinberg, 2000, 2011). The first two

hallmarks maintain cancer cells in a proliferative state through modulation of the signalling environment, whereas hallmarks three to five support the survival of dysregulated cells by stifling intrinsic safety mechanisms designed to prevent uncontrolled hyperproliferation and supplying enough nutrients and oxygen. Finally, the sixth hallmark promotes the spread of the tumour to other parts of the body.

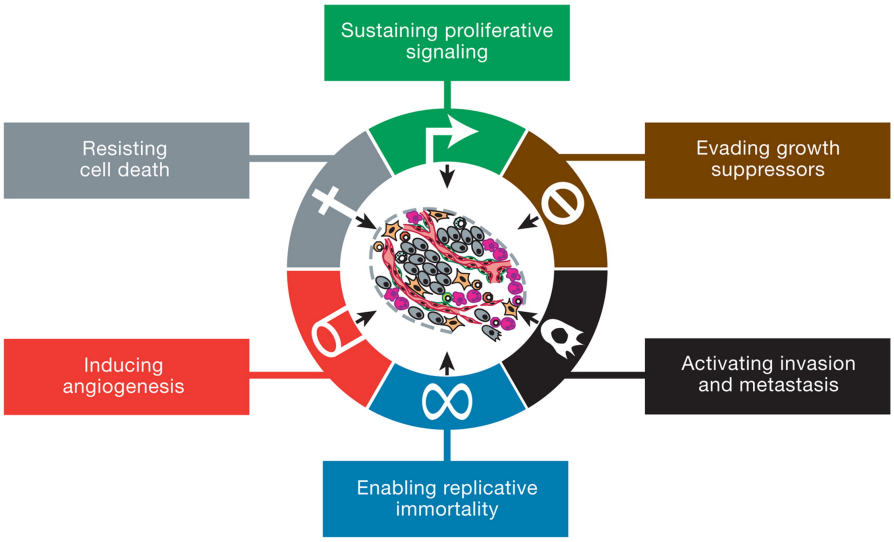

Figure 1.1: The hallmarks of cancer. The six hallmarks of cancer as originally proposed by Hanahan and Weinberg in 2000.
Reprinted from Hanahan and Weinberg (2011), Copyright 2011, with permission from Elsevier.

Sustained proliferative signalling

Cancer cells can be rendered self-sufficient in growth signals by either a manipulated growth factor (GF) environment or independence from GF stimulation. For the GF environment, two determinants are important, the stimulus (i.e. GFs) and the sensing (i.e. receptors), both of which can be influenced in cancer. Glioblastoma cells, for instance, produce platelet-derived growth factor (PDGF), thus generating a positive feedback loop for growth (Lokker et al., 2002). Moreover,

an increased number of GF receptors on the cellular surface can cause cancer cells to propagate despite the low, ambient growth signal, insufficient to induce proliferation in somatic cells (Korc et al., 1992; Farley et al., 2000; Haugsten et al., 2010). Furthermore, the abundance of receptors in the cellular membrane can trigger ligand-independent signalling. This phenomenon is for instance observed in breast, stomach and brain cancer overexpressing the human epidermal growth factor receptor 2 (Her2/*neu*) (Slamon et al., 1987).

The second possibility of growth signal autonomy besides manipulation of the GF environment is via intracellular signal processing. In somatic cells, growth signals registered by receptors on the cellular surface are transferred via several cytoplasmic mediators to their respective intracellular effectors. An activating mutation in one of these intracellular mediators, rendering it constitutively active, provides the cell with a constant mitogenic signal regardless of the surrounding GF environment. Two prominent examples are the mitogen-activated protein kinase (MAPK) pathway, with many known activating mutations in the Ras subfamily (Bos, 1989; Pylayeva-Gupta et al., 2011) and the Raf kinases (Holderfield et al., 2014), and the phosphatidylinositol-3-kinase (PI3K) pathway, with frequent mutations in PI3K and protein kinase B (PKB, also known as AKT) (Liu et al., 2009).

A further mechanism leading to uncontrolled growth of cells is insensitivity to anti-growth signals. In healthy tissue, homeostasis is maintained by a tightly knit regulatory network of proliferative and anti-proliferative signals linked to the cell cycle. During growth phase (G_1), cells proliferate, temporarily quiesce (G_0) or enter a permanent, post-mitotic state dependent on the cellular environment (Bertoli et al., 2013). The anti-growth signals for quiescence and post-mitotic

arrest are thereby mainly enacted by the retinoblastoma protein (RB) through sequestering members of the E2F transcription factor (TF) family, thus inhibiting the progress from G_1- into S-phase (Weinberg, 1995). Hence, disruption of the RB pathway renders cells insensitive to signals blocking the $G_1 - S$ transition, resulting in uncontrolled cell cycle progression, a phenomenon frequently observed in cancer (Ho and Dowdy, 2002; Sherr and McCormick, 2002).

Restriction of intrinsic safety mechanisms

The rapid proliferation of cancer cells and the substantial dysregulation of their cellular signalling networks, blocking or severely impairing intrinsic safety mechanisms, leads to significant intracellular stress. Replicative stress, due to continuous replication of DNA without sufficient time and activity of proofreading agents, increases the mutation rate and DNA damage within cancer cells (Loeb, 2001). Stress of the endoplasmic reticulum (ER), due to the high load of protein synthesis, in turn, enhances the occurrence of misfolded proteins (Clarke et al., 2014). In somatic cells, the apoptotic machinery senses these stress signals and induces programmed cell death once they surpass a threshold (Adams and Cory, 2007). In cancer cells however, dysregulated signalling pathways provide a way to evade apoptosis and sustain high levels of cellular stress (Hanahan and Weinberg, 2000; Fernald and Kurokawa, 2013).

Probably the most prominent sensor for intracellular stress is the tumour suppressor TP53, the so-called guardian of the genome (Lane, 1992). As a key regulatory TF, it controls the expression of a multitude of factors involved among others in DNA repair, cell cycle control and apoptosis, thus playing a crucial role in cellular stress response. In human cancer, TP53 is one of the most frequently mutated

or inactivated genes, interfering with the stress response pathways (Hollstein et al., 1991; Olivier et al., 2010).

A second safety mechanisms to protect somatic cells from harmful uncontrolled growth is an irreversible growth arrest, termed senescence. This signalling network has also been shown to be dysregulated in cancer cells, a topic discussed in more detail below (Section 1.3).

Sufficient nutrient supply

In addition to avoiding the intrinsic safety mechanisms, tumours can only rise with enough nutrients and oxygen available to support their growth. Once grown to a size of 1-2 mm^3, the diffusion limit for oxygen and nutrients is reached and new blood vessels are necessary for a sufficient supply (Hillen and Griffioen, 2007). An enhanced vascularisation of tumour tissue has already been described 100 years ago (Goldmann, 1907), but only in the last 40 years the underlying molecular mechanisms have become more evident. The process of neovascularisation is regulated by a balance of pro- and anti-angiogenic signals and several distinct mechanisms have been identified; a) sprouting angiogenesis, the formation of vessels from pre-existing vasculature, b) intussusceptive angiogenesis, the splitting of pre-existing vessels into two new, separate vessels, and c) the recruitment of endothelial progenitor cells (EPC) to form blood vessels (Carmeliet and Jain, 2000; Hillen and Griffioen, 2007).

Sprouting angiogenesis is a tightly controlled process mainly governed by the fibroblast growth factor (FGF) family and the vascular endothelial cell growth factor (VEGF) family. Both are involved in all major steps of angiogenesis, facilitating the activation of endothelial cells, their migration and proliferation, and

at the same time, increasing the expression of ECM degrading enzymes, such as matrix metalloproteinases and plasminogen activators (Hillen and Griffioen, 2007). Both families of GF have been shown to be produced and secreted by cancer cells, thus enabling vascularisation of tumours (Hillen and Griffioen, 2007; Holmes et al., 2007).

During intussusceptive angiogenesis, a transvascular tissue pillar is formed inside the lumen of an existing vessel, splitting the vessel into two through continuous growth in diameter (Burri et al., 2004). The exact mechanism is not yet fully understood, but alterations in blood flow dynamics and elevated shear stress on the endothelial cells have been shown to stimulate the process (Hillen and Griffioen, 2007).

The recruitment of EPCs to form blood vessels is promoted by endocrine signals, generated among others during tumour growth. Upon stimulation by angiogenic factors such as placental growth factor (PLGF) or VEGF, EPCs are released from the bone marrow and subsequently recruited and integrated at the site of neovascularisation in tumours (Hillen and Griffioen, 2007). The contribution of EPCs to overall tumour vessel growth is still debated in the field, but nevertheless a factor worth considering.

Another, very intriguing phenomenon related to tumour vascularisation is vasculogenic mimicry (VM), first demonstrated in uveal melanoma (Maniotis et al., 1999). It describes the formation of *de novo* vascular networks by dedifferentiated tumour cells, enhancing the perfusion of rapidly growing tumours. The vasculogenic-like networks are lined with tumour cells, co-expressing endothelial, embryonic/stem cell, and tumour markers, highlighting the remarkable plasticity of tumour cells (Seftor et al., 2012). Moreover, resulting channels and tubular

structures have been shown to be morphological similar to endothelial-lined vasculature, and rich in ECM proteins, such as laminin, collagens and proteoglycans (Hillen and Griffioen, 2007). Detected plasma and red blood cells within these networks indicate a functionally equivalent perfusion pathway to endothelial-lined vasculature for rapidly growing tumours (Seftor et al., 2012). In recent studies, induction of VM has been attributed to a hypoxic microenvironment, emphasising the importance of the tumour microenvironment as a contributing factor to tumourigenesis (van der Schaft et al., 2005; Mihic-Probst et al., 2012).

Metastasis formation

The probably most severe aspect of cancer from a patient's survival point of view is the formation of metastases, with a significantly worse prognosis for patients with already metastasising tumours (Steeg, 2006). In order to disseminate and form metastases, tumour cells undergo a sequence of discrete steps, the so-called invasion-metastatic cascade (Fidler, 2003). First, tumour cells invade the local tissue to enter the nearby blood and lymphatic vessels. Once in the vessels, the cells circulate through the lymphatic and hematogenous systems until they escape from the lumen of the vessel into the parenchyma of the secondary site. Subsequently, the engrafted tumour cells form small nodules, so called micrometastases, which finally grow into secondary, macroscopic tumours (Figure 1.2) (Talmadge and Fidler, 2010).

An early developmental programme, called the epithelial-mesenchymal transition (EMT), is suggested to be re-activated in cancer cells facilitating invasion and metastasis. The same TFs orchestrating EMT and migratory functions during embryonic development, such as SNAIL, SLUG, or TWIST, are also expressed

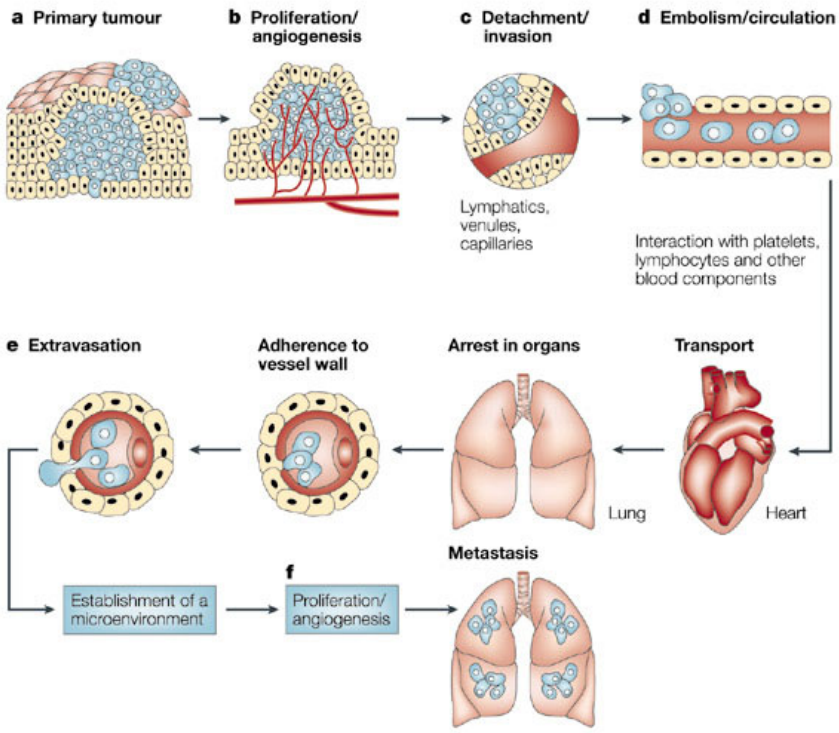

Figure 1.2: The invasion-metastatic cascade. Dissemination of a tumour and metastases formation is a stepwise process. After establishment of the primary tumour (a,b), tumour cells invade the local tissue to enter the nearby blood and lymphatic vessels (c,d). Once in the vessels, the cells circulate through the lymphatic and hematogenous systems until escaping from the lumen of the vessel into the parenchyma of the secondary site (e) to form micrometastases, that eventually grow into macroscopic tumours (f).
Reprinted by permission from Macmillan Publishers Ltd: Nature Reviews Cancer, Fidler (2003), Copyright 2003.

in several malignant tumour types in various combinations (Larue and Bellacosa, 2005). As a consequence, loss of adherens junctions, expression of matrix-degrading enzymes, and increased motility, among others, can be observed. One of the well-known targets of these TFs is E-cadherin, a key cell-to-cell adhesion molecule,

repressed by the above mentioned TFs, leading to a more invasive, metastasis prone phenotype (Peinado et al., 2004). However, it is not clearly understood which conditions and triggers lead to the phenotype of invasive growth and metastasis.

1.1.2 Enabling characteristics

In addition to the described functional characteristics of cancer cells, arisen over time in a multi-step process, two enabling characteristics, facilitating the emergence of tumours, have been outlined: genomic instability and tumour-promoting inflammation (Figure 1.3) (Hanahan and Weinberg, 2011).

Genomic instability generates random mutations including chromosome rearrangements in the cell's genome, which as a matter of stochastic probability produce the rare mutations enabling hallmark capabilities. These mutations can confer a selective advantage and consequently result in clonal outgrowth of a subpopulation of cells (Nowak et al., 2002; Aguilera and García-Muse, 2013). Hence, there are several protective genome maintenance systems in somatic cells limiting the mutation rate during cell replication (Ciccia and Elledge, 2010). However, in cancer cells members of the DNA maintenance machinery, responsible for detecting and repairing DNA damage or counteracting mutagenic agents, were found to be mutated (Negrini et al., 2010; Aguilera and García-Muse, 2013). As a consequence, genomic stability is decreased and the likelihood of a cancer supporting mutation to occur raised.

Tumours have long been recognised as being infiltrated by cells of the immune system, a phenomenon compared to wound healing, which was thought to be an anti-tumoural response by the immune system (Dvorak, 1986). Yet, in recent

years the paradoxical nature of this immune activation has become clear. The inflammatory response can also supply tumour-supportive molecules to the tumour microenvironment, hence, enabling the above discussed hallmarks of cancer. In some cases, this can occur already at the earliest stages of neoplastic progression, facilitating the development of an incipient cancer nodule into a fully developed tumour (de Visser et al., 2006).

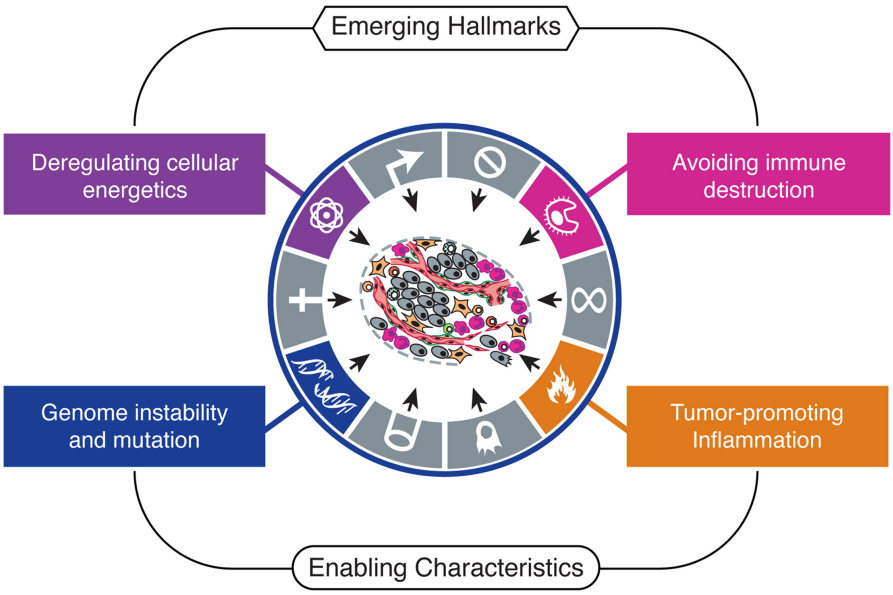

Figure 1.3: Emerging Hallmarks and Enabling Characteristics. Recent research findings suggest two additional emerging hallmarks, involved in cancer pathogenesis, a modified cellular metabolism to support neoplastic proliferation and the capacity to avoid immune destruction. Additionally, two enabling characteristics of incipient cancer cells facilitate the acquisition of hallmark capabilities, genomic instability and inflammation.
Reprinted from Hanahan and Weinberg (2011), Copyright 2011, with permission from Elsevier.

1.1.3 Emerging hallmarks

Advances in the understanding of cancer biology have led to the addition of two emerging hallmarks in the second edition of the review of hallmarks of cancer: dysregulated cellular energetics and avoidance of immune destruction (Figure 1.3) (Hanahan and Weinberg, 2011).

To fuel the high level of proliferation, adjustments to the energy metabolism have been detected in cancer cells (Dang, 2012). Under normoxic conditions, somatic cells process glucose to pyruvate via glycolysis, which is then further oxidised to carbon dioxide in the mitochondria. In anaerobic conditions, energy production is limited to glycolysis as mitochondrial oxidisation requires high amounts of oxygen. In contrast, Warburg et al. described already in 1926 the propensity of tumours to limit energy production to glycolysis even under normoxic conditions, a phenomenon termed aerobic glycolysis or the Warburg-Effect (Warburg et al., 1926). Since oxidative phosphorylation is ~18-fold more efficient than glycolysis alone, the significantly lower adenosine triphosphate (ATP) production from glycolysis can be compensated in cancer cells by a higher glucose consumption, facilitated by up-regulation of glucose transporters (Gillies et al., 2008).

A functional explanation for the glycolytic switch remains elusive. One hypothesis suggests a higher supply of intermediary products of the glycolytic pathway due to enhanced glycolysis to the cell, fuelling downstream biosynthetic pathways, such as nucleoside or amino acid production. This, in turn, provides necessary building blocks for the biosynthesis of macromolecules and organelles to foster cell growth and division (Vander Heiden et al., 2009). Interestingly, aerobic glycolysis has also been noted in fast dividing embryonic tissues, indicating a potentially

developmental programme for rapid cell proliferation re-activated by cancer cells (Vander Heiden et al., 2009).

The second emerging hallmark is immune evasion. The prevailing theory of immune surveillance proposes a permanent monitoring of cells and tissue by the immune system, recognising and eliminating all dysregulated, abnormal cells. Accordingly, the majority of early cancer cells and nascent tumours are thought to be identified and cleared (Finn, 2012). As a consequence, emerging tumours must have avoided recognition by the immune system and subsequent eradication in order to develop.

The production and secretion of immunosuppresive molecules, such as transforming growth factor beta (TGF-β) or interleukin-10 (IL-10), can result in immune evasion of cancer cells (Igney and Krammer, 2002). Alternatively, neoplastic cells recruit immunosuppresive cells, such as T_{reg} cells, via the cytotoxic T-lymphocyte associated antigen 4 (CTLA-4), to dampen the immune response (Mocellin and Nitti, 2013). Furthermore, in order to limit the cytotoxic effects of T-cells, cancer cells express members of the programmed death-ligand (PD-L) family on their cell surface, inducing a self-tolerance response via binding to programmed cell death protein 1 (PD-1) receptors (Quezada and Peggs, 2013). Both molecules, CTLA-4 and PD-1, are hence potent mediators of immune evasion.

1.1.4 Tumour heterogeneity

Originally, a tumour was considered a mass of identical cells, having acquired the potential of unlimited proliferation. Over time, however, research elucidated tumours as very heterogeneous structures, resembling an organ in terms of com-

plexity and variety (Hanahan and Weinberg, 2011). There are two types of tumour heterogeneity, between different tumours (inter-tumoural heterogeneity), and within a single tumour (intra-tumoural heterogeneity) (Marusyk and Polyak, 2010; Burrell et al., 2013).

Inter- and intra-tumoural heterogeneity

There is increasing evidence in many different cancer types for inter-tumoural heterogeneity, describing distinct morphological and phenotypic profiles of tumours from the same location (Marusyk and Polyak, 2010). As a consequence, a breast cancer, for instance, might be pathologically more related to a tumour of a different location, than another breast cancer. Strikingly, inter-tumoural heterogeneity is not only observed between different, independent tumours of the same location, but also between primary tumours and their respective metastases (Yancovitz et al., 2012).

Additionally, heterogeneity is also found within a single tumour, so called intra-tumoural heterogeneity, provoking the idea of a tumour as an organ, although structurally and functionally abnormal (Figure 1.4) (Hanahan and Weinberg, 2011). Just like organs, tumours contain multiple cell types, interact with the surrounding tissue and develop using processes resembling developing organs (Egeblad et al., 2010). There are two different types of intra-tumoural heterogeneity, cellular heterogeneity, manifested in the presence of distinct cell types forming the tumour, and genetic heterogeneity, a diverging genetic make-up of cells of the same type.

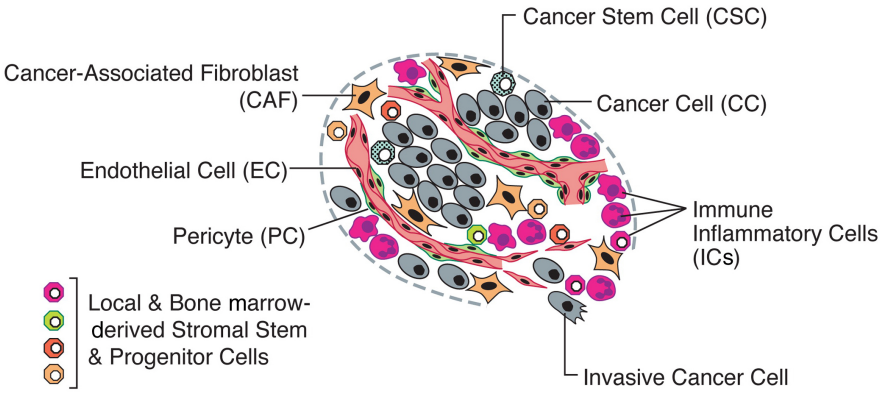

Figure 1.4: Tumour heterogeneity. Tumours are very heterogeneous structures, resembling an organ in terms of complexity and variety. Several distinct cell types contribute to the tumour mass with individual functions. This intra-tumoural heterogeneity has important implications for the understanding of cancer biology and subsequent treatment.
Reprinted from Hanahan and Weinberg (2011), Copyright 2011, with permission from Elsevier.

Cellular and genetic heterogeneity

The main contributor of tumours are cancer cells, harbouring one or several of the above mentioned hallmarks. Further cell types comprising the tumour are endothelial cells, forming tumour associated vasculature and lymphatic vessels, as well as pericytes, supporting the tumour endothelium, cancer associated fibroblasts and cells of the immune system (Hanahan and Weinberg, 2011). Moreover, an increasing body of work suggests another cell type to be present in tumours, cancer stem cells (CSC), initially described in hematopoietic neoplasias (Bonnet and Dick, 1997; Reya et al., 2001). CSCs are functionally defined by the ability to seed new tumours, giving rise to all individual cancer cell types within the tumour, and sharing a number of properties and markers with normal stem cells (Magee et al., 2012; Visvader and Lindeman, 2012). As these cells, nevertheless, still bear

mutations in key signalling pathways, the term stem cell-like cancer cells might be more accurate (Hoek and Goding, 2010).

The existence of CSC is heavily debated, on the one hand, due to their relative scarcity, with reported frequencies as low as 0.2 CSC in 10^6 cells (Bonnet and Dick, 1997), on the other hand, due to the lack of understanding of their origin. Two plausible hypotheses have been, emergence through a de-differentiation mechanism after establishment of the tumour or through oncogenic transformation of normal tissue stem cells (Hanahan and Weinberg, 2011).

Nevertheless, the concept of CSC holds important implications for understanding cancer biology particularly in respect to the plasticity of tumours. As mentioned above, cancer cells are very versatile and capable of adapting to changing external influences of the microenvironment, an attribute that gave rise to the idea of phenotype-switching. According to this model, cancer cells switch back-and-forth between phenotypes, e.g. CSC, invasive, or proliferating cell depending on microenvironmental conditions (Hoek and Goding, 2010). This could potentially explain the low abundance of CSCs, as there might only be a very small niche with the right microenvironment within a tumour for them to exist, but it could also explain the lack of understanding of their origin, as there might not be the one origin for these cells.

Finally, genetic heterogeneity, the second type of heterogeneity found within a tumour, describes the multi-clonal nature of tumours. Despite originating from the same cell initially, genetic instability and selective pressure by the tumour environment leads to clonal expansion of several, genetically different cell populations, forming a heterogeneous tumour of the same cell type (Burrell et al., 2013).

1.2 Melanoma

Melanoma is a sub-type of cancer originating from melanocytes, specialised pigment producing cells predominantly found in the skin. Furthermore, melanoma can also emerge in any part of the body containing melanocytes, such as the choroid layer of the eye (Tsao et al., 2012). Although melanoma accounts for only 4% of all dermatological cancers, it is responsible for 75-80% of skin cancer related deaths (Jerant et al., 2000; Miller and Mihm, 2006). Accordingly, melanoma is among the most aggressive cancers, metastasising already at a very early stage of primary tumour development. As a consequence, if diagnosed early, 5-year survival rates in the UK for malignant melanoma are above 90%, but plummet as low as 5% for patients with metastasising melanoma (Cancer Research UK, Melanoma statistics).

1.2.1 Melanoma epidemiology

Melanoma is particularly common among Caucasians in Oceania, North America, Europe, Southern Africa and Latin America (Ferlay et al., 2010), a pattern reflecting elevated exposure to ultraviolet radiation (UVR) in conjunction with low skin pigmentation. The individual's risk for developing melanoma depends on intrinsic and environmental factors. Intrinsic factors are genetic predispositions and a family history of melanoma, accounting for 10% of all melanoma cases (Hayward, 2003). Two susceptibility genes with high penetrance have been identified, *CDK4* and *CDKN2A* (Zuo et al., 1996; Soufir et al., 1998).

A point mutation in codon 24 of *CDK4* prevents inactivation of cyclin-dependent kinase 4 (CDK4), the protein product of *CDK4*, by p16, a cyclin-dependent

kinase inhibitor (CKI), unable to bind the mutant (Zuo et al., 1996). The binding to cyclin D, however, is not affected by the mutation, thus the cyclin-dependent kinase complex is still able to phosphorylate RB, releasing as a consequence the E2F protein family, which results in cell cycle progression (Zuo et al., 1996; Hayward, 2003). *CDKN2A*, however, is a tumour suppressor gene with inherited inactivating germline mutations, encoding for the cell cycle regulator p16 involved in the control of the G_1 to S cell cycle transition, inhibiting CDK4 among others. Therefore, mutations in these genes confer an enhanced proliferative potential, a hallmark of cancer (Hayward, 2003).

Certainly, the most important environmental risk factor for developing melanoma is UVR (Bennett, 2008). Both, DNA and RNA contain strongly absorbing chromophores for UVR, resulting in a photochemical reaction upon UVR exposure causing mainly C→T base mutations (Tran et al., 2008). Furthermore, UVR can induce base linkage of neighbouring bases, disrupting the replication and transcription of DNA. Strikingly, a high proportion of TP53 mutations in melanoma are C→T transitions, and NRAS mutations, another frequently mutated oncogene in melanoma, has been linked to T-T linkage lesions, underpinning the role of UVR in melanoma formation (Tran et al., 2008). In a whole genome sequencing study of 25 metastatic melanomas, a remarkable 10-fold difference in mutation rate was found dependent on the level of previous UVR exposure. Moreover, the majority of observed mutations were C→T and G→A transitions, consistent with UVR-induced photochemical reactions (Berger et al., 2012).

1.2.2 Melanoma pathophysiology

Melanoma can develop from normal melanocytes in five steps as described in the Clark-model (Figure 1.5). The first step is a hyperproliferation of structurally normal melanocytes forming a benign nevus due to overexpression or constitutive activation of a pro-proliferation pathway. Subsequently, there is aberrant growth leading to a dysplastic nevus with a higher proliferative activity than a benign nevus (Urso et al., 1992). The radial-growth phase is the third step in which cells start proliferating intraepidermally and show morphologically atypical signs. During the fourth step, cells invade vertically into the dermis followed by the last step, the formation of metastases (Clark et al., 1984; Miller and Mihm, 2006).

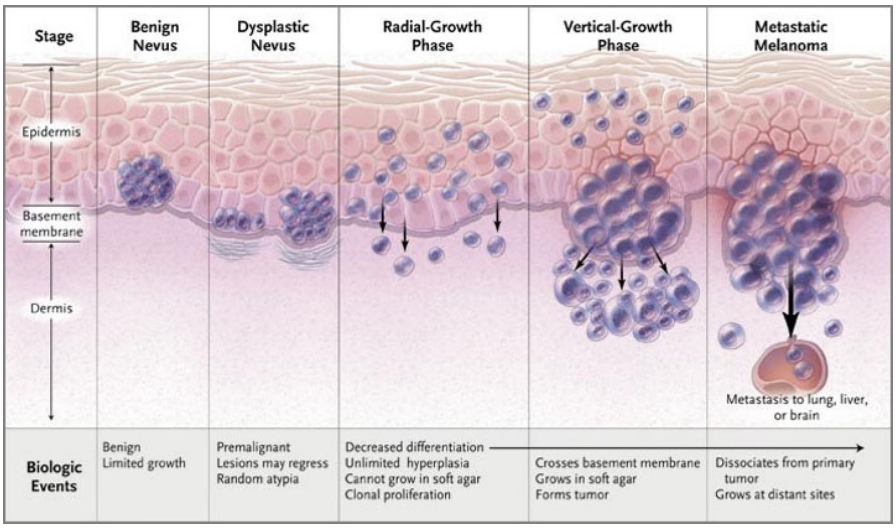

Figure 1.5: The Clark-model of melanoma development. see text for details.
Reproduced with permission from Miller and Mihm (2006), Copyright Massachusetts Medical Society.

For a nevus to form, melanocytes need to hyperproliferate by sustaining a proliferative signalling, a hallmark of cancer as described above. In the majority of malignant melanoma, an activating mutation in the MAPK pathway, a growth re-

lated pathway stimulated under normal conditions by external GFs (Figure 1.6), confers that capability. Mutations in NRAS, a kinase of the RAS kinase family in the MAPK pathway, were identified first as candidates driving melanocyte transformation, occurring in 20% of all melanoma cases (Albino et al., 1984; Fedorenko et al., 2015). In the majority of melanoma tumours (66%), however, the kinase BRAF, downstream of RAS, is mutated. Several activating mutations are described, but the V600E mutation is with 80% by far the most abundant (Davies et al., 2002; Wellbrock et al., 2004b). The finding, that oncogenic $BRAF^{V600E}$ induces proliferation in cultured melanocytes, by constitutively activating mitogen-activated protein kinase kinase (MEK) and extracellular-signal-regulated kinase (ERK) signalling, confirms the significance of this mutation (Wellbrock et al., 2004a). Moreover, mutant BRAF promotes benign melanocytic hyperplasia in mouse models, which progress to malignant melanoma dependent on BRAF expression level and secondary mutations, i. a. in *PTEN* or *CDKN2A* (Goel et al., 2009; Dankort et al., 2009). In addition, BRAF driven melanomas have been shown to be addicted to MEK signalling (Solit et al., 2006), further supporting the importance of the MAPK signalling pathway in melanoma.

As mentioned earlier, activation of BRAF is not sufficient for the development of melanoma in mouse models, but only leads to the formation of benign hyperplasia. This phenomenon can be explained by the induction of senescence, following activation of an oncogene, such as BRAF or NRAS (Serrano et al., 1997; Michaloglou et al., 2005). Senescence is an irreversible growth arrest discussed in more detail later. Indeed, human benign nevi have been shown to harbour oncogenic mutations, such as BRAF or PTEN, without progressing to melanoma (Pollock et al., 2003; Tsao et al., 2003). Necessary secondary mutations and le-

sions deployed by tumours and melanoma in particular to by-pass or overcome the senescence barrier will be discussed in section 1.3.

1.2.3 Treatment

If diagnosed early, surgery can be curative in melanoma, later-stage, metastatic melanoma, however, is highly refractive to conventional treatment, such as radio-, chemo-, or immunotherapy (Bhatia et al., 2009). Hence, with increasing understanding of melanoma cancer biology more specific, targeted treatment options became available in recent years.

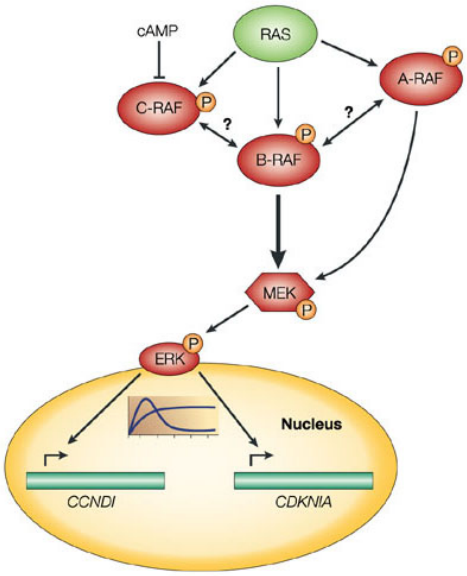

Figure 1.6: Mitogen-activated protein kinase (MAPK) signalling pathway. MAPK signalling cascade signals via phosphorylation events from RAS protein kinase family upstream of the RAF protein kinase family with its three members A-RAF, B-RAF and C-RAF, via MEK to ERK, inducing its nuclear localisation and consequent activation of downstream targets. (adapted from Wellbrock et al., 2004b)

$BRAF^{V600E}$ is an ideal target for therapy due to its high prevalence and restriction to the cancerous state. Accordingly, two selective $BRAF^{V600E}$ inhibitors, vemurafenib and dabrafenib, strongly binding the constitutively active mutant but not the wild-type inactive or active form, have been developed in recent years (Tsai et al., 2008; Bollag et al., 2010; Menzies et al., 2012; Rheault et al., 2013). Both inhibitors showed remarkable results in clinical trials, result-

ing in complete or partial tumour regression in the majority of patients and an estimated median progression-free survival among all patients of up to 16 months. Accordingly, both drugs received approval from the authorities for the treatment of melanoma patients (Flaherty et al., 2010; Sosman et al., 2012; Menzies et al., 2012). Yet, after initial regression of the tumour, most of the patients suffer from a relapse and regrowth of partially even more aggressive tumours. Strikingly, recurring tumour nodules reappear at exactly the same locations as the primary lesions, indicating resistance to therapy by a few cancer cells within the original tumours subsequently spurring the regrowth of a resistant tumour (Wagle et al., 2011).

Several resistance mechanisms have been reported to date, aberrant activation of growth signals upstream of BRAF, such as receptor tyrosine kinases or activation of NRAS (Nazarian et al., 2010), flexible switching between RAF isoforms (Villanueva et al., 2010), expression of a truncated variant of $BRAF^{V600E}$, showing enhanced dimerisation to stimulate ERK signalling, or activation of MAPK signalling by ECM-mediated activation of SRC kinases (Poulikakos et al., 2011; Hirata et al., 2015). These findings highlight the importance of the above mentioned intra-tumoural heterogeneity for a successful therapy.

Another target for treatment in the MAPK pathway is MEK, downstream of BRAF, as malignant melanoma with a $BRAF^{V600E}$ mutation have been shown to be addicted to MEK signalling (Solit et al., 2006). Indeed, the MEK inhibitor trametinib shows efficacy in the clinic and is approved by the authorities for single-agent use in melanoma (Flaherty et al., 2012a), but yet again shows progression of the disease after an initial regression of the tumour. Consequently, to account for the intra-tumoural heterogeneity, combination therapies have been devised. One very promising approach is to combine BRAF with MEK inhibitors in a cocktail

at full monotherapy doses, showing an increased median progression-free survival and enhanced response rate of patients compared to monotherapy (Flaherty et al., 2012b).

In addition to small molecule inhibitors, there is also an immunotherapy approach for melanoma treatment available. The monoclonal antibody ipilimumab targets the protein receptor CTLA-4, a receptor sensing inhibitory signals during priming of cytotoxic T-cells (CTL). By suppressing the inhibitory stimulus, ipilimumab facilitates successful priming of CTLs, enabling recognition and cytotoxic destruction of the cancer cells (Ribas, 2012). Another target for immunotherapy is the PD-1 receptor on T-cells, inhibiting a cytotoxic response when bound to PD-L expressed on melanoma cells. The monoclonal antibody nivolumab interrupts this inhibitory signal and promotes antitumour immunity by facilitating T-cell activation (Topalian et al., 2012; Ribas, 2012; Johnson et al., 2015). Both antibodies showed durable response rates in metastatic melanoma during clinical trials and have been approved by the authorities. Due to their remarkable success, a combination treatment with both monoclonal antibodies is currently examined in a phase 1 clinical trial (Johnson et al., 2015; Weber et al., 2015).

Concluding, a single agent curative treatment for melanoma has not yet been found and, considering the numerous described resistance mechanisms, is unlikely to ever be found. The complexity and heterogeneity within tumours represent such a high selective advantage, that, from an evolutionary point of view, the selective pressure of a single agent will presumably be not enough to stop tumour growth. Furthermore, as melanoma derives from somatic cells, it is increasingly difficult to find unique tumour targets, allowing a specific strike to cancer cells only, excluding somatic cells. Most likely, a successful treatment strategy will comprise several

different targets in a staged regimen to eliminate a tumour. A unique tumour signature amenable for treatment will then be defined by the combination of a handful of broader characteristics, potentially distinct to each presented tumour. To enable such treatment options, a precise assessment of the molecular make-up of the individual cancer and a subsequent stratification of patients will be paramount.

1.3 Cellular senescence

Cellular senescence has been defined as an irreversible arrest of proliferation, activated upon cellular stress (Lanigan et al., 2011). It was first described in the context of normal diploid fibroblasts, which cease to divide after a given amount of cell divisions in culture, referred to as replicative senescence (Hayflick, 1965). Later, in the context of cancer biology, it was discovered that cells undergo senescence upon activation of an oncogene without reaching the replicative limit (Serrano et al., 1997). Recently, senescence was also discovered during embryonic development, suggesting a conserved role in human physiology (Muñoz-Espín et al., 2013; Storer et al., 2013). To reflect the recent findings, the definition of cellular senescence was refined as a response to stress that disables cell proliferation and orchestrates an inflammatory process that eliminates damaged cells (Serrano, 2015).

1.3.1 Replicative senescence

In 1965 Hayflick demonstrated a limited number of cell divisions of human diploid fibroblasts *in vitro* (Hayflick, 1965). These results were repeated in many cell types of different animal species and some studies have also passaged cells *in vivo*, suggesting senescence to be a principle mechanism in the animal kingdom. The

number of divisions completed by normal cells varies and depends on species, age, cell type and genetic background, totalling up to 60-80 doublings (Campisi, 1997). Once cells have undergone replicative senescence, cell growth is arrested in G_1 and transition into S-phase cannot be stimulated. Cells are still responsive to mitogens, remain alive and metabolically active, however, a deficiency of key positive growth regulators, such as the E2F family of proteins and phosphorylated Rb, prevents proliferation (Beltrami et al., 2011; Rodier and Campisi, 2011). In addition, two cell cycle inhibitors, p21 and p16, are overexpressed, firmly stalling cell cycle progression (Campisi, 1997).

The cause for this growth arrest was attributed to telomere attrition (Harley et al., 1990). Telomeres comprise the end of each linear chromosome, consisting of long TTAGGG repeats, and protect, in conjunction with their binding proteins, the chromosome from fusion and translocation (Blasco, 2005). During DNA replication, the telomere is shortened at the 3' end, due to the unidirectionality of DNA polymerase. Telomerase, an enzyme adding telomeric repeats to the end of the chromosome, can counteract that shortening, but is not expressed in somatic cells (O'Sullivan and Karlseder, 2010). Consequently, the length of telomeric DNA decreases as a function of serial passages (Harley et al., 1990). Critically short telomere regions cause genome instability and activate the DNA damage response, inducing replicative senescence (O'Sullivan and Karlseder, 2010).

1.3.2 Oncogene induced senescence (OIS)

After the initial discovery of cellular senescence, phenotypically similar growth arrests have been described, occurring in response to cellular stresses, such as

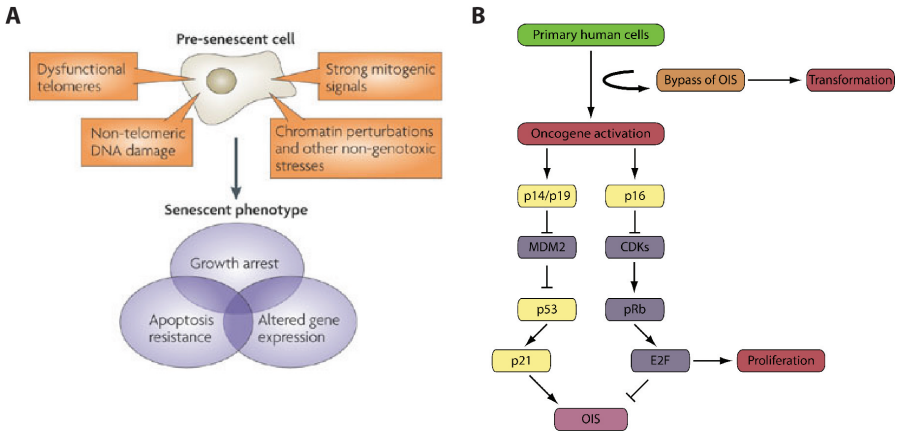

Figure 1.7: Trigger and pathways leading to senescence. (A) Pre-senescent cells enter a senescent phenotype upon several different signals. (B) OIS is executed through the TP53 and RB pathway. (adapted from Zhang and Yang, 2011)

(A) Reprinted by permission from Macmillan Publishers Ltd: Nature Reviews Molecular Cell Biology, Campisi and d'Adda di Fagagna (2007), Copyright 2007.

DNA damage, oxidative stress or oncogene expression (Lanigan et al., 2011). In the context of cancer, senescence due to oncogene expression, termed oncogene induced senescence (OIS), is of particular importance as a major barrier to tumour growth (Courtois-Cox et al., 2008; Collado and Serrano, 2010).

OIS, unlike replicative senescence, is independent of telomere attrition, as overexpression of the telomerase reverse transcriptase hTERT cannot rescue the phenotype (Wei et al., 1999). An accumulation of DNA damage has hence been proposed as trigger for OIS, with two possible origins, reactive oxygen species (ROS) and replicative stress (Figure 1.7 A). Elevated levels of ROS have been detected in many different cancer types (Liou and Storz, 2010) and their DNA-damaging effects are widely known. Moreover, ROS have been shown to be able to trigger cellular senescence themselves (Chen et al., 1998; Frippiat et al., 2000). Furthermore, the continuous proliferation of tumours causes significant replicative stress,

resulting in accumulation of DNA damage, the internal repair machinery cannot cope with. Consistently, senescent cells have been shown to stall in S-phase, exhibit an elevated number of replicons and reveal defects in DNA replication fork progression (Di Micco et al., 2006). All upstream signals eventually funnel into the same two effector pathways, executing the senescence programme, the TP53 and RB pathways (Figure 1.7 B) (Ben-Porath and Weinberg, 2005; Courtois-Cox et al., 2008; Kuilman et al., 2010).

TP53 executes its pro-senescence potential via activating p21, a CKI, which inactivates cyclin-CDK complexes to inhibit cell cycle progression through the G_1/S checkpoint (Lanigan et al., 2011). TP53 itself is regulated by an autoregulatory feedback loop via mouse double minute 2 homolog (MDM2), an E3 Ubiquitin-ligase recognising the N-terminus of TP53 and marking it for degradation (Zhang and Yang, 2011). Upstream of that regulatory loop is the $p14^{ARF}$ protein ($p19^{ARF}$ in mice) inhibiting MDM2, thus preventing degradation of TP53 (Lanigan et al., 2011).

RB exerts its anti-proliferative activity by binding and thus inactivating the E2F family of transcription factors while hypophosphorylated (Buchkovich et al., 1989; Burke et al., 2010; Lanigan et al., 2011). Upon phosphorylation by cyclin-CDK complexes, the E2F transcription factors are released, orchestrating the progression through the cell cycle (Lanigan et al., 2011). The CDKs phosphorylating RB are themselves regulated by CKIs, notably $p16^{INK4a}$ (Zhang and Yang, 2011). Interestingly, p21, the executor downstream of TP53, acts also as a CKI linking the TP53 pathway with RB (Lanigan et al., 2011).

Strikingly, the two prominent upstream regulators $p14^{ARF}$ and $p16^{INK4a}$ are both encoded by the same alternatively spliced gene locus, the *CDKN2A* or

INK4A-ARF locus (Lanigan et al., 2011). Consequently, this genomic arrangement implies a simultaneous disruption of the RB and TP53 pathway, the two crucial pathways in cellular senescence, by mutating or silencing a single locus.

In addition to the already described cell cycle arrest, senescent cells display a number of characteristics, defining the senescent state. In general, senescence is accompanied by morphological changes, cells tend to become flat, large and multinucleated. Additionally, cells may display huge vacuoles due to ER stress caused by the unfolded protein response (UPR) (Kuilman et al., 2010). The most widely used biomarker for senescence is senescence associated β-galactosidase activity (Dimri et al., 1995; Debacq-Chainiaux et al., 2009), reflecting an increase in lysosomal content of senescent cells (Kurz et al., 2000). Furthermore, senescent cells undergo a profound transcriptomic change, leading to the secretion of many factors, among others cytokines and chemokines, a phenomenon termed the senescence-associated secretory phenotype (SASP) (Campisi, 2005; Coppe et al., 2008; Rodier et al., 2009). Interestingly, the resulting pro-inflammatory environment shows a pro-oncogenic effect on the neighbouring cells, enhancing proliferation, migration and invasion (Krtolica et al., 2001; Yang et al., 2006). The two secreted factors IL-6 and IL-8 have been demonstrated to play a crucial role in the establishment and maintenance of the senescent arrest (Acosta et al., 2008; Kuilman et al., 2008; Acosta et al., 2013). In summary, there is evidence for two opposing effects of senescence, tumour suppression on the one hand, limiting the expansion of pre-cancerous cells, and an oncogenic effect on the other hand, promoting cancer progression through the SASP (Muñoz-Espín and Serrano, 2014).

1.3.3 Senescence in development

In 2013, two independent groups discovered the existence of senescent cells during embryonic development (Muñoz-Espín et al., 2013; Storer et al., 2013). These findings uncover a new role for cellular senescence in remodelling and patterning of the embryo, suggesting an evolutionary origin of senescence. The occurrence of senescent cells during development happens in distinct patterns and at clearly defined stages, as observed in mouse, chick and human embryos. Storer et al. demonstrated their findings in the developing limb and the neural tube, while Muñoz-Espín et al. focused on the mesonephros and the endolymphatic sac of the inner ear. Still, both groups concluded a senescent phenotype governed by p21, as it is compromised in p21 deficient mice, but independent of DNA damage and other pathophysiological senescence mediators (Muñoz-Espín et al., 2013; Storer et al., 2013). Yet, the developmental defects in senescence inhibited embryos were minor, indeed, development of the mesonephros was only delayed by one day as compared to a normal embryo (Muñoz-Espín et al., 2013). Interestingly, both groups indicated a connection between the senescence and apoptosis pathways, presumably accounting for the mild phenotype due to compensatory mechanisms. Furthermore, an efficient clearance of senescent cells by macrophages has been identified as vital for development of the studied structures (Muñoz-Espín et al., 2013; Storer et al., 2013).

Given the recently presented evidence, it is tempting to speculate, that senescence is a developmental three step process of firstly, growth arrest, secondly, clearance of arrested cells, and thirdly regeneration of the damaged tissue (Figure 1.8). This sequence would give the organism a way to eliminate superfluous cells in a

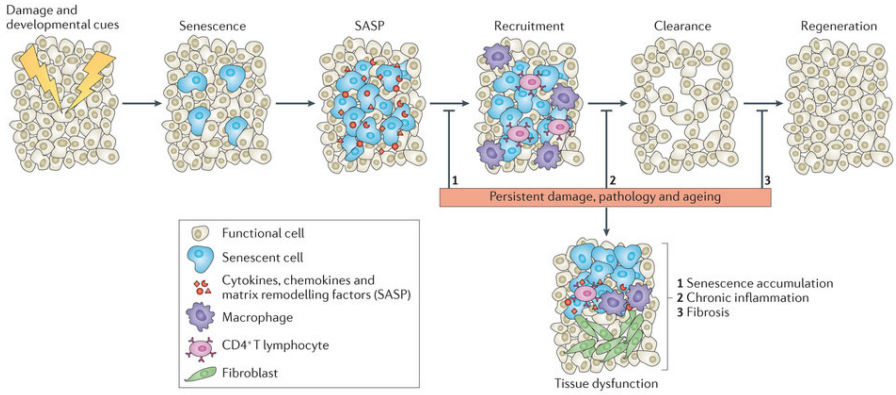

Figure 1.8: Unified model of senescence. Senescence can be described as a three step process, consisting of growth arrest, clearance of arrested cells, and regeneration of the damaged tissue. Clearance is thereby executed by the immune system recruited by the SASP. Impairment of this sequence leads to an insufficient clearance of senescent cells and incomplete regeneration of the tissue. The resulting fibrotic scar with senescent cells, inflammatory cells and fibrotic tissue can ultimately cause pathological complications.
Reprinted by permission from Macmillan Publishers Ltd: Nature Reviews Molecular Cell Biology, Muñoz-Espín and Serrano (2014), Copyright 2014.

timed fashion as opposed to apoptosis, a mechanism for immediate cell elimination. Hence, remodelling and patterning during embryonic development would rely on an intricate interplay between both senescence and apoptosis (Muñoz-Espín and Serrano, 2014). The time delay, introduced by the growth arrest during senescence, would allow the surrounding tissue to react to the insult, either to replenish the niche, replace it with a different type of cell or build a new barrier to the emerging gap. Clearance is subsequently executed by the immune system. This two step process could be flexibly timed, with clearance not necessarily following growth arrest immediately. This would give a rationale for cells to enter senescence upon stress, rather than apoptosis. Senescence would represent a stress checkpoint before the cells are lost, with the possibility to adapt to the changes, potentially

explaining reversion of senescence under certain circumstances.

Ultimately, this hypothesis would lead to the conclusion that pathological, senescent cells *in vivo*, as for instance found in melanocytic nevi, are indeed misregulated cells, that underwent the first step of the senescent programme, growth arrest, but failed to accomplish the second, immune clearance, and never reached the third, tissue regeneration. Thus, the originally beneficial aspect of growth arrest via senescence, an immediate addressing of cellular stress with the possibility of alleviation, is turned into a detrimental long-term effect via SASP and other mechanisms, as discussed above, due to the evasion of immune clearance (Muñoz-Espín and Serrano, 2014). The exact mechanism of evasion of immune clearance, however, remains elusive to date.

1.4 T-box factors

T-box factors comprise an evolutionary ancient family of transcription factors serving various roles during embryonic development (Figure 1.9 A) (Bollag et al., 1994; Sebé-Pedrós et al., 2013). T-box gene expression has been reported to be highly specific, and active during the entire developmental cycle, from the oocyte to the adult, acting through multiple downstream target genes (Naiche et al., 2005; Papaioannou, 2014). Most family members are transcriptional activators (e.g. TBR1 (Wang et al., 2004), TBX19 (Maira et al., 2003)), TBX2 and TBX3, however, function mainly as transcriptional repressors (Carreira et al., 1998; Lingbeek et al., 2002; Paxton et al., 2002). Furthermore, TBX2 and TBX3 were reported to be abnormally expressed in various cancer types, among others melanoma, breast, liver and lung cancer, suggesting a specific role for these two T-box factors in

melanoma (Lu et al., 2010).

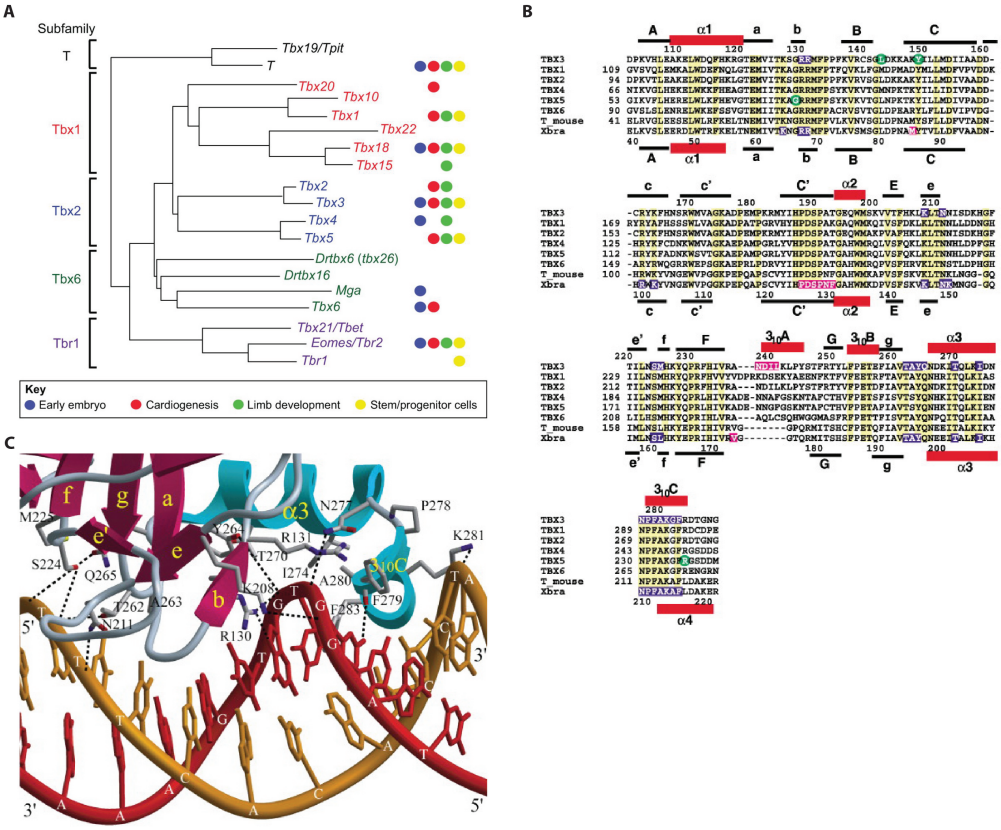

Figure 1.9: T-box factor family. The T-box factor family is an ancient family of transcription factors. (A) The phylogenetic tree shows distinct sub-groups within the family, involved in different fundamental processes during embryogenesis. (B) The T-box binding domain is evolutionary conserved throughout the family. Residues involved in DNA binding are shaded in light purple, those involved in binding the second monomer in magenta, point mutations associated with pathologies are marked in green. (C) Crystal structure of TBX3 monomer binding a T-half site, demonstrating to contact DNA only at two bases, once in the major, once in the minor groove.
(A) Reproduced with permission from Development, Papaioannou (2014), (B) and (C) Reprinted from Coll et al. (2002), Copyright 2002, with permission from Elsevier.

On a molecular level, all members of the family share a common N-terminal DNA-binding motif, called the T-box domain, spanning 180-200 amino acids (Fig-

ure 1.9 B). It recognises the T-box binding element (TBE) and binds to the consensus T-half site 5'-AGGTGTGAAA-3' mainly as a monomer, even though homodimers have also been described to exist (Kispert and Herrmann, 1993; Müller and Herrmann, 1997; Papapetrou et al., 1997). Interestingly, T-box factors have been shown to make base-specific contact with DNA only at two bases, once in the major, once in the minor groove, conferring little gene selectivity on its own (Figure 1.9 C) (Coll et al., 2002). Hence, T-box factors are suggested to achieve specificity in conjunction with interaction partners, allowing for context dependent regulation, in line with its above described widespread activity. The C-terminus, in contrast, has been shown to regulate transcription and presumably orchestrates interactions with other TFs (Wilson and Conlon, 2002).

1.4.1 T-box factors in development

During embryogenesis, T-box factors contribute to a plethora of different developmental programmes, such as craniofacial development (TBX1, TBX10, TBX15, TBX22), development of the brain (TBR1, EOMES), heart (EOMES, TBX1, TBX2, TBX3, TBX5, TBX18 and TBX20), limb (TBX4, TBX5), mammary gland (TBX2, TBX3), pituitary gland (TBX3, TBX19), thymus (TBX1), liver (TBX3), lung (TBX2, TBX4, TBX5), pigmentation (TBX15) and the immune system (TBX21) (Papaioannou, 2014). Already at the pre-implantation stage, TBX3 is expressed in the inner cell mass involved in pluripotency and later contributes to yolk sac development (Davenport et al., 2003), whereas EOMES drives differentiation and proliferation of the trophectoderm (Russ et al., 2000). At a later stage T-box factors crucially contribute to lineage specification and embryo

patterning of the vertebrate gastrula, with an heavily interwoven and overlapping web of signalling interactions with each other (Naiche et al., 2005; Papaioannou, 2014). Members of the T-box family have been described to be involved in the development of all three germ layers, mesoderm, ectoderm and endoderm, orchestrating such important biological processes as proliferation, cell survival, migration and EMT (Suzuki et al., 2004; Papaioannou, 2014).

At later stages in development T-box factors participate in the specification and maintenance of cell identity in the respective organs, e.g. T-box factors are crucially involved in heart and limb formation (Naiche et al., 2005). During heart formation, T-box factors coordinate the initial specification of the cardiac mesoderm, the regionalisation of the primitive heart tube into chamber and non-chamber myocardium, the formation of the valves and septa that separate the chambers, the recruitment of second heart field cells to the outflow tract, and formation of the cardiac conduction system (Cai et al., 2005; Stennard and Harvey, 2005; Papaioannou, 2014). Also during limb development several members of the T-box factor family are expressed (T, EOMES, TBX2, TBX3, TBX4, TBX5, TBX1, TBX15 and TBX18), with TBX2 and TBX3 being involved in digit formation (King et al., 2006), and TBX5 and TBX4 playing a critical roles in forelimb and hindlimb bud initiation, respectively (Duboc and Logan, 2011).

Given the central role of T-box factors during development, it is not surprising that TBX2 and TBX3 knock-outs are embryonic lethal due to heart malformation (Davenport et al., 2003; Harrelson et al., 2004). Furthermore, there are several human disorders known, resulting from mutations in various T-box factors. A TBX1 haploinsufficiency for instance results in DiGeorge Syndrome, a congenital heart defect and facial dysmorphism, mutations in TBX3 causes ulnar-mammary

syndrome, and mutations in TBX5 causes Holt-Oram Syndrome, leading to cardiac and skeletal congenital abnormalities (Packham and Brook, 2003).

1.4.2 T-box factors in cancer

T-box factors have been discovered and their function mainly described in the context of embryogenesis, however, their role in the adult organism, in particular in tumours, is only being recently appreciated. The key biological processes they are involved in during development, such as differentiation, proliferation, tissue integrity and EMT, are also relevant with respect to cancer and metastasis. Especially TBX2 and TBX3 have been found upregulated in breast cancer (Rowley et al., 2004; Douglas and Papaioannou, 2013) and melanoma (Vance et al., 2005; Jonsson et al., 2007; Johansson et al., 2007), indicating a potential role during tumourigenesis. Indeed, overexpression of both factors has been reported to promote bypass of senescence by suppression of $p14^{ARF}$ and p21 expression (Jacobs et al., 2000; Carlson et al., 2001; Prince et al., 2004; Vance et al., 2005; Peres et al., 2010). Furthermore, TBX2 was shown to functionally interact with RB where RB determines the functional specificity of TBX2 (Vance et al., 2010). In addition, TBX3, and potentially TBX2, downregulate the expression of E-cadherin, a cell-cell adhesion glycoprotein, resulting in a higher motility of these cells within their local niche (Rodriguez et al., 2008). Eventually, this leads to an invasive phenotype in melanoma. Concluding, there is a growing evidence for pro-tumourigenic activity of TBX2 and TBX3 via interference with the senescence pathway.

However, little is known so far about the regulation of TBX2 and TBX3 protein levels and expression as well as their exact mechanism of action during tumouri-

genesis. Furthermore, targets of TBX2 and TBX3 activity, both on DNA and protein level remain elusive.

1.5 Aim of the project

Senescence is a major barrier to tumour progression in melanoma. TBX2 and TBX3, members of the developmentally important T-box factor family, are over-expressed in melanoma and have been implicated in senescence bypass, thus promoting melanoma development. So far, their integration into the wider melanoma signalling landscape, i.e. upstream regulator and downstream effectors, and mechanism of action is unclear.

The aim of this project, therefore, is to understand the involvement of TBX2 and TBX3 in melanoma, specifically their roles in bypassing senescence. The following three main questions will be addressed:

1. Which genes are regulated by TBX2 and TBX3?
2. What signalling pathways regulate TBX2 and TBX3 and which co-factors are involved?
3. Which transcription factors regulate TBX2 and TBX3?

Chapter 2

Materials and Methods

2.1 Materials

Chemicals and reagents were purchased from Sigma-Aldrich unless stated otherwise. PI3K inhibitor GDC0941 was purchased from Selleckchem, AKT inhibitor MK-2206 was from Selleckchem and the proteasome inhibitor MG-132 was purchased from Calbiochem (Merck Millipore).

Throughout the study, autoclaved double-distilled 18 MΩ water was used for DNA and RNA solutions. Double-distilled 15 MΩ water was used to prepare all buffers and solutions.

2.1.1 Plasmids

The following plasmids were used throughout this study.

Table 2.1: List of plasmids used in this study

Construct	**Source and note**
p3XFLAG-CMV-14	3×FLAG expression vector, available in the laboratory
p3XFLAG-CMV-14-Tbx2fl	3×FLAG expression vector for Tbx2, available in the laboratory
p3XFLAG-CMV-14-Tbx3(+20aa)fl	3×FLAG expression vector for Tbx3(+), available in the laboratory
p3XFLAG-CMV-14-Tbx3(-20aa)fl	3×FLAG expression vector for Tbx3(-), available in the laboratory
pcDNA3	mammlian expression vector, available in the laboratory

Continued on next page

Table 2.1 – *Continued from previous page*

Construct	**Source and note**
pcDNA3-FoxO1a	mammalian expression vector for FoxO1, available in the laboratory
pcDNA3-FoxO3a	mammalian expression vector for FoxO3, available in the laboratory
pCMV-SV5-Pax3	mammalian expression vector for Pax3, available in the laboratory
pGL3-basic	Firefly luciferase expression construct lacking any promoter region; Promega, available in the laboratory
pGL3-basic-Tbx2promoter	human *Tbx2* promoter up to -1604 bp, available in the laboratory
pGL3-basic-Tbx3promoter	-968 to +168 bp of human *Tbx3* promoter, available in the laboratory
pPB-hCMV1-cHApA-MCS-3xFLAG	piggyBAC construct with 3×FLAG-tag, prepared by the candidate
pPB-hCMV1-cHApA-Tbx2-3xFLAG	piggyBAC construct with Tbx2-3×FLAG, prepared by the candidate
pPB-hCMV1-cHApA-Tbx3(+)-3xFLAG	piggyBAC construct with Tbx3(+)-3×FLAG, prepared by the candidate
pPB-hCMV1-cHApA-Tbx3(-)-3xFLAG	piggyBAC construct with Tbx3(-)-3×FLAG, prepared by the candidate
pCD NLBH* lenti	available in the laboratory
pMDG-VSV-G	available in the laboratory

Continued on next page

Table 2.1 – *Continued from previous page*

Construct	**Source and note**
pTRIP-GFP-shCtrl	lentiviral construct for shCtrl, co-expressing GFP, generous gift by M. Hrdinka (Gyrd-Hansen Lab, Ludwig Institute for Cancer Research, Oxford)
pTRIP-GFP-shPax3-3UTR	lentiviral construct for shPax3 targeting 3' UTR, co-expressing GFP, prepared by the candidate
pTRIP-GFP-shPax3-CDS	lentiviral construct for shPax3 targeting CDS, co-expressing GFP, prepared by the candidate
pTRIP-puro-shCtrl	lentiviral construct for shCtrl, puromycin selection cassette, prepared by the candidate
pTRIP-puro-shPax3-3UTR	lentiviral construct for shPax3 targeting 3' UTR, puromycin selection cassette, prepared by the candidate
pTRIP-puro-shPax3-CDS	lentiviral construct for shPax3 targeting coding sequence, puromycin selection cassette, prepared by the candidate

2.1.2 Antibodies

The following primary antibodies were used for both Western Blot and immunocytochemical stainings in this study.

Table 2.2: List of primary antibodies and their dilutions used in this study

Target	Source	Species	Dilution	
			Western Blot	IF
α 53BP1	Cell Signaling	rabbit	n/a	1:200
α Actin (AC-40)	Sigma Aldrich	mouse	1:5000	n/a
α BRN-2/POU3F2	Cell Signaling	rabbit	1:1000	n/a
α CDK1	Santa Cruz	mouse	1:500	1:100
α CDK2	Santa Cruz	goat	1:500	1:200
α Cyclin B1 (V152)	Cell Signaling	mouse	1:500	1:100
α Cyclin E	Santa Cruz	mouse	1:500	1:50
α E2F-1	Cell Signaling	rabbit	1:600	n/a
α E-Cadherin clone 36	BD Bioscience	mouse	1:1000	n/a
α ERK2 (C-14)	Santa Cruz	rabbit	1:5000	n/a
α EZH2 clone BD43	Millipore	mouse	1:500	n/a
α FLAG® M2	Sigma Aldrich	mouse	1:2000	1:500
α FLAG®	Sigma Aldrich	rabbit	1:1000	n/a
α FOXO1A [EP927Y]	Abcam	rabbit	1:1000	1:300
α GFP	Abcam	rabbit	1:1000	n/a
α FOXO3a (75D8)	Cell Signaling	rabbit	1:1000	1:300

Continued on next page

Table 2.2 – *Continued from previous page*

Target	**Source**	**Species**	**Dilution**	
			Western Blot	IF
α H2A.X, phospho (Ser139)	Millipore	mouse	1:1000	1:250
α HA clone 7	Sigma Aldrich	mouse	1:1000	n/a
α HP1α	Millipore	mouse	1:500	1:100
α MITF	in house	mouse	1:1000	n/a
α MYC 9E10	Sigma Aldrich	mouse	1:500	n/a
α p16 (F-12)	Santa Cruz	mouse	1:300	n/a
α p21 (M-19)	Santa Cruz	rabbit	1:500	n/a
α p27 (C-19)	Santa Cruz	goat	1:500	n/a
α p53 (DO-1)	Santa Cruz	mouse	1:500	n/a
α PAX3	DSHB Iowa	mouse	1:1000	n/a
α Pericentrin	Abcam	rabbit	n/a	1:500
α PTEN clone A2B1	Pharmingen	mouse	1:500	1:100
α S6 Ribosomal Protein (5G10)	Cell Signaling	rabbit	1:2000	n/a
α S6 Ribosomal Protein, phospho (Ser235/236)	Cell Signaling	rabbit	1:2000	n/a
α TBX2 NAs32	in house	mouse	1:1000	1:250
α TBX3 (A-20)	Santa Cruz	goat	1:500	1:50
α TBX3	Life Technologies	rabbit	1:500	1:50

The following secondary antibodies were used in this study.

Table 2.3: List of secondary antibodies and their dilutions used in this study

Target	Source	Conjugation	Species	Dilution
α goat	Santa Cruz	HRP	donkey	1:3000
α mouse	BioRad	HRP	goat	1:10,000
α rabbit	BioRad	HRP	goat	1:10,000
α goat	Life Technologies	Alexa-488/564/647	donkey	1:1000
α mouse	Life Technologies	Alexa-488/546/647	donkey	1:1000
α rabbit	Life Technologies	Alexa-488/546/647	donkey	1:1000

2.1.3 Oligodeoxynucleotides

The following oligodeoxynucleotides were used for ChIP analyses and bought from IDT, Integrated DNA Technologies.

Table 2.4: List of oligodeoxynucleotides used for ChIP analysis in this study

Sequence	Comment
5'-CAGGAGAGTCTCTTGAACCC-3'	human *E-cadherin* promoter (-800 bp), fwd
5'-TTTGTAGAGAGACAAGTCGG-3'	human *E-cadherin* promoter (-505 bp), rev
5'-CAATACAGGGAGACACAGCG-3'	human *E-cadherin* promoter (-566 bp), fwd
5'-GGTGGCTCACTAAGACCTGG-3'	human *E-cadherin* promoter (-249 bp), rev
5'-GATCCCAGGTCTTAGTGAGC-3'	human *E-cadherin* promoter (-273 bp), fwd

Continued on next page

Table 2.4 – *Continued from previous page*

Sequence	**Comment**
5'-TGGAGTCTGAACTGACTTCC-3'	human *E-cadherin* promoter (+55 bp), rev
5'-ATCTTCGAGGGAAGGAGAG-3'	human *E-cadherin* coding region, fwd
5'-TCACCCCCTCAAGACCTAG-3'	human *E-cadherin* coding region, rev

The following oligodeoxynucleotides were used for gene expression studies and bought from IDT, Integrated DNA Technologies.

Table 2.5: List of oligodeoxynucleotides used for gene expression analysis in this study

Sequence	**Comment**
5'-CTGACAAGCACGGCTTCA-3'	human TBX2, fwd
5'-GTTGGCTCGCACTATGTGG-3'	human TBX2, rev
5'-AAAAATAGACAACAACCCTTTTGC-3'	human TBX3, fwd
5'-TGCAGGGTGAGCTGTTTTC-3'	human TBX3, rev
5'-CCGACTTGGAGAGGAAGGA-3'	human PAX3, fwd
5'-CATCTGATTGGGGTGCTGA-3'	human PAX3, rev
5'-AGAAAATCTGGCACCACACC-3'	human Actin, fwd*
5'-GGGGTGTTGAAGGTCTCAAA-3'	human Actin, rev*
5'-TGCTGTCTCCATGTTTGATGTATCT-3'	human Beta-2-microglobulin, fwd*
5'-TCTCTGCTCCCCACCTCTAAGT-3'	human Beta-2-microglobulin, rev*
5'-TGCACCACCAACTGCTTAGC-3'	human Glyceraldehyde 3-phosphate dehydrogenase, fwd*

* housekeeping gene

Continued on next page

Table 2.5 – *Continued from previous page*

Sequence	**Comment**
5'-GGCATGGACTGTGGTCATGAG-3'	human Glyceraldehyde 3-phosphate dehydrogenase, rev*
5'-TGACACTGGCAAAACAATGCA-3'	human Hypoxanthine-guanine phosphoribosyltransferase, fwd*
5'-GGTCCTTTTCACCAGCAAGCT-3'	human Hypoxanthine-guanine phosphoribosyltransferase, rev*
5'-CCCCAGCTGTATTTCCAAAATGTC-3'	human Phosphoglycerate kinase 1, fwd*
5'-GCAGCCTTAATCCTCTGGTTGT-3'	human Phosphoglycerate kinase 1, rev*
5'-ACTACACACCGACTATCTCACG-3'	human Proteasome subunit beta type-2, fwd*
5'-TCGAACACTGAAGGTTGGCA-3'	human Proteasome subunit beta type-2, rev*
5'-TTCTGGGATTGTACCGCAGC-3'	human TATA-binding protein. fwd*
5'-CAAACCGCTTGGGATTATATTCGG-3'	human TATA-binding protein, rev*
5'-GTTCTTCGACATTGCCGTCG-3'	human Cyclophilin A, fwd*
5'-AAATTTTCTGCTGTCTTTGGGACC-3'	human Cyclophilin A, rev*
5'-TCTGGGTATCGGAAAGCAAGCC-3'	human Heat shock protein 90, fwd*
5'-GTGCACTTCCTCAGGCATCTTG-3'	human Heat shock protein 90, rev*
5'-CGCATGCCAGGGAAGACTAC-3'	human Succinate dehydrogenase complex, subunit A, fwd*
5'-GAGTGACCTTCCCAGTGCCAA-3'	human Succinate dehydrogenase complex, subunit A, rev*

* housekeeping gene

The following antisense oligonucleotides were used for transient knock-downs of endogenous genes and were bought from Qiagen.

Table 2.6: List of antisense oligonucleotides used for transient knock-down in this study

Sequence	**Target**
5'-r(GUUCCACAACUCGCGCUGG)d(TT)-3'	human TBX2
5'-r(CAGCUCACCCUGCAGUCCA)d(TT)-3'	human TBX3
5'-r(CCACAUCCGCCACAAGAUC)d(TT)-3'	human PAX3
5'-r(CCAGGCAUCUCAUAACAAA)d(TT)-3'	human FOXO1 SMARTpool
5'-r(CCAGAUGCCUAUACAAACA)d(TT)-3'	human FOXO1 SMARTpool
5'-r(GGAGGUAUGAGUCAGUAUA)d(TT)-3'	human FOXO1 SMARTpool
5'-r(AGGACAAUAAGUCGAGUUA)d(TT)-3'	human FOXO1 SMARTpool
5'-r(CGAAUCAGCUGACGACAGU)d(TT)-3'	human FOXO3 SMARTpool
5'-r(GUACUCAACUAGUGCAAAC)d(TT)-3'	human FOXO3 SMARTpool
5'-r(CAGUAAAGAGGUACGAAAA)d(TT)-3'	human FOXO3 SMARTpool
5'-r(UGCAUUAACUUGCGGUAUU)d(TT)-3'	human FOXO3 SMARTpool

The following short hairpin sequences were used for lentiviral knock- of endogenous genes.

Table 2.7: List of short hairpin sequences used for knock-down in this study

Sequence	Target
5'-GAAAGCGAGAAGAAGGCCAAA-3'	human PAX3 fwd, coding region
5'-TTTGGCCTTCTTCTCGCTTTC-3'	human PAX3 rev, coding region
5'-GTAACGACATGGAACTGAAAG-3'	human PAX3 fwd, 3' UTR
5'-CTTTCAGTTCCATGTCGTTAC-3'	human PAX3 rev, 3' UTR

2.2 Bacterial Methods

2.2.1 Cultivation of bacteria

To obtain clonal colonies, bacteria were streaked on agar plates, comprised of Luria-Bertani broth (LB; 1% w/v bactotryptone, 0.5% w/v yeast extract, 1% w/v NaCl, pH 7.5) containing 1.5% agar, supplemented with appropriate antibiotics (ampicillin [100 µg/ml] or kanamycin [30 µg/ml]), and poured into Petri dishes (Sterilin). Plates were stored at 4℃ after solidification, and air dried and warmed to 37℃ before use. Incubation overnight at 37℃ allowed for colony formation.

For liquid bacterial cultures LB supplemented with appropriate antibiotics was inoculated with a single colony and incubated (225 rpm, 37℃, over night with shaking).

The specialised components of all media were purchased from Difco Laborat-

ories Ltd., and media were autoclaved prior use.

2.2.2 Transformation of competent bacteria

For transformation of competent bacteria, one aliquot of 25 µl was thawed on ice, plasmid DNA added at no more than 10% v/v and the mix incubated (on ice, 30 minutes). Uptake of DNA was facilitated by subjecting the bacterial mix to heat shock (42℃, 30 seconds). After recovery (on ice, 2 minutes), 100 µl S.O.C. medium (2% w/v tryptone, 0.5% w/v yeast extract, 10 mM NaCl, 2.5 mM KCl, 10 mM $MgCl_2$, 10 mM $MgSO_4$, 20 mM glucose; Invitrogen) was added and the bacterial mixture was incubated (700 rpm shaking, 37℃, 1 hour) before plating on LB-agar plates supplemented with the appropriate selection antibiotic.

2.3 Mammalian Cell Methods

2.3.1 Cultivation of mammalian cell lines

All human melanoma cell lines used in this study (Table 2.8) were available from long-term laboratory stocks and were grown in a monolayer at 37℃ and humidified air containing 10% CO_2, using Roswell Park Memorial Institute Medium-1640 (RPMI; Life Technologies) supplemented with 10% foetal bovine serum (FBS; Sigma Aldrich).

501mel cells stably expressing 3×FLAG-tagged Tbx2, Tbx3(+) and Tbx3(-) (section 2.3.4) were maintained as for parental 501mel cells, but with a further supplement of Geneticin® (600 µg/ml; Life Technologies). When plated for experiments, selection was removed to avoid potential side-effects.

Table 2.8: Human melanoma cell lines used in this study and their respective mutational status, where known

Cell line	Metastasis	BRAF	NRAS	PTEN	p53
501mel		V600E	WT	WT	C277W
SKmel28	lung/liver	V600E	WT	T167A	L145R
IGR37		V600E			
IGR39		V600E			

Phoenix-Ampho cells, a cell line derived from the human embryonic kidney cell line 293T containing the SV40 Large T-antigen, were cultured in Dulbecco's Modified Eagle Medium (DMEM; Lonza) supplemented with 10% FBS.

Cells were regularly passaged when 80-90% confluent. To passage cells, medium was aspirated, cells washed once with PBS and subsequently detached from the cell culture dish with 0.25% Trypsin-EDTA (Life Technologies). Upon dissociation of the cells, Trypsin was inactivated with two volumes of complete medium, and the collected cells pelleted (800 g, 4 minutes). The cell pellet was resuspended in an appropriate volume of complete medium, allowing either passage or experimental use.

All described handling steps were performed under sterile conditions in a sterile laminar flow cabinet with sterile media and consumables certified for tissue culture. Cell lines were routinely checked for mycoplasma infection using MycoAlert™ mycoplasma detection kit (Lonza) according to manufacturer's protocol.

2.3.2 Cryoconservation of mammalian cell lines

For storage of cell lines, 2.5 x 10^6 cells were detached from the cell culture dish, centrifuged (800 g, 4 minutes) and resuspended in freezing medium (complete medium supplemented with 10% DMSO). Cells were then transferred into an isopropanol freezing container and immediately stored at -80℃ to allow gradient cooling. After at least 8 hours, cells were transferred to liquid nitrogen for long-term storage.

2.3.3 Transient expression of proteins of interest

For transient expression of proteins of interest, human melanoma cells were transfected with plasmid DNA containing the respective coding sequences under the control of an appropriate promoter. Cells were plated at 50-70% confluency and allowed to attach to the cell culture dish. Then, FuGENE® 6 Transfection Reagent (Promega), a blend of lipids, used at the manufacturer's recommended ratio of 3 µl FuGENE® 6 : 1 µg DNA was mixed with Opti-MEM® (Life Technologies) and incubated (RT, 5 minutes) to allow micelle formation. Plasmid DNA was subsequently added, followed by incubation of the mix (RT, 15 minutes) before drop-wise addition to the cells. Expression of protein of interest was allowed for up to 72 hours prior analysis.

2.3.4 Inducible stable expression of proteins of interest

For a stable expression of proteins of interest, the respective DNA sequence under the control of an appropriate promoter needs to be integrated into the cell lines' genome. To achieve this, two different approaches were used, a passive and an

active. For the passive approach, an expression vector of the protein of interest containing an antibiotic resistance cassette was transfected into human melanoma cells using FuGENE® 6 Transfection Reagent (Promega) as described above. After 48 h of incubation, the appropriate antibiotic was added to the culture medium for 7-10 days to select for cells with randomly integrated expression vector. To obtain a population with homogeneous transgene expression, monoclonal cell lines were subcloned.

Active integration of the DNA sequence of the protein of interest was achieved using the piggyBAC transposase (PB). For this purpose, the desired sequence of the protein of interest including its promoter was flanked with terminal repeats recognised by PB transposase and co-transfected into human melanoma cells together with an expression vector for the PB transposase at a ratio of 10:1 using FuGENE® 6 Transfection Reagent (Promega) as described above. Upon expression of the PB, it randomly integrates the DNA sequence of the protein of interest from the provided plasmid into the cell's genome at TTAA sites allowing a stable, long-term expression.

In addition, in this study the protein of interest is driven by the minimal, reverse tetracycline transactivator (rtTA) controlled promoter hCMV*-1 only transcriptionally active when bound upstream by a rtTA/tetracycline complex. This facilitates an inducible expression of the protein of interest upon administration of doxycycline (dox), a tetracycline analogue. The rtTA sequence is also integrated into the cell's genome via PB-mediated integration and bears a neomycin resistance cassette to allow selection for successful integration. Again, to obtain a population with homogeneous transgene expression, monoclonal cell lines were subcloned.

2.3.5 Transient knock-down of endogenous proteins of interest

For a transient knock-down of endogenous proteins of interest, human melanoma cells were transfected with short interfering RNA (siRNA) targeting specific mRNA sequences of the respective protein (Table 2.6 for exact sequences). First, siRNA (to a final concentration of 0.4 µM) and Lipofectamine® RNAiMAX Transfection Reagent (2% v/v) were separately diluted in Opti-MEM® and incubated (RT, 5 minutes). After mixing the two solutions and further incubation (RT, 15 minutes), the mixture was added to the empty cell culture dish followed by adding the passaged and appropriately diluted cells. This method allows a reverse transfection by settling of the cells onto the micelles enhancing transfection efficiency. Cells were incubated for 48-72 h prior harvest. AllStars Negative Control siRNA (Qiagen) was used as negative control.

2.3.6 Lentivirus production

To produce lentiviral particles Phoenix cells were plated on tissue culture dishes previously coated with polylysine (0.1 mg/ml, 15 minutes in incubator) to a confluency of 60-70%. The next day, cells were triple transfected with the plasmid containing the sequence of interest flanked by long terminal repeats (LTR) for lentiviral recognition, pCD NLBH* plasmid, providing necessary lentiviral structural and enzymatic proteins, and pMDG-VSV-G, providing an envelope protein conveying broad tropism to the virus; transfection was carried out using Lipofectamine® 2000 (Life Technologies). The following day, transfection medium was discarded and fresh complete DMEM was added twice for 24 hours each.

After each 24 hours, medium was collected, filtered (ø 45 µm) and stored (4℃). The two collected batches of medium were pooled and centrifuged (70,000 g, 2 hours, 4℃) to concentrate the virus particles. The virus pellet was resuspended in HBSS [+$CaCl_2$, +$MgCl_2$] (Life Technologies) and polybrene was added (final concentration 1 µg/ml).

The virus particle were either directly used for infection of human melanoma cells or stored until use (-80℃).

2.3.7 Lentiviral infection

For integration of a DNA sequence of interest human melanoma cells were infected with lentiviral particles containing the respective sequence. Culture medium was aspirated from cells and virus at the respective titre was administered in a thin film and allowed to incubate (RT, 5 minutes). Subsequently, fresh complete medium was added and cells were grown over night. The next day, medium was changed for appropriate selection medium to select for successful integration of the DNA sequence of interest for 48-72 hours.

2.4 Nucleic Acid Methods

2.4.1 Isolation of nucleic acid

Plasmid DNA

To isolate plasmid DNA, liquid bacterial cultures of *E.coli* carrying the plasmid of interest were harvested (small scale: 2 ml culture at 15,000 g, 1 minute, 4℃; large scale: 150 ml culture at 6000 g, 10 minutes, 4℃) and DNA was isolated using a

QIAprep Spin Miniprep Kit (Qiagen) for small-scale and a QIAGEN Plasmid Maxi Kit (Qiagen) for large-scale purification according to the manufacturer's protocol. Small-scale purifications were eluted in water, the DNA pellet from large-scale purification was suspended in water.

mRNA

For isolation of mRNA from human melanoma cells, respective cells were grown until 90% confluency, harvested using 0.25% Trypsin-EDTA (Life Technologies), lysed in RLT buffer containing β-mercaptoethanol (1% v/v), and homogenised using a syringe (19G). Purification was then performed using the RNeasy Mini Kit (Qiagen) according to the manufacturer's manual and RNA was eluted with an appropriate volume nuclease free water.

2.4.2 Quantification of nucleic acids

Nucleic acids were quantified with a NanoDrop 2000 (Thermo Scientific). According to the Beer-Lambert law the concentration c $(\mu g/ml)$ of a sample with the absorbance at 260 nm of A_{260} and an extinction coefficient ϵ $([\mu g/ml]^{-1}\, cm^{-1})$ measured at a path length l (cm) can be calculated as:

$$c = \frac{A_{260}}{\epsilon\, l}$$

For double stranded DNA $\epsilon = 0.02\,(\mu g/ml)^{-1}\, cm^{-1}$, for single stranded RNA $\epsilon = 0.025\,(\mu g/ml)^{-1}\, cm^{-1}$. The absorbance ratio at 260 nm and 280 nm was used to assess sample purity; pure DNA shows $A_{260} : A_{280} \cong 1.8$ and pure RNA $A_{260} : A_{280} \cong 2$.

2.4.3 Polymerase chain reaction

Polymerase chain reaction (PCR) was used to amplify specific DNA regions from plasmids for downstream cloning purposes or screening. For high accuracy amplification, necessary for cloning, Phusion High-Fidelity DNA Polymerase (2 U, Thermo), a proof-reading polymerase, was used in a 50 µl reaction with 100 ng DNA template, 0.4 µM of each oligonucleotide primer and 0.5 µM deoxyribose nucleoside triphosphates (dNTPs) in the supplied buffer. The enzymatic reaction was carried out in a T100 Thermal Cycler (BioRad) by denaturing the DNA template (94℃, 3 minutes); followed by 30 cycles of denaturation (94℃, 30 seconds), annealing (melting temperature, 45 seconds), and elongation (72℃, 1-2 minutes depending on amplicon); and concluded with a final elongation step (72℃, 5 minutes). For downstream applications, the PCR product was purified using the QIAquick PCR Purification Kit (Qiagen) according to the manufacturer's manual and eluted with water.

For screening purposes illustra PuReTaq Ready-To-Go PCR Beads (GE Life Science) or MyTaq™ Red Mix (Bioline) was used according to manufacturer's recommendations. The enzymatic reaction was carried out in a T100 Thermal Cycler (BioRad) by denaturing the DNA template (94℃, 1 minute); followed by 30 cycles of denaturation (94℃, 20 seconds), annealing (melting temperature, 45 seconds), and elongation (72℃, 45 seconds); and concluded with a final elongation step (72℃, 3 minutes). The resulting fragments were analysed by agarose gel electrophoresis.

2.4.4 Cleavage of double-stranded DNA by restriction endonucleases

For cloning of fragments, or screening for successful ligations, enzymatic digest using restriction endonucleases was used. The enzymatic reaction was carried out in the manufacturer's recommended buffer system (assigned temperature, 1 hour). Restriction digests were analysed by agarose gel electrophoresis.

All restriction endonucleases were purchased from New England BioLabs Inc.

2.4.5 Ligation

To ligate previously digested DNA fragments the receiving backbone vector was treated with Calf Intestinal Alkaline Phosphatase (20 U, 37℃, 30 minutes; New England BioLabs) to remove 5'-phosphate groups to prevent re-ligation of the vector unless non-complementary ends were used for cloning. Ligation itself was carried out using T4 DNA ligase (400 U; New England BioLabs) in 1× reaction buffer (RT, 30 minutes) with a 3- to 5-fold excess of insert. For a better yield, ligation was carried out over night (4℃). 2 µl of the reaction was transformed into competent bacteria and resulting colonies were screened for incorporation of the insert via restriction digest or PCR. Successful integration at the desired orientation was confirmed by DNA sequencing.

2.4.6 Agarose gel electrophoresis

To separate double-stranded DNA fragments according to size agarose gel electrophoresis was performed. Agarose (1% w/v, Appleton) was dissolved in 1× TBE buffer (Life Technologies) and heated until homogenised. After addition of the

nucleic acid dye peqGREEN (1:20,000 Peqlab), the mixture was poured into a gel tray with a comb forming wells of the desired size and allowed to polymerise. DNA samples were blended with loading dye (New England BioLabs) and electrophoresis was carried out at 120 V. DNA fragments were subsequently visualised under ultraviolet (UV) light (λ = 400 nm) using a BioDoc-It® Imaging System (UVP).

Respective DNA fragments were excised and purified from gels using QIAquick Gel Extraction Kit (Qiagen) according to the manufacturer's manual.

2.4.7 Quantitative polymerase chain reaction (qPCR)

In order to determine the abundance of a specific mRNA in a cell population, reverse transcription followed by qPCR was performed. First, 1 µg extracted whole cell mRNA (Section 2.4.1) was reverse transcribed using the QuantiTect Reverse Transcription Kit (Qiagen) according to the manufacturer's protocol. The resulting cDNA is then amenable to PCR amplification using target specific primers, ideally spanning intron boundaries to avoid amplification from contaminating genomic DNA (Table 2.5 for exact sequences). qPCR reaction was performed in technical triplicates in 15 µl total volume, containing 1× GoTaq® qPCR Master Mix (Promega), forward and reverse primer (each 0.67 µM), and an appropriate amount of cDNA as template.

PCR reaction was carried out in a Corbett Rotor-Gene 6000 (Qiagen) and after a first denaturation (95℃, 10 minutes), 55 cycles of denaturation (96℃, 5 seconds), annealing (61℃, 10 seconds), and elongation (72℃, 5 seconds) followed. At the end, melting curves for the primers used were created by gradually increasing the

temperature (72℃ to 96℃ in steps of 1℃, every 5 seconds). Only reactions having passed an empirically determined threshold and exhibiting a faithful amplification rather than primer dimerisation as judged by the melting curve, were subsequently analysed.

The comparative Ct method according to Livak and Schmittgen was applied for analysis of the raw data, expressing the amount of mRNA of the protein of interest relative to a housekeeping gene:

$$Amount\ of\ target = 2^{-\Delta\Delta C_T}$$

$$-\Delta\Delta C_T = -(\Delta C_{T[sample]} - \Delta C_{T[reference]})$$

with $\Delta C_{T[sample]}$ being the threshold value of the gene of interest, and $\Delta C_{T[reference]}$ the threshold value of the reference housekeeping gene.

This method heavily depends on stable transcription levels of the housekeeping gene regardless of the treatment applied. Hence, to determine an appropriate housekeeping gene for each treatment used in this study, 10 potential housekeeping genes (Table 2.5) were screened, ranked according to their consistency in transcription levels and the most stable gene chosen as housekeeping gene for that particular treatment (RefFinder, http://www.leonxie.com/referencegene.php).

2.4.8 Gene expression arrays

For the analysis of transcribed mRNA species, 500 ng mRNA was hybridised to a HumanHT-12 v4 Expression BeadChip (Illumina) and scanned on an IScan (Illumina). Array processing and initial analysis to extract average probe intensities

were conducted by Dilair Baban (High Throughput Genomics, The Wellcome Trust Centre for Human Genetics, University of Oxford). See section 2.7.1 for details of subsequent analysis.

2.4.9 DNA-Sequencing

For sequencing of plasmid DNA the external service of Source BioScience was used.

2.5 Protein Methods

2.5.1 Cell Extracts

Whole cell extract

To analyse whole cell proteomes, whole cell extracts were prepared. Cells were washed in PBS, detached from the cell culture dish with 0.25% Trypsin-EDTA (Life Technologies) and pelleted by centrifugation (4000 g, 2 minutes, 4℃). The resulting cell pellet was directly lysed in 2× SDS-PAGE loading buffer (78 mM Tris [pH 6.8], 4% SDS, 20% glycerol, dash of bromophenol blue, supplemented with 1.43 M β-mercaptoethanol). Extracts were boiled (95℃, 10 minutes) to allow denaturation of all proteins and stored until use (-20℃).

Nuclear cell extract

To distinguish between nuclear and cytoplasmic proteins, nuclear extracts were prepared. Cells were harvested as before and the resulting pellet was resuspended in nuclear isolation buffer (10 mM HEPES [pH 7.9], 1.5 mM $MgCl_2$, 10 mM KCl, 0.5 mM DTT, 1× protease inhibitor cocktail (PIC; Roche), 10 mM sodium butyr-

ate), and incubated (on ice, 10 minutes). NP-40 was added (0.2%, RT, 5 minutes) to dissolve the cellular membrane, leaving the nuclear membrane intact. Successful nuclear exposure was monitored under the microscope. Nuclei were pelleted by centrifugation (600 g, 4℃, 5 minutes) and lysed in nuclear extraction buffer (20 mM HEPES [pH 7.9], 420 mM NaCl, 1.5 mM $MgCl_2$, 0.2 mM EDTA, 0.5 mM DTT, 25% glycerol, 1× PIC, 10 mM sodium butyrate; on ice, 10 minutes). Insoluble matter was pelleted by centrifugation (10,000 g, 10 minutes), the supernatant transferred to a new tube and blended with 2× SDS-PAGE loading buffer. After boiling (95℃, 10 minutes), nuclear cell extracts were stored until use (-20℃).

2.5.2 Determination of Protein Concentration

To determine the concentration of a protein solution, the Bradford Assay was used. Dilution series of protein standards of known concentration and of the protein solution of interest were prepared, mixed with Quick Start™ Bradford 1× Dye Reagent (BioRad) and incubated to allow the protein-dye complex to form (RT, 5 minutes). Then, absorbance at 595 nm wavelength of each sample was measured with a 6300 Spectrophotometer (Jenway) and a standard curve was compiled plotting the absorbance of the standards against their concentration. Subsequently, concentrations of the protein solution of interest could be calculated by means of this standard curve.

For a reliable result, all sample values had to be within the linear range of the standard curve.

2.5.3 Immunoprecipitation

To isolate specific proteins of interest and its interaction partner out of a whole cell lysate, immunoprecipitation was performed. Cells were harvested as described before and the cell pellet resupended in lysis buffer (50 mM Tris [pH 8.0], 150 mM NaCl, 1 mM EDTA, 1% Triton X-100, 1× PIC (Roche)) for lysis (on ice, 10 minutes). The cell lysate was cleared by centrifugation (13,000 g, 10 minutes) and 10% of the supernatant stored as input fraction. The remaining cleared lysate was incubated with Anti-FLAG® M2 affinity gel (Sigma), previously equilibrated in lysis buffer to remove storage buffer, to allow binding of the protein of interest (4℃, 2 hours). Beads were washed in PBS twice and boiled directly in 2× SDS-PAGE loading buffer. Alternatively, to avoid interference of the light and heavy chain of the applied antibody, bound protein was eluted off the beads using 3×FLAG® peptide (150 µg/ml, 4℃, 30 minutes with mild shaking). Beads were subsequently pelleted by centrifugation (1500 g, 1 minute) and the supernatant, containing the eluted protein of interest, was blended with 2× SDS-PAGE loading buffer and boiled (95℃, 10 minutes).

2.5.4 SDS-polyacrylamide gel electrophoresis

To resolve previously prepared protein extracts (Section 2.5.1) SDS-polyacrylamide gel electrophoresis (SDS-PAGE) was performed. Gels consisted of two parts, a lower resolving gel overlain by a stacking gel with a comb forming appropriately sized wells for applying sample.

Resolving gel was prepared using an appropriate amount of acrylamide in resolving gel buffer (375 mM Tris, 0.1% SDS (v/v), adjusted to pH 8.9), and poly-

merised using 0.1% ammonium persulfate (APS) and Tetramethylethylenediamine (TEMED). Until the resolving gel was polymerised it was overlaid with isopropanol to form a level gel border and avoid oxidation. For the preparation of resolving gels 30% stock acrylamide (37.5:1 acrylamide:bis-acrylamide; Severn Biotech) was used, unless resolving phosphorylated species of a protein when 45% stock acrylamide (200:1 acrylamide:bis-acrylamide; Severn Biotech) was used.

The stacking gel comprised 5% acrylamide (30%, 37.5:1 acrylamide:bis-acrylamide; Severn Biotech) in stacking gel buffer (122 mM Tris, 0.1% SDS (v/v), adjusted to pH 6.8), and polymerised with 0.1% APS and TEMED. The mixture was poured on top of the resolving gel after removing the isopropanol.

Gels were run at 170 V in running buffer (52 mM Tris, 53 mM glycine, 0.1% SDS) until sufficient resolution of the protein extracts.

2.5.5 Coomassie staining

To directly visualise resolved proteins, SDS-PAGE gels were stained with Coomassie Brilliant Blue R250, a stain forming a protein-dye complex resulting in a blue colour. For the staining, proteins were fixed to the acrylamide matrix by submerging the gel in fixing solution (10% glacial acetic acid [Fisher], 20% ethanol [Fisher]; RT, 10 minutes). Fixing solution was subsequently replaced by Coomassie staining solution (0.1% Coomassie Brilliant Blue R250 (w/v), 10% glacial acetic acid, 40% methanol, filtered to remove particulates), boiled (20 seconds), and rocked (RT, 10 minutes). To remove excess stain, the gel was rinsed twice in water and destained in destaining solution (10% glacial acetic acid, 40% methanol; 4℃, over night) with occasional change of destaining solution. Stained gels were

then either photographed using a ChemiDoc™ MP System (BioRad) or dried on Whatman™ paper (Fisher Scientific) using a Gel Dryer (80℃, 2 hours; Aurogene Life Science).

2.5.6 Western blot

To detect specific proteins of interest out of a whole cell extract western blot was performed. After separating proteins according to size with SDS-PAGE, they were electro-transferred (100 mA per membrane, 1 hour, 24 V max) in transfer buffer (31 mM Tris, 192 mM glycine, 20% methanol) to methanol-soaked polyvinylidene difluoride (PVDF; GE Healthcare) membranes using a Owl™ HEP-1 Semidry Electroblotting System (Thermo Scientific). Subsequently, the membranes were blocked in blocking solution (5% nonfat milk in PBS supplemented with 0.1% Tween-20 (PBS-T), 1 hour), and incubated with primary antibody diluted as indicated (Table 2.2) in blocking solution (4℃, over night). Following three washes in PBS-T, membranes were incubated with appropriate horseradish peroxidase-conjugated secondary antibody (RT, 1 hour; Table 2.3), washed again three times and visualised with enhanced chemiluminescence detection reagent (Amersham). Blots were developed using Super RX X-ray films (Fujifilm) with an SRX-101A developer (Konica Minolta).

2.5.7 Chromatin immunoprecipitation (ChIP)

In order to determine the binding of a protein of interest to a specific DNA region, chromatin immunoprecipitation (ChIP) was performed. Cells were grown to 80% confluence, washed in cold PBS, and fixed with cold fixation solution (0.4% form-

aldehyde in PBS; 10 minutes, rocking), to cross-link primary amino groups of proteins with neighbouring nitrogen atoms in protein or DNA via a $-CH_2-$ linkage. To quench fixation, glycine was added (final concentration of 0.2 M; 10 minutes, rocking) and washed with cold PBS. Cross-linked cells were subsequently scraped off the plate in presence of PBS, and pelleted (1500 g, 5 minutes). Cells were resuspended in ChIP lysis buffer (50 mM Tris [pH 8.0], 10 mM EDTA, 1% SDS, 1× PIC, 0.5 mM phenylmethylsulfonyl fluoride (PMSF)), lysed (on ice, 10 minutes) and sonicated in a Covaris S220 (140 W Peak Incident Power, 5% Duty Cycle, 200 Cycles per Burst; 4℃, 16 minutes) with the water bath being continuously degassed. For confirmation of sufficient fragmentation of chromatin (approximately 300 bp fragments), cross-linking was reversed for an aliquot of chromatin (see below), and the chromatin concentration measured. This aliquot was retained as the input fraction.

80 µg chromatin was subsequently diluted 8 times in ChIP dilution buffer (16.7 mM Tris [pH 8.0], 167 mM NaCl, 1.2 mM EDTA, 0.01% SDS, 1.1% Triton X-100) and Dynabeads® Protein G (0.9 µg; Life Technologies), previously equilibrated in ChIP dilution buffer, were added for pre-clearing the chromatin (4℃, 2 hours, rotating). Beads were separated using a DynaMag™-2 Magnet (Life Technologies) and the supernatant incubated with primary antibody (5 µg, 4℃, over night, rotating). Antibody-bound material was captured with Dynabeads® Protein G (1.5 µg; 4℃, 1 hour, rotating) and the beads washed twice (4℃, 10 minutes) in each of the following buffers: low salt buffer (20 mM Tris [pH 8.0], 150 mM NaCl, 2 mM EDTA, 0.1% SDS, 1% Triton X-100), high salt buffer (20 mM Tris [pH 8.0], 500 mM NaCl, 2 mM EDTA, 0.1% SDS, 1% Triton X-100), lithium chloride buffer (0.25 M LiCl, 10 mM Tris [pH 8.0], 1 mM EDTA, 1% NP-40, 1% sodium

deoxycholate), and TE buffer (10 mM Tris [pH 8.0], 1 mM EDTA). Beads were subsequently separated using a DynaMag™-2 Magnet and bound protein-DNA complexes eluted twice (RT, 15 minutes each) in elution buffer (100 mM $NaHCO_3$, 1% SDS).

Cross-links were reversed chemically (300 µM NaCl, 10 µg RNase A; 65℃, over night) followed by enzymatic peptide digestion with Proteinase K (20 µg in 40 mM Tris [pH 8.0], 10 mM EDTA; 42℃, 1 hour; Thermo Scientific). Finally, DNA was extracted through equal volumes of phenol-chloroform, with an additional purification step in chloroform (Fisher Scientific), and precipitated (0.1 volumes 3 M sodium acetate, 2 volumes 100% ethanol; -20℃, over night) before centrifugation (16,000 g, 30 minutes). The pellet was washed in 70% ethanol, dried and resuspended in an appropriate amount of water.

Assessment of the protein of interest's binding to a specific DNA section was done via PCR or qPCR. Both times, an appropriate amount of extracted DNA (see above) as template together with specific oligonucleotide primer (0.6 µM) was used (Table 2.4 for exact sequences).

For normal PCR, allowing for a qualitative assessment of DNA binding, MyTaq™ Red Mix (Bioline) was used in a T100 Thermal Cycler (BioRad) by denaturing the DNA template (94℃, 2 minutes), 30 cycles of denaturation (94℃, 20 seconds), annealing (60℃, 30 seconds), and elongation (72℃, 30 seconds), and a final elongation step (72℃, 5 minutes). PCR products were separated via agarose gel electrophoresis and amplification of the specific DNA product indicated binding of the protein of interest to the respective DNA region.

For qPCR, allowing for a quantitative assessment, GoTaq® qPCR Master Mix (Promega) with a Corbett Rotor-Gene 6000 (Qiagen) was used by denaturing

the DNA template (95℃, 10 minutes), 55 cycles of denaturation (96℃, 5 seconds), annealing (61℃, 10 seconds), and elongation (72℃, 5 seconds). At the end, melting curves for the primers used were created by raising the temperature from 72℃ to 96℃ in steps of 1℃ every 5 seconds. Only reactions having passed an empirically determined threshold and exhibiting a faithful amplification rather than primer dimerisation as judged by the melting curve, were subsequently analysed. For quantitation, a dilution series of input DNA was prepared for each target amplicon an ChIP condition and the fold enrichment of each target in the ChIP product relative to the amount of DNA present in the input control was calculated.

ChIP-Sequencing

For an agnostic, genome-wide assessment of the DNA binding of a protein of interest, ChIP-Sequencing (ChIP-Seq) was performed. DNA of 10 parallel ChIP experiments were pooled to a final volume of 50 µl, and samples were subjected to 50 bp, single-end sequencing using an Illumina HiSeq 2500. Library preparation and sequencing was carried out by Angie Green (High Throughput Genomics, The Wellcome Trust Centre for Human Genetics, University of Oxford). For details of the bioinformatic processing and analyses see section 2.7.2.

2.6 Cell Biology Methods

2.6.1 Brightfield Imaging

To assess cell morphology and β-galactosidase staining, brightfield images were obtained by photography at 10× magnification with a Nikon microscope and Meta-

morph software.

2.6.2 Senescence-associated β-galactosidase assay

To detect senescent cells on the basis of their enhanced lysosomal β-galactosidase activity, a β-galactosidase assay was performed as published by (Debacq-Chainiaux et al., 2009). In brief, after two washes in PBS cells were fixed in fixation solution (2% formaldehyde (v/v), 0.2% glutaraldehyde (v/v) in PBS; RT, 5 minutes), washed again twice with PBS and immersed in staining solution (40 mM citric acid/Na phosphate buffer, 5 mM $K_4[Fe(CN)_6] \cdot 3\,H_2O$, 5 mM $K_3[Fe(CN)_6]$, 150 mM NaCl, 2 mM $MgCl_2$, 1 mg/ml X-gal in distilled water). Cells were incubated until a blue staining was visible (37℃, ambient CO_2).

2.6.3 Scratch-wound healing assay

To assess the motility of human melanoma cells, scratch-wound healing assays were used. First, cells were grown to 100% confluency. After treating the cells as desired, three vertical scratches were introduced using a P200 pipette tip. Closing of the introduced wound was monitored on a time-lapse microscope taking a bright-field image at 10× magnification (every 15 minutes, 48 hours). For each condition at least three different areas of the wound were monitored. ImageJ with custom macros from Mark Shipman (Ludwig Institute for Cancer Research, University of Oxford) was used to analyse the resulting data.

2.6.4 Immunocytochemical staining of human melanoma cells

To assess intracellular abundance and localisation of specific proteins of interest, immunocytochemical staining was performed. Human melanoma cells were grown to 80% confluence on glass cover slips (VWR), washed twice in PBS and fixed in formaldehyde (4% in PBS; RT, 5 minutes). After two further washes in PBS, cells were blocked and permeabilised in blocking solution (5% BSA in PBS containing 0.1% Triton X-100; RT, 20 minutes) and subsequently incubated with primary antibody, diluted as indicated (Table 2.2) in blocking solution (RT, 20 minutes). Cells were washed again twice in PBS, before incubated with appropriate Alexa Fluor-conjugated secondary antibodies (Invitrogen), diluted as indicated (Table 2.3) in blocking solution (20 minutes, RT). To counterstain cell nuclei, DAPI (0.5 µg/ml; Invitrogen) was added at this step. Coverslips were finally washed three times in PBS and mounted on Polysine™ microscopy slides (VWR) with a drop of Mowiol mounting medium (10% Mowiol (w/v) [Calbiochem], 25% glycerol, 0.1 M Tris [pH 8.5]) or dried by successive washes in increasing percentage of ethanol (70%, 90%, 100%) and a final wash in xylene before mounting with a drop of DePeX mounting medium (VWR). Slides were imaged on a LSM710 confocal microscope (Zeiss) with appropriate magnification using ZEN software.

2.6.5 Flow cytometry

For determining the cell cycle profile of a human melanoma cell population, flow cytometry after propidium iodide (PI) staining was used. Cells were grown and treated as indicated before harvest with 0.25% Trypsin-EDTA (Life Technologies)

and centrifugation (4000 g, 2 minutes). Following ethanol fixation (70% in PBS; on ice, 1 hour), cells were again pelleted (4000 g, 2 minutes), and resuspended in 250 µl PI solution (50 µg/ml PI, 0.1 mg/ml RNase A, 0.05% Triton X-100 in PBS) and incubated to allow DNA to stain (37°C, 40 minutes). After adding 750 µl PBS and another centrifugation step (4000 g, 2 minutes), stained cells were resuspended in staining solution (5% FBS, 2 mM EDTA, 0.01% NaN_3 in PBS) and PI fluorescence was measured using a BD FACSCanto™ (BD Bioscience). Cell cycle profiles were derived by plotting PI fluorescence intensities of 10,000 cells.

2.6.6 Luciferase reporter assay

For the analysis of a protein's ability to activate or suppress transcription of a specific target protein, luciferase reporter assays were performed. A luciferase reporter, containing the coding region for firefly (*Photinus pyralis*) luciferase under the control of the promoter of the target protein, was transfected into human melanoma cells together with an expression vector of the protein of interest in a 24-well format. 48 hours after transfection, cells were lysed in 50 µl Passive Lysis Buffer (Promega; RT, 10 minutes, with rocking). 25 µl of the lysate was mixed with 50 µl Luciferase Assay Reagent and luminescence was measured using a GloMax® Multi-detection System (Promega) with 0.5 seconds integration time.

2.7 Bioinformatics

2.7.1 Microarrays

Average probe intensities for each probe on the Illumina chip were analysed in R (version 3.1.1), a software environment for statistical computing and graphics (www.r-project.org), with the use of the limma package (version 3.22.1) (Ritchie et al., 2015) provided by Bioconductor, a tool collection for bioinformatic analyses (www.bioconductor.org). After initial quality control assessing hybridisation efficiency for each chip based on on-chip controls, background correction and either variance stabilisation and normalisation, or quantile normalisation were performed for all samples. Principal component analysis of the resulting data set was subsequently computed within R and used to assess grouping of the samples.

Subsequently, differentially expressed genes were identified by fitting a linear model to the pre-processed data sets and comparing the doxycycline induced samples of interest to either the same cell line without doxycycline induction or the equally treated 3×FLAG-only negative control. Only genes, individually detected as differentially expressed after both normalisation methods (variance stabilisation and normalisation, and quantile normalisation) and against both backgrounds, the same monoclonal cell line uninduced and the negative control line induced, at a p-value < 0.05, were considered for subsequent analyses. Venn diagrams, heatmaps and resulting gene lists of regulated target genes were generated within R.

2.7.2 ChIP-Sequencing

In order to obtain biologically meaningful and robust information of single-end sequencing reads after ChIP, reads were first subjected to a quality control step, before aligning them to the human genome and finally calling significant peaks for downstream analyses.

For quality control, low quality bases at the 5' and 3' end were trimmed according to their quality scores using Sickle (version 1.2) (Joshi and Fass, 2011) and FastQC (version 0.10.1), a quality control tool for high throughput sequence data (http://www.bioinformatics.babraham.ac.uk/projects/fastqc/), provided an overall assessment of quality of reads. Subsequently, high quality reads were aligned to the human genome build hg19 (GRCh37, February 2009) using Bowtie2 (version 2.1.0) in end-to-end mode (Langmead and Salzberg, 2012). Genome coverage of the aligned reads was then calculated with Bedtools (version 2.17.0) (Quinlan and Hall, 2010) and the resulting bedGraph files were uploaded to the University of California at Santa Cruz (UCSC) Genome Browser for visualisation.

Significant peaks above background were finally detected with MACS2 (version 2.0.10) (Zhang et al., 2008). Two different samples were used as a control for normalisation, a chromatin input sample collected before IP and a negative ChIP control sample produced with the established stable 3×FLAG-only 501mel cell line. Only peaks significantly enriched above both backgrounds were considered for further downstream analyses.

Annotation of peaks to nearby genes was performed using the annotatePeak program of the Hypergeometric Optimization of Motif Enrichment suite (HOMER,

version 4.7). For *de novo* prediction of enriched motifs in the identified peaks, the sequences 50 bp around the peak summit were extracted and analysed with the findMotifsGenome/annotatePeak program of the HOMER suite. The same was done for the analysis of co-enrichment of known motifs next to identified peaks with sequences 200 bp around the peak summit.

To predict potential directly regulated targets, the DNA binding information from the ChIP-Seq experiment was integrated with the expression information derived from the microarray data (Section 2.7.1) using Binding and Expression Target Analysis (BETA) (Liu et al., 2011; Wang et al., 2013), a software package from the Cistrome Project (www.cistrome.org). Each gene with an annotated peak gets a binding potential, dependent on the peak's distance to the transcriptional start site (TSS), and its differential expression assigned. After ranking both factors within the entire data set, the rank product of the two is used to identify potential direct targets.

2.7.3 Gene ontology and pathway analysis

To identify enriched annotation terms of genomic regions from ChIP-Seq experiments the Genomic Regions Enrichment of Annotations Tool (GREAT) with the 'two nearest genes' definition for gene regulatory domains was used (McLean et al., 2010). Gene ontology (GO) and Kyoto encyclopaedia of genes and genomes (KEGG) pathway analysis was conducted for proteins differentially expressed in the microarray study using the Database for Annotation, Visualization and Integrated Discovery (DAVID) against a whole-genome background using default settings (Huang et al., 2009a,b).

Chapter 3

Role of TBX2 and TBX3

3.1 Introduction

Elevated protein levels of TBX2 and TBX3 have been reported for several cancer types, i. a. in melanoma (Vance et al., 2005). In recent years, growing evidence arose for an involvement of these two proteins in tumourigenesis, linking the observed overexpression to oncogenic potential. However, the exact consequences of the increased protein levels and the underlying mechanism as to how these T-box transcription factors contribute to tumourigenesis remains elusive.

Individual targets, such as $p14^{ARF}$ ($p19^{ARF}$ in mice), p21, and E-cadherin, all repressed by T-box factors (Jacobs et al., 2000; Prince et al., 2004; Rodriguez et al., 2008), have been identified, but no broader understanding of the regulatory activity of TBX2 and TBX3 in oncogenesis has been obtained to date. As transcription factors, TBX2 and TBX3 mainly exert their function via binding regulatory elements of target genes in the genome, thereby activating or repressing their transcription. To obtain an agnostic, genome-wide view of DNA binding of TBX2 and TBX3, ChIP-Seq analysis was performed. In addition to identifying potentially regulated genes, the resulting genome-wide information of DNA binding sites enables the analysis of DNA binding motifs in a cellular context, allowing their correlation to the consensus T-half site determined in *in vitro* binding assays. Moreover, co-enriched binding motifs of other, known TFs in the vicinity of T-box binding sites can elucidate potential interaction partners, binding cooperatively to the respective sites. This information taken together can give further insights into T-box factor regulation.

To supplement the DNA binding information obtained via ChIP-Seq, expression analysis upon overexpression of TBX2 and TBX3 using human microarrays

was conducted to identify TBX2- and TBX3-dependent differentially expressed genes. This gives an additional layer of information for physiological targets of TBX2 and TBX3 regulation as it also expands the information obtained from the ChIP-Seq experiment to indirect targets. Furthermore, by intersecting the two genome-wide data sets, ChIP-Seq and microarray, potential directly regulated targets of TBX2 and/or TBX3, exhibiting both, binding of TBX2 and/or TBX3 in their promoter or enhancer region and a differential transcription, can be identified. This comprehensive, agnostic approach will help to elucidate the role of TBX2 and TBX3 in the context of melanoma tumourigenesis.

3.2 Generation of human melanoma cell lines expressing epitope-tagged TBX2 and TBX3

Due to the lack of reliable and high-grade antibodies against TBX2 and TBX3, transgenic human melanoma cell lines, stably expressing epitope-tagged TBX2 and TBX3, respectively, were established. For the generation of the stable cell lines used throughout this study, the human non-invasive melanoma cell line 501mel was chosen as it is well described and widely used in the laboratory. Additional genome-wide data sets have been generated with this cell line by other member of the laboratory, allowing comparison and integration of the different data sets due to the same genetic background. Furthermore, 501mel cells are amenable to easy genetic manipulations and simple to maintain.

3.2.1 Stable human melanoma cell lines expressing *in vivo* biotinylated TBX2 and TBX3

Biotin is a widely used epitope tag in biochemistry. Due to its small size (244 Da) it is unlikely to interfere with the tagged protein's biological activity and the high affinity to streptavidin allows a specific identification of the tagged protein. Here, the biotin holoenzyme synthetase BirA of *Escherichia coli* was deployed specifically biotinylating an acceptor peptide of 15 amino acids called Avitag (Schatz, 1993; Beckett et al., 1999).

First, a stable cell line constitutively expressing BirA was established, subsequently infected with a lentivirus integrating the cDNA of TBX2 or TBX3 respectively with an N-terminal Avitag under the control of the constitutively active EF1α promoter into the cell's genome. A transferred antibiotic resistance allowed for selection of clones with a successful integration of the respective T-box construct. Thereafter, single colonies were picked to establish monoclonal cell lines for both, TBX2- and TBX3-biotin expressing cell lines. In addition, a negative control cell line was generated, using a lentivirus integrating only the Avitag sequence.

For the analysis of successful expression of biotinylated protein, whole cell extracts of the monoclonal cell lines were assessed using Western Blot (WB). Three different clones for both cell lines were analysed and one clone each overexpressed the respective T-box factor with no biotinylated protein detected in the negative control cell line (Figure 3.1 A). However, TBX2 seemed not to be biotinylated, despite the overexpression of the protein as detected with a TBX2-specific antibody (Figure 3.1 A). Furthermore, subsequent analysis of sub-cellular localisation of the protein with immunocytochemical staining (ICC) revealed a predominantly

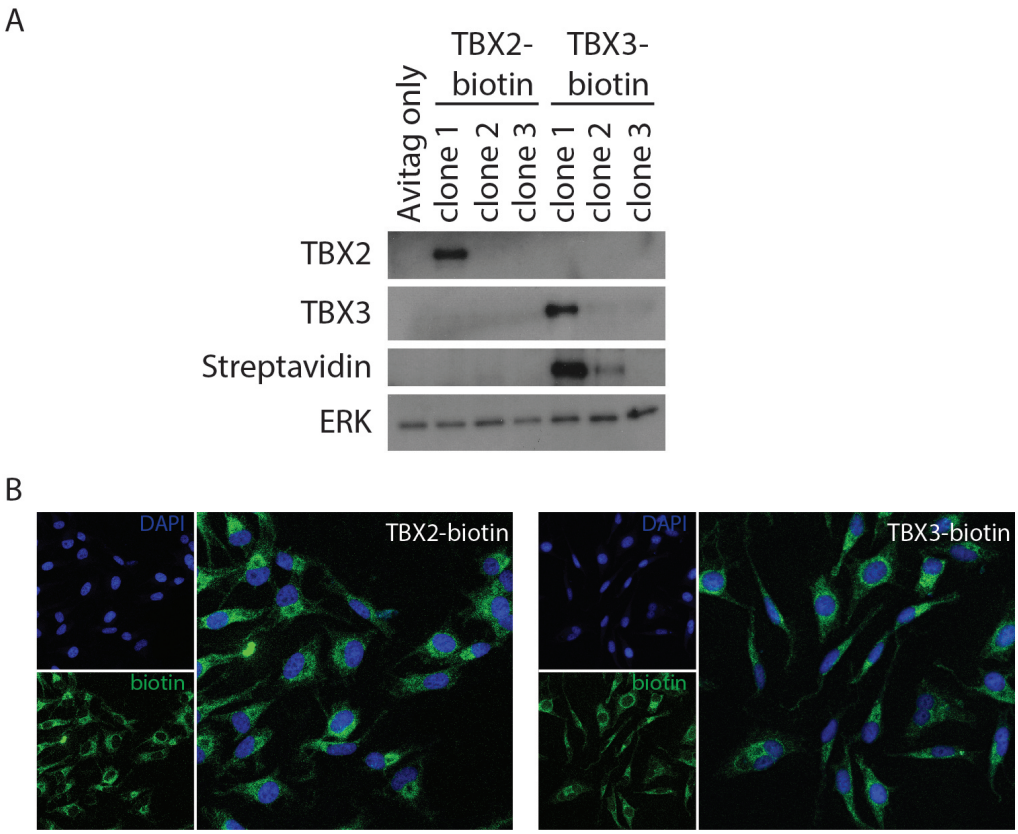

Figure 3.1: Stable human melanoma cell line expressing *in vivo* biotinylated TBX2 and TBX3.
(A) Whole cell protein extracts of three clones for both stable cell lines expressing *in vivo* biotinylated TBX2 and TBX3, respectively, were analysed using WB with the indicated antibodies and streptavidin-HRP conjugate. ERK was used as a loading control. (B) The sub-cellular localisation of *in vivo* biotinylated TBX2 and TBX3 in the stable cell line (clone 1 each) was analysed using ICC with a streptavidin-fluorophore conjugate.

cytoplasmic signal of biotinylated protein (Figure 3.1 B), not expected for TFs like TBX2 and TBX3, shown to reside in the nucleus (Prince et al., 2004; Vance et al., 2005; Li et al., 2013). Interestingly, the cell line expressing TBX2 showed a biotin signal in ICC, which was not detected earlier in the WB analysis.

The cytoplasmic signal of the protein could have two possible explanations.

Either, the biotinylated protein is unable to enter the nucleus, or biotinylated protein gets exported from the nucleus. Taken together, the generated cell lines could not be used for the devised ChIP-Seq analysis, for which a reliable biotin-tagging and nuclear localisation would have been paramount.

3.2.2 Stable human melanoma cell lines constitutively expressing polypeptide-tagged TBX2 and TBX3

To obtain a more robust tagging and avoid the localisation issues encountered with the *in vivo* biotin-tagging system, recombinant polypeptide tags directly attached to the T-box factor sequence were assessed. Two different tags, the 3×FLAG tag and the human influenza hemagglutinin (HA) tag, were deployed (Field et al., 1988; Einhauer and Jungbauer, 2001). In addition, a nuclear localisation signal (NLS) was used in conjunction with the HA-tag to drive the expressed protein into the nucleus (Kalderon et al., 1984; Dingwall et al., 1988).

In humans, TBX2 occurs only in one isoform, whereas two isoforms are described in the literature for TBX3. TBX3(+) differs from TBX3(-) in the DNA binding domain with an extra 20 amino acids present in the (+) form produced by alternative splicing. Both isoforms of TBX3 are evolutionary conserved and have been described to be functional equivalent (Hoogaars et al., 2008). For this study, stable cell lines were established for both isoforms separately.

To generate stable cell lines, 501 human melanoma cells were transfected with a plasmid containing the respective T-box factor's cDNA with the C-terminal epitope tag driven by the constitutively active CMV promoter. Successful integration of the plasmid was selected for via the conferred antibiotic resistance. In addition,

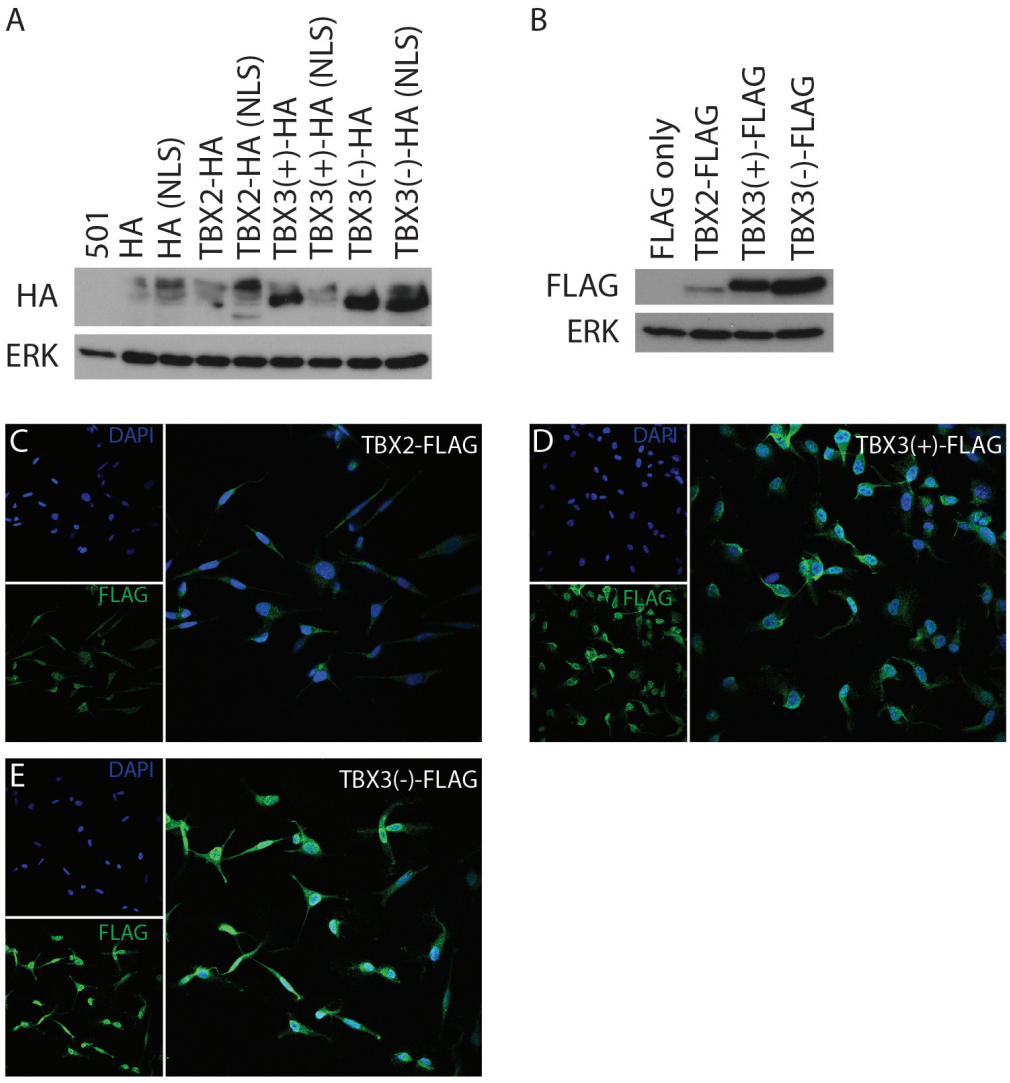

Figure 3.2: Stable human melanoma cell line expressing epitope-tagged TBX2 and TBX3. (A) Whole cell protein extracts of cell lines expressing HA-tagged T-box factors with or without NLS were analysed using WB with an antibody against the HA epitope. ERK was used as a loading control. (B) Whole cell protein extracts of cell lines expressing FLAG-tagged T-box factors were analysed using WB with an antibody against the FLAG epitope. ERK was used as a loading control. (C-E) The sub-cellular localisation of FLAG-tagged TBX2 and TBX3 in the stable cell lines was analysed using ICC with an antibody against the FLAG epitope.
NLS, nuclear localisation signal

a negative cell line was produced using the empty plasmid with only the epitope tag present.

After 10 days of selection, the transgene expression was evaluated by analysing whole cell protein extracts via WB. The stable cell lines expressing HA-tagged T-box factors showed a variable and slightly erratic expression level for both variants, with and without NLS (Figure 3.2 A). The cell lines expressing FLAG-tagged T-box factors, however, produced a reliable expression, with the expression level of TBX2-FLAG lower than both TBX3-FLAG isoforms (Figure 3.2 B). Consequently, the FLAG-tagged cell lines were characterised further.

Analysis of the sub-cellular localisation of the 3×FLAG-tagged proteins was achieved using ICC with an αFLAG antibody. All three cell lines exhibit a nuclear signal for the expressed transgene with a proportion of the expressed protein residing in the cytoplasm (Figure 3.2 C-E).

These 3×FLAG-tagged cell lines were then used to prepare samples for ChIP-Seq (Section 2.5.7). Alignment of the resulting reads to the human genome produced no significant binding peaks, indicating some technical problems with the stable cell lines. Subsequent analysis of the transgene expression over time of culturing revealed declining transgene expression levels with increasing passages (data not shown). Hence, during characterisation and preparation of ChIP-Seq samples, transgene expression levels presumably decreased in the stable cell lines, so that no successful DNA-binding of tagged T-box factors could be detected, explaining the failed ChIP-Seq experiment.

3.2.3 Inducible stable human melanoma cell lines expressing 3×FLAG-tagged TBX2 and TBX3

Subsequently, to avoid the previously encountered problems with loosing the constitutive overexpression of epitope-tagged T-box factors, inducible transgenic human melanoma cell lines were generated, expressing TBX2 and TBX3 respectively, with a C-terminal 3×FLAG-tag upon induction shortly before sample generation. For the generation of the cell lines, a tetracycline-controlled transcriptional activation (tet-on) system combined with the piggyBAC (PB) transposase mediated genomic integration was deployed. The tet-on system allows an inducible expression of TBX2-FLAG and TBX3-FLAG, respectively, upon administration of doxycycline (dox), a tetracycline derivative. The cDNAs for TBX2 and both isoforms of TBX3 including the 3×FLAG peptide were cloned under the control of the minimal promoter hCMV*-1 with an up-stream tetracycline response element (TRE), not transcriptionally active by itself. Administered dox binds the constitutively expressed reverse tetracycline transactivator (rtTA) enabling its binding to the TRE, subsequently activating the expression of *TBX2* and *TBX3* (Figure 3.3 A).

The PB transposase system was used to efficiently integrate the coding sequences of *TBX2* and *TBX3* with their minimal promoter into the genomic DNA. The above described sequences were inserted between inverted terminal repeat sequences (ITRs), recognised by the PB transposase. Upon recognition, the PB transposase excises the sequence from the plasmid and mediates efficient integration into genomic DNA at TTAA sites (Figure 3.3 B).

To establish the stable cell lines, the piggyBAC constructs of *TBX2* and *TBX3*, as described above, were transfected into 501mel cells together with rtTA under

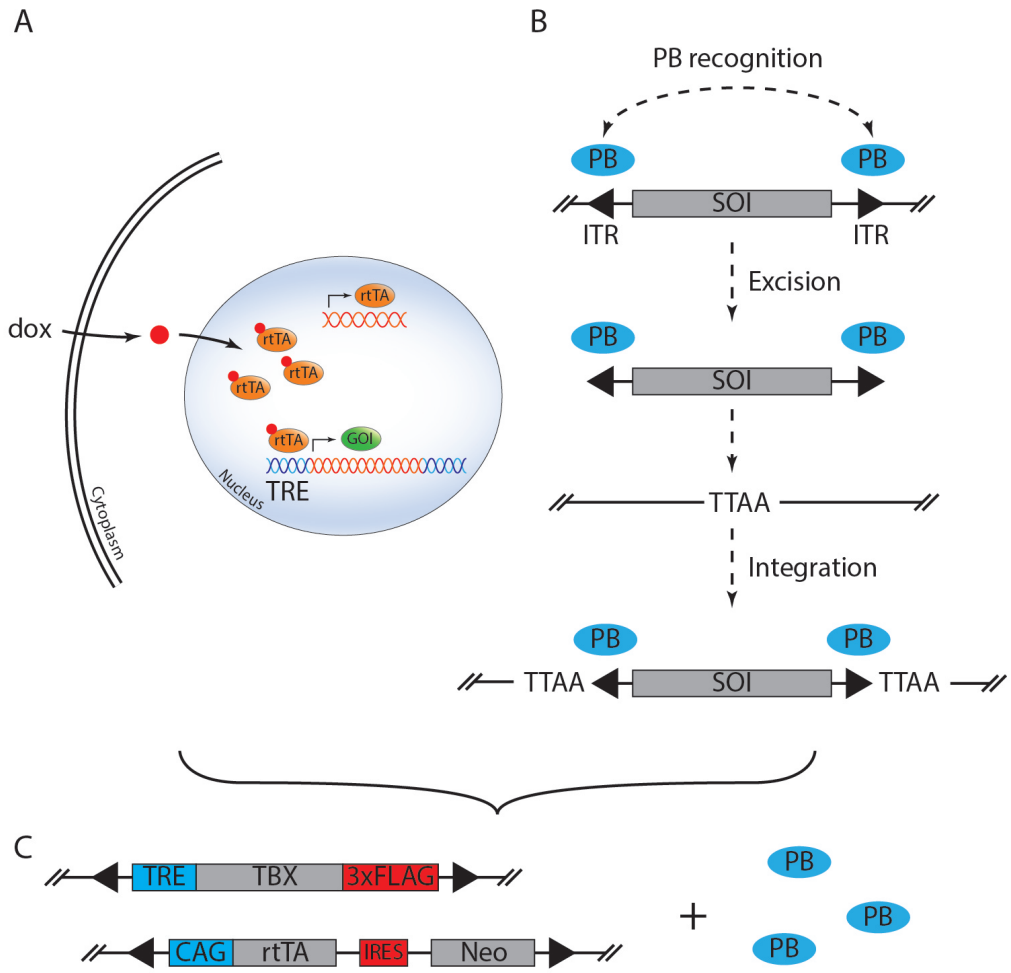

Figure 3.3: The piggyBAC-tet-on system used in this study.
(A) *Tet-on system.* The GOI is under the control of a minimal promoter, transcriptionally inactive by itself. Dox binds to rtTA, and the complex then binds the TRE, driving expression of the GOI. (B) *piggyBAC mediated integration.* ITRs flanking the SOI are recognised by PB transposase, excised, together with the SOI, and integrated at accessible TTAA sites in the genome. (C) *Combined piggyBAC-tet-on system.* The piggyBAC constructs for TBX2 and TBX3, respectively, were transfected together with the rtTA construct, also flanked by ITRs, and PB transposase to execute integration into the genomic DNA.
dox, doxycycline; GOI, gene of interest; ITR, inverted terminal repeat sequence; Neo, neomycin resistance cassette; PB, piggyBAC transposase; rtTA, reverse tetracycline transactivator; SOI, sequence of interest; TRE, tetracycline response element

the control of the constitutively active CAG promoter and a neomycin resistance cassette, also flanked by ITRs enabling PB transposase-mediated integration, and a plasmid constitutively expressing the PB transposase (Figure 3.3 C). In addition to the constructs of the T-box factors, the empty vector, containing only the ITR-flanked minimal promoter and the C-terminal 3×FLAG-tag, was transfected together with the other two components of the system to generate a negative control cell line. Polyclonal cell lines with successfully integrated sequences were derived via neomycin selection, the resistance being conferred via the rtTA construct. Due to highly heterogeneous expression levels in the polyclonal population, monoclonal cell lines were subsequently established for all four cell lines from their respective polyclonal pool.

Characterisation of monoclonal cell lines

To characterise the monoclonal cell lines, transgene expression upon dox induction was analysed by WB and sub-cellular localisation was assessed using ICC.

All three cell lines express the respective 3×FLAG-tagged T-box factor upon dox administration, confirmed to be the respective T-box factor with a protein specific antibody (Figure 3.4 A). The expression level of TBX3(+)-FLAG, however, is lower than for the other isoform TBX3(-)-FLAG, but shows similar levels to TBX2-FLAG. In all three cell lines, the transgene expression level after dox induction was significantly higher than endogenous T-box factor protein levels. Endogenous proteins could be detected in the FLAG only control cell line after longer exposure (data not shown). Upon longer exposure, background expression of the transgenes without dox addition, indicating a leakiness of the minimal promoter, can be detected. However, protein levels are significantly increased upon

induction with dox above the observed background levels, ERK levels were used as loading control.

Furthermore, to assess the dynamic range and titratability of the inducible system and determine the optimal dox concentration for reliable transgene expression, a dox dose curve was performed and protein levels analysed with WB. Very weak protein expression was already detected with 10 ng/ml dox with a strong signal at 100 ng/ml already after 4h, indicating a responsive, dox dependent transgene expression (Figure 3.4 B). The cell line for TBX3(+)-FLAG showed a lower expression level and less responsiveness than the other two cell lines. Further experiments were performed with 100 ng/ml dox and up to 24h incubation time to allow sufficient time for transgene expression and subsequent activity of the protein.

In addition, all monoclonal cell lines show an exclusive, pan-nuclear expression pattern in ICC as expected for a TF (Figure 3.4 C-F). To assess the proportion of transgene-expressing cells in the monoclonal population, positively stained cells for FLAG over the total number of cells stained by DAPI were counted in three different fields of view (300-400 cells total). Each clone showed 90% and more of the cells stained positive for the 3×FLAG transgene.

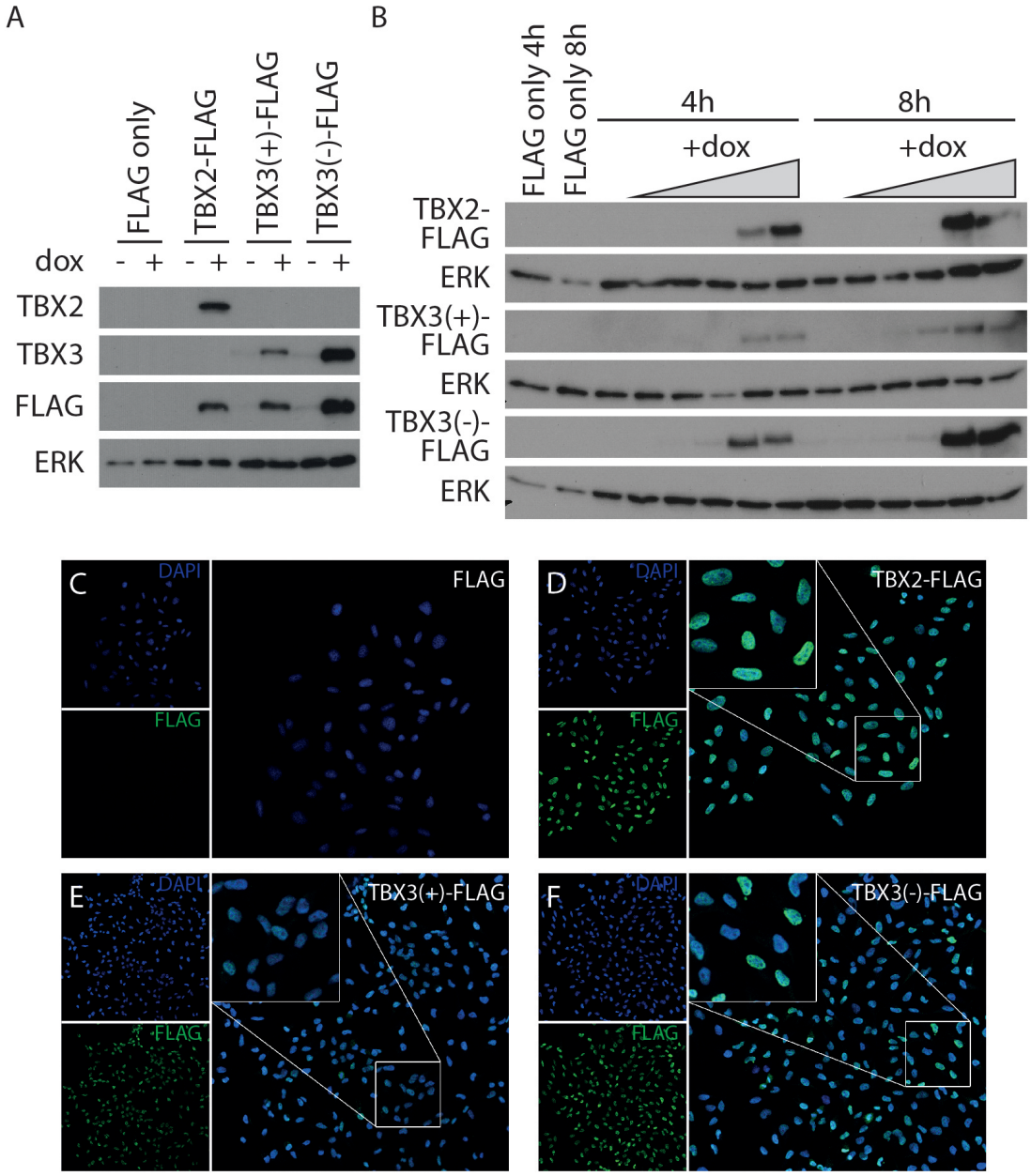

Figure 3.4: Characterisation of the stable 501mel cell lines. *Legend continues at the bottom of the next page.*

3.3 DNA binding analysis of TBX2 and TBX3

The monoclonal cell lines expressing the epitope tagged T-box factors upon induction enabled the genome-wide analysis of their DNA binding via ChIP-Seq using an antibody against the 3×FLAG epitope. Samples were generated as described (Section 2.5.7) and subjected to single-end sequencing. The negative control cell line was included to control for possible systemic effects of dox administration and input samples for all cell lines, taken just before the immunoprecipitation step of the ChIP experiment, were sequenced as further negative control to account for potential sonication bias due to tertiary or quaternary DNA structures.

3.3.1 Overview

For the analysis of the raw reads obtained from the sequencing facility, a bioinformatic pipeline was devised (Figure 3.5). First, the sequenced DNA reads were trimmed for low quality bases using Sickle (Joshi and Fass, 2011) to avoid inaccurate alignment of the reads to the human genome. The subsequent quality

Figure 3.2: Characterisation of the stable 501mel cell lines. (A) Whole cell protein extracts of the four stable, monoclonal cell lines treated with or without dox (500 ng/ml) for 24 h were analysed using WB with the indicated antibodies. ERK was used as a loading control. (B) WB of whole cell protein extracts of the three inducible, transgene expressing cell lines after administration of different dox concentrations (0 ng/ml, 1 ng/ml, 5 ng/ml, 10 ng/ml, 50 ng/ml, 100 ng/ml) for 4 h and 8 h using a FLAG-tag antibody. ERK was used as a loading control. (C-F) The four stable, monoclonal cell lines FLAG (C), TBX2-FLAG (D), TBX3(+)-FLAG (E) and TBX3(-)-FLAG (F) were treated with dox (100 ng/ml) for 24 h and stained using ICC with a FLAG-tag antibody.

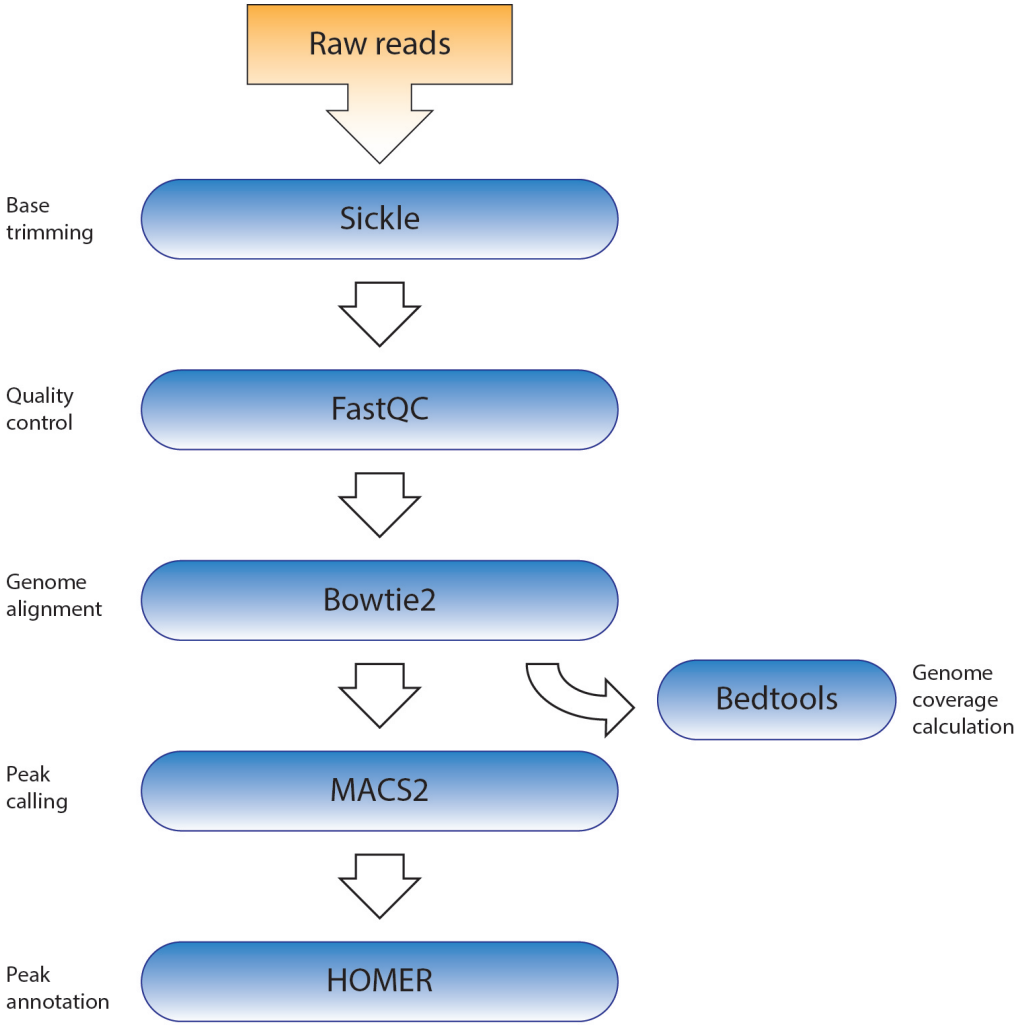

Figure 3.5: ChIP-Seq analysis pipeline. Schematic depiction of the bioinformatic pipeline used for ChIP-Seq analysis.

assessment with FastQC provided an overview of the successful trimming and the resulting high quality of DNA reads. Following, the processed DNA reads were aligned to the human genome with Bowtie2 (Langmead and Salzberg, 2012) in end-to-end mode forcing the algorithm to take every single base of the read into account. For visualisation, the genome coverage of the aligned reads was calcu-

lated using Bedtools (Quinlan and Hall, 2010) and viewed in either the UCSC genome browser or the Integrative Genomics Viewer (IGV) from the Broad Institute. Subsequent peak calling using MACS2 (Zhang et al., 2008) returned 4710 peaks genome-wide for TBX2-FLAG when using the input control as background and 6165 peaks compared to the peaks of the negative 3×FLAG cell line. The plus isoform of TBX3-FLAG showed 58 and 639 peaks, respectively, for the minus isoform 4407 and 3269 peaks, respectively, were called (Table 3.1). In similar DNA binding studies for brachyury, another member of the T-box factor family, 6420 reproducible peaks were found using a human chordoma cell line (Nelson et al., 2012) and 3,160 high-confidence peaks in a mouse ES-cell derived primitive streak model (Lolas et al., 2014), showing comparable figures to the number of peaks found here.

To consolidate the two sets of peaks obtained from the two different negative control backgrounds and identify high-confidence peaks, common peak regions, present in both lists, were determined for each TF. Intersection using Bedtools (Quinlan and Hall, 2010) resulted in 3797 common peaks for TBX2-FLAG, 39 for TBX3(+)-FLAG and 2782 for TBX3(-)-FLAG and subsequent analyses were performed only with these common peaks. As several peaks can be annotated to the same gene, the number of genes featuring peaks is lower than the overall number of common peaks (Table 3.1).

The peak height, representing the number of individual DNA reads aligned to the summit position of the peak, was calculated for each peak using the 'pileup' function of MACS2. The majority of peaks have a height between 20-60, as shown by plotting the peak height distribution of all peaks with bins of 20 reads increment. This distribution remains roughly the same independent of the background sample

used for peak calling, suggesting no strong bias in the samples (Figure 3.6 A). Subsequently, all peaks were assigned to the closest gene in the genome, respectively, according to the distance to the transcription start site (TSS) and the genomic annotation of the region occupied by the center of the peak was determined using HOMER. The global view revealed the majority of peaks to reside in the promoter regions of genes, followed by intronic and intergenic regions (Figure 3.6 B). The TBX3(+)-FLAG isoform features the biggest proportion of peaks in the promoter region, however, unlike TBX2-FLAG and TBX3(-)-FLAG, only a small fraction of the peaks are located in introns, with a much higher proportion of peaks in intergenic regions (Figure 3.6 B). Yet, there are much fewer peaks with TBX3(+)-FLAG in total potentially skewing the assessment.

To analyse the spatial pattern of binding within the promoter region, the distance of the peak's summit to the TSS of the corresponding assigned gene was plotted. By far the majority of peaks for both T-box factors occupy the region close to the TSS, suggesting a direct regulatory influence on the transcription of the target genes. Only very few peaks bind more than 1 kb up- or downstream of

Table 3.1: Number of peaks in each ChIP-Seq data set

cell line	**# peaks**		**# common peaks**	**# unique genes**
	vs. Input	**vs. Flag-ChIP**		
3×FLAG only	30	n/a	n/a	n/a
TBX2-FLAG	4710	6165	3797	3386
TBX3(+)-FLAG	58	639	39	37
TBX3(-)-FLAG	4407	3269	2782	2534

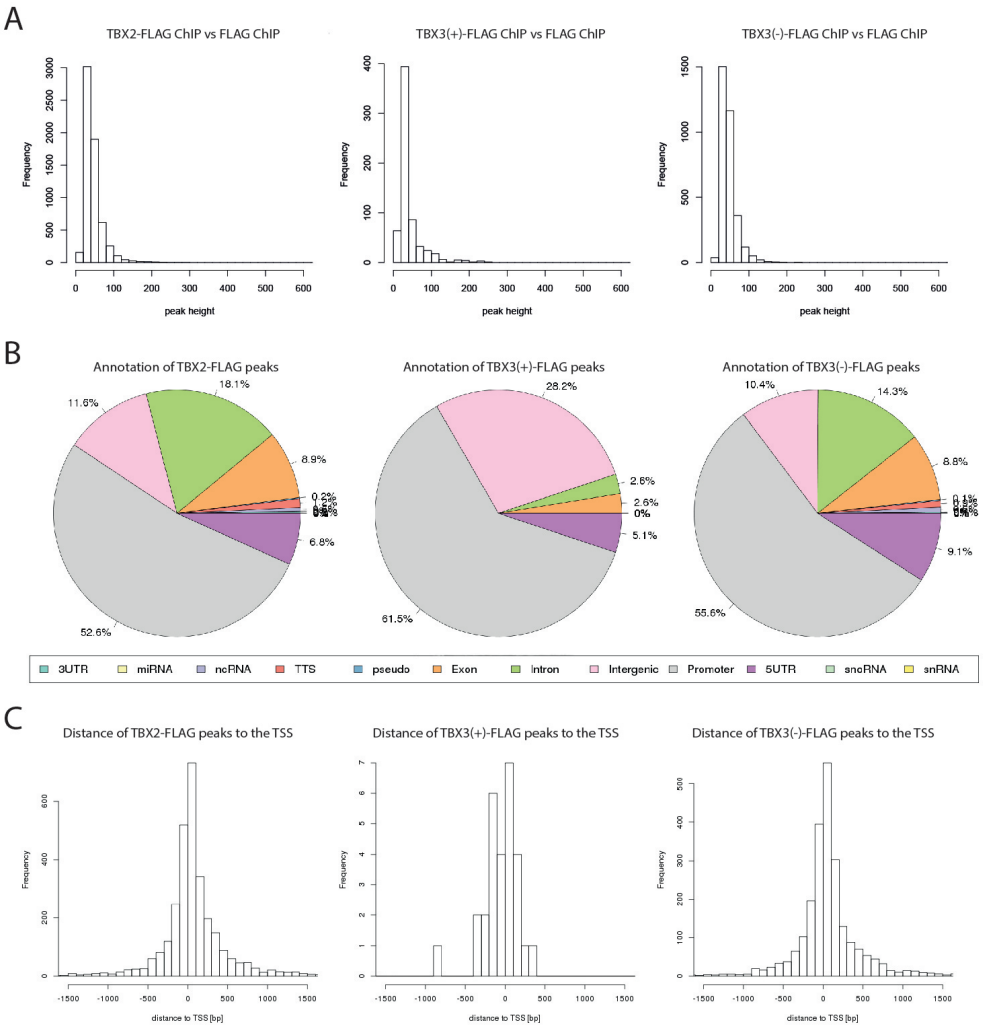

Figure 3.6: Global overview of ChIP-Seq results for the different cell lines. (A) Frequency distribution for each data set of the peaks called in comparison to the peaks of the control FLAG only cell line binned in 20 read increments according to their peak height. (B) Pie charts of each peak's annotation to the respective genomic regions for each data set using the HOMER suite. (C) Frequency distribution for each data set of the peak's distance to the TSS binned in 20 bp increments.

the TSS (Figure 3.6 C).

The global view of the data shows reliable, good quality reads for all three monoclonal cell lines. The number of raw reads after sequencing, subsequently

aligned to the genome, are similar and during quality control of the raw data, no striking differences were determined. However, the number of DNA-binding peaks identified in the sample generated with the TBX3(+)-FLAG cell line was significantly lower than with the TBX3(-)-FLAG cell line. Presumably, this difference can be accounted for by the lower expression levels of TBX3(+)-FLAG in the monoclonal cell line compared to TBX3(-)-FLAG (Figure 3.4 A). Hence, further in-depth analyses for TBX3 are based on the data generated with the TBX3(-)-FLAG monoclonal cell line due to the lack of statistical power with the low number of peaks observed with the TBX3(+)-FLAG cell line.

3.3.2 Potentially regulated genes

To further structure the list of potential target genes and extract biological meaning by predicting functions of *cis*-regulatory regions, enriched cellular pathways were assessed by calculating overrepresented gene annotation terms associated with TBX2-FLAG and TBX3(-)-FLAG binding peaks with the Genomic Regions Enrichment of Annotations Tool (GREAT). The pathway clustering is based on the Molecular Signatures Database (MSigDB) Pathway of the Broad Institute.

The most significantly enriched annotation terms associated with TBX2-FLAG binding can be subdivided into three main functions, transcriptional regulation, cell cycle regulation, and growth regulation (Figure 3.7 A). Genes with TBX2-FLAG binding in the regulatory region related to transcriptional regulation include histones, such as *H2AFX* and *H2AFZ* of the Histone 2A family, and *H3F3A* of the Histone 3A family. Furthermore, TBX2 was found to bind the promoter of *KAT2B*, coding for the K(lysine) acetyltransferase 2B (KAT2B) (Figure 3.7 B), also known

A

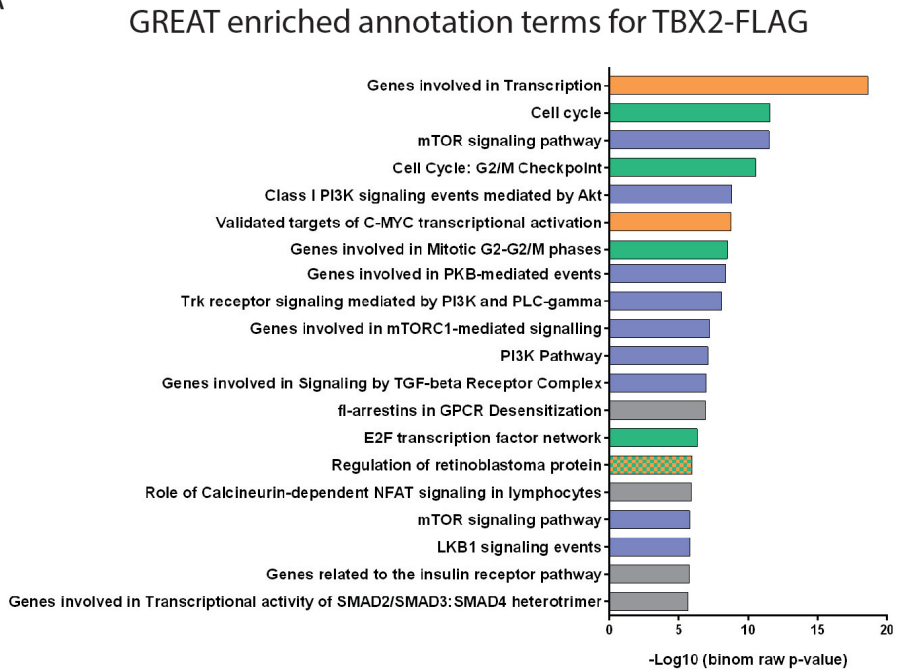

B

Transcriptional regulation	Cell cycle regulation	Growth regulation
CBX3	*ANAPC10*	*FOXO1*
ELL	*ANAPC11*	*FOXO3*
GTF2A1	*ANAPC13*	*GSK3B*
GTF2E2	*CDC25A*	*KRAS*
H2AFX	*CDC25B*	*MAP3K5*
H2AFZ	*CDK4*	*MAPK1*
H3F3A	*CUL1*	*PDPK1*
KAT2B/PCAF	*E2F1*	*PIK3R1*
TAF4	*E2F2*	*PRKAA1*
TCEB3	*E2F3*	*PRKAA2*
	GADD45A	*RICTOR*
	HDAC2	*RPTOR*
	Rb	*SHC1*
	Wee1	*SMAD4*

Figure 3.7: Potential target genes and pathways for TBX2-FLAG.
(A) Enriched annotation terms associated with TBX2-FLAG peaks as calculated by GREAT, three main groups can be distinguished, transcription (orange), cell cycle regulation (green), and growth regulatory pathways (purple). (B) List of selected targets, potentially regulated by TBX2-FLAG.

as p300/CBP-associated factor (PCAF). PCAF associates with the p300/CBP complex suggesting a direct role in transcriptional regulation via histone acetylation (Wallberg et al., 2002). The ChIP-Seq results further suggest a binding of TBX2-FLAG in the promoter of genes involved in transcription initiation. For example, *TAF4*, coding for a subunit of the transcription initiation factor TFIID, and *GTF2E2*, coding for a subunit for the general transcription factor IIE, show both a clear peak in their promoter. Interestingly, some genes coding for elongation factors, responsible for maintaining transcription after initiation, are also potentially regulated by TBX2-FLAG. There is, for instance, a distinct peak for TBX2-FLAG in the promoter of *ELL*, coding for the eleven-nineteen Lys-rich leukaemia (ELL) protein, a component of the super elongation complex (SEC) required to increase the catalytic rate of RNA polymerase II transcription and to stabilise the pre-initiation complex and early elongation (Luo et al., 2012). Taken together, the results indicate a role for TBX2-FLAG in regulating transcription at several levels and stages.

In addition to transcription, annotation terms for cell cycle regulation are also enriched when analysing the regions bound by TBX2-FLAG. *ANAPC10*, *ANAPC11*, and *ANAPC13*, three subunits of the anaphase-promoting complex (APC), all feature a TBX2-FLAG binding peak in their promoter region. APC is a cell cycle regulatory complex, triggering the meta-to-anaphase transition (Vodermaier, 2004). Furthermore, TBX2-FLAG seems to bind the promoter region of *CDC25A* and *CDC25B*, two subunits of CDC25, another cell cycle regulatory complex forcing an irreversible entry into mitosis (Malumbres and Barbacid, 2005). Besides, a binding peak for TBX2-FLAG can also be found in the promoter of *CDK4*, a cyclin-dependent kinase involved in G_1 phase progression (Vermeulen

et al., 2003), indicating different points of regulatory intervention of TBX2-FLAG. In addition, TBX2-FLAG binding peaks can also be found in several members of the E2F family and Rb, adding another pathway to the potential targets affecting cell cycle regulation.

Growth regulation is the third predicted function emerging from the enriched annotation terms analysis for TBX2-FLAG binding peaks. Three prominent pathways have been identified in that context, the PI3K pathway, the PKB/Akt pathway, and the mTOR pathway, all connected with each other via direct regulation or feedback loops. PI3K is one of the main effector pathways of RAS and upstream receptor tyrosine kinases (RTK), regulating cell growth, cell cycle entry, cell survival, cytoskeleton reorganization, and metabolism (Castellano and Downward, 2011). PI3K signals through PKB/Akt, which in turn among others regulates mTOR complex 1 (mTORC1) to exert its function. Furthermore, mTOR complex 2 (mTORC2) regulates PKB/Akt signalling (Fruman and Rommel, 2014).

Peaks of TBX2-FLAG binding can be found in all three signalling pathways. A peak in the promoter region of *PIK3R1*, coding for the phosphatidylinositol 3-kinase regulatory subunit 1 (alpha) (PIK3R1), the 85 kDa regulatory subunit of PI3K, indicates a direct potential regulatory influence of TBX2-FLAG on PI3K. Furthermore, *RICTOR*, a gene coding for rapamycin-insensitive companion of mammalian target of rapamycin (RICTOR), features a clear peak for TBX2-FLAG binding just upstream of the TSS. RICTOR is the scaffold protein in the mTORC2 enabling the binding of the substrate (Mendoza et al., 2011). The mTORC2 has been shown to activate PKB/Akt, a kinase deregulated in cancer, through phosphorylation. Further potentially regulated genes appearing in context with mTOR signalling are *AMPK*, *TSC1*, *TSC2* and *RHEB*, feeding into mTORC1.

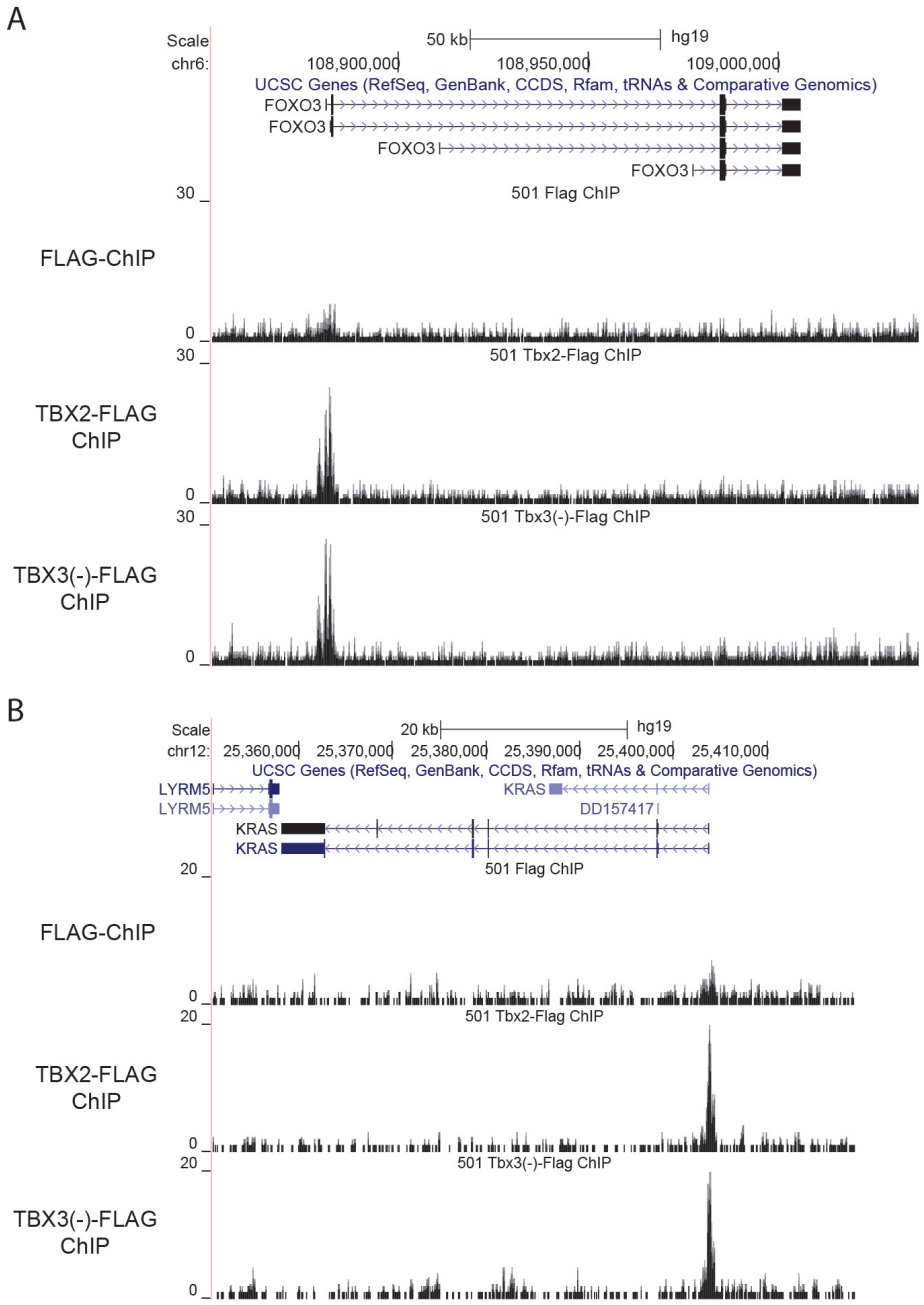

Figure 3.8: Example ChIP-Seq peaks. Exemplary binding peaks of TBX2-FLAG and TBX3(-)-FLAG in the promoter region of *FOXO3* (A) and *KRAS* (B).

Moreover, *FOXO1* and *FOXO3* exhibit TBX2-FLAG binding in their promoter (Figure 3.8 A). The genes code for Forkhead box protein O1 (FoxO1) and O3 (FoxO3), respectively, two downstream effectors of the PI3K pathway, inactivated by phosphorylation of PKB/Akt (Brunet et al., 1999). Of note, *KRAS* also seems to be bound by TBX2-FLAG in the promoter region (Figure 3.8 B), interacting high up in the hierarchy of the pathway. In addition, *GSK3B*, the gene for glycogen synthase kinase 3 beta (GSK3β), an enzyme involved in energy metabolism and also an effector pathway of PI3K, seems to be regulated as well.

The GREAT analysis for TBX3(-)-FLAG binding regions returned fewer enriched annotation terms compared to TBX2-FLAG. Nevertheless, cell cycle regulation and growth regulation also emerge as subsuming functions in the enriched annotation terms (Figure 3.9 A), indicating a functional overlap with TBX2-FLAG regulatory activity. However, annotation terms related to transcriptional regulation are not enriched with TBX3(-)-FLAG, showing differences in the regulatory potential of the two transcription factors.

Potentially regulated target genes of TBX3(-)-FLAG with enriched annotation terms for cell cycle control contribute to the same regulatory complexes and pathways described above for potential TBX2-FLAG targets. The APC and CDC25 complexes are both potentially regulated by TBX3, indicated by peaks in the promoter regions of their subunits *ANAPC11* and *CDC25B*, respectively. Furthermore, binding peaks for members of the E2F family can also be found with TBX3(-)-FLAG. In addition, TBX3(-)-FLAG binds more prominently than TBX2-FLAG in the promoter region of *MDM2*, coding for the E3 ubiquitin ligase of p53, promoting the degradation of p53 (Momand et al., 1992; Oliner et al., 1992). This is particularly interesting as p53 regulates, among others, the G_1/S checkpoint

A

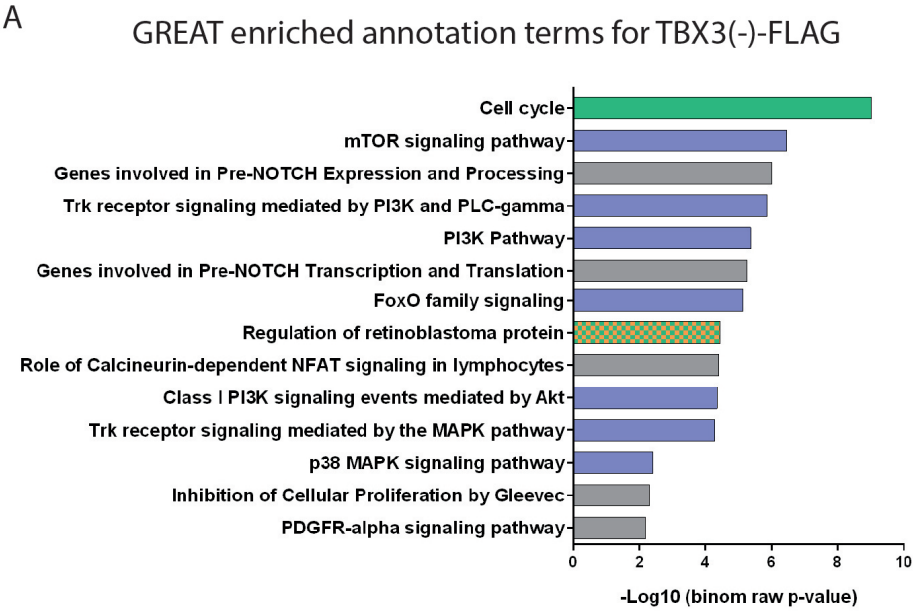

B

Cell cycle regulation	Growth regulation
ANAPC11	*CREB1*
CDC25B	*FOXO1*
CDKN1B	*FOXO3*
CUL1	*GSK3B*
E2F2	*KRAS*
E2F3	*MAP3K1*
GADD45A	*MAP3K5*
MDM2	*MAPK1*
SMAD2	*PIK3R1*
STAG1	*PRKAA1*
WEE1	*PRKAA2*
	RICTOR

Figure 3.9: Potential target genes and pathways for TBX3(-)-FLAG. (A) Enriched annotation terms with TBX3(-)-FLAG as calculated by GREAT, cell cycle regulation (green), and growth regulatory pathways (purple) are two emerging themes. (B) List of selected targets, potentially regulated by TBX3(-)-FLAG.

during cell cycle, an important step during cell cycle progression.

Possible targets for TBX3(-)-FLAG enriched for annotation terms in the context of growth regulation are members of the same three pathways already identified with TBX2-FLAG, the PI3K pathway, the PKB/Akt pathway, and the mTOR pathway. There are peaks of TBX3(-)-FLAG binding the promoter of genes related to the PI3K pathway, such as *KRAS* (Figure 3.8 B), *PIK3R1*, *GSK3B*, *FOXO1* and *FOXO3* (Figure 3.8 A). Furthermore, the MAPK pathway with peaks in *MAPK1*, *MAP3K1* and *MAP3K5* and mTOR pathway with a peak in *RICTOR* are also potential targets for TBX3 (Figure 3.9 B).

Assessing all genes potentially regulated by TBX2-FLAG and TBX3(-)-FLAG through binding in the promoter region, there is a significant overlap between the two gene sets. Roughly 60% of TBX2-FLAG regulated genes are shared with TBX3(-)-FLAG, equalling almost 80% of TBX3(-)-FLAG regulated genes (Figure 3.10). This underlines the close relatedness of TBX2-FLAG and TBX3(-)-FLAG within the T-box factor family, binding a similar set of regulatory elements. Hence, the significant overlap in predicted functions of *cis*-regulatory regions of TBX2-FLAG and TBX3(-)-FLAG, as seen above, is not surprising.

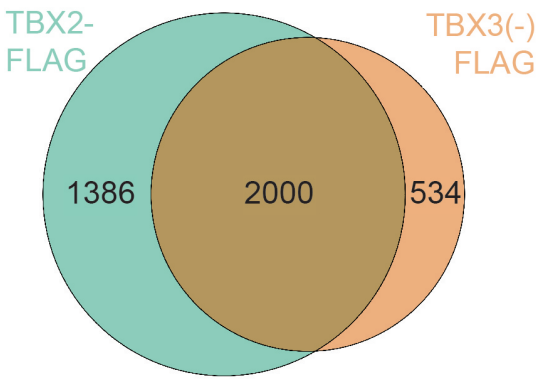

Figure 3.10: Peak overlap between TBX2-FLAG and TBX3(-)-FLAG. Venn diagram of potentially regulated genes by TBX2-FLAG and TBX3(-)-FLAG.

GREAT analysis of the uniquely regulated genes for TBX2-FLAG or TBX3(-)-

FLAG, only featuring a binding peak for one of the two TF and not for the other, resulted in no new predicted pathways or functions. Genes exclusively bound by TBX2-FLAG in the promoter region were mainly related to growth regulation, in line with previous findings, whereas no significant enrichment was found for genes only bound by TBX3(-)-FLAG in the promoter region. Genes with an exclusive binding of TBX2-FLAG in their promoter included for instance *PRKAB1* and *PRKAB2*, coding for the 5'-AMP-activated protein kinase subunit beta-1 and 2, two catalytic subunits of the 5'-AMP-activated protein kinase (AMPK), implicated in nutrient and cellular energy homoeostasis (Hardie et al., 2012). Another example of exclusive TBX2-FLAG binding is *TSC1*, a gene coding for tuberous sclerosis 1 (TSC1), forming a complex with TSC2 to regulate mTORC1 and mTORC2 signalling (Huang et al., 2008).

An example for exclusive TBX3(-)-FLAG binding is the promoter region of *RYBP*, a gene coding for the RING1 and YY1-binding protein (RYBP) involved in mediating specificity of E2F proteins (Schlisio et al., 2002), and stabilising p53 via inhibition of its ubiquitination by MDM2 (Chen et al., 2009). *PSEN2* is a further gene only bound by TBX3(-)-FLAG in the promoter region, coding for presenilin-2 (PSEN2). Presenilin is the catalytic subunit of the γ-secretase complex involved in Notch signalling via cleavage of membraneous Notch-1 releasing the Notch intracellular domain (NICD), which translocates into the nucleus to activate canonical Notch target genes (De Strooper et al., 1999; Okochi et al., 2002). These examples illustrate distinct roles for the two T-box factors TBX2-FLAG and TBX3(-)-FLAG with both being involved in the potential regulation of different target genes and hence exerting divergent functions. The overlap in target genes suggests a common regulatory activity for some functions, potentially even

complementing each other, but not for all functions.

Summarising, the presented data suggests a regulatory role for TBX2-FLAG in transcriptional regulation and an involvement of both, TBX2-FLAG and TBX3(-)-FLAG, in crucial cellular pathways related to cell cycle progression and proliferation. Considering the largely repressive function reported for T-box factors, a role for TBX2-FLAG in dampening overall transcription levels in cancer cells could be hypothesised. This could allow cancer cells to maintain an equilibrium of stresses by restraining excessive demand for nutrients and molecular building blocks through suppressing transcriptional activity, given the highly pro-proliferative signature of cancer cells. Subsequently, this dampening of cell cycle and growth pathways, as suggested by the ChIP-Seq data presented here, could ensure maintainable levels of proliferation. One could hence hypothesise a role for T-box factors in sustaining a growth-supporting equilibrium within cancer cells, just enduring enough stress without crossing a critical threshold, causing severe cellular damage. This would enable indefinite, elevated proliferation without cellular catastrophe as the cell is neither depleting the pool of nutrients due to exaggerated demand, nor accumulating too much damage due to an unsustainable proliferation rate. The maintenance of this elevated, but sustainable equilibrium could be termed cancer homoeostasis.

However, the here presented findings and hypotheses are based on DNA binding alone and can only give an indication for potential regulatory roles of TBX2-FLAG and TBX3(-)-FLAG, the functional consequences of this binding are still to be determined.

3.3.3 Enriched DNA binding motifs

The genome-wide availability of DNA sequences underlying TBX2-FLAG and TBX3-FLAG binding sites allows the assessment of enriched sequence motifs within the peak region and directly adjacent. The T-half site 5'-AGGTGTGAAA-3' is described as the canonical binding site for T-box factors (Naiche et al., 2005). However, the crystal structure of the DNA-binding domain of TBX3 bound to DNA identified only two direct contacts with DNA bases, conveying little binding specificity on their own (Coll et al., 2002). This raises the question of how T-box factors gain their target specificity. Thus, analysing enriched DNA motifs within the binding peaks can verify the canonical motif and, in addition, identify further potential sequence-specific aspects of DNA binding. Furthermore, enriched binding motifs of known TFs with well-characterised binding motifs adjacent to TBX2-FLAG and/or TBX3-FLAG binding peaks can elucidate potential interaction partners, that may act to increase DNA binding specificity for the T-box factors.

For the identification of enriched motifs within the TBX2-FLAG and TBX3(-)-FLAG binding peaks, the 50 bp DNA fragments surrounding the summit of each peak, 25 bp either side, were extracted and analysed with the findMotifGenome programme of the HOMER suite. For both T-box factors the most significantly enriched DNA binding motif is indeed the T-half site with variation on the seventh base, a G in the consensus sequence and with similar frequency for C, T, and G in the position specific frequency matrices (PSFM) enriched in the data set (Figure 3.11 A).

In this analysis only known TF binding motifs were used to search and only 15%

of TBX2-FLAG peaks, and 10% of TBX3(-)-FLAG peaks contained the T-half site. Interestingly, for TBX2-FLAG peaks the next most significantly enriched motifs were similar to the T-half site, exhibiting a few modified bases. These motifs are attributed to Eomesodermin, also known as TBR2, and TBET, also known as TBX21, two TFs of the T-box family, indicating a similar binding pattern within the entire T-box protein family. In the TBX3(-)-FLAG peaks, on the other hand, the most significantly enriched motifs after the consensus T-half site are binding motifs for ELK1 and ELK4, two members of the TCF subfamily of the ETS TF family. Strikingly, for both proteins, ELK1 and ELK4, a TBX3 binding peak can be found in their promoter region, indicating a potential cross-regulatory loop (Figure 3.11 B). The resemblance to the T-half site of the second most significantly enriched motif for the TBX2-FLAG peaks is more apparent when reading the complement sequence on the reverse strand.

While the above analysis identified enriched motifs based on a curated database of known TF binding site, the same 50 bp DNA fragments around the peak summits were also used to determine enriched *de novo* motifs within the TBX2-FLAG and TBX3(-)-FLAG binding peaks. For this analysis, overrepresented motifs relative to a random background control, derived from non-regulated promoter regions matched for GC-content and fragment size, were calculated. The resulting motifs were subsequently matched to resembling motifs of known TFs.

For both T-box factors slightly modified versions of the T-half site emerged among the results, giving further confidence in the identified peaks being related to T-box factor binding. Moreover, there is a subset of peaks for both, TBX2-FLAG and TBX3(-)-FLAG, with an enriched DNA binding motif associated with E2F2, a TF of the E2F family controlling the cell cycle in conjunction with RB (Fig-

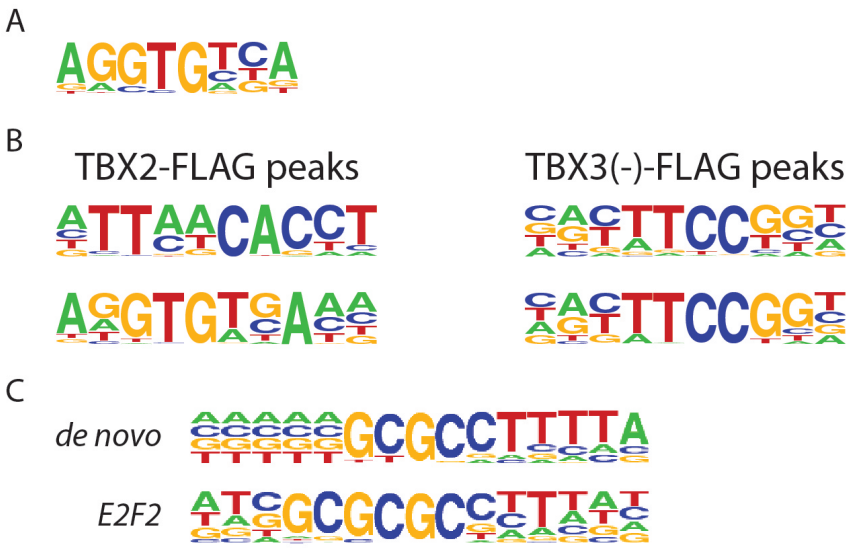

Figure 3.11: Enriched DNA binding motifs for TBX2-FLAG and TBX3(-)-FLAG.
(A) PSFM of the most significantly enriched consensus DNA binding motif for TBX2-FLAG and TBX3(-)-FLAG. (B) PSFM of subsequent significantly enriched motifs found in TBX2-FLAG and TBX3(-)-FLAG peaks. (C) PSFM of *de novo* binding motif prediction for both TBX2-FLAG and TBX3(-)-FLAG binding peaks.

ure 3.11 C). Again, as with ELK1 and ELK4 above, the promoter region of E2F2 itself features distinct peaks for TBX2-FLAG and TBX3(-)-FLAG binding, potentially indicating a feedback loop. As the binding motif of the entire E2F family is very similar, these sites can be potentially bound by the other members of the E2F family as well. Indeed, the identified enriched *de novo* motifs assigned to E2F2 also resemble the binding motifs of E2F1 and E2F3.

Furthermore, in the minor groove of DNA T and C bases offer similar chemical interaction possibilities for DNA binding proteins via electron acceptors and donors, so that recognition in the minor groove is not as base specific as in the major groove and TFs with the same recognition site can bind both, T and C bases.

Hence, the underlying binding motif might feature either base, further expanding the spectrum of potential binding sites.

The presence of binding sites of other TFs at the summit of TBX2-FLAG and TBX3(-)-FLAG peaks gives three possible scenarios. Either both TFs compete for binding the respective regions and as the ChIP-Seq experiment represents an average of a large population of cells, the T-box factors occupy enough sites within the entire cell population to be detected in the analysis. A further possibility is the binding of the two TFs adjacent to each other, one in the major groove, the other in the minor groove, with or without interaction between the two. The last possibility is an interaction between the two TFs with the interaction partner binding to the DNA binding motif and the T-box factor executing its regulatory function without immediate or with just partial DNA interaction. A definite explanation, however, will require biochemical analysis of DNA binding of the factors identified in an *in vitro* reconstituted system.

3.3.4 Co-enriched motifs of known TF

To further analyse possible interaction partners, potentially conferring more binding specificity to T-box factors, co-enrichment of known TFs in the close vicinity of the 3×FLAG-tagged T-box factor binding sites were assessed. For that, a larger DNA fragment of 200 bp around the summit of each peak, 100 bp either side, was extracted and analysed with findMotifGenome of the HOMER suite.

In addition to the already identified binding motifs, further enriched binding sites for members of the ETS TF family were found, such as ETS1, FLI1, ETV1, GABPA and ELF1 (Figure 3.12 A, B). The ETS family of TF have been described

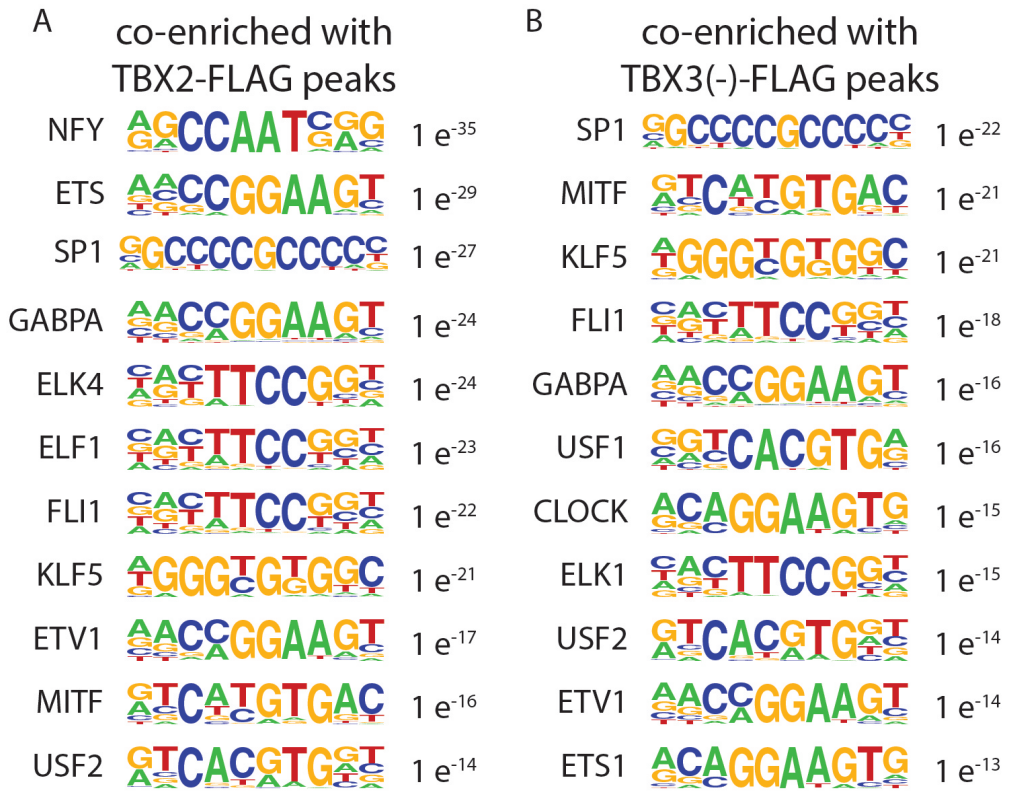

Figure 3.12: Co-enriched DNA binding motifs in close vicinity to TBX2-FLAG and TBX3(-)-FLAG binding sites. Selected PSFM of co-enriched binding motifs of known TFs in the 200 bp DNA fragments surrounding the DNA binding peaks of TBX2-FLAG (A) or TBX3(-)-FLAG (B). The number next to each PSFM indicates the respective p-value.

as important regulators in both, early development and the adult organism, and dysregulated expression has been linked to tumourigenesis (Oikawa and Yamada, 2003). Moreover, ETS-domain proteins are known to function in collaboration with other TFs, promoting specificity of the individual members. Due to the differing protein partners for each member they can act in an either repressive or activating manner, indicating a context-dependent activity (Sharrocks, 2001).

Another enriched binding motif in the region around TBX2-FLAG and

TBX3(-)-FLAG binding sites is of the microphthalmia-associated transcription factor (MITF), the master regulator of the melanocyte lineage (Figure 3.12 A, B). MITF has been linked to pro- and anti-proliferative activity, a contradiction being resolved by the rheostat model, whereby MITF protein levels determine the regulatory function (Carreira et al., 2006). Interestingly, TBX2 is upregulated by MITF (Carreira et al., 2000) and is here suggested to be a potential interaction partner for regulation of target genes. Furthermore, MITF binding motifs can also be bound by the upstream stimulatory factor 1 (USF1) and 2 (USF2) (Galibert et al., 2001). The USF proteins are cellular TFs involved in regulating stress and immune responses, cell cycle and proliferation, and lipid and glucid metabolism. In addition, USF1 has been implicated in the regulation of pigmentation upon UV-radiation in melanocytes (Corre and Galibert, 2005). As these TFs are capable of binding the same MITF binding site, they could also represent potential interaction partner of TBX2 and TBX3.

Finally, there are also enriched binding motifs next to TBX2-FLAG and TBX3(-)-FLAG binding peaks for member of the Kruppel-like factors (KLF), in particular KLF1, KLF4, and KLF5 (Figure 3.11 A). The KLF family is a family of zinc finger-containing TF, regulating multiple biological processes, such as proliferation, growth, and survival. In order to exert the multitudinous functions, KLFs recruit transcriptional regulatory proteins including transcriptional co-activators and co-repressors.

Summarising, the analysis of co-enriched binding motifs in the vicinity of TBX2-FLAG and TBX3(-)-FLAG binding region has identified interesting candidates, either interacting or recruiting T-box factors to their target sites. This interaction could add binding specificity to T-box factor binding despite their own

weak DNA interaction. Furthermore, context-dependent cooperation with different TF could also potentially explain the described disparate regulatory function of T-box factors of both, repression and activation.

3.4 Gene expression analysis

To expand the assessment of the regulatory potential of TBX2 and TBX3 to the RNA level and include potentially indirectly regulated targets, gene expression analysis using microarrays was performed. For that purpose, the monoclonal cell lines described above were deployed, inducibly expressing the 3×FLAG tagged T-box factors. Whole cell RNA extracts were prepared after 6 h and 24 h dox treatment in independent triplicates from the three monoclonal cell lines, TBX2-FLAG, TBX3(+)-FLAG, and TBX3(-)-FLAG, and hybridised to an Illumina HumanHT-12 v4 Expression BeadChip, covering the entire human transcriptome. In order to account for technical variation between microarray chips, each triplicate sample was run on a different chip. In addition, whole cell RNA extracts from the same monoclonal cell lines without dox induction were run, to identify target proteins, potentially regulated by TBX2-FLAG and TBX3-FLAG, through differential expression analysis comparing the expression profiles of induced versus uninduced cell lines. The 3×FLAG negative control cell line was also included with and without dox treatment to account for potential dox effects as two recent publications have shown alterations of the metabolism and mitochondrial function upon tetracycline administration (Ahler et al., 2013; Moullan et al., 2015).

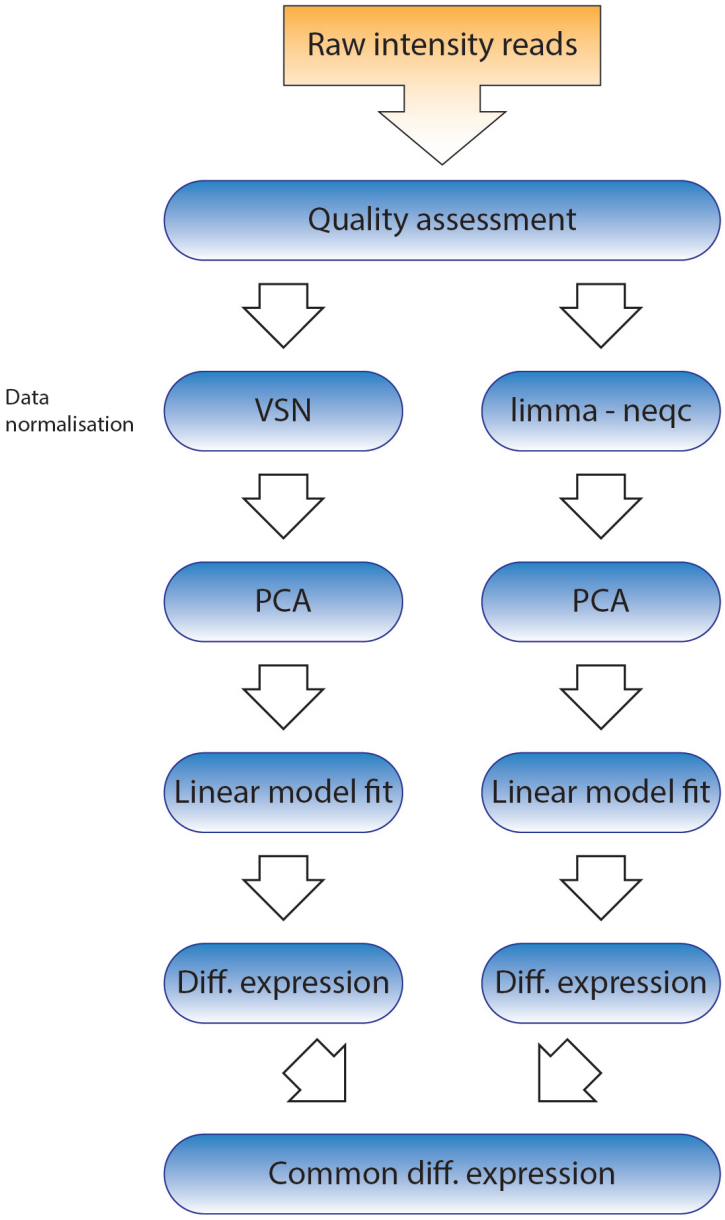

Figure 3.13: Microarray analysis pipeline. Schematic depiction of the bioinformatic pipeline used for microarray analysis.
PCA, principal component analysis; VSN, variance and stabilisation normalisation

3.4.1 Overview

For the analysis of the raw intensity reads obtained from the High Throughput Genomics facility a bioinformatic pipeline was established (Figure 3.13). First, for quality assessment of the obtained data average probe intensities for each sample were analysed (Figure 3.14 A). The internal positive control of biotin binding showed a satisfactory hybridisation efficiency for the samples, only chip 1 exhibited a slightly lower sample hybridisation. The average intensity signal was consistent throughout all samples and the number of genes detected above background ranged from 12,000 to 15,000, roughly half of the represented genes on the chip. This is a normal value for these kind of experiments, indicating overall high quality data.

Thereafter, background correction and normalisation of the probe intensities were performed with two different approaches, variance stabilisation and normalisation (VSN) and neqc. VSN is a native statistical function from the R language, whereas neqc is a pre-defined function from the limma package. After background correction, data was subjected to cluster analysis and principal component analysis (PCA) to identify possible outliers and major contributors to variance within the sample set. The cluster analysis of all samples revealed a clear difference of the samples derived from the 3×FLAG negative control cell line, clustering all to the left main branch, whereas all samples derived from the three sample cell lines, expressing the 3×FLAG-tagged T-box factors, clustered in the right main branch. No clear clustering within the sample cell lines on the right main branch was observed (Figure 3.14 B). Subsequent PCA based on all samples identified a strong technical batch-to-batch variation between the chips, which can occur even under strict chip manufacture and experimental conditions, as the primary source

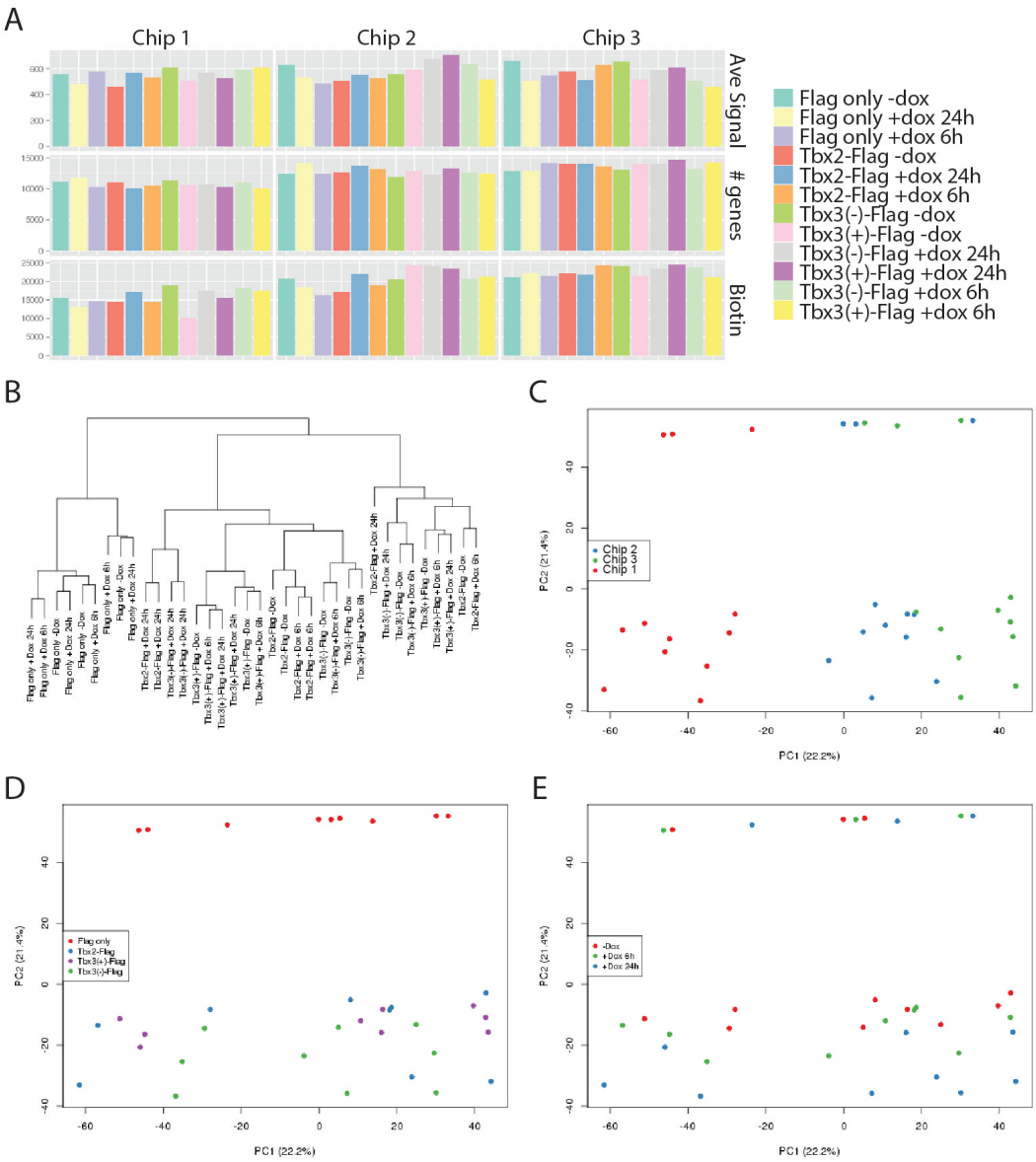

Figure 3.14: Global overview of microarray results for the different cell lines. (A) Overview of hybridisation statistics for all samples on the different chips. (B) Cluster analysis of all individual samples. (C-E) PCA of all individual samples coloured according to array chips (C), cell line (D), and time of dox induction (E).

for variance in the data set (PC1). Chip 1 is clearly different to chip 2 and 3, but also between chip 2 and 3 a difference can be noticed (Figure 3.14 C). This is an inherent, systemic issue that cannot be circumvented and could potentially explain the lack of further clustering within the samples derived from the T-box factor cell lines. Due to the strong contribution, this chip effect was accounted for in the subsequent statistical analysis for differentially expressed genes.

The second most prominent contributor to variance (PC2) are the cell lines (Figure 3.14 D) and to a lesser extent treatment with dox (Figure 3.14 E). The 3×FLAG negative control cell line is very distant from the other cell lines, as already seen in the cluster analysis. This presumably reflects the earlier described leakiness of the tet-on system, expressing the epitope tagged T-box factors at low levels even without dox administration (Section 3.2.3). Again, this is a technical limitation of the applied system, considered during analysis. In addition, a segregating effect of dox treatment can be detected within the samples derived from the T-box factor expressing cell lines (Figure 3.14 E, lower half). RNA samples extracted after 24 h dox treatment differ significantly from the untreated samples, indicating an effect of the induction of T-box factors on the overall expression profiles of the melanoma cell line, as the 3×FLAG negative control samples remain the same on the PC2 axis. Only a minor difference is detected for the samples extracted after 6 h dox treatment, suggesting a longer time frame necessary for the induced T-box factors to exert their function.

Table 3.2: Number of differentially expressed genes

cell line	vs. uninduced		vs. Flag
	limma	VSN	
3×FLAG only	0	0	n/a
TBX2-FLAG	4511	4124	6947
TBX3(+)-FLAG	227	158	4942
TBX3(-)-FLAG	3219	2853	6928

3.4.2 Differentially expressed genes

To identify potential targets regulated by TBX2-FLAG and TBX3-FLAG, differentially expressed genes upon overexpression of the two T-box factors were detected. This was achieved by comparing the normalised probe intensities of the dox treated samples with the untreated samples of the same cell line and the samples of the equally treated 3×FLAG negative control cell line after fitting a linear model to the data set.

For normalisation and background correction before calculating differentially expressed genes compared to the uninduced samples, two different statistical approaches were used, variance stabilisation normalisation (VSN) and the in-built normalisation of the limma package (Section 2.7.1). Both algorithms resulted in a similar number of identified differentially expressed genes, 4511 and 4124 genes, respectively, for TBX2-FLAG overexpression, 227 and 158 for T-box(+)-FLAG, and 3219 and 2853, respectively, for TBX3(-)-FLAG overexpression. The comparison with the samples derived from the 3×FLAG negative cell line resulted in many more differentially expressed genes, 6947 for TBX2-FLAG, 4942 for TBX3(+)-FLAG, and 6928 for TBX3(-)-FLAG overexpression (Table 3.2). Given the signi-

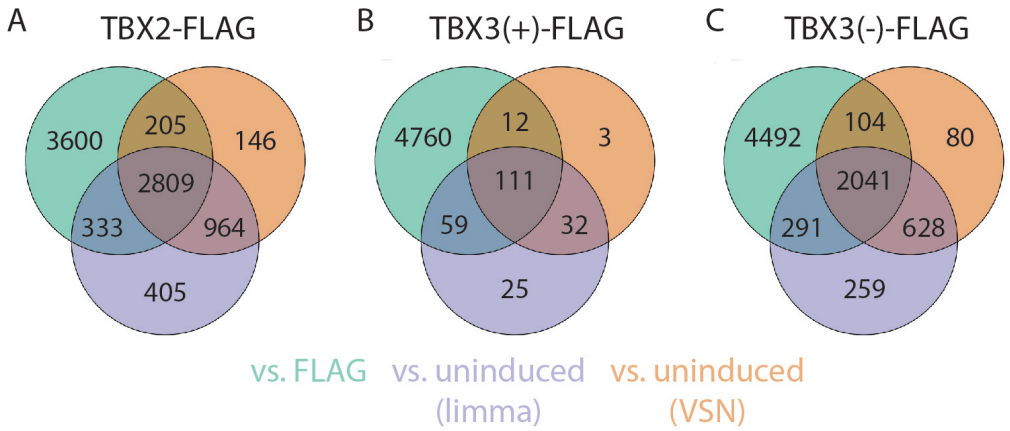

Figure 3.15: Number of differentially expressed genes. Venn diagrams of differentially expressed genes determined with the three different contrasts when overexpressing TBX2-FLAG (A), TBX3(+)-FLAG (B), and TBX3(-)-FLAG (C).

ficant difference between the samples of the 3×FLAG and the T-box expressing cell lines as determined in the PCA, this higher number of genes identified is not surprising. One factor contributing to this difference might be the leakiness of the tet-on system, as the stable cell lines expressing the 3×FLAG-tagged T-box factors upon induction might have slightly adapted to elevated expression levels of the T-box factors during preparation of the samples. As a consequence, the difference in protein levels upon induction is not as big as compared to the 3×FLAG negative cell line, still expressing physiological levels of the T-box factors.

As the induction of T-box factor expression for 6 h did not result in many differentially expressed genes (Figure 3.16 A), the analyses presented here concentrate on the samples induced for 24 h, showing more promising results.

Only genes detected as differentially expressed in all three data sets, VSN and limma normalised compared to the uninduced samples, and compared to the induced 3×FLAG sample, were considered for the downstream assessment as high-

confidence targets. This criteria was met by 2809 genes for TBX2-FLAG, 111 for TBX3(+)-FLAG, and 2041 for TBX3(-)-FLAG (Figure 3.15 A-C). With this selection criterion potential bona fide target genes are excluded, detected in the comparison with the 3×FLAG negative control sample, but not recognised via the contrast with the uninduced cell line due to the leakiness in the system. However, the stringent criterion still resulted in plenty of differentially expressed genes potentially regulated by T-box factors, to justify this approach. At a later stage, a more lenient criterion can be applied to determine further potentially regulated genes, excluded this time.

When plotting all differentially expressed genes with an adjusted p-value < 0.05 and their respective expression difference in a heat map, the earlier observed little effect of 6 h dox induction is corroborated, with only a few genes exhibiting a differential expression profile. Furthermore, within the samples derived from the TBX3(+)-FLAG cell line, a significantly lower number of differentially expressed genes of high-confidence was identified for both, 6 h and 24 h induction (Table 3.2 and Figure 3.16 A). Already in the genome-wide DNA binding analysis, the samples generated with this cell line produced fewer binding site peaks (Section 3.3), suggesting a general concern with the monoclonal cell line. Consequently, further analyses are focused on the data generated with the monoclonal cell lines expressing TBX2-FLAG and TBX3(-)-FLAG.

The heat map of all differentially expressed genes also indicates a predominantly repressive function for both T-box factors, with only a few genes upregulated upon overexpression of TBX2-FLAG and TBX3(-)-FLAG (Figure 3.16 A). This finding is further substantiated using the function prediction analysis of the binding and expression target analysis (BETA) software package for the entire list of

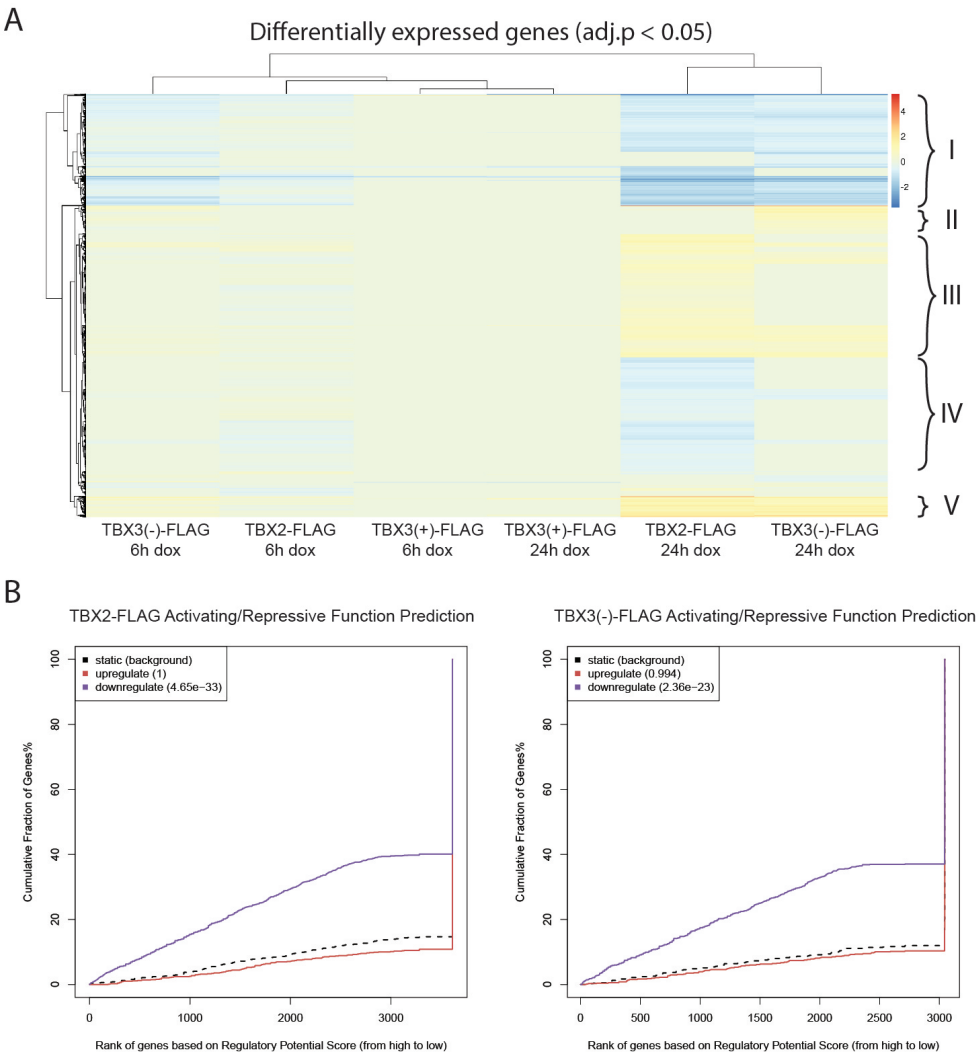

Figure 3.16: Global view of differentially expressed genes. (A) Heat map of all differentially expressed genes with five distinct sets of genes comparing TBX2-FLAG and TBX3(-)-FLAG expression profiles after 24 h induction: (I) genes downregulated with both, (II) genes upregulated with TBX3(-)-FLAG but not with TBX2-FLAG, (III) genes upregulated with TBX2-FLAG but not with TBX3(-)-FLAG, (IV) genes downregulated with TBX2-FLAG but no change in TBX3(-)-FLAG, (V) and genes upregulated with both. (B) Functional prediction for TBX2-FLAG and TBX3(-)-FLAG overexpression.

differentially expressed genes of the two T-box factors (Figure 3.16 B).

Comparing the differentially expressed genes of TBX2-FLAG and TBX3(-)-FLAG in the clustered heat map, one can observe a block of genes downregulated in both gene lists (I), a small set of genes being upregulated by TBX3(-)-FLAG with no change upon TBX2-FLAG induction (II), a block of slightly upregulated genes upon TBX2-FLAG induction and no change with TBX3(-)-FLAG (III), then downregulated genes with TBX2-FLAG overexpression but not with TBX3(-)-FLAG (IV), and a small set of genes upregulated by both (V) (Figure 3.16 A).

KEGG and GO analysis of differentially expressed genes

To categorise the differentially expressed genes and predict potential biological roles, enriched Kyoto encyclopaedia of genes and genomes (KEGG) pathways and gene ontology (GO) terms were determined for the entire list of differentially expressed genes and subsequently for up- and downregulated genes separately for both, TBX2-FLAG and TBX3(-)-FLAG (Figure 3.17).

The most prominent pathways enriched in the KEGG analysis and hence potentially regulated by T-box factors are related to metabolism. A whole plethora of different metabolic pathways, for instance purine and pyrimidine, the building bases for nucleotides, several amino acids, the building blocks for proteins, pyruvate and fatty acid metabolism, providing energy to the cells, are enriched within the differentially expressed genes identified upon TBX2-FLAG and TBX3(-)-FLAG overexpression. Strikingly, analysis of the up- and downregulated genes separately reveals a correlation between upregulated genes upon TBX2-FLAG and TBX3(-)-FLAG overexpression and energy providing metabolic pathways, such as pyruvate and fatty acid metabolism. Furthermore, the KEGG pathway 'lysosome' is also

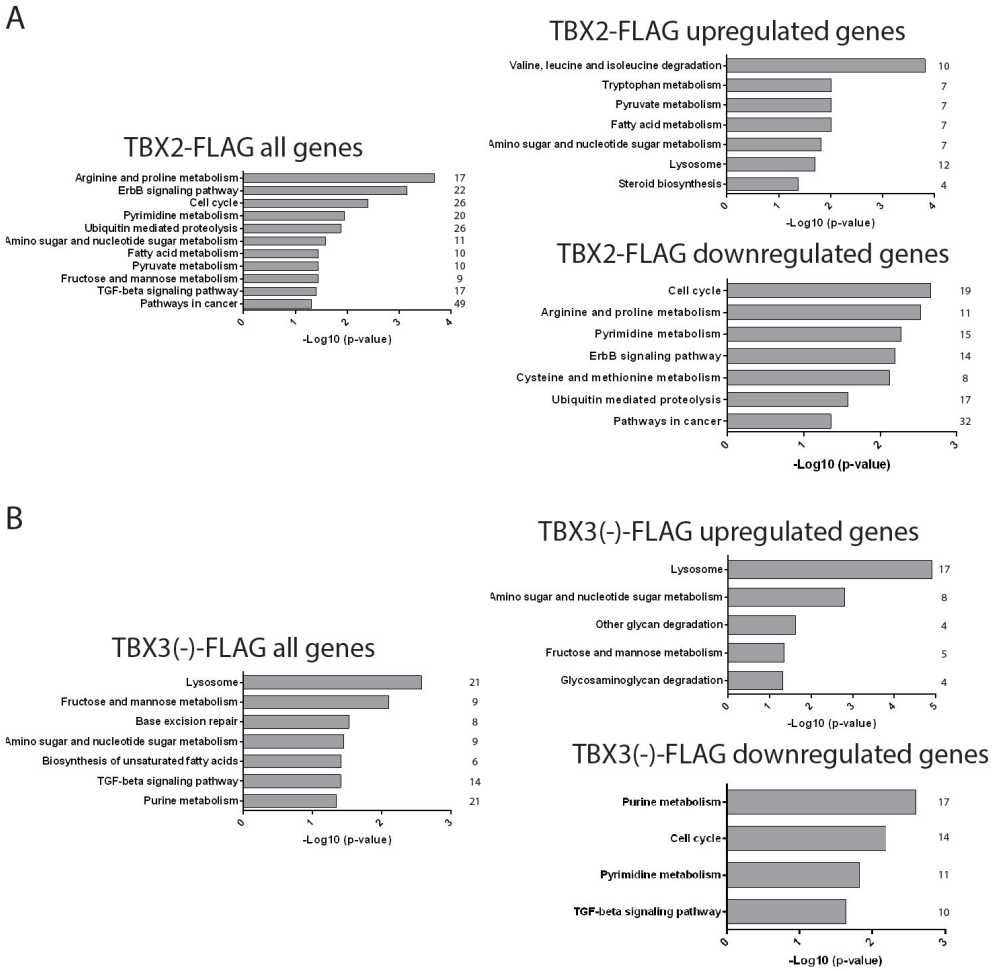

Figure 3.17: Enriched KEGG pathways in differentially expressed genes. Selected enriched KEGG pathways for all differentially expressed genes (left) and up- and downregulated genes separately (right) for TBX2-FLAG (A) and TBX3(-)-FLAG overexpression (B). The number next to each column indicates the count of genes assigned to the respective GO term.

enriched in the upregulated genes, enhancing degradation of waste products within the cell and further provide needed building blocks for proliferation. This finding supports the idea of a potential role for T-box factor in energy provision for fast dividing cancer cells.

Another enriched KEGG pathway found in this analysis is 'cell cycle', in line with the results of the ChIP-Seq analysis, where several significant peaks were found in the promoter region of cell cycle related genes (Figure 3.7 and Figure 3.9). For both 3×FLAG-tagged T-box factors it emerges as enriched in the downregulated genes, indicating a role in cell cycle repression. This is rather surprising, given the pro-proliferative, cell cycle dysregulated nature of a cancer cell. However, in terms of cancer homoeostasis, it might make sense under certain circumstance to control the cell cycle, in order to maintain a long-term proliferative potential and not end up in cellular catastrophe for example under conditions of nutrient limitation, which would impose a dominant inhibitory effect on the cell cycle even in cells bearing an activated pro-proliferative oncogene. T-box factors might hence be involved in supporting the long-term proliferation of melanoma cells by limiting the consumption of nutrients to a sustainable level via adaptive, negative cell cycle regulation. This would allow the cell to circumvent cellular catastrophe by nutrient depletion and accumulation of cellular damage due to unsustainable stresses and maintain cancer homoeostasis.

A further interesting pathway, identified in this analysis, is the TGF-β signalling pathway, described to regulate tumour progression by controlling G_1 arrest and thus enacting a tumour suppressor function during early phase of tumour progression (Ikushima and Miyazono, 2010; Meulmeester and ten Dijke, 2011). Downregulation by T-box factors would subsequently allow the cancer cell to retain a proliferative potential, progressing through the cell cycle. This result is at first sight contradictory to the above described negative cell cycle control, however, as this analysis is based on a population of cells, the described regulations do not necessarily happen in the same cell. The contradiction could thus be recon-

ciled with the already previously hypothesised modulating role of T-box factors, enhancing or repressing cell cycle progression in a context-dependent manner.

The differentially expressed genes upon TBX2-FLAG and TBX3(-)-FLAG overexpression have also been assessed for enriched GO terms. The enriched terms all reflected the already described enriched KEGG terms, further corroborating the findings, but no additional roles for T-box factors could be found.

Highly differentially expressed genes

For the identification of individual genes likely to be regulated by 3×FLAG-tagged T-box factors, highly differentially expressed target genes showing at least 4-fold up- or downregulation ($|logFC| > 2$) upon TBX2-FLAG or TBX3(-)-FLAG induction were selected. Plotting these genes together with the corresponding expression level upon overexpression of the other 3×FLAG-tagged T-box factor in a heat map showed a considerable congruency between the two factors (Figure 3.19 and Figure 3.18).

Among the upregulated genes, the most differentially expressed gene for both T-box factors is VGF nerve growth factor inducible (VGF). The gene has been linked to energy homoeostasis, metabolism, and cell-cell interaction and is primarily described in the context of neurobiology (Hahm et al., 1999). A more interesting candidate, also upregulated upon overexpression of both, TBX2-FLAG and TBX3(-)-FLAG, is transforming growth factor-β 2 (TGF-β2), an isoform of the transforming growth factor β (TGF-β). TGF-β has been demonstrated to be upregulated in cancer cells, supporting the here presented findings (Elliott and Blobe, 2005). Given its ascribed anti-proliferative activity by inducing a G_1 arrest (Kletsas et al., 1995; Mukherjee et al., 2010), an upregulation is initially

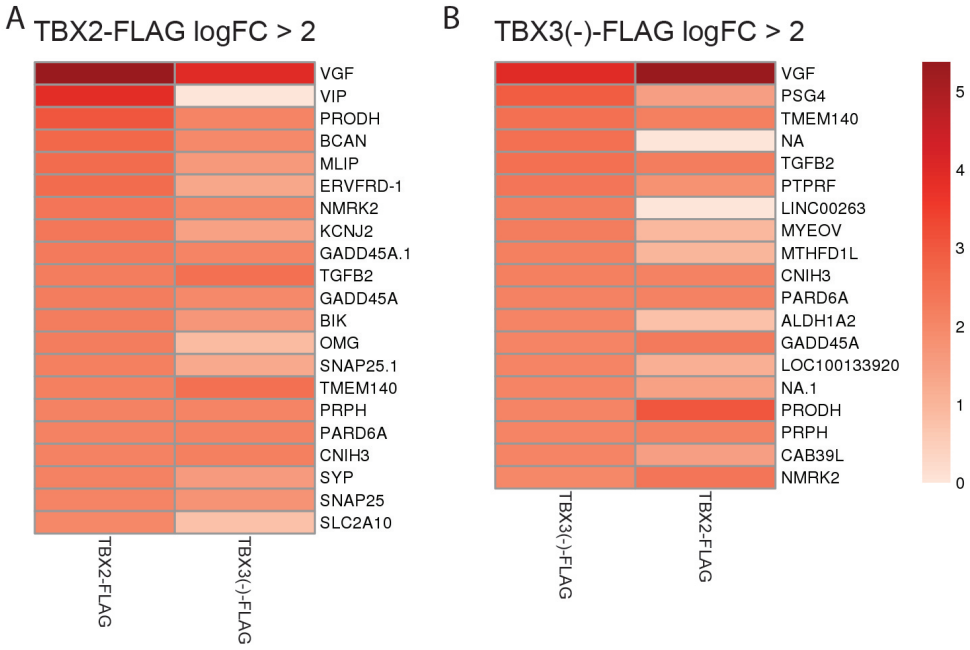

Figure 3.18: Highly upregulated genes upon TBX2-FLAG and TBX3(-)-FLAG induction. Heat maps of upregulated genes with at least 4-fold change upon TBX2-FLAG (A) and TBX3(-)-FLAG induction (B) with the expression level of the same gene upon induction of the respective other T-box factor.
NA, not assigned

counterintuitive, however, in established tumours the TGF-β signalling pathway is mostly mutated, thus blocking the anti-proliferative activity. The overexpressed TGF-β, subsequently, acts on the tumour environment via paracrine signalling and induces immunosuppression and angiogenesis (Blobe et al., 2000; Siegel and Massague, 2003). Interestingly, TBX3 is a downstream target and mediator of the TGF-β pathway, that also regulates TBX2 (Li et al., 2013, 2014). In addition, the data presented here suggests a further regulatory layer, by adding a positive feedback loop for TGF-β.

Another potentially regulated target of TBX2-FLAG and TBX3(-)-FLAG is

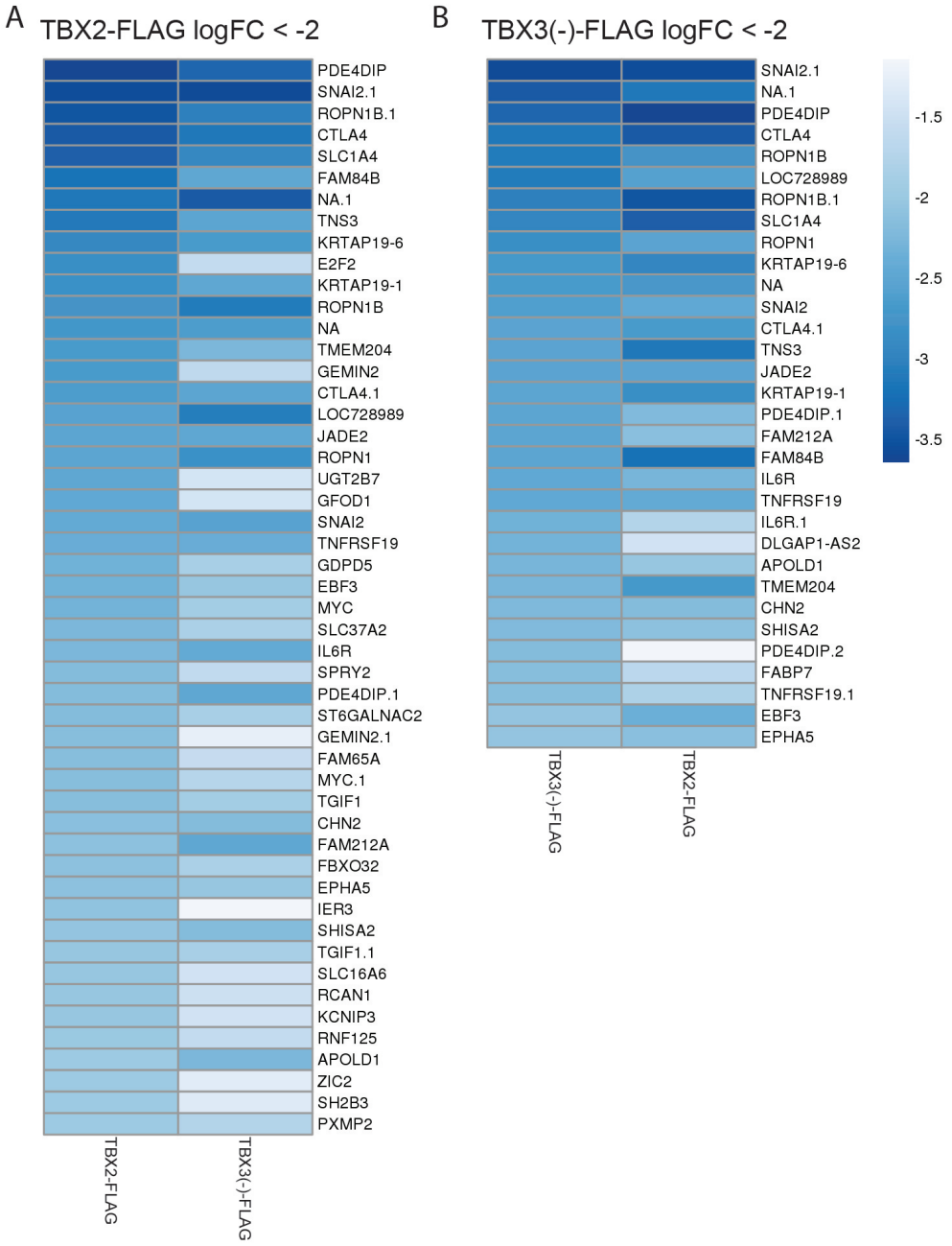

Figure 3.19: Highly downregulated genes upon TBX2-FLAG and TBX3(-)-FLAG induction. Heat maps of downregulated genes with at least 4-fold change upon TBX2-FLAG (A) and TBX3(-)-FLAG induction (B) with the expression level of the same gene upon induction of the respective other 3×FLAG-tagged T-box factor.
NA, not assigned

growth arrest and DNA-damage-inducible protein 45 α (GADD45A), also upregulated upon overexpression of the T-box factors. The GADD45 family of proteins act as stress sensors within the cell, mediating the cellular response to genotoxic stress and regulating cell cycle arrest and DNA repair (Liebermann and Hoffman, 2002). This could be a pro-survival mechanism for cancer cells to avoid excessive cellular stress and DNA damage, a constant risk due to their heavily dysregulated signalling cascades.

The assessment of potential target genes highly downregulated upon TBX2-FLAG and TBX3(-)-FLAG induction revealed three proteins emerging for both T-box factors, snail family zinc finger 2 (SNAI2), cytotoxic T-lymphocyte-associated protein 4 (CTLA4), and interleukin 6 receptor (IL6R). SNAI2 is a transcriptional repressor, that modulates basal transcription and is involved in EMT during embryonic development (Peinado et al., 2004, 2007). CTLA4 is a protein receptor, acting as an immune checkpoint on T-cells, exerting a immunosuppressive signal (Walunas et al., 1994, 1996). In contrast, IL6R is the receptor for interleukin 6 (IL-6), a pro-inflammatory cytokine, secreted by T-cells and macrophages (Heinrich et al., 2003). This contradicting immunoregulation of T-box factors, immunostimulating on the one hand side via repressing CTLA4, and immunosuppresive via repressing IL6R on the other hand, suggests an immunobalancing function of T-box factors within cancer. Inflammation has been shown to be able to accelerate tumour progression by inducing angiogenesis and stroma growth. An extensive immune response, however, can elicit immunoclearance of the tumour by the adaptive immune system (Coussens and Werb, 2002). Hence, an intricate balancing of the immune response is necessary for a tumour to optimise growth conditions, potentially regulated by T-box factors.

In addition, TBX2-FLAG, more pronounced than TBX3(-)-FLAG, seems to repress the TFs E2F2, MYC, and sprouty homolog 2 (Drosophila) (SPRY2). E2F2 is a member of the E2F protein family, a TF family whose activating member E2F1, E2F2, and E2F3a orchestrate the G_1/S cell cycle transition (Weinberg, 1995). Downregulation of members of the E2F family, consequently, stops cells from progressing in the cell cycle. The TF MYC has been ascribed mainly activating transcriptional activity and has a potential to regulate as much as 15% of the entire genome, indicating a function as widespread regulator of transcription (Patel et al., 2004). Lower levels of MYC will result in less transcriptional activity in the cell. This is in line with the previous hypothesis of TBX2 dampening transcriptional activity, based on its binding peaks showing enriched annotation terms related to transcriptional regulation (Section 3.3.2). A further highly downregulated gene upon T-box factor overexpression is SPRY2, a negative feedback regulator of receptor tyrosine kinases. The inhibitory activity antagonises growth factor mediated pathways, such as the FGF, the epidermal growth factor (EGF), and the hepatocyte growth factor (HGF) pathway (Lee et al., 2004). The repression of SPRY2, thus, enhances growth signalling in these pathways.

Summarising, the 3×FLAG-tagged T-box factors show a wide spectrum of potentially regulated cellular functions, ranging from immunomodulation via TGF-β, CTLA4, and IL6R, over stress response via Gadd45A, cell cycle regulation via the E2F family of TF, transcriptional activity via MYC, and finally growth regulatory pathways via SPRY2. The role of T-box factors might hence be balancing the impulse to proliferate uncontrolled with a very high demand on resources while maintaining the high proliferative potential. This could aptly be integrated into the earlier formulated hypothesis of cancer homoeostasis.

3.5 Integration of DNA binding with gene expression information

The availability of genome-wide data for TBX2-FLAG and TBX3(-)-FLAG for both, DNA binding and differential gene expression, enables an integrated analysis to associate DNA binding in the promoter region of genes with a physiological consequence in form of expression changes of the corresponding proteins. This analysis could give further indications for potential direct targets of T-box factor regulation. Both data sets have been produced with the same monoclonal cell lines under identical culture conditions and using the same antibodies for sample generation, allowing a direct correlation of the two.

For the analysis, the genomic region of previously identified differentially expressed genes 5 kb around the TSS was assessed for DNA binding by TBX2-FLAG and TBX3(-)-FLAG and the corresponding logFC was then interrelated with this DNA binding information using the binding and expression target analysis (BETA) programme. Out of the 2809 differentially expressed genes for TBX2-FLAG, 694 also exhibit at least one binding peak in the genomic region around the TSS, of which 105 genes are up- and 589 downregulated. For TBX3(-)-FLAG there are 454 out of 2041 differentially expressed genes with at least one peak, of which 85 are up-and 369 downregulated (Table 3.3).

The BETA analysis identified some genes already found in the previous individual analyses, supporting these findings. Among the downregulated genes with a 3×FLAG-tagged T-box binding peak in the promoter region are, for instance, *E2F2* and *E2F7*, two member of the E2F TF family implicated in cell cycle progression (Attwooll et al., 2004), indicating a direct regulation by T-box factors.

Also related to cell cycle is *CDKN2A*, determined as a potential direct target. Furthermore, proteins involved in the MAPK pathway, such as *MAPK6*, *MAP2K3*, and *MAP2K6*, processing cellular growth signals (Cargnello and Roux, 2011) are also presumably directly downregulated by T-box factors, as already suggested earlier. Further, proteins processing growth signals within the PI3K/AKT pathway are revealed by this analysis, either, such as *PIK3R1* and *FOXO3*. Also the role of T-box factors in transcriptional regulation is further supported, with *MYC* being identified as potential direct target.

Among the already described upregulated genes with a DNA binding peak of TBX2-FLAG and TBX3(-)-FLAG, *GADD45A*, involved in cellular stress response (Liebermann and Hoffman, 2002), and *VGF*, linked to energy homoeostasis and metabolism (Hahm et al., 1999), were determined. These results reflect the pathways already described above in the individual assessment of DNA binding and differential gene expression of 3×FLAG-tagged T-box factors, strengthening the discovery of their supposed regulation by TBX2-FLAG and TBX3(-)-FLAG.

In addition, new candidate genes emerged with this integrated analysis, previously rejected possibly due to a less significant peak in the DNA binding assessment or a lower logFC in the gene expression analysis. However, genes identified

Table 3.3: Number of potential direct targets of TBX2-FLAG and TBX3(-)-FLAG

cell line	**total # of potential targets**	**upregulated**	**downregulated**
TBX2-FLAG	694	105	589
TBX3(-)-FLAG	454	85	369

Table 3.4: Selected potential direct targets of TBX2-FLAG and TBX3(-)-FLAG regulation

TBX2-FLAG		**TBX3(-)**-FLAG	
upregulated	**downregulated**	**upregulated**	**downregulated**
VGF	CDKN2A	VGF	E2F2
GADD45A	E2F2	GADD45A	CDKN2A
EGR2	E2F7	EGR2	EEF2K
MAPK3	MC1R	CASP9	SIAH2
TRIM63	RUNX3	HES4	MYC
ACP5	SIAH2	DUSP10	IL6R
HES4	MAPK6	IL1RAP	CASP3
ARL4A	EEF2K	ZNF696	RUNX3
BIK	EZH2		MAP2K3
KDM1A	IL6R		PIK3R1
	MAP2K3		CDK2AP1
			MAP2K6

with this combined analysis have an increased significance compared to the individual approaches due to their recognition in two independent experiments, thus bypassing the set threshold.

One interesting newly discovered gene potentially directly repressed by both 3×FLAG-tagged T-box factors is enhancer of zeste homolog 2 (EZH2), the functional enzymatic component of the polycomb repressive complex 2 (PRC2) (Morey and Helin, 2010) As such, EZH2 participates in DNA methylation and, ultimately, transcriptional repression via heterochromatin formation. Through its activity, it can maintain among others epigenetic marks over generations of dividing cells (Hansen et al., 2008). This very interesting, possibly directly regulated candidate

can be added to the supposed regulatory function of T-box factors in transcriptional regulation.

Another newly identified, possible target gene repressed by T-box factors is the eukaryotic elongation factor-2 kinase (EEF2K), implicated in the regulation of protein synthesis via phosphorylation of eukaryotic elongation factor 2 (EEF2) (Ryazanov and Spirin, 1990). By repressing protein synthesis, a cancerous cell can potentially balance nutrient supply and demand to maintain the pro-proliferative signature. A similar function might be enacted by seven in absentia homolog 2 (SIAH2), an E3 ubiquitin ligase whose activity is implicated in regulating cellular response to hypoxia (Nakayama et al., 2009). This regulation poses another layer of cellular stress maintenance, potentially counteracting GADD45 activity, shown to be upregulated by 3×FLAG-tagged T-box factor in this study, and thus balancing cellular stress response.

A newly identified gene, upregulated upon 3×FLAG-tagged T-box factor overexpression, is early growth response protein 2 (EGR2), a member of the EGR family of zinc finger TF. EGR2 has been mainly described as a tumour suppressor, via induction of TGF-β and p53 (Krones-Herzig et al., 2005; Baron et al., 2005). Furthermore, it has been identified as a modulator of the immune response by transcriptional regulation of key cytokines and costimulatory molecules (Gómez-Martín et al., 2010). This upregulation of EGR2 would also fit into the hypothesis of cancer homoeostasis by titrating growth signals and modulating the immune response.

3.6 Validation of selected target genes identified in the genome-wide analyses

In order to validate some of the identified targets from the genome-wide study, independent whole cell protein extracts and RNA extractions were prepared with and without dox induction and analysed via WB and qPCR. The protein levels of EZH2 and EGR2, two targets determined to be repressed in the genome-wide analyses, decrease slightly upon induction of TBX2-FLAG and TBX3(-)-FLAG and more prominently upon induction of TBX3(+)-FLAG (Figure 3.20 A). Moreover, RNA levels also decrease for EZH2 and E2F2 as shown by qPCR (Figure 3.20 B). Unfortunately, no signal could be obtained in WB analysis with the antibody against E2F2 and the specifically designed primer for qPCR analysis for EGR2 did not work, either.

Summarising, the observed differences in protein levels are not large, which is in line with the results from the genome-wide analyses. Especially assuming an overall modulating role for T-box factors in different cellular functions, rather than a switch-like function, a moderate regulatory effect is perhaps advantageous. Nevertheless, validation of further candidates is desirable.

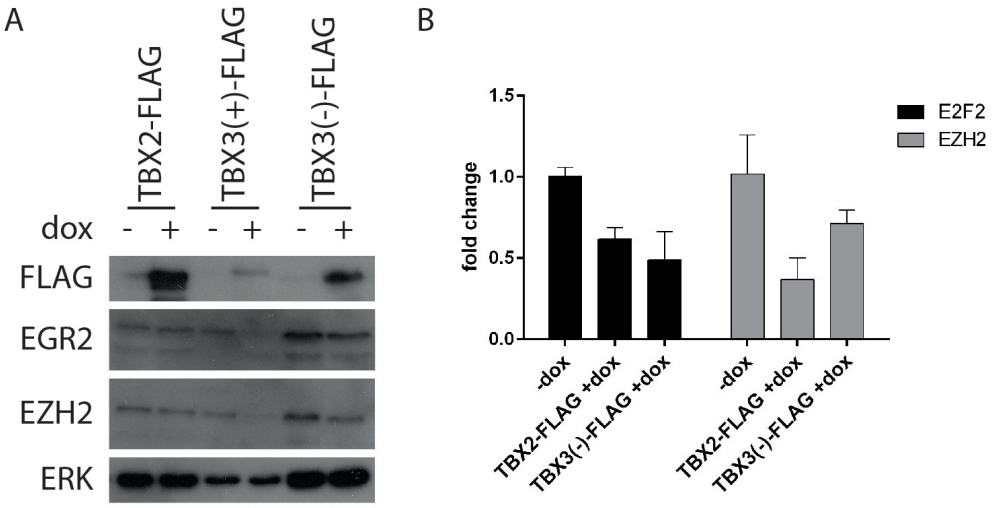

Figure 3.20: Validation of target genes identified in the genome-wide analyses. (A) Whole cell protein extracts of the four stable, monoclonal cell lines after 24 h treatment without or with dox were analysed with the indicated antibodies using WB. ERK was used as a loading control. (B) mRNA levels of the indicated genes without dox and upon induction of TBX2-FLAG and TBX3(-)-FLAG with dox were determined using qPCR. Data are represented as mean (n=3) with standard deviation (SD).

3.7 Discussion

In this chapter an agnostic, genome-wide view on potential targets regulated by the two T-box factors TBX2 and TBX3 was taken. Both, DNA binding analysis using ChIP-Seq and expression analysis upon overexpression of the TFs using microarrays, were integrated to obtain an extensive assessment of the role of the two T-box factors in melanoma.

The identified targets potentially regulated by the T-box factors TBX2 and TBX3 offered a broad spectrum of regulatory roles and could not be assigned to a single class of cellular function. The three main clusters of regulatory activity identified upon enrichment analysis were cell cycle regulation, growth regulation

and transcriptional regulation. For all three categories, TBX2 and TBX3 predominantly exert a repressive function, but activating influences could also be detected for a subset of potential targets, demonstrating a very versatile regulatory activity. To consolidate the different determined functions into one overarching role for the two T-box factors, the concept of cancer homoeostasis was proposed.

Cancer homoeostasis describes the balancing of nutrient supply and demand to keep the cell in a sustainable equilibrium for long-term proliferation. If demand, especially in cancer cells due to their elevated proliferation, would not be met by the supply, the cell would sooner or later run into cellular catastrophe due to depletion of nutrients. This equilibrium is at an elevated level in cancer cells compared to physiological cells, allowing enhanced proliferation. The binding of both T-box factors in the promoter region of E2F proteins, for instance, allows the cell to influence nutrient demand via cell cycle regulation, as a temporary repression of cell cycle progression via downregulation of E2F proteins would require less nutrients in the cell. In line, TBX2 and TBX3 have been determined to be involved in transcriptional regulation, another way to regulate nutrient demand, as transcription is one of the main consumers of nutrients in the cell. Hence, balancing the levels of transcription allows the cell to maintain the balance between supply and demand, avoiding depletion of nutrients due to exaggerated demand, not met by the supply. Furthermore, the identified upregulation of GADD45A, a cellular stress sensor (Liebermann and Hoffman, 2002), allows the cell to closely monitor stresses and adjust the nutrient equilibrium appropriately.

Taken together, this modulating role of nutrient demand might provide a potential explanation for the multiple different functions identified for TBX2 and TBX3 in the genome-wide approach, without one major effect. For the balancing

of an equilibrium it is probably more important to be able to adjust several different levers in moderate ways, rather than having a big, switch-like impact on one. Only if the equilibrium has severely lost balance, a big regulatory intervention would be necessary to revert the cell to its sustainable equilibrium, which would presumably show a bigger regulatory activity of the T-box factors. In this study, however, the cells were analysed under normal culture conditions without any induced stresses, resulting in only moderate changes of target gene expression.

This might also explain the weak changes observed in the WB and qPCR analysis when validating some of the previously identified target genes. The cells were again analysed under normal culture conditions, with plenty of nutrients provided in the cell culture medium. Consequently, there were sufficient nutrients available to the cell leaving the T-box factors little to regulate as the equilibrium was easily sustained. Furthermore, the hybridisation of isolated mRNA to a microarray chip is presumably more sensitive than a WB, resulting in the detection of differential expression of genes in the genome-wide microarray study, not immediately evident in the WB analysis.

Strikingly, the stable, monoclonal cell line expressing TBX3(+) upon dox induction showed the strongest differential expression of the potential target genes *EGR2* and *EZH2* in WB analysis, even though the data sets for ChIP-Seq and microarray analysis generated with this cell line produced the lowest number of DNA binding peaks and differentially expressed genes. The expression levels of the FLAG-tagged transgene was lower in this cell line as compared to the TBX2 and TBX3(-) cell lines. Hence, one possible explanation might be, that the observed leakage of the piggyBAC system affected the TBX3(+) cell line less than the other two due to the lower expression level. Subsequently, the stable TBX3(+) cell line

was less exposed to elevated T-box factor expression during the establishment of the cell lines, and thus less adjusted to the elevated protein levels upon induction.

Another possibility for the relatively moderate changes in the genome-wide assessment could be cell cycle regulation. TBX2 has been demonstrated to be tightly regulated throughout the cell cycle (Bilican and Goding, 2006), which might imply a strongly context-dependent function. Consequently, the genome-wide assessment of potentially regulated targets by TBX2 and TBX3 using an asynchronous, steadily growing cell population, might mask their specific roles, as the analysed cell population represents an average over all the cell cycle states of each individual cell. In a considerable proportion of the assessed cells, the ectopically expressed T-box factors might thus reside in an inappropriate cell context, i.e. cell cycle state, to conduct its actual function. This might explain the relatively low levels of change observed in the genome-wide assessment, manifested in moderate peak heights for the DNA binding of the two T-box factors in the ChIP-Seq analysis and modest fold changes of differentially expressed genes in the microarray analysis. It could hence proof useful for future work to use a homogeneous, synchronised cell population and analyse the role and function of T-box factors at specific, well-defined cell cycle states.

The exact reason for the moderate changes detected in this study might in the end be a blend of the above offered explanations and future work will have to address the mentioned possibilities to improve the signal. Nevertheless, this chapter provides valuable insights into the regulatory activities of TBX2 and TBX3 and potential interaction partner, reassuringly confirming some already described functions, and eliciting interesting, new candidates to follow up on in the future.

To integrate the regulatory function of the two T-box factors into the cellular

signalling context, not only their potential regulated targets are of interest, but also their regulation themselves. This question will be addressed in the next chapter.

Chapter 4

Regulation of Tbx2 and Tbx3

4.1 Introduction

In the previous chapter target genes potentially regulated by the T-box factors TBX2 and TBX3 were identified to obtain a better understanding of their role in tumourigenesis. Here, the regulation of TBX2 and TBX3 themselves will be analysed to integrate their suggested role into the cellular regulatory networks.

The functions for TBX2 and TBX3 in the context of cancer described so far give some indications for possible signalling pathways, they might be regulated by. Specifically, their reported ability to promote the bypass of senescence via suppression of $p14^{ARF}$ and p21 expression (Jacobs et al., 2000; Carlson et al., 2001; Prince et al., 2004; Vance et al., 2005; Peres et al., 2010) was of interest. In a recent publication, Vredeveld et al. demonstrated PTEN depletion and thus constitutive activation of the PI3K pathway to be sufficient to abrogate OIS in melanocytes (Vredeveld et al., 2012). However, how PI3K can mediate senescence bypass is not known.

PI3K signalling is an important cellular, growth regulating pathway, implicated in cell cycle regulation and protein synthesis via various effectors highlighted below (Vanhaesebroeck et al., 2012). Activation of PI3K plays a central role in tumour cell biology and has been linked to several types of cancer (Fruman and Rommel, 2014). PI3K is located at the cellular membrane, activated by receptor tyrosine kinases (RTK) on the cell surface upon GF binding. It catalyses the phosphorylation of phosphatidylinositol (4,5)-bisphosphate (PIP2) forming phosphatidylinositol (3,4,5)-trisphosphate (PIP3), which serves as docking phospholipid recruiting downstream effectors to the cellular membrane, such as the phosphoinositide-dependent kinase-1 (PDK1) and the protein kinase PKB/AKT (Vivanco and Saw-

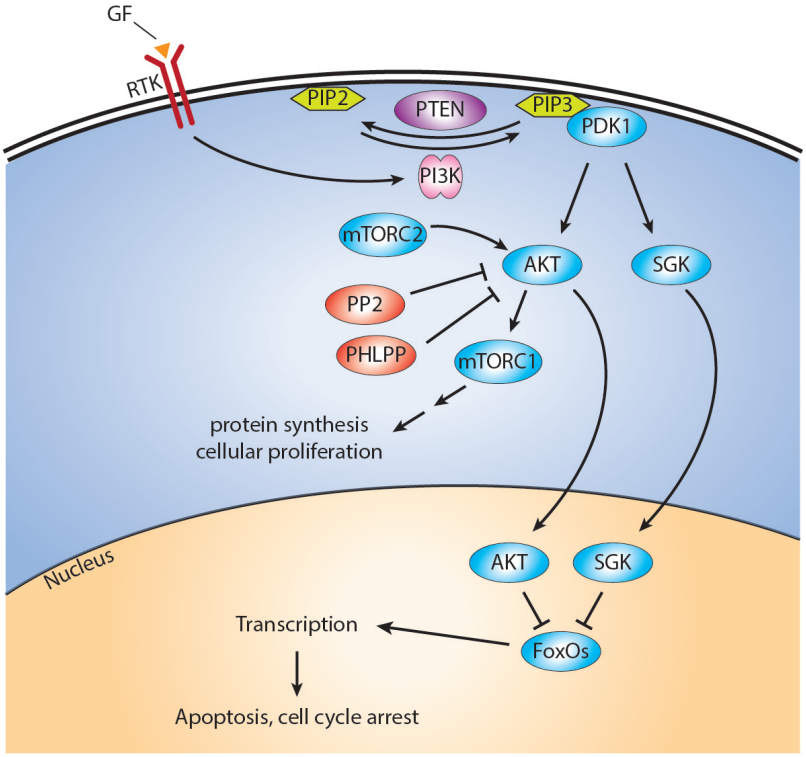

Figure 4.1: Overview of the PI3K pathway. Upon activation by RTK, PI3K phosphorylates PIP2 to PIP3, which in turn recruits PDK1 to the cellular membrane to activate PKB/AKT to exert the downstream processes, such as protein synthesis and cellular proliferation via mTORC1, or proliferation and cell cycle control via FoxO proteins. SGK is a second downstream effector of PI3K signalling, also activated by PDK1, promoting cell survival via FoxO proteins. The dephosphoryation of PIP3 to PIP2 is catalysed by PTEN, inhibiting as a consequence PI3K signalling.
AKT, Protein kinase B; FoxOs, Forkhead box proteins; GF, Growth factor; mTORC1, mTOR complex 1; mTORC2, mTOR complex 2; PDK1, Phosphoinositide-dependent kinase-1; PI3K, Phosphatidylinositol-3-kinase; PIP2, Phosphatidylinositol (4,5)-bisphosphate; PIP3, Phosphatidylinositol (3,4,5)-trisphosphate; PTEN, Phosphatase and tensin homolog; RTK, Receptor tyrosine kinases; SGK, Serum/glucocorticoid-regulated kinase

yers, 2002). Upon recruitment, PDK1 phosphorylates PKB/AKT leading to its partial activation, sufficient for regulating protein synthesis and cellular proliferation via mTORC1 (Hemmings and Restuccia, 2012). A second phosphorylation by mTORC2 fully activates PKB/AKT, subsequently exerting additional regulatory functions, such as growth, proliferation, or survival via several downstream effectors, i.a. mTOR and FoxO proteins (Hemmings and Restuccia, 2012). Another downstream effector of PI3K signalling are serum/glucocorticoid-regulated kinases (SGK), a kinase subfamily of the serine/threonine-protein kinases. SGK are also activated via PDK1 and promote cell survival in part by phosphorylating and inactivating FoxO3a (Brunet et al., 2001) (Figure 4.1).

The PI3K growth stimulating pathway is repressed by PTEN, a hydrolase catalysing the dephosphorylation of PIP3 to PIP2, thus suppressing the activation of PKB/AKT (Liu et al., 2009). Furthermore, AKT can be dephosphorylated by protein phosphatase 2 (PP2) (Ugi et al., 2004) and PH domain and leucine rich repeat protein phosphatases (PHLPP) (Gao et al., 2005) to inactivate the signalling cascade (Figure 4.1).

In melanoma, the PI3K pathway is often upregulated (Aziz et al., 2009), and is able to promote tumourigenesis and metastatic growth in combination with the RAS/RAF pathway (Dankort et al., 2009; Nogueira et al., 2010). The upregulation could be linked to activating mutations in the gene encoding PI3K (Curtin et al., 2006; Omholt et al., 2006; Shull et al., 2012), or loss-of-function mutations in *PTEN* (Tsao et al., 1998; Shull et al., 2012).

Considering the described role of T-box factors in bypassing senescence (Jacobs et al., 2000) and the bypass of OIS in melanocytes by activation of the PI3K pathway (Vredeveld et al., 2012), we hypothesised TBX2 and TBX3 could be

regulated by the PI3K pathway, executing the anti-senescence programme initiated by the hyperactivation of PI3K.

4.2 PI3K regulation of TBX2 and TBX3

Throughout this chapter two different melanoma cell lines, 501mel and SKmel28, available in the laboratory, were used to dissect the underlying signalling cascades of TBX2 and TBX3 regulation. Both are derived from malignant melanoma biopsies and harbour the common $BRAF^{V600E}$ mutation. Furthermore, 501mel cells are non-invasive, whereas SKmel28 have an invasive phenotype and form tumours in nude mice (Fogh et al., 1977), allowing to study the regulation of the two T-box factors in two different cellular contexts. Both cell lines are amenable to genetic manipulations and have been widely studied by our laboratory and others.

To test the potential regulation of the T-box factors TBX2 and TBX3 by the PI3K pathway as suggested above, the melanoma cell lines 501mel and SKmel28 were treated for 24 h with two different PI3K inhibitors, LY294002 (20 µM) and GDC0941 (10 µM) (Vlahos et al., 1994; Folkes et al., 2008), and a PKB/AKT inhibitor downstream of PI3K, triciribine (20 µM) (Yang et al., 2004). WB analysis of the whole cell protein extracts, using ERK as a loading control, revealed a downregulation of TBX2 and TBX3 in 501mel cells upon treatment with the PI3K inhibitors. TBX2 expression was also downregulated in SKmel28 cells, though in these cells TBX3 expression was at low levels. The inhibition with triciribine did not affect TBX2 or TBX3 protein levels (Figure 4.2 A).

To check for successful inhibition of the pathway upon inhibitor treatment, activation of ribosomal S6 kinase (S6K), an effector of the PI3K pathway downstream

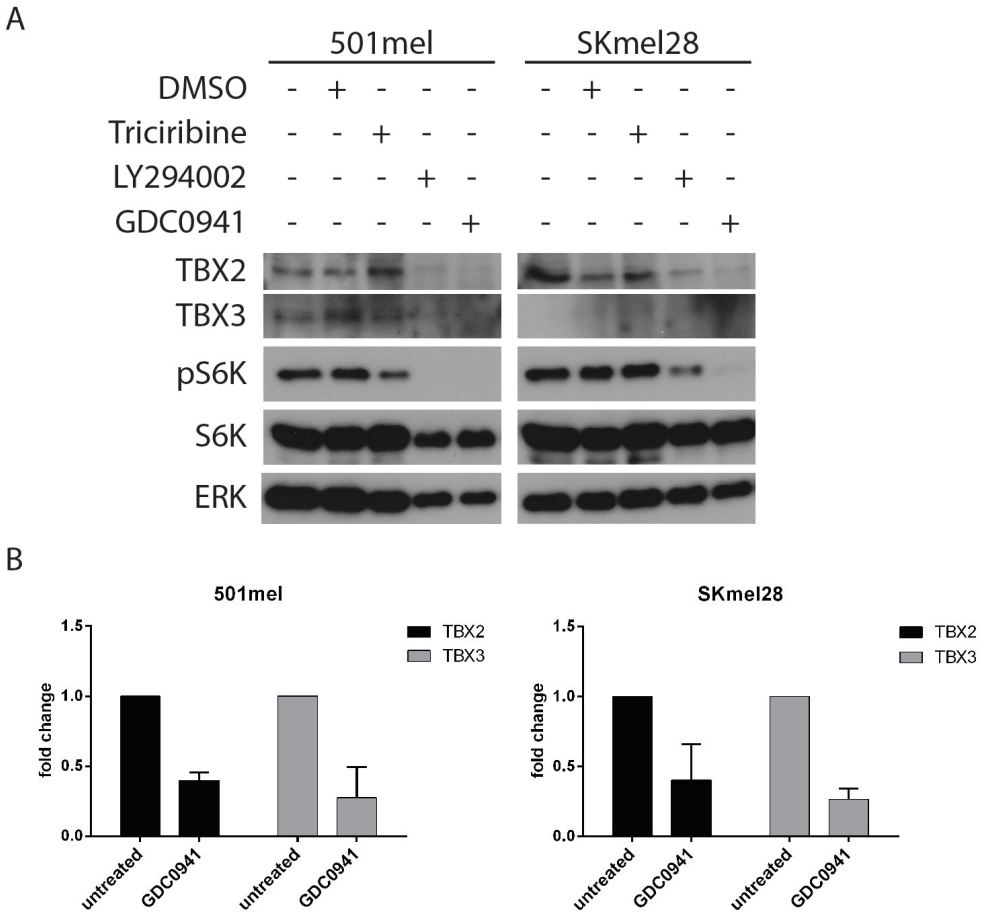

Figure 4.2: T-box factors are regulated by the PI3K pathway in melanoma cell lines. (A) WB of whole cell protein extracts of 501mel and SKmel28 cells individually treated with the PI3K inhibitors LY294002 (20 µM) and GDC0941 (10 µM), and triciribine (20 µM), a PKB/AKT inhibitor, for 24 h. The phosphorylation status of S6K is used as indicator for successful inhibition of the PI3K pathway and ERK was used as loading control. (B) qPCR analysis of RNA levels for TBX2 and TBX3 upon treatment with 10 µM GDC0941 in 501mel and SKmel28 cells. Data are represented as mean (n=3) with standard deviation (SD).

of PI3K and PKB/AKT (Hemmings and Restuccia, 2012), by phosphorylation was analysed. In 501mel, administration of LY294002 and GDC0941 inhibited the PI3K pathway as S6K is dephosphorylated upon treatment, in SKmel28 GDC0941

treatment also leads to a total abolition of signalling via S6K, whereas LY294002 treatment only reduced the levels of phosphorylated S6K. Activation of S6K seems not to be affected by the PKB/AKT inhibitor triciribine, most likely indicating an inactivity of the inhibitor, presumably explaining the observed unchanged TBX2 and TBX3 protein levels upon treatment with this inhibitor (Figure 4.2 A).

The PI3K inhibitor GDC0941 clearly inhibits the PI3K pathway in both melanoma cell lines tested, whereas LY294002 seems to only partially inhibit PI3K in SKmel28. Furthermore, GDC0941 is very specific and its class I PI3K specificity is much higher than with LY294002 (Kong et al., 2010). LY294002, in contrast, has been shown to not only inhibit PI3K, but also other unrelated targets, such as BET bromodomains and adenosine receptor activation (Gharbi et al., 2007; Dittmann et al., 2014; Searl and Silinsky, 2005). Consequently, to be able to specifically dissect the T-box factor regulation by PI3K and avoid unspecific side-effects, GDC0941 was used for further experiments.

Next, to corroborate the regulation of T-box factors by the PI3K pathway, RNA levels for both genes were assessed upon PI3K inhibition. 501mel and SKmel28 cells were treated with 10 µM GDC0941 for 24 h and whole cell RNA was extracted for qPCR analysis. The results show a clear reduction of RNA levels for both factors upon PI3K inhibition in both melanoma cell lines, further substantiating the previous results of a potential regulation of TBX2 and TBX3 by the PI3K pathway (Figure 4.2 B).

To better understand the kinetic of TBX2 and TBX3 regulation upon GDC0941 treatment, a time course experiment was performed, treating 501mel cells with 10 µM GDC0941 for 4 h, 8 h, 12 h, and 24 h, respectively. Blotting of the whole cell protein extracts showed a decrease in protein levels after 12 h, with a further

reduction after 24 h. Interestingly, consistent with the downregulation of the two T-box factors, PI3K inhibition upregulates the known T-box factor target p21, demonstrated to be suppressed by TBX2 and TBX3 (Prince et al., 2004; Vance et al., 2005) (Figure 4.3 A).

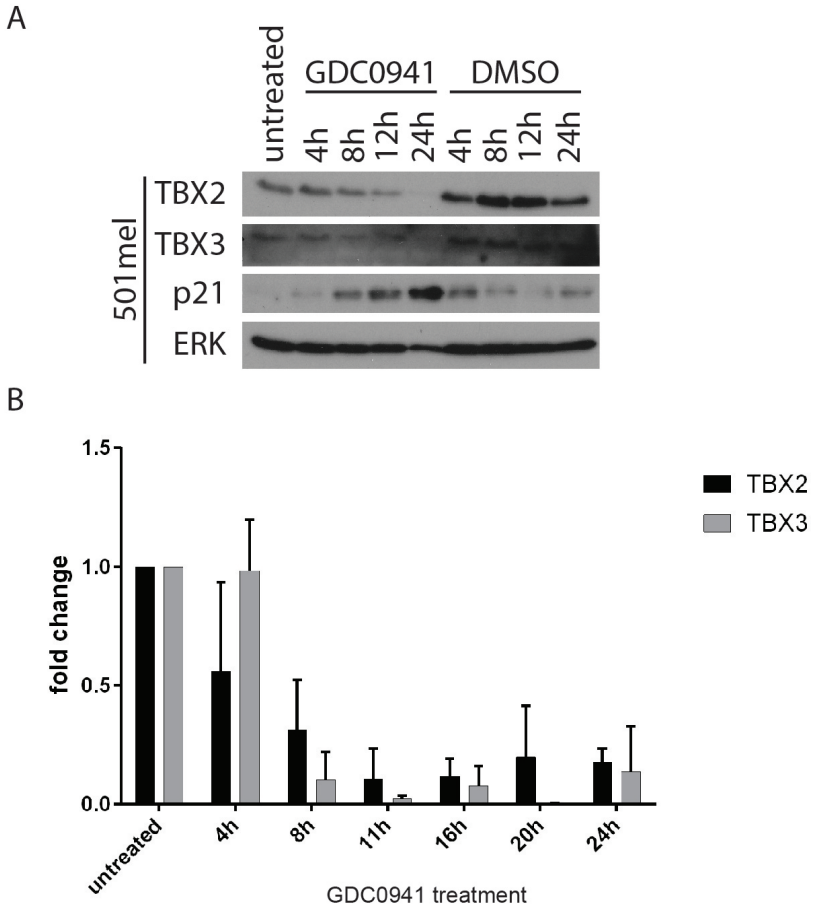

Figure 4.3: Protein and RNA level of TBX2 and TBX3 decrease in a time dependent manner upon PI3K inhibition. (A) WB analysis for TBX2 and TBX3 protein levels with whole cell protein extracts of 501mel cells treated with 10 µM GDC0941 in a time course (4 h, 8 h, 12 h, 24 h). ERK was used as loading control. (B) qPCR analysis of whole cell RNA extracts for RNA levels of *TBX2* and *TBX3* upon PI3K inhibition with 10 µM GDC0941 in a time course (4 h, 8 h, 11 h, 16 h, 20 h, 24 h). Data are represented as mean (n=3) with standard deviation (SD).

To understand, whether the observed regulation occurs on transcriptional or translational level, RNA levels of TBX2 and TBX3 were determined over time upon PI3K inhibition. 501mel cells were treated for 4 h, 8 h, 11 h, 16 h, 20 h, and 24 h with 10 µM GDC0941 and whole cell RNA was extracted for qPCR analysis. RNA levels for both, TBX2 and TBX3, decrease in a time dependent manner upon GDC0941 treatment. The RNA levels of TBX2 already decline after 4 h of treatment, while RNA levels of TBX3 start decreasing after 8 h of treatment, with both reaching a plateau after 11 h (Figure 4.3 B). Comparing the decline of the RNA levels of both T-box factors with the protein levels, one can note a decline of RNA levels already after 4-8 h of treatment, whereas reduction of protein levels are observed from 8-12 h onwards. The results strongly suggest a positive regulation of *TBX2* and *TBX3* mRNA expression by PI3K signalling.

The PI3K inhibitor GDC0941 used in this work has a reported IC_{50} of 3 nM for the PI3K subunit p110α (Folkes et al., 2008), thus, the used concentration of 10 µM in the here presented experiments seems high potential eliciting unspecific inhibitory activity towards other kinases. However, the determination of IC_{50} is based on *in vitro* biochemical assays using purified kinase in an artificial reaction environment. When using the inhibitor in a cellular environment, the conditions change and a higher concentration is necessary for a cellular effect. In line, Folkes et al. report in the original publication, describing the inhibitor, a cell line dependent proliferation IC_{50} of up to 1 µM (Folkes et al., 2008), shining a different light on the here used concentration. Nevertheless, to further substantiate the here presented findings, future experiments should include lower inhibitor concentrations and knock-down experiments of PI3K to exclude potential off-target effects.

Summarising, the data presented so far implicates a regulation of the two T-box

factors TBX2 and TBX3 by the PI3K signalling pathway. To further understand the signalling cascade through which PI3K exerts this regulation, mediators upstream of the T-box factors and downstream of PI3K are to be identified.

4.3 PAX3, a potential mediator of PI3K signalling

Paired box 3 (PAX3) is a key regulator of the melanocyte lineage, widely expressed in melanomas (Plummer et al., 2008). It is a member of the highly conserved family of paired box TF, contributing to the regulation of such important cellular functions as proliferation, migration, and resistance to apoptosis (Kubic et al., 2008; Medic et al., 2011). Interestingly, PAX3 can repress PTEN in rhabdomyosarcoma cells to promote cell survival, linking it to the PI3K signalling pathway (Kubic et al., 2008). Given its important regulatory role within the melanocyte lineage and wide expression in melanoma, we asked whether PAX3 could regulate the T-box factors TBX2 and TBX3.

4.3.1 PAX3 regulates TBX2 and TBX3

To investigate the potential regulatory link between PAX3 and the T-box factors TBX2 and TBX3, PAX3 was knocked down in 501mel and SKmel28 melanoma cell lines using a lentiviral expression system for a short hairpin RNA (shRNA) against PAX3, co-expressing green fluorescent protein (GFP). The cells were infected with serial dilutions of the lentivirus preparation allowing for a titre-dependent knock-down of PAX3. Whole cell extracts were prepared 48 h post infection and

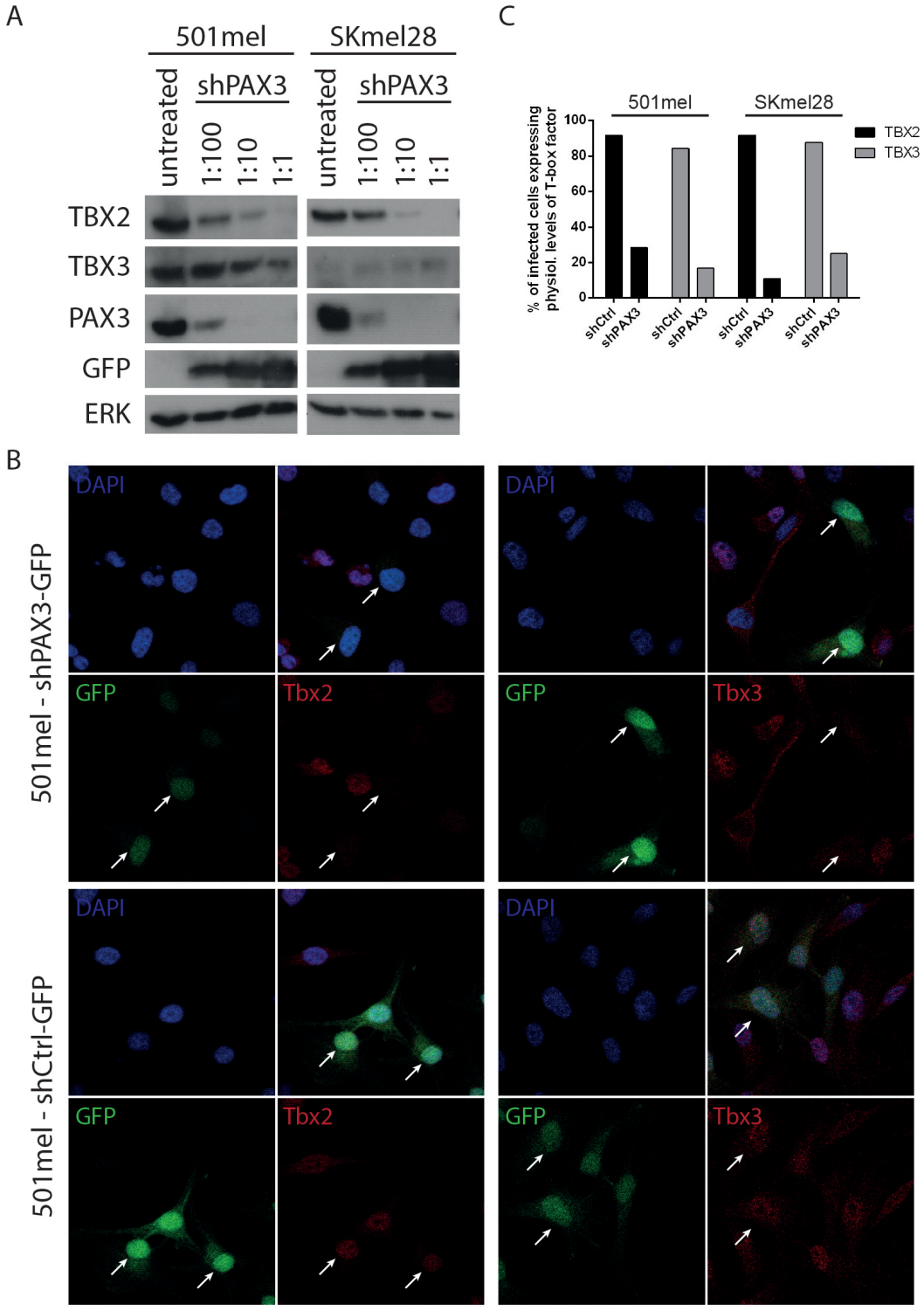

Figure 4.4: T-box factors are regulated by PAX3. *Legend continues at the bottom of the next page.*

protein levels analysed using WB. The assessment showed a titre dependent increasing expression of GFP, indicating a successful infection of the cells with the lentivirus, and a concurrent downregulation of PAX3, demonstrating a successful knock-down. Furthermore, TBX2 protein levels were strongly reduced upon increasing PAX3 downregulation in both cell lines, indicating a regulation of TBX2 by PAX3 (Figure 4.4 A). TBX3 protein levels, however, reduce to a much lesser extent only with a strong PAX3 knock-down at high titres in 501mel. In SKmel28 cells the physiological protein levels of TBX3 are much lower than in 501mel cells and seem to remain unchanged upon knock-down of PAX3 even at high titres, if not slightly increased (Figure 4.4 A).

Figure 4.4: T-box factors are regulated by PAX3. (A) Whole cell protein extracts of 501mel and SKmel28 were analysed using WB for the indicated proteins 48 h post infection with different dilutions of a shPAX3 lentivirus co-expressing GFP. ERK was used as loading control. (B) 501mel cells were infected with indicated shRNA expressing lentiviruses for 48 h before analysis by ICC for indicated proteins. Arrows indicate exemplary lentivirus infected cells. (C) 501mel and SKmel28 cells were infected with a low titre of lentivirus expressing shPAX3 or non-targeting shCtrl and GFP (10 – 20% of total cells were infected). GFP-expressing cells still expressing the indicated T-box factor at comparable physiological levels to uninfected, neighbouring cells were counted. For each condition, three independent fields of view were analysed and the percentage of the total GFP-expressing cells are presented.

To further substantiate the finding of a potential TBX2 and TBX3 regulation by PAX3, 501mel and SKmel28 cells were infected with a lentivirus expressing shPAX3 and GFP, thus marking every infected, PAX3-deficient cell green. An appropriate virus titre was chosen to only infect 10 – 20% of the total number of cells providing internal controls of uninfected cells, still expressing physiological levels of PAX3, in each field of view. Subsequently, 48 h post infection cells

were stained for TBX2 and TBX3 protein levels using ICC with T-box factor specific antibodies and GFP-positive cells were analysed for the respective protein levels. Both T-box factors appear to be specifically downregulated in cells infected with the lentivirus, indicating a PAX3-dependent regulation. Cells infected with a lentivirus expressing a non-targeting control shRNA (shCtrl) and GFP show unchanged protein levels of T-box factors, demonstrating a specific effect of the PAX3 knock-down (Figure 4.4 B). This regulation is also observed in the melanoma cell line SKmel28 (ICC images not shown). Potentially, this downregulation of the T-box factors is linked to the cell cycle, a possibility further assessed in future experiments.

To quantify the observed effect, GFP-expressing cells still expressing TBX2 or TBX3 at comparable physiological levels to uninfected, neighbouring cells were counted in three independent fields of view. In 501mel cells infected with the shPAX3 expressing lentivirus, 29% of GFP-positive cells expressed TBX2 at comparable physiological levels to uninfected, neighbouring cells, while this was the case for 92% of cells infected with the lentivirus expressing a non-targeting shCtrl. 17% of GFP-positive 501mel cells still expressed TBX3 at comparable physiological levels after infection with the shPAX3 lentivirus, and 84% of the cells infected with the shCtrl lentivirus. SKmel28 cells showed similar ratios, 11% with shPAX3 and 92% with shCtrl for TBX2, and 25% with shPAX3 and 88% with shCtrl for TBX3 (Figure 4.4 C). These results corroborate the PAX3-specific regulation of both T-box factors.

4.3.2 PAX3 is regulated by the PI3K pathway

So far, TBX2 and TBX3 protein levels have been shown to be reduced upon PI3K signalling inhibition and PAX3 has been identified as a possible activating regulator of the two T-box factors. Hence, it was tested next, whether PAX3 itself is regulated by the PI3K pathway, serving as a potential mediator for PI3K signalling to the T-box factors TBX2 and TBX3.

To test the PI3K regulation of PAX3, 501mel cells were treated for 24 h with the two different PI3K inhibitors, LY294002 (20 µM) and GDC0941 (10 µM), and the PKB/AKT inhibitor triciribine (20 µM), and the whole cell protein extracts were analysed for PAX3 protein levels using WB. Indeed, PAX3 protein levels are reduced upon PI3K inhibition with both inhibitors. The diminished levels of S6 phosphorylation indicated a successful inhibition of PI3K (Figure 4.5 A). No changes of PAX3 protein levels were observed with the PKB/AKT inhibitor triciribine, which most likely is inactive as discussed above. To substantiate the potential regulation, RNA levels of PAX3 were assessed upon PI3K inhibition. 501mel cells were treated with GDC0941 for 24 h and whole cell RNA extracted for qPCR analysis. Reduced RNA levels of PAX3 could be determined in these samples, supporting the suggested regulation of PAX3 by the PI3K pathway (Figure 4.5 B).

Subsequently, a time course of treatment with 10 µM GDC0941 for 4 h, 8 h, 12 h, and 24 h was performed to determine the repressive kinetic of PI3K inhibition of PAX3 expression. WB analysis of the whole cell extracts showed decreasing PAX3 protein levels after 8 h of treatment (Figure 4.5 C), earlier than the reduction of T-box factors upon PI3K inhibition (Figure 4.3 A). This observation corrob-

orates the potential regulatory link between PAX3 and the T-box factors TBX2 and TBX3, with PAX3 potentially activating TBX2 and TBX3 to mediate the proliferative signal of the activated PI3K pathway (Section 4.3.1).

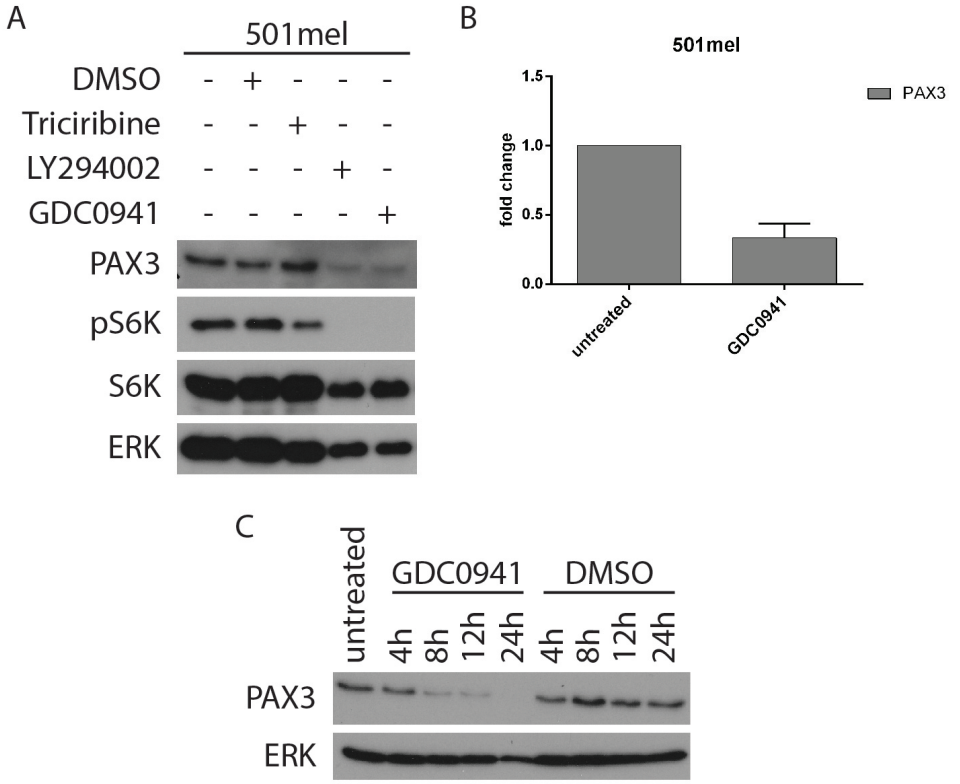

Figure 4.5: PAX3 is regulated by the PI3K pathway. (A) Whole cell protein extracts of 501mel cells individually treated with LY294002 (20 µM), GDC0941 (10 µM), and triciribine (20 µM) for 24 h were analysed by WB for PAX3 protein levels. ERK was used as loading control. The experiment was performed at the same time as Figure 4.2, hence the same loading control and S6K inhibitor controls are shown. (B) qPCR analysis for RNA levels of *PAX3* of whole cell RNA extracts from 501mel cells upon treatment with 10 µM GDC0941 for 24 h. Data are represented as mean (n=3) with standard deviation (SD). (C) WB analysis for PAX3 protein levels with whole cell protein extracts of 501mel cells treated with 10 µM GDC0941 in a time course (4 h, 8 h, 12 h, 24 h). ERK was used as loading control. The experiment was performed at the same time as Figure 4.3, hence the same loading control is shown.

Additional data in the laboratory shows a potential direct regulation of TBX2 and TBX3 by PAX3. *TBX2* and *TBX3* gene expression was shown to be activated by PAX3 in a luciferase reporter assay. Furthermore, in an electrophoretic mobility shift assay (EMSA), potential PAX3 binding sites in the *TBX3* promoter were identified, further supported by the demonstration of PAX3 binding in the *TBX3* promoter by ChIP (H. Shaw, Goding Lab, Ludwig Institute for Cancer Research, unpublished).

4.3.3 Knock-down of PAX3 induces a senescent phenotype in melanoma cell lines

The hitherto presented data suggests a regulatory link between PI3K via PAX3 to TBX2 and TBX3. Next, the functional consequences of this regulatory cascade and the potential link to the anti-senescence phenotype upon hyperactivation of PI3K as described by Vredeveld et al. were investigated.

To determine the implications of the regulatory cascade, PAX3 was silenced, thus interrupting the signalling cascade, and the cells were analysed for proliferation over time. 10^5 501mel and SKmel28 cells were seeded in duplicate and infected the next day with a lentivirus expressing a shRNA targeting PAX3 or a negative, non-targeting control sequence. Subsequently, cells were counted every day for seven days with an automated cell counter. Plotting of the respective growth curves normalised to the initial cell count at d1 showed reduced cell growth upon PAX3 knock-down for both cell lines, 501mel and SKmel28, indicating a growth stimulating role for PAX3 (Figure 4.6 A).

Furthermore, upon analysis of the PAX3 deficient cells under the microscope, a

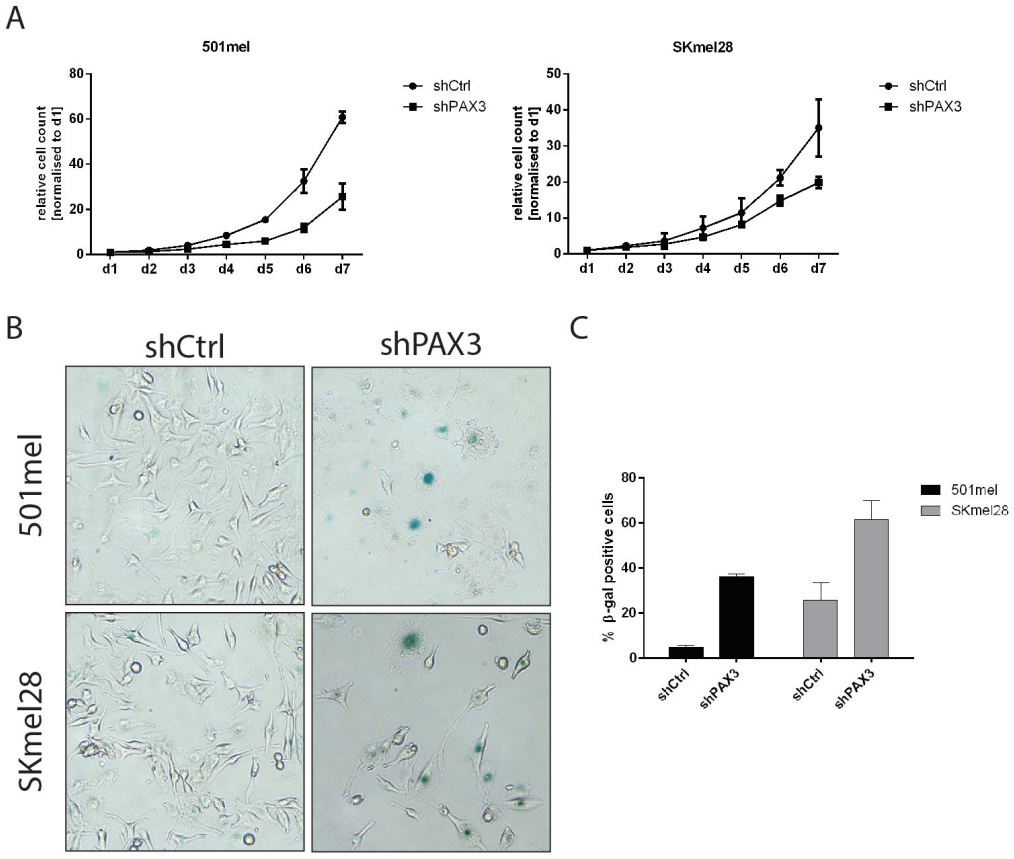

Figure 4.6: Knock-down of PAX3 impairs cell growth and induces a senescence phenotype. (A) 10^5 cells of 501mel and SKmel28 were infected with a lentivirus expressing shPAX3 or shCtrl and number of cells were counted every day. Data are represented as mean (n=2) with standard deviation (SD) normalised to the cell count at day 1. (B) 501mel and SKmel28 cells were infected with a lentivirus expressing shPAX3 or shCtrl and stained for β-galactosidase activity 72 h post infection. (C) β-gal positive 501mel and SKmel28 cells were counted 72 h after infection with a lentivirus expressing the indicated shRNA. At least 150 cells were counted for each condition and the percentage of total cells are reported. Data are presented as mean (n=2) with standard deviation (SD).

change in cell morphology compared to the control cells was observed. Many cells infected with the shPAX3 lentivirus became large and flat, and in addition, distinct vacuolisation occurred in the cytoplasm (Figure 4.6 B). These morphological

transformations have been described in the context of senescent cells (Kuilman et al., 2010), hence a β-galactosidase (β-gal) assay was performed to further substantiate the identification of a senescent phenotype. Seeded cells were infected with the shPAX3 expressing lentivirus and fixed after 72 h to perform the β-gal staining. Indeed, the staining revealed an enhanced β-gal activity in PAX3 deficient melanoma cells compared to the negative control cells, indicating the onset of senescence upon PAX3 knock-down (Figure 4.6 B).

Subsequently, to quantify the effect, cells with enhanced β-gal staining were counted for both, 501mel and SKmel28 cells, 72 h after infection with a lentivirus expressing either shPAX3 or shCtrl. At least 150 cells were counted for each condition in two biological replicates, and 5% of 501mel cells showed an enhanced β-gal staining after infection with the shCtrl expressing lentivirus, whereas this was the case for 36% of 501mel cells after infection with the shPAX3 lentivirus. SKmel28 cells exhibited a generally higher level of β-gal activity, with 26% of the cells showing an enhanced staining upon infection with the shCtrl lentivirus, but after infection with the shPAX3 lentivirus, this number increased to 61% (Figure 4.6 C). These results showed an considerably increased number of cells with elevated β-gal activity upon PAX3 knock-down compared to the negative control, suggesting the induction of senescence in PAX3-deficient cells.

4.3.4 TBX2 and TBX3 can rescue the senescent phenotype induced by PAX3 deficiency

T-box factors, in particular TBX2, have been implicated in the bypass of senescence (Jacobs et al., 2000; Carlson et al., 2001; Prince et al., 2004; Vance et al.,

2005; Peres et al., 2010) and are here shown to be downregulated upon PAX3 knock-down. Furthermore, the knock-down of PAX3 leads to a senescent phenotype in melanoma cell lines. Taking this observations together, it was hypothesised, that the observed senescent phenotype might be caused by the reduced levels of T-box factors.

To test this, the genetically engineered stable 501mel cell lines, ectopically overexpressing TBX2 and TBX3 respectively upon dox administration as described earlier (Section 3.2.3), were deployed. PAX3 protein levels were reduced in these cells via lentiviral shPAX3 knock-down to evoke the senescent phenotype and the consecutive loss of endogenous TBX2 and TBX3 was compensated by the ectopic expression of the two T-box factors via dox induction. If the downregulation of TBX2 and TBX3 as a consequence of PAX3 knock-down is responsible for the senescent phenotype as hypothesised, the ectopic overexpression in the engineered cell line should rescue the phenotype. 72 h post infection, cells were fixed and stained for β-gal activity. Indeed, much lower β-gal activity could be detected in cells overexpressing TBX2 or TBX3 than in cells without dox administration, indicating a rescue of the senescent phenotype (Figure 4.7 A). The effect was specific for TBX2 and TBX3 as the negative control cell line, generated with the empty Flag vector, demonstrated similar enhanced β-gal activity with and without dox administration. In addition, infecting the cell lines with the scrambled shCtrl lentivirus did not reproduce the enhanced β-gal staining (Figure 4.7 A).

To quantify the effect, at least 150 cells were counted for all conditions in biological duplicates 72 h post infection with the shPAX3 lentivirus. The 501mel cell line inducibly expressing TBX2-FLAG showed 31% β-gal positive cells without dox administration, whereas upon dox-induced TBX2-FLAG overexpression only

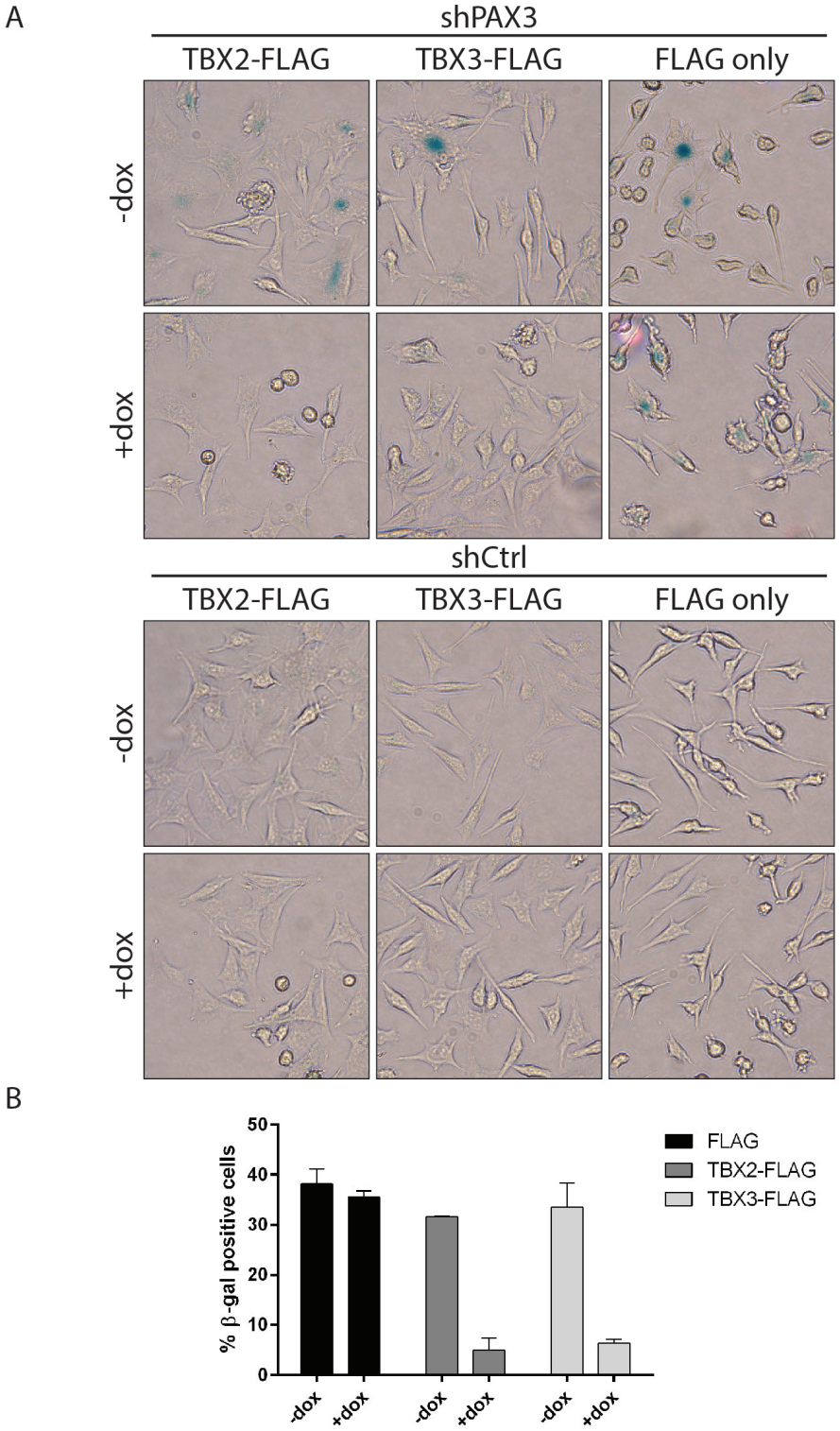

Figure 4.7: Overexpression of TBX2 or TBX3 rescues the senescent phenotype induced by PAX3 knock-down. *Legend continues at the bottom of the next page.*

5% stained positive. For the inducible TBX3(-)-FLAG cell line 33% of cells showed an elevated β-gal staining without dox induction, and only 6% after dox-induced TBX3(-)-FLAG overexpression (Figure 4.7 B). These results f the potential for TBX2 and TBX3(-) to rescue the senescent phenotype induced upon PAX3 knock-down. The negative cell line expressing the 3×FLAG peptide only upon dox administration showed 38% of cells with an enhanced β-gal staining without dox, and 36% with dox addition, indicating a specific effect by the two T-box factors TBX2 and TBX3 (Figure 4.7 B).

Summarising, the presented data suggests a signalling cascade from PI3K via PAX3 to T-box factors executing the bypass of senescence. The activation of PI3K signalling increases PAX3 protein levels and activity, in turn activating the T-box factors TBX2 and TBX3, triggering the bypass of senescence via its described suppression of expression of $p14^{ARF}$ and p21. This regulatory axis might provide the elusive mechanism for the described bypass of senescence upon constitutive PI3K activation via PTEN abrogation as published by Vredeveld et al. (2012).

Figure 4.7: Overexpression of TBX2 or TBX3 rescues the senescent phenotype induced by PAX3 knock-down. (A) The stable 501mel cell lines inducibly expressing TBX2-FLAG and TBX3(-)-FLAG upon dox administration, respectively, and the negative cell line expressing the 3×FLAG peptide only were infected with a lentivirus expressing shPAX3 (upper panel) or shCtrl (lower panel). After infection, culture medium was added without (upper row) or with dox (lower row) to induce transgene expression. All cell lines were assessed for β-gal activity 72 h post infection. (B) β-gal positive cells were counted 72 h after infection with a lentivirus expressing shPAX3 without and with addition of dox as indicated. At least 150 cells were counted for each condition and the percentage of total cells are reported. Data are presented as mean (n=2) with standard deviation (SD).

4.4 SGK, a potential mediator of PI3K signalling

A signalling mediator in the PI3K pathway downstream of PI3K is SGK, a family of protein kinases structurally related to PKB/AKT (Park et al., 1999). SGK, like PKB/AKT, is activated through PIP3-dependent phosphorylation by PDK1 and subsequently translocates to the nucleus to propagate its functions, such as glucose transport, glycogen synthesis, anti-apoptotic activity, and cell proliferation (Kobayashi and Cohen, 1999; Brunet et al., 2001; Sakoda et al., 2003; Tessier and Woodgett, 2006). The catalytic domain of SGK is 54% identical with PKB/AKT, hence, they are likely to phosphorylate related substrates (Kobayashi et al., 1999; Brunet et al., 2001). However, despite their similarity, SGK and PKB/AKT display unique features (Sakoda et al., 2003; Bruhn et al., 2010). For instance, SGK protein expression unlike PKB/AKT is induced upon treatment of cells with extracellular stimuli, such as GFs (Firestone et al., 2003). Furthermore, SGK seems not to be recruited to the plasma membrane prior to its activation due to its lack of a pleckstrin homology domain (Sakoda et al., 2003). Finally, notwithstanding the homology of the catalytic domain, substrate specificity of SGK seems to be different to PKB/AKT (Kobayashi et al., 1999; Kobayashi and Cohen, 1999; Sakoda et al., 2003). These differences suggest complementary rather than redundant functions of the two kinases.

Interestingly, SGK expression is induced by the ERK/MAP kinase signalling, linking the PI3K pathway to the MAPK pathway, which is often constitutively activated in melanoma (Mizuno and Nishida, 2001). Furthermore, a suppression of BRAF activity by SGK has been found, indicating a negative feedback loop to the MAPK pathway and an intricate regulatory interplay between the two major

proliferative pathways (Zhang et al., 2001).

To date, the role of PKB/AKT as the mediator of PI3K signalling has been addressed in a number of studies (Bellacosa et al., 2005; Manning and Cantley, 2007), but the contribution of SGK to tumourigenesis is largely uncharacterised. Despite its assumed overlap in regulated targets with PKB/AKT, the understanding of the roles of SGK remains limited and physiological targets are largely unknown. Considering its role in anti-apoptotic activity and cell proliferation, we next asked, whether T-box factors might be affected by SGK regulation and potential downstream targets.

4.4.1 SGK affects TBX2 and TBX3 protein levels

To test whether SGK affects the protein levels of the T-box factors TBX2 and TBX3, 501mel and SKmel28 melanoma cells were treated with 10 µM of the specific SGK inhibitor GSK650394 (Sherk et al., 2008) and protein levels of TBX2 and TBX3 were analysed in whole cell extracts using WB. The initial treatment for 24 h did not result in any change of protein levels (data not shown), but after 72 h of treatment decreased levels of TBX2 could be noted in both melanoma cell lines. TBX3 levels stayed unchanged in 501mel cells and were not detected in the samples generated with SKmel28 (Figure 4.8 A).

To better understand the time response of TBX2 protein levels upon SGK inhibition, a time course was performed. 501mel cells were treated with 10 µM of GSK650394 and DMSO as negative control for 4 h, 8 h, 12 h, 24 h, 48 h, and 72 h and whole cell protein extracts were subsequently assessed for protein levels of TBX2 and TBX3. After an initial increase of TBX2 protein levels after 8 h,

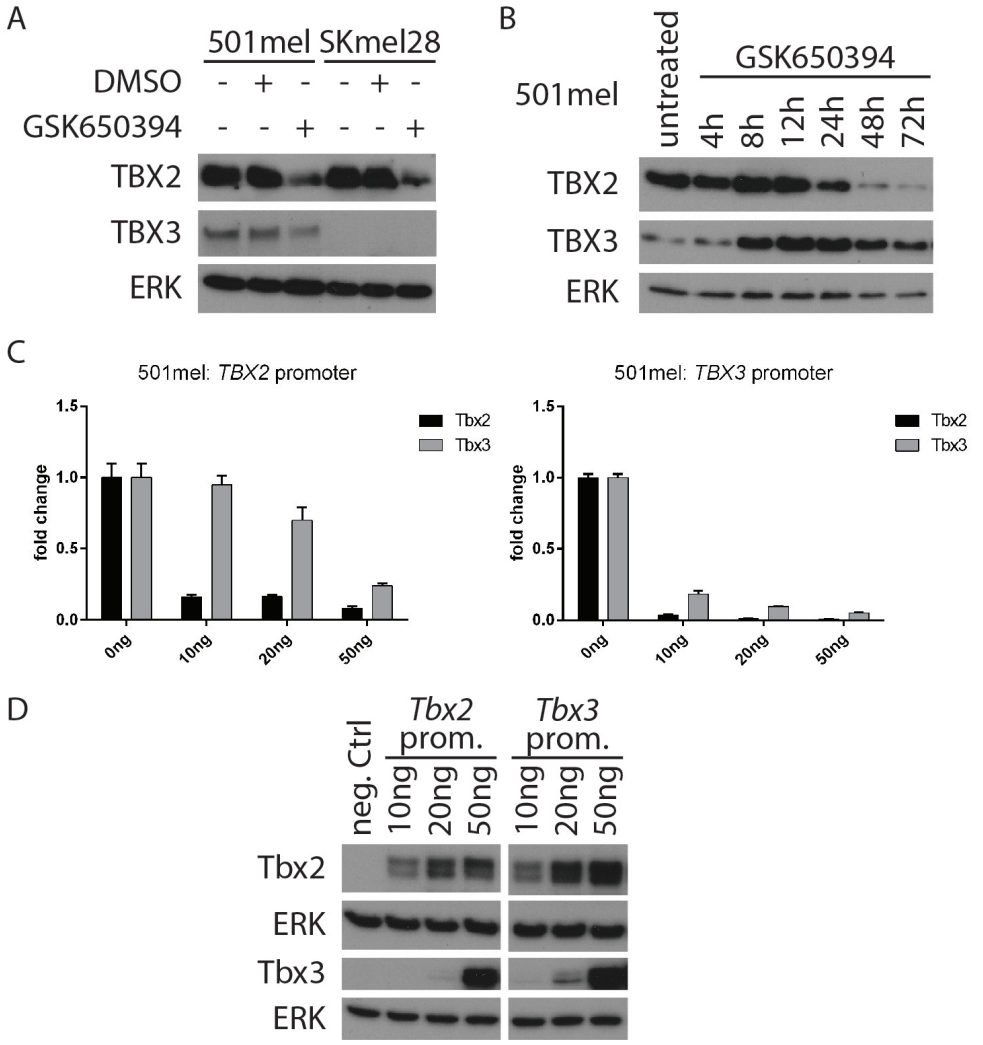

Figure 4.8: SGK affects protein levels of T-box factors TBX2 and TBX3. (A) Whole cell protein extracts of 501mel and SKmel28 cells treated with 10 µM of the SGK inhibitor GSK650394 for 72 h were analysed by WB for the indicated proteins. (B) WB analysis for the indicated proteins with whole cell protein extracts of 501mel cells treated with 10 µM GSK650394 in a time course. (C) 501mel cells were co-transfected with the indicated amount of expression plasmid for TBX2 or TBX3 and 100 ng of a luciferase reporter plasmid carrying the *TBX2* or *TBX3* promoter, respectively. The luciferase activity was measured 48 h post transfection. Data are represented as mean (n=3) with standard deviation (SD) normalised to the reporter plasmid alone. (D) Whole cell lysates of the transfected cells were analysed for transient expression of the T-box factors after the luciferase assay. ERK was used as loading control for all WBs.

WB analysis showed reducing protein levels after 48 h further diminishing after 72 h, indicating a late onset regulation by SGK. TBX3 protein levels, however, increase after 8 h and then remain mostly unchanged until 72 h of treatment with GSK650394 (Figure 4.8 B).

Earlier experiments in the laboratory indicated a negative cross-regulation between TBX2 and TBX3 (M. Rodriguez, Goding lab, unpublished), which might explain the detected downregulation of TBX2 while TBX3 is upregulated. Hence, a luciferase assay was performed with 501mel cells transfected with 100 ng of a luciferase reporter plasmid featuring the *TBX2* and *TBX3* promoters, respectively, to drive luciferase expression. The cells were co-transfected with different amounts of TBX2 or TBX3 expression plasmid (10 ng, 20 ng, 50 ng) and the luciferase activity was measured 48 h post transfection with a luminometer. With increasing amounts of transfected T-box factor expression vector the activity of both promoters, *TBX2* and *TBX3*, was progressively repressed, further substantiating a negative cross-regulation between TBX2 and TBX3 (Figure 4.8 C). WB of the whole cell lysates used for the luciferase assay demonstrated successful transfection and increasing, transient expression of the T-box factors consistent with the amount of transfected expression vector (Figure 4.8 D). To corroborate the finding, a mutated reporter construct preventing T-box factor binding in the promoter would have to be tested. Concluding, the inhibition of SGK with GSK650394 in the melanoma cell lines 501mel and SKmel28 might increase TBX3 protein levels, which in turn represses TBX2, leading to the determined downregulation of TBX2.

4.4.2 Inhibition of SGK induces a G_2/M arrest in melanoma cells

Upon treatment of the melanoma cells with the SGK inhibitor GSK650394 for 72 h, quite drastic morphological changes were noted. To better understand the development of this morphological phenotype better, a time-lapse experiment upon SGK inhibition was performed. 501mel and SKmel28 cells were treated with 10 µM GSK650394 or DMSO as negative control and bright field images were taken every 15 minutes for 3 days while still cultured under standard culture conditions (37℃, 10% CO_2, humidified air). The resulting footage revealed an enormous inflation of the cytoplasm over time, an increased size of the nucleus, and a more prominent ER upon GSK650394 treatment (Figure 4.9 A, only data for 501mel shown).

A possible explanation for the observed phenotype in the time-lapse experiment could be an impaired cell cycle upon SGK inhibition, with seemingly no cell cycle progression. To test this and characterise the phenotype in more detail, the cell cycle profiles of 501mel and SKmel28 cells were analysed upon SGK inhibition. The cells were treated for 24 h, 48 h, and 72 h with 10 µM GSK650394 or DMSO as a negative control, and the cell cycle profile was subsequently determined using flow cytometry after propidium iodide (PI) staining of the cells' DNA content. Already after 24 h, an increased proportion of cells accumulated in the G_2/M phase of the cell cycle was noted, and after 72 h almost the entire cell population was arrested in G_2/M (Figure 4.9 B, only data for 501mel shown). These results suggest an impaired cell cycle progression, with cells possibly incapable of exiting mitosis.

The progress of the cell through the cell cycle is predominantly governed by two

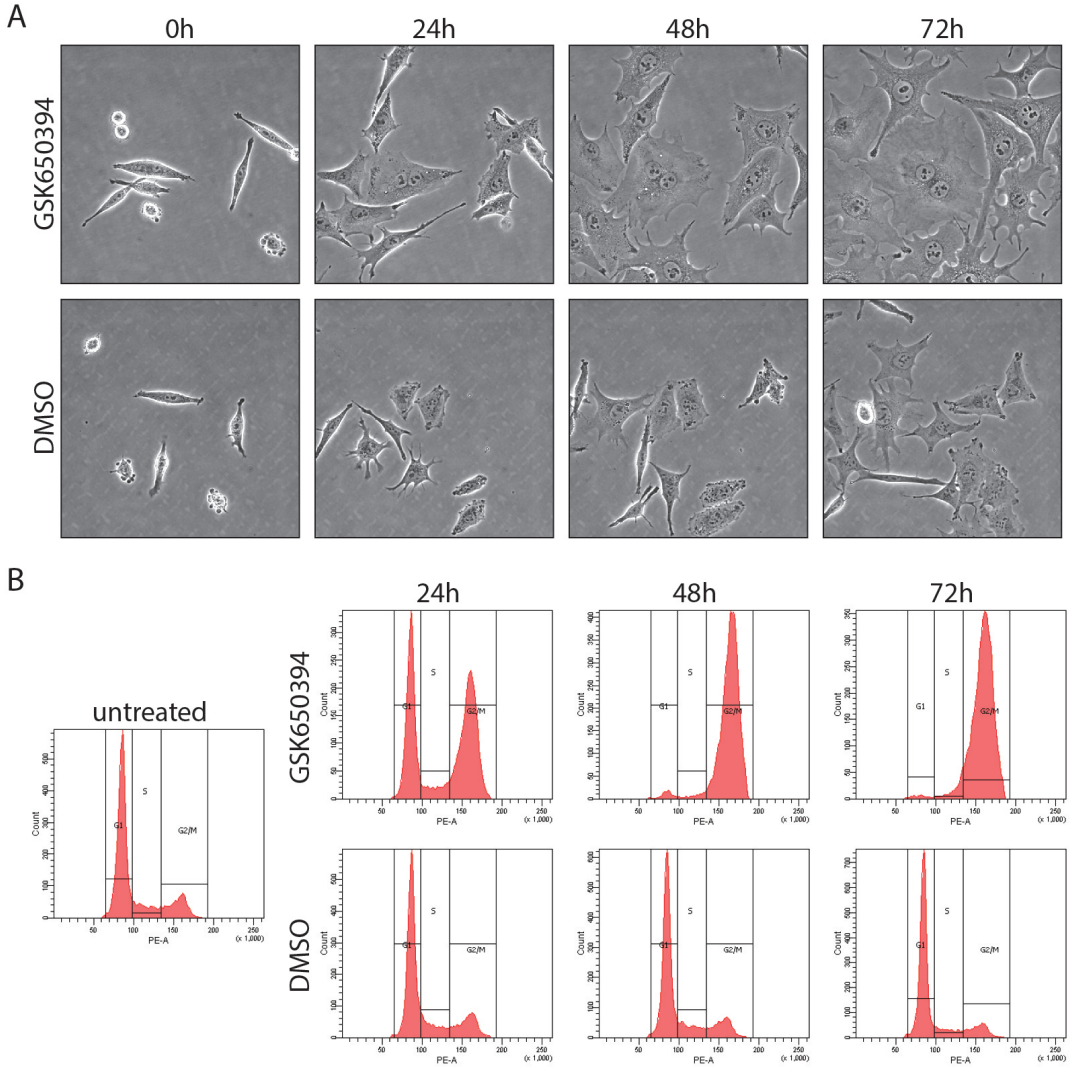

Figure 4.9: SGK inhibition causes marked changes in cell morphology and cell-cycle arrest. (A) 501mel cells were treated with 10 µM GSK650394 or DMSO as a control and bright field images were taken every 15 minutes for 3 days while still cultured under standard culture conditions. Exemplary images taken throughout the time-lapse are presented here. (B) Cell cycle profiles of 501mel cells treated for 24 h, 48 h, or 72 h with 10 µM GSK650394 or DMSO as a control were determined using flow cytometry after PI staining.

classes of regulatory proteins, cyclins and cyclin-dependent kinases (CDKs) (Nurse, 2000). CDKs are the executors of the tightly regulated cell cycle programme, phosphorylating selected downstream proteins to induce progression through the cell cycle. Their protein levels remain stable during the cell cycle and they only get activated by cyclins, forming specific cyclin/CDK complexes for the respective cell cycle stages (Vermeulen et al., 2003). The cyclin proteins are expressed periodically throughout the cell cycle, with different cyclins required at different phases of the cell cycle, facilitating the tight control throughout the cell cycle (Morgan, 1995). The G_1/S transition is governed by the cyclin E/CDK2 complex, whereas cyclin B and CDK1 form the maturation-promoting factor (MPF) governing the G_2/M transition and driving the cell through mitosis (Malumbres and Barbacid, 2005, 2009).

To follow up on the observed cell cycle phenotype, potential impairments of the cell cycle programme were assessed. For that, the protein levels of Cyclin B1 and CDK1, implicated in the G_2/M transition and during mitosis, as well as Cyclin E, CDK2, and E2F1, important cell cycle regulators for the G_1/S transition, were determined. Whole cell protein extracts of 501mel and SKmel28 cells were analysed using WB after treatment with 10 µM GSK650394 for 72 h. The results showed elevated cyclin B1 protein levels upon SGK inhibition and stable CDK1 protein levels (Figure 4.10 A). In contrast, the protein levels of E2F1 and cyclin E were reduced upon SGK inhibition with CDK2 protein levels being constant (Figure 4.10 B).

The unchanged protein levels of CDK1 and CDK2 are in line with the literature, where they have been described as stably expressed throughout the cell cycle (Vermeulen et al., 2003). Furthermore, given the observed G_2/M arrest of the

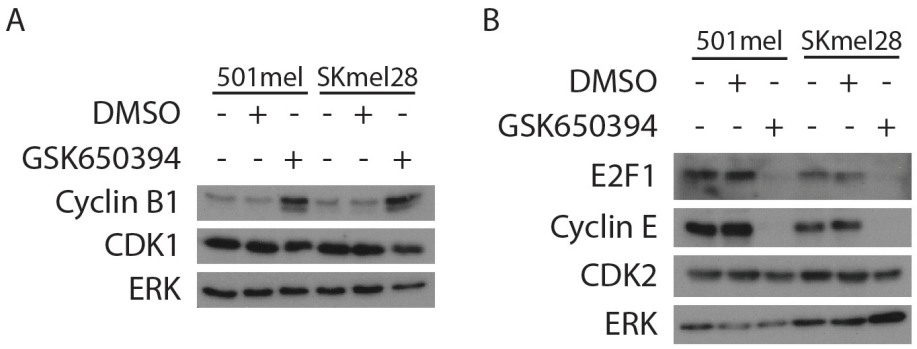

Figure 4.10: Cell cycle specific proteins for G_2/M phase are upregulated upon SGK inhibition. (A, B) Whole cell protein extracts of 501mel and SKmel28 cells either treated with 10 µM GSK650394, DMSO, or untreated as a control for 72 h were analysed for protein levels of the indicated proteins. ERK was used as loading control.

melanoma cells upon SGK inhibition as described above, the reduced protein levels of E2F1 and cyclin E are not surprising, as these proteins are only upregulated during the G_1 phase of the cell cycle, inducing the transition into S phase, and then being rapidly degraded (Vermeulen et al., 2003; Malumbres and Barbacid, 2005). However, it demonstrates the cell cycle machinery not to be dysregulated at the G_1/S check point of the cell cycle. The elevated cyclin B1 protein levels, yet, corroborate an impaired cell cycle progression through the G_2/M phase. Initially, it confirms the majority of cells accumulated in the G_2 phase, but, with elevated cyclin B1 and stable CDK1 protein levels, one could assume the MPF to form and guide the cell through mitosis, not leading to the observed cell cycle arrest in G_2/M. For the proper exit of mitosis, the MPF needs to be inactivated, accomplished by the degradation of cyclin B1 (Malumbres and Barbacid, 2005). Consequently, two possible options could explain the described phenotype: either upon SGK inhibition the binding of cyclin B1 to CDK1 is disrupted, preventing the MPF to

form; or the MPF is formed, but CDK1 is inactive, and consequently incapable of phosphorylating downstream targets to complete mitosis progression. The exact reason for the described phenotype remains elusive and further work is necessary to address the outstanding questions.

4.4.3 Inhibition of SGK evokes a senescence-like phenotype

The described cellular characteristics upon SGK inhibition could also suggest a potential senescent phenotype. On the one hand, the morphological changes are indicative for senescence and have been described to occur in senescent cells (Kuilman et al., 2010). On the other hand, senescence has been mainly associated with a G_1 cell cycle arrest (Serrano et al., 1997), rather than a G_2/M arrest as observed here. Nevertheless, to test for a senescent phenotype, the two melanoma cell lines were assessed for enhanced β-gal activity upon GSK650394 treatment. First, 501mel and SKmel28 cells were treated with different concentrations of GSK650394 (1 µM, 5 µM, 10 µM) for 72 h to analyse dose-dependent β-gal activity. Already with 1 µM of inhibitor, single cells show an enhanced β-gal staining, becoming increasingly prevalent at higher concentrations. The intensity of the staining also increases with the concentration, suggesting a strong dose-dependent upregulation of β-gal activity (Figure 4.11 A).

Subsequently, to analyse the time-dependent β-gal activity a time course of treatment with 10 µM GSK650394 for 24 h, 48 h, and 72 h was performed. Indeed, already after 24 h isolated flat cells with enhanced β-gal activity were observed, and after 48 h almost every cell showed elevated β-gal activity, further fortified after

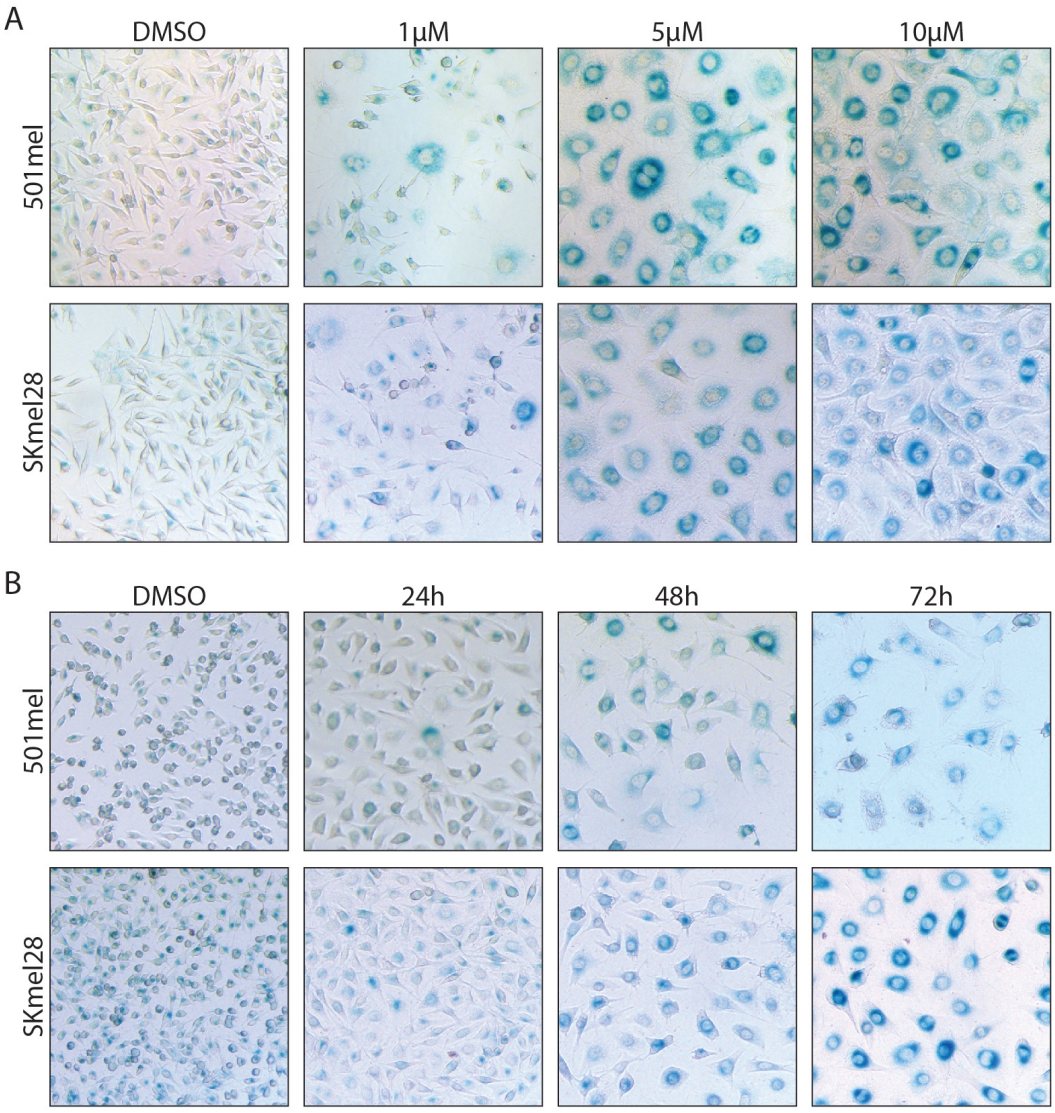

Figure 4.11: SGK inhibition results in a senescent-like phenotype. (A) 501mel and SKmel28 cells were treated with increasing concentrations of GSK650394 (1 µM, 5 µM, 10 µM) and DMSO as a control for 72 h and stained for β-gal activity. (B) 501mel and SKmel28 cells were treated with 10 µM GSK650394 for different lengths of time (24 h, 48 h, 72 h) and DMSO as a control and stained for β-gal activity.

72 h (Figure 4.11 B). This phenotype was not only observed in the two melanoma cell lines, 501mel and SKmel28, but also in the breast cancer cell lines MCF-7

and T-47D, in human embryonic kidney cells (HEK293), and in the human lung embryonic fibroblast line CT-1 (data not shown), indicating a more widespread phenomenon, not restricted to melanoma or cancer.

Next we asked, whether the observed phenotype upon SGK inhibition is dependent on PI3K signalling. For that, 501mel cells were treated with 10 µM of the SGK inhibitor GSK650394 alone or in combination with 10 µM of the PI3K inhibitor GDC0941 and stained for β-gal activity after 72 h of treatment. The cells treated with GSK650394 alone showed the expected elevated β-gal staining and morphological changes described above, whereas no enhanced β-gal activity and no morphological changes were observed with the cells treated with the inhibitor combination (Figure 4.12 A). Furthermore, the cell cycle profiles of 501mel cells treated with either 10 µM of the SGK inhibitor GSK650394 alone or in combination with 10 µM of the PI3K inhibitor GDC0941 were determined after 72 h treatment with flow cytometry. The cells treated with the combination showed a considerable proportion of cells in the G_1 phase of the cell cycle, not observed with GSK650394 treatment alone, indicating an at least partial reversion of the phenotype (Figure 4.12 B). These results suggest a PI3K dependency of the observed, senescence-like phenotype upon SGK inhibition with GSK650394.

To further elaborate on the senescence-like phenotype, protein levels of key executors of the senescence pathway were assessed. p16 and p21 are two cyclin-dependent kinase inhibitors (CKI) inactivating CDKs via phosphorylation to inhibit cell cycle progression (Vermeulen et al., 2003; Malumbres and Barbacid, 2005). Both proteins are upregulated in senescent cells and are used as senescence markers (Collado and Serrano, 2010). p53, described as the guardian of the genome (Lane, 1992), is a key stress sensor in cells, triggering a variety of antiprolifer-

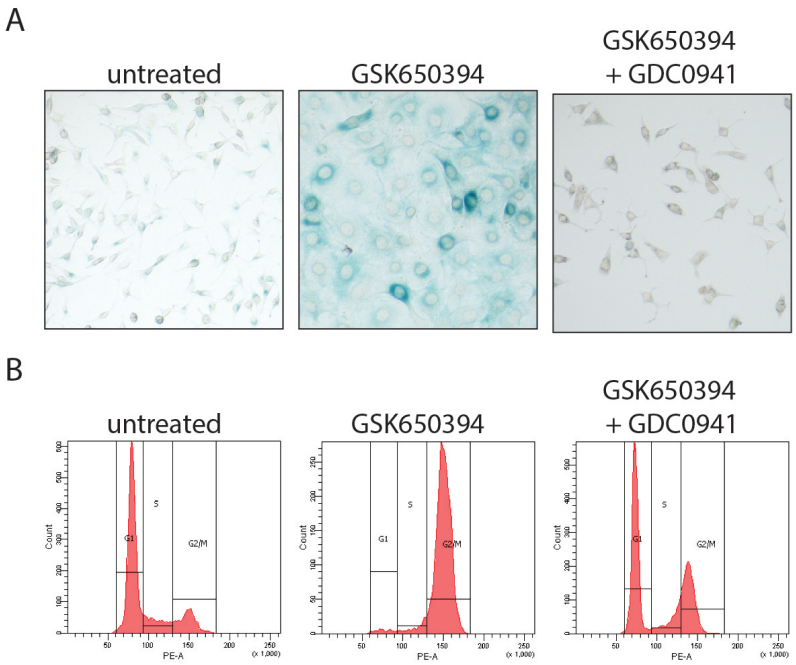

Figure 4.12: SGK inhibition results in a senescent-like phenotype. (A) 501mel cells were treated with 10 µM GSK650394 alone or in combination with 10 µM GDC0941 for 72 h and subsequently stained for β-gal activity. Untreated 501mel cells were used as negative control. (B) The cell cycle profile of 501mel cells treated with 10 µM GSK650394 alone or in combination with 10 µM GDC0941 was determined after 72 h treatment using flow cytometry after PI staining. Untreated 501mel cells were used as negative control.

ative programs through activation or repression of key effector genes (Zilfou and Lowe, 2009). Increased activity of p53 has been demonstrated to, among others, induce senescence mainly through activation by the DNA damage response pathway (Rufini et al., 2013). Consequently, all three proteins are expected to be upregulated in senescent cells.

501mel and SKmel28 were treated with 10 µM GSK650394 for 72 h and the whole cell protein extracts were analysed for p16, p21, and p53 protein levels.

Strikingly, neither p16, nor p21 were upregulated upon SGK inhibition, in contrary, substantially reduced protein levels were detected, whereas protein levels for p53 remained unchanged (Figure 4.13 A). Moreover, PTEN levels also seem to decrease upon treatment of 501mel and SKmel28 melanoma cells with 10 µM GK650394 for 72 h (Figure 4.13 B). Reduced levels of PTEN results in an activation of the PI3K pathway, upstream of SGK, which could potentially be a compensatory mechanism to counteract the inhibition of SGK. However, hyperactivation of the PI3K pathway via abrogation of PTEN signalling has been associated with the bypass of senescence (Vredeveld et al., 2012), rather than induction.

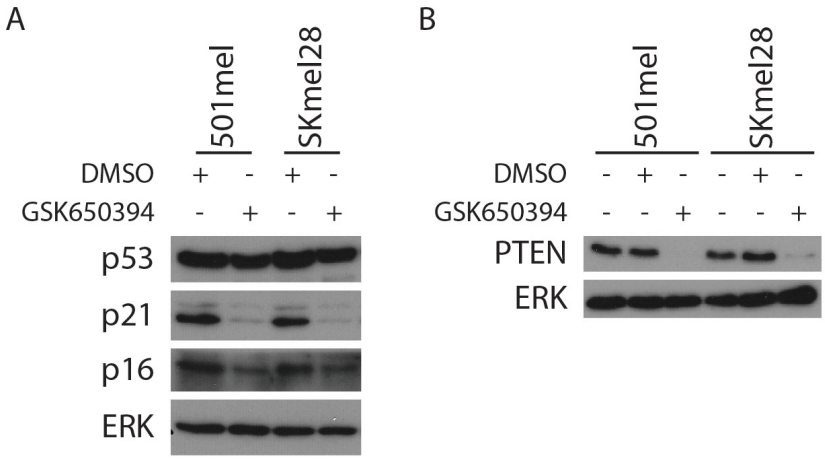

Figure 4.13: Key mediators of senescence are downregulated upon SGK inhibition. (A, B) Whole cell protein extracts of 501mel and SKmel28 cells either treated with 10 µM GSK650394 or DMSO as a control for 72 h were analysed for protein levels of the indicated proteins. ERK was used as loading control.

Taking these results into account, it is uncertain whether the cells indeed undergo senescence upon GSK650394 treatment. The enhanced β-gal activity observed upon SGK inhibition and initially interpreted as indication for a senescence

phenotype might ultimately not be related to senescence. Possibly, the accumulation of β-gal just represent generally elevated lysosomal activity due to cellular stress. Revisiting the data, the phenotype could potentially derive from a cell cycle failure in G_2/M, disallowing the cell to progress through mitosis, subsequently getting stuck in G_2/M. At the same time, the hyperactivated PI3K pathway, due to downregulation of PTEN, stimulates the cell to keep growing and progressing through mitosis. This could thus explain the enormous increase of the cytoplasm as the cells keep producing cellular macromolecules despite the cell cycle arrest. As a consequence, the cell would experience severe ER stress, resulting in enhanced lysosomal activity to cope with the stress, potentially explaining the observed enhanced β-gal activity.

Furthermore, when using the alternate, supposedly also specific SGK inhibitor EMD638683 (Ackermann et al., 2011) at 10 µM, the described phenotype could not be reproduced. As downstream targets of SGK are poorly described, it was difficult to check for the inhibitory activity of EMD638683 in the used melanoma cell lines. Additionally, the knock-down of SGK with target-specific siRNA, potentially yielding further insights into the regulation, could not yet been achieved due to the lack of an appropriate antibody for SGK. Hence, it was not possible to definitely determine the contribution of the T-box factors TBX2 and TBX3 in the SGK signalling branch of the PI3K pathway.

Concluding, more experiments are necessary to elucidate the underlying mechanism of this striking phenotype upon treatment with GSK650394 and dissect the contribution of T-box factors.

4.5 Discussion

In this chapter, the regulation of the T-box factors TBX2 and TBX3 was investigated. A potential regulation of the T-box factors TBX2 and TBX3 by the PI3K signalling pathway through PAX3 has been detected, a finding also reported by two recent publications published during the work on this thesis, which showed a regulation of PAX3 by the PI3K pathway and a direct regulation of TBX2 by PAX3, both in the mouse melanoma cell line B16 (Bonvin et al., 2012; Liu et al., 2013). This study demonstrates the regulation in two individual human melanoma cell lines, the invasive SKmel28 cell line and the non-invasive 501mel cell line. Furthermore, the regulation of TBX3 was included in the analysis and the PAX3 – TBX regulatory axis could be linked to a physiological phenotype, namely senescence. Hence, these results expand the understanding of the regulation of the T-box factors TBX2 and TBX3 beyond the published knowledge.

Common regulation of TBX2 and TBX3

As both T-box factors have been reported to serve distinct roles during melanoma progression (Peres et al., 2010), it was of interest to see, whether differences in their regulation could be observed. Throughout the study, TBX2 seemed to be the more prominently regulated factor, as the results showed a much clearer response to inhibitory intervention. TBX3, on the contrary, seemed to either not respond as strongly or not as promptly. Partially, this could be explained with technical restraints of the antibody against TBX3. Unfortunately, there is no fully reliable antibody against TBX3 for WB or ICC analyses available to date, making the analysis of TBX3 regulation and changes of protein levels challenging. Fur-

thermore, the SKmel28 melanoma cell line, one of the two cell lines deployed in this study, seems to have low levels of TBX3, making it difficult to confirm findings from 501mel cells for TBX3.

In addition, there is evidence of a cross-regulation between TBX2 and TBX3, with both factors repressing each other's transcription (Figure 4.8 C). Consequently, a slight change in protein levels of one of the two factors, might already be sufficient to cause the one factor to be repressed by the other disturbing the equilibrium between the two factors and resulting in a cellular state of one upregulated and one downregulated factor. This might mask or exaggerate possible additional effects and thus further complicate the interpretation of experiments, when trying to dissect the role of the two TFs.

Despite the published distinct roles of TBX2 and TBX3, both factors were individually capable to rescue the senescence phenotype induced via PAX3 knockdown in this study (Figure 4.7), indicating an overlapping regulatory potential. However, upon inhibition of SGK with the inhibitor GSK650394 a differential regulation of TBX2 and TBX3 could be detected, with increasing TBX3 protein levels and decreasing TBX2 protein levels, which could also be a consequence of the negative cross-regulation of the two T-box factors. Consequently, one could argue, that both TFs are regulated by the same pathway, but to a different extent. The resulting balance amplified by the cross-regulation between the two factors then exerts a specific regulatory outcome, with overlapping targets and effects, potentially also complementing each other, with no complete overlap.

Senescence upon PAX3 knock-down

In this chapter, a senescence phenotype was detected upon knock-down of PAX3 in the two melanoma cell lines 501mel and SKmel28. However, not all cells infected with the shPAX3 lentivirus showed the senescent morphology of flat and large cells, and also only 37% of 501mel and 68% of SKmel28 cells exhibited an enhanced β-gal staining. Moreover, the growth curve of 501mel and SKmel28 cells infected with the shPAX3 expressing lentivirus is not flat, as one would expect for senescent cells, but a certain level of proliferation was still detected. This suggests either an inefficient infection or PAX3 knock-down with the lentivirus or a possible escape of some cells from the senescent phenotype induced by PAX3-deficiency.

Indeed, when infecting 501mel cells with a lentivirus expressing shPAX3 and in addition integrating a puromycin resistance cassette into the cell's genome, a subset of cells kept proliferating and a stable cell line could be propagated, after initial cell death of uninfected cells. It would have been expected to not being able to establish a proliferating cell line as only PAX3-deficient cells would survive the selection process and subsequently senesce. Presumably, cells undergoing senescence induced by PAX3-deficiency were lost during early passaging of the cells, and cells escaping the phenotype were selected for, subsequently forming a proliferating cell line.

Interestingly, the stable cell line still showed reduced levels of PAX3 after up to nine passages, indicating the shRNA still to be expressed in these cells. This observation suggests an escape mechanism rather than inefficient infection with the lentivirus or knock-down of PAX3. The sub-population of cells escaping the senescence phenotype could consequently also explain the fact, that not all cells

showed the senescence-associated morphological changes, the low proportion of β-gal positive cells and also the residual growth detected in the growth curve upon PAX3 knock-down.

SGK inhibition

The PI3K pathway plays an important role in tumour cell biology. Downstream of PI3K, the pathway is bifurcated, with PKB/AKT and SGK separately propagating the respective signals after activation by PDK1. Hence, to better understand the regulation of T-box factors by that pathway, it is important to identify the respective branch, responsible for the regulation, PKB/AKT, SGK, or possibly both. Unfortunately, triciribine, the used PKB/AKT inhibitor in this study, appeared to be inactive and hence did not result in any insights into the regulation. Future work could include MK-2206, an alternate PKB/AKT inhibitor (Hirai et al., 2010), to gain further insights into potentially differential regulations in the PKB/AKT branch of the PI3K pathway.

However, upon treatment with the SGK inhibitor GSK650394, TBX2 protein levels were diminished, indicating a possible regulatory axis, and the treated cells showed a striking phenotype. Further analysis of the phenotype suggested a cell cycle impairment with cells getting stuck in the G_2/M phase of the cell cycle. Protein levels for cyclin B1 were elevated in these cells and CDK1 stably expressed, indicating a functional MPF to guide the cell through G_2/M. However, for the cell to exit the mitotic programme, the MPF needs to be inactivated by ubiquitin-mediated degradation of cyclin B1, not observed upon SGK inhibition. Two possible explanations were offered above for this phenomenon, either the MPF is not able to form upon SGK inhibition or CDK1, as the catalytic subunit of the MPF, is not

activated upon binding to cyclin B1. Both times, the mitotic programme would not be properly initiated and cells remain in G_2/M. To check for the two options, future work would need to analyse the complex formation via co-immunoprecipitation to determine whether the complex is disrupted. To assess the activity of CDK1, phospho-specific antibodies for the activation and inactivation sites of CDK1 could be used, indicating its phosphorylation and thus activation status (Coulonval et al., 2011). Moreover, the cellular localisation of the two proteins could be determined as a further indication of their activity. Only MPFs translocating into the nucleus have been demonstrated to govern chromosome condensation and break-down of the nuclear lamina to guide the cell through mitosis. Cytoplasmic complexes target the golgi apparatus causing it to disassemble, but have no effect on DNA condensation or the nuclear lamina (Draviam et al., 2001). Consequently, the localisation of the MPF could give further indication of potential impairments in the G_2/M phase of the cell cycle due to SGK inhibition.

Interestingly, PAX3 protein levels are also down upon SGK inhibition with GSK650394, potentially linking the PAX3 regulation of T-box factors to SGK signalling (data not shown). However, the morphological phenotype observed upon PAX3 knock-down was not as marked as with GSK650394. Furthermore, the timing of downregulation is also different. Whereas the protein levels for PAX3 and T-box factor are already markedly reduced after 24 h of PI3K inhibition, no change is observed after the same time of SGK inhibition, but the onset of phenotype is much later, after 72 h. It is difficult to tell, whether the observed phenotype upon SGK inhibition is a consequence of the reduced protein levels of TBX2 and presumably TBX3 or vice versa. This can be addressed in the future by deploying the stable 501mel cell lines expressing TBX2 or TBX3 upon dox

induction established in this thesis (Section 3.2.3).

Aside from all these considerations, there is also the possibility of some unspecific side-effects of the inhibitor GSK650394 causing the observed phenotype rather than downstream effects. In the characterisation of the inhibitor, Aurora kinases (AK) were identified as a potential unspecific target of GSK650394 with a selectivity of less than 10-fold (Sherk et al., 2008). AK play a crucial role in cellular division, governing the segregation of chromatids (Bolanos-Garcia, 2005) and inhibition consequently results in the impairment of the cell cycle during G_2. The reported IC_{50} concentration for GSK650394 is 103 nM (Sherk et al., 2008), 100-fold less than what has been used in this study. However, the determination of the IC_{50}-value was performed using an *in vitro* activity-based scintillation proximity assay with purified enzyme and a synthetic biotinylated peptide substrate (Sherk et al., 2008), not reflecting cellular conditions. Effective concentrations in a cellular context to observe physiological effects can be significantly higher than the *in vitro* IC_{50} concentration. Nevertheless, unspecific inhibition of AK due to high concentration of GSK650394 could potentially explain the observed phenotype. Yet, no phenotype as described here for the GSK650394 inhibition has been reported for AK inhibitors (Kollareddy et al., 2012; Xie et al., 2013), indicating at least a contribution of SGKs in the phenotype.

For further analyses, a second supposedly specific SGK inhibitor, EMD638683, was used and did not recapitulate the striking phenotype. This could be explained with different specificities for SGK between the two inhibitors as SGK comprises a family of 3 members functionally related but distinct (Tessier and Woodgett, 2006). So different specificities for individual members of the family could result in different phenotypic outcomes. Furthermore, a specific knock-down of the indi-

vidual members of the SGK family using siRNA or shRNA could help excluding unspecific effects of the inhibitor. It could also provide further evidence for the possible regulation of T-box factors by SGKs and elucidating the underlying causes for the observed phenotype. Unfortunately, the knock-down using specific siRNAs has to date been unsuccessful, thus future experiments could include a lentiviral guided shRNA knock-down.

Chapter 5

Discussion

The T-box factors TBX2 and TBX3 are members of an ancient family of TFs implicated in embryonic development (Bollag et al., 1994; Sebé-Pedrós et al., 2013). Unlike the majority of members of the T-box family, TBX2 and TBX3 predominantly function as transcriptional repressors of their target genes (Carreira et al., 1998; Lingbeek et al., 2002; Paxton et al., 2002). Moreover, TBX2 and TBX3 have been demonstrated to be abnormally expressed in several different cancer types (Lu et al., 2010), but their repertoire of target genes remain elusive. In this study, a comprehensive assessment of genes potentially regulated by the two T-box factors via DNA-binding and gene expression analysis was performed, revealing an entire set of novel TBX2 and TBX3 target genes. The multitude of potentially regulated genes could be grouped into three main functions, cell cycle regulation, growth regulation, and transcriptional regulation. Subsequently, cancer homoeostasis was proposed as an overarching role for TBX2 and TBX3 during cancer tumourigenesis, incorporating the variety of regulatory activities into one concept.

Furthermore, due to their overexpression in several cancer types, the regulation of TBX2 and TBX3 themselves by growth-regulatory pathways, that are dysregulated in cancer, was analysed. PI3K regulation of the two T-box factors was established, mediated by PAX3, a member of the paired box family of TFs involved in the cell survival and growth of the melanocytic lineage (Scholl et al., 2001; He et al., 2005). This regulation was furthermore linked to the potential of bypassing senescence, a role previously described for TBX2 and TBX3 (Jacobs et al., 2000; Carlson et al., 2001; Prince et al., 2004; Vance et al., 2005; Peres et al., 2010). PI3K regulation and subsequent bypass of senescence can be integrated into the overarching role of TBX2 and TBX3 in cancer homoeostasis.

5.1 The concept of cancer homoeostasis

For a cancer cell to support its indefinite proliferation, it needs to keep a balance between nutrient supply and demand. Supply describes thereby the provision of essential, basic building materials for all cellular processes. Examples are nutrients like carbohydrates used to generate ATP, the main energy carrier of the cell, or lipids to allow compartmentalisation of the cell. Further crucial building materials are nucleotides, necessary for the synthesis of nucleic acids, and amino acids, the building blocks of all proteins in the cell, the executor of cellular processes. Some of the basic materials can be taken up from the extracellular space via diffusion, membrane channels or endocytosis, others are produced internally from the previously absorbed building materials via intracellular, biochemical processes. This allows the cell to tightly regulate the production and provision of necessary materials according to the cellular state.

Demand is then the other side of the equation, the consumptive need of a cell. For the basic maintenance of the cellular functions, the cell consumes energy in form of ATP. Lipids are used to build lipid layer membranes for the compartmentalisation of the cell, creating physical boundaries and spatial separation for biological processes providing specific biochemical conditions, such as pH or oxidising environments. Moreover, they represent a major form of energy storage being available and consumed during high metabolic activities. Furthermore, for gene transcription and subsequent protein synthesis the cell expends nucleotides and amino acids to generate mRNAs and proteins, allowing the cell to proliferate and react to external cues via its intricate intracellular signalling network. Finally, nucleotides are also used for DNA replication, necessary for successful cell division

and thus proliferation, as the entire DNA needs to be duplicated before mitosis. Consequently, a coordination of supply and demand is paramount for the functioning of the cellular processes, to ensure the availability of sufficient building blocks for every active process without over- or underproduction.

In cancer cells, the demand of nutrients is markedly increased, in order to fuel the proliferation driven by oncogene activation. The activation of an oncogene or inactivation of a tumour suppressor gene increases the proliferative rate and uncouples the cells from the regulatory control circuits (Hanahan and Weinberg, 2000). So what happens, when the equilibrium of nutrient supply and demand is out of balance? In the case of a much higher supply than demand, either arising from an elevated supply or a decreased demand without regulatory adjustments in the respective other part, the cell would accumulate too many building blocks without using them, resulting in a surplus and a very inefficient use of resources.

Much more detrimental, however, would be a significantly higher demand than supply, emanating from either an increased demand or decreased supply. In that case, many more building blocks would be consumed than the cell could provide, leading to a shortage and eventual depletion of these building blocks within the cell. In the case of an amino acid depletion, protein production would be impaired, as ribosomes would not be able to incorporate the respective necessary amino acid as encoded by the mRNA (Murguía and Serrano, 2012). In case of a nucleotide shortage, mRNA transcription would be affected due to lack of appropriate nucleotides, leading to transcriptional stress. Also DNA replication would be harmed with the replication fork either stalling, consequently being at a higher risk for S-phase-associated DNA damage (Labib and Hodgson, 2007), or incorporating wrong nucleotides leading to an increased mutation rate (Kunz, 1988;

Meuth, 1989). Ultimately, if the imbalance in supply and demand of nutrients is not resolved via cell cycle checkpoints, cells would undergo quiescence, apoptosis or necrosis (Lieberthal et al., 1998; Sakagami et al., 1998; Martinet et al., 2005; Fu et al., 2006; Kim and Forbes, 2008).

Interestingly, nucleotide depleted cancer cells have also been demonstrated to undergo OIS due to the induction of DNA damage (Mannava et al., 2012; Aird et al., 2013; Mannava et al., 2013). The DNA damage thereby presumably originates from DNA damage sites preexistent to DNA replication causing the DNA replication fork to stall or collapse. The preexistent lesions might be caused by nucleotide misincorporation due to the lack of appropriate nucleotides and consequent activation of the DNA mismatch repair machinery (Boucher et al., 2002; Mannava et al., 2013). If the DNA repair machinery is overwhelmed by too many misincorporated nucleotides, it would generate single and/or double strand breaks in the DNA (O'Konek et al., 2009). In addition, the DNA mismatch repair system uses *de novo* DNA synthesis for filling existing gaps (Jiricny, 2006), which also requires nucleotides. Hence, the fidelity of the DNA repair would also be affected by low levels of nucleotides.

Consequently, for a cancer cell to keep proliferating, it would have to avoid the severe imbalance and keep a sustainable equilibrium of nutrient supply and demand. This cellular function was termed cancer homoeostasis in this thesis, to indicate the elevated, but still controlled, balance of supply and demand to fuel the oncogene-driven proliferation of cancer cells, in contrast to physiological homoeostasis (Figure 5.1). Cancer homoeostasis in the context of high demand due to activated oncogenes can either be achieved by increasing the supply or decreasing the demand. Indeed, cancer cells increase the supply of building ma-

terials for instance through upregulation of nutrient importers (Flier et al., 1987; Ying et al., 2012), or oncogene-induced macropinocytosis of amino acids (Commisso et al., 2013), or degradation of ECM to provide additional nutrients (White, 2013). Furthermore, at a macroscopic level, tumours induce vasculogenesis to establish additional blood vessels to provide more nutrients and essential building blocks for the cancer cells (Carmeliet and Jain, 2000; Hillen and Griffioen, 2007).

Moreover, in the situation of nutrient and/or building block shortage, the cell might undergo autophagy, a catabolic recycling pathway within the cell degrading cytoplasmic constituents to make the metabolites bound in the macromolecules available again for other cellular processes (Boya et al., 2013). This adaptive response would allow a cancer cell to temporarily increase the supply of metabolites to meet the demand and potentially resolve the shortage (Martinet et al., 2005).

However, increasing the supply might not always suffice to counteract the imminent imbalance in nutrient supply and demand. This might happen either because of physical limitations of the cell, already internalising and producing supply at its limits without the capacity to increase any more, or limitations in the environment with insufficient nutrients and building blocks available to fuel the cell's demand. Hence, it might be necessary for a cancer cell to also reduce demand to allow continuous proliferation and maintaining the balance. Even though this might result in a slower proliferation rate due to the limiting regulation, it will ensure the long-term proliferation of the tumour avoiding depletion of supplies and subsequent cell death or senescence.

5.2 The T-box factors TBX2 and TBX3 in cancer homoeostasis

In this study, the T-box factors TBX2 and TBX3 have been suggested to contribute to cancer homoeostasis by regulating the balance of demand and supply downstream of the PI3K pathway. Through DNA binding studies using ChIP-Seq experiments strong binding was elucidated in major growth-related pathways, often mutated during tumourigenesis, such as the MAPK pathway (Dhillon et al., 2007), with peaks in the promoter region of *KRAS* and *MAPK1*, and the PI3K pathway (Fruman and Rommel, 2014), with peaks in the promoter region of *PIK3R1* and *RAPTOR* (Figure 3.7 B and Figure 3.9 B). Considering the mainly repressive function of TBX2 and TBX3 (Carreira et al., 1998; Lingbeek et al., 2002; Paxton et al., 2002), also confirmed here with microarray analyses (Figure 3.16 B), a repression of growth stimulating signals by TBX2 and TBX3 was inferred. This would provide a mechanism by which cancer cells would be able to lower the demand to sustain cancer homoeostasis. This idea is further supported by the identification of MYC repression upon TBX2 and TBX3 overexpression in microarray analyses (Figure 3.19 B). MYC is a common transcriptional activator involved in the regulation of approximately 15% of genes (Patel et al., 2004). Hence, repression of MYC by TBX2 and/or TBX3 would lead to reduced overall transcription in the cell and consequently lower nutrient demand.

However, exaggerated suppression of growth stimuli, or transcription, and thus reduction of demand would be disadvantageous to the cancer cell, as it would restrict the proliferative potential. Thus, a cancer cell would need to closely monitor the balance to reduce demand just enough to ensure maximal proliferation within

sustainable nutritional boundaries. In line with this hypothesis, one of the up-regulated proteins upon overexpression of TBX2 and TBX3 as identified in the microarray study is GADD45A (Figure 3.18 A), a member of the GADD45 proteins, acting as an intracellular stress sensor reacting to genotoxic and physiological stress within the cell (Liebermann and Hoffman, 2002). Upregulating GADD45A via TBX2 and TBX3 would give the cancer cell the possibility to detect current stress level to control the appropriate proliferative rate, i.e. nutrient demand.

Interestingly, the T-box factors TBX2 and TBX3 seem not only to control cancer homoeostasis by reducing demand, but can also increase demand, indicating a role as a two-sided modulator. The integrated analysis of DNA binding peaks of TBX2 and TBX3 and differential expression upon overexpression of the two T-box factors revealed a potential direct repression of EZH2 (Section 3.5), involved via the PRC2 complex in transcriptional repression via heterochromatin formation (Hansen et al., 2008). Thus, repression of EZH2 results in enhanced transcription and consequently enhanced demand of nutrients by the cell. Considering the earlier described decrease of transcription via repression of MYC, the T-box factors TBX2 and TBX3 seem to be able to regulate demand in both directions. This two-sided regulation would allow a cancer cell to finely adjust the demand to the necessary levels, in order to support maximal proliferation under the existing nutritional circumstances.

The role for TBX2 and TBX3 as both, positive and negative modulator is further corroborated by the results of the KEGG analysis of differentially expressed genes from the microarray analysis upon overexpression of the two T-box factors showing the regulation of several metabolic pathways for both, amino acids and carbohydrates, in the cell (Figure 3.17). This indicates a further role for TBX2

and TBX3 in the supply of the cells with nutrients. Strikingly, individual metabolic pathways are enriched for both up- and down-regulated genes, hinting again towards a two-sided regulatory role.

Furthermore, to add another regulatory layer, TBX2 and TBX3 are regulated by cellular signalling cascades themselves. In this study, a regulation by the PI3K pathway, an important, often dysregulated growth regulatory pathway in cancer (Vanhaesebroeck et al., 2012), via PAX3 has been demonstrated. PAX3 plays an crucial role in melanocyte specification from neural crest cells (Kubic et al., 2008), but is also frequently found expressed in melanomas and naevi (Plummer et al., 2008; Medic and Ziman, 2010). In the adult organism, PAX3 is essential for the maintenance of the melanocyte stem cell niche in blocking terminal differentiation of melanoblasts (Lang et al., 2005), and has been further implicated in melanocytic proliferation and resistance to apoptosis (Borycki et al., 1999; Margue et al., 2000). The induction of TBX2 and TBX3 expression by PAX3, as identified in this work, and the proposed regulation of cancer homoeostasis by the two T-box factors could hence provide a novel mechanism for the described functions of PAX3, especially proliferation and resistance to apoptosis.

In addition, the novel finding of the induction of a senescent phenotype upon knock-down of PAX3 in human melanoma cells (Figure 4.6) and its subsequent rescue via overexpression of TBX2 or TBX3 respectively (Figure 4.7) provided a physiological function for this signalling axis. Considering the above described establishment of OIS in nutrient depleted cancer cells (Mannava et al., 2012; Aird et al., 2013; Mannava et al., 2013), one could argue, that the modulating role of TBX2 and TBX3 in cancer homoeostasis, triggered by PAX3 downstream of the PI3K pathway, provides a possible mechanism for the observed bypass of OIS. By

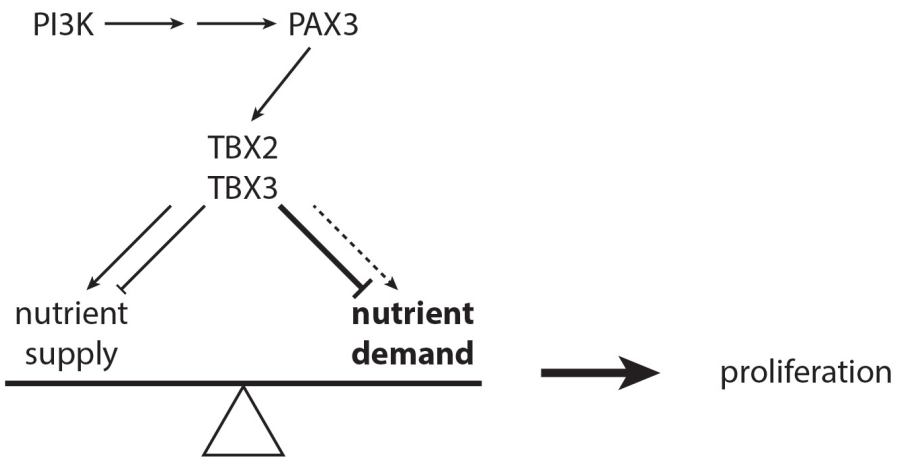

Figure 5.1: Illustration of the proposed model of cancer homoeostasis. The two T-box factors TBX2 and TBX3 maintain the balance between nutrient supply and demand through the positive and negative regulation of factors involved in both processes, subsequently allowing elevated proliferation of the cancer cell. The T-box factors are thereby regulated themselves by PI3K signalling mediated via PAX3. The bold typeface of nutrient demand signifies the markedly increased nutrient demand of fast proliferating cancer cells.

enabling the melanoma cell to avoid nutrient depletion and maintain a sustainable nutrient equilibrium, despite the enhanced stress levels due to the oncogenic insults, the activity of the two T-box factors TBX2 and TBX3 can circumvent the onset of senescence. This newly established regulatory path, mechanistically linking PI3K signalling with the bypass of senescence, might also constitute the elusive mechanism of the described bypass of senescence upon activation of the PI3K pathway via the abrogation of PTEN (Vredeveld et al., 2012).

The regulation of the activity of TBX2 and TBX3 by PI3K also conforms with their proposed role in cancer homoeostasis. The PI3K pathway is an important growth regulatory pathway and often mutated or dysregulated in cancer (Van-

haesebroeck et al., 2012; Fruman and Rommel, 2014). In melanoma, the PI3K pathway is often upregulated (Aziz et al., 2009), consequently also increasing the levels of TBX2 and TBX3. Without the activity of TBX2 and TBX3, the constitutively activated PI3K would possibly exhibit an unsustainably high level of nutrient demand, eventually driving the melanoma cells into OIS, due to depletion of nutrients and subsequent DNA damage. However, the upregulation of the two T-box factors allows the melanoma cells to establish an elevated equilibrium for long-term, sustainable growth. The linkage of the modulating function of the T-box factors with the activating, pro-proliferative function of PI3K thereby enables the establishment of an elevated equilibrium, still fostering sustainable proliferation. The potential differential regulation through PKB/AKT on the one hand and SGK on the other hand, would offer an additional lever to modulate the equilibrium appropriately.

Interestingly, the hippo pathway, another cellular signalling pathway controlling organ size via restraining cell proliferation and promoting apoptosis (Saucedo and Edgar, 2007), has been implicated in PAX3 regulation. Yes-associated protein (YAP), a member of the hippo signalling pathway has been demonstrated to directly regulate PAX3 during development in the neural crest and stimulate its expression (Mo et al., 2014). Furthermore, YAP and transcriptional coactivator with PDZ-binding motif (TAZ) act as synergistic coactivators of PAX3-dependent transcription (Manderfield et al., 2014). This could suggest PAX3 as a nodal point in the cellular signalling circuitry integrating signals of several proliferation-related pathways to modulate their activity and enable cancer homoeostasis orchestrated by the T-box factors TBX2 and TBX3.

To further elaborate on the regulation of the two T-box factors themselves,

a cross-regulation of TBX2 and TBX3, repressing each other's expression, was demonstrated in this study (Figure 4.8 C), further supported by unpublished data in the laboratory. Both T-box factors show a considerable overlap in potentially regulated target genes in the DNA binding analysis, but also exhibit a subset of genes exclusively bound in the promoter region by only one of the TFs (Figure 3.10). Considering the detection of both proteins under normal culture conditions with WB, one could speculate, that under normal, non-stress conditions the protein levels of both T-box factors are balanced, repressing each other's transcription just that much to maintain a cellular equilibrium. As soon as the protein level of one of the two factors increase above the balance threshold, however, repression of the respective other T-box factor leads to the domination of the factor via this positive feedback loop.

For instance, in this study an increase of the protein levels of TBX3 upon SGK inhibition with the specific inhibitor GSK650394 in the two human melanoma cell lines 501mel and SKmel28 has been demonstrated, followed by reduced protein levels of TBX2 (Figure 4.8 B). Consequently, a context dependent target specificity of the T-box factors would be an attractive possibility, with regulation of the target genes common to the two T-box factors under equilibrium conditions, while both factors are expressed, and a switch to regulation of the target genes exclusive to only one factor upon its dominant expression condition. Further work, however, is necessary to substantiate this hypothesis.

Besides, TBX2 has been demonstrated to be tightly regulated during the cell cycle in transformed and non-transformed cell lines, with protein levels rising in late S/G_2-phase, and a sudden drop at the onset of mitosis (Bilican and Goding, 2006). Thus, the majority of target gene regulation presumably happens during

late S- and G_2-phase, during DNA replication and preparation for cell division when the protein levels of the T-box factors peak. During the remaining cell cycle, TBX2 and TBX3 protein levels can still be detected, though at a lower level, indicating a continuous basal level throughout the cell cycle. Consequently, the regulatory functions of the two T-box factors could be potentially divided into two groups, cell cycle dependent and independent functions.

For instance, TBX2 and TBX3 have been found in this study to repress members of the E2F protein family (Section 3.5), important regulators of the G1/S transition of the cell cycle, inducing the expression of proteins orchestrating the transition into S phase of the cell cycle. This regulation could be an example for a cell cycle dependent function of the two T-box factors, as during late S- and G_2-phase, the peak of TBX2 and TBX3 activity, the E2F protein family, exerting their function during the G1/S transition, is not needed and hence a repression by the T-box factors would fit in the current understanding of the cell cycle.

It would hence be very interesting, to be able to assign the here identified novel target genes to the two different groups, in order to obtain a deeper understanding of the specific functions of TBX2 and TBX3. For that, future work would have to comprise the analysis of cell cycle synchronised cells to dissect the regulated target genes at the respective stage of the cell cycle. Presumably, the individual functions involve different interaction partner, activating or repressing the regulatory activity of the two T-box factors in a context-dependent manner. To elucidate potential proteins interacting with TBX2 and TBX3, the stable, monoclonal melanoma cell lines, expressing 3×FLAG-tagged upon dox induction established in this study were sent to a collaboration partner for mass spectrometry analysis. The results will provide further valuable insights into the role and regulation of the two T-box

factors TBX2 and TBX3.

Integrating this cell cycle specific regulation of the two T-box factors with the above identified role in modulating nutrient demand, one could speculate, that the two T-box factors lower the nutrient consumption of the cell specifically during the late S/G_2 phase of the cell cycle, enabling the cell to get through mitosis. At that stage, the DNA has been duplicated and the subsequent growth of the cell during G_2 is limited by the T-box factors to avoid an imbalanced nutrient equilibrium and subsequent stop at the G_2/M DNA damage checkpoint. This regulation would ensure an orderly preparation of and transition to mitosis.

An entirely different, but nevertheless noteworthy role for TBX2 and TBX3, identified in this study, is immune modulation (Section 3.4.2), important for the long-term survival of a cancer cell. Dysregulated cancer cells can be recognised by the immune system via tumour-associated antigens due to aberrant expression or mutation-specific antigens derived from point mutations in normal genes during tumourigenesis. Following the recognition, the immune system can trigger the immune-mediated destruction of these cells (Woo et al., 2015). Therefore, to evade immune clearance especially at an early stage of tumourigenesis, it is crucial for a cancer cell to avert a full immune response. However, pro-inflammatory signals can also support and enhance tumour growth by supplying additional nutrients and growth stimulatory signals (Lu et al., 2006). Consequently, moderate inflammation levels without full activation of an immune response, that would lead to clearance of the cells, would provide a cancer cell with increased proliferative potential and long-term survival.

The possible activation of TGF-β, inducing immuno suppression and angiogenesis (Blobe et al., 2000; Siegel and Massague, 2003), the suppression of CTLA4,

activating T-cells (Parry et al., 2005), and the suppression of IL6R, repressing the signalling of pro-inflammatory cytokines (Scheller et al., 2011), by the two T-box factors indicate a possible mechanism, by which a cancer cell might be able to modulate the immune response. Interestingly, IL6 signalling has been shown to repress PAX3 protein and mRNA levels (Kamaraju et al., 2002), suggesting a regulatory feedback loop between PAX3, T-box factors and IL6. Furthermore, the activation of TGF-β signalling has been suggested to induce a high metastatic potential in melanoma cells by driving the expression of inhibitory factors to Wnt-signalling (Hoek et al., 2006).

As modulation of the immune response would be beneficial for the cancer cell throughout the cell cycle, this function could conceivably be a candidate for cell cycle independent regulation by the two T-box factors not restricted to a certain cell cycle stage. However, further work is necessary to validate this assumption.

5.3 Implications

With the suggested concept of cancer homoeostasis the seemingly uncontrolled growth of tumours is proposed to be controlled itself, adding a further layer of regulation to cancer cell biology. This might open up a new avenue for a potential cancer treatment by targeting the modulators of cancer homoeostasis. In this study, the two T-box factors TBX2 and TBX3 have been proposed to perform that role, but there are supposedly more modulators influencing cancer homoeostasis to be identified. By inhibiting the activity of these modulators, cancer cells would no longer be able to maintain the delicate balance of supply and demand, establish a nutritional imbalance over time and be forced into cellular catastrophe. The

consequence would be cell death via apoptosis or necrosis, respectively, or a cell cycle arrest via senescence, reducing the tumour burden of the patient or at least stop the proliferation.

One could even argue, that stimulating the already activated cancer cells even further while inhibiting the modulating role of the T-box factors, could potentially provide an additional avenue to push cancer cells out of the equilibrium, and inducing apoptosis or senescence. Combining this regimen with a treatment limiting the supply of tumours, for instance a anti-VEGF treatment to inhibit neovascularisation, might prove even more efficient due to a much more severe impact on the equilibrium of supply and demand.

5.4 Future perspectives

The presented data in this study were generated with a stable, monoclonal cell line derived from the human melanoma cell line 501mel under standard culture conditions. The thereby obtained results showed mainly medium peak heights in DNA binding sites and moderate expression changes of regulated target genes. This could presumably be explained with the nutrient rich cell culture medium used for the maintenance of the cell lines, supplying the cells with plenty of building materials. As a consequence, the activity of the two T-box factors in their proposed role of maintaining cancer homoeostasis, the balancing of nutrient supply and demand, was presumably not required much due to the high nutrient supply, resulting in the observed moderate changes in gene expression following their induction. Consequently, future work could analyse the identified target genes under more tumour-like, stress-induced conditions, such as nutrient limitation, to obtain

a more prominent regulation. One could even try and assess their role and function in recently developed 3D cancer models, even more resembling the prevailing conditions within a tumour mass (Nyga et al., 2011; Tanner and Gottesman, 2015).

Furthermore, the analysed samples were generated from a non-synchronised cell population, with only a subset of them being in late S/G_2-phase, when due to the cell cycle regulation of the T-box factors most of the regulation would be expected. Thus, the observed cell cycle dependent changes in the genome-wide data sets originate only from a subset of cells, potentially explaining the moderate changes observed in this study. The analysis of a purely late S/G_2 cell population in the future would presumably result in higher DNA binding peaks and bigger gene expression changes. Moreover, assessing cell populations of the other specific cell cycle stages, G_1 and G_1/early S-phase, would enable the categorisation of the identified functions of the two T-box factors into the two hypothesised classes, cell cycle dependent and independent regulation.

In addition, it would be very interesting to investigate the nutrient levels of human melanoma cells upon induction or depletion of the T-box factors in a metabolic study to further elaborate on their role in cancer homoeostasis. Especially the levels of nucleotides would be very interesting to explore due to the link to the onset of senescence upon depletion, a role TBX2 and TBX3 have been demonstrated to be involved in.

Finally, the determination of interacting proteins with TBX2 and TBX3 via mass spectrometry is already underway. The analysis of the results and subsequent integration with the genome-wide data of DNA binding and gene expression of the two T-box factors in the future will further unravel and corroborate regulated target genes and their role and function within the cellular signalling network.

References

Ackermann, T. F., Boini, K. M., Beier, N., Scholz, W., Fuchß, T., and Lang, F. EMD638683, a Novel SGK Inhibitor with Antihypertensive Potency. *Cellular Physiology and Biochemistry*, 28(1):137–146, 2011.

Acosta, J. C., O'Loghlen, A., Banito, A., Guijarro, M. V., Augert, A., Raguz, S., Fumagalli, M., Da Costa, M., Brown, C., Popov, N., Takatsu, Y., Melamed, J., d'Adda di Fagagna, F., Bernard, D., Hernando, E., and Gil, J. Chemokine signaling via the CXCR2 receptor reinforces senescence. *Cell*, 133(6):1006–1018, 2008.

Acosta, J. C., Banito, A., Wuestefeld, T., Georgilis, A., Janich, P., Morton, J. P., Athineos, D., Kang, T.-W., Lasitschka, F., Andrulis, M., Pascual, G., Morris, K. J., Khan, S., Jin, H., Dharmalingam, G., Snijders, A. P., Carroll, T., Capper, D., Pritchard, C., Inman, G. J., Longerich, T., Sansom, O. J., Benitah, S. A., Zender, L., and Gil, J. A complex secretory program orchestrated by the inflammasome controls paracrine senescence. *Nature Cell Biology*, 15(8):978–990, 2013.

Adams, J. M. and Cory, S. The Bcl-2 apoptotic switch in cancer development and therapy. *Oncogene*, 26(9):1324–1337, 2007.

Aguilera, A. and García-Muse, T. Causes of Genome Instability. *Annual Review of Genetics*, 47(1):1–32, 2013.

Ahler, E., Sullivan, W. J., Cass, A., Braas, D., York, A. G., Bensinger, S. J., Graeber, T. G., and Christofk, H. R. Doxycycline Alters Metabolism and Proliferation of Human Cell Lines. *PLoS ONE*, 8(5):e64561, 2013.

Aird, K., Zhang, G., Li, H., Tu, Z., Bitler, B., Garipov, A., Wu, H., Wei, Z., Wagner, S., Herlyn, M., and Zhang, R. Suppression of Nucleotide Metabolism Underlies the Establishment and Maintenance of Oncogene-Induced Senescence. *Cell Reports*, 3(4):1252–1265, 2013.

Albino, A. P., Le Strange, R., Oliff, A. I., Furth, M. E., and Old, L. J. Transforming ras genes from human melanoma: a manifestation of tumour heterogeneity? *Nature*, 308(5954):69–72, 1984.

Attwooll, C., Denchi, E. L., and Helin, K. The E2F family: specific functions and overlapping interests. *EMBO Journal*, 23(24):4709–4716, 2004.

Aziz, S. A., Davies, M., Pick, E., Zito, C., Jilaveanu, L., Camp, R. L., Rimm, D. L., Kluger, Y., and Kluger, H. M. Phosphatidylinositol-3-Kinase as a Therapeutic Target in Melanoma. *Clinical Cancer Research*, 15(9):3029–3036, 2009.

Baron, V., Adamson, E. D., Calogero, A., Ragona, G., and Mercola, D. The transcription factor Egr1 is a direct regulator of multiple tumor suppressors including TGF[beta]1, PTEN, p53, and fibronectin. *Cancer Gene Therapy*, 13 (2):115–124, 2005.

Beckett, D., Kovaleva, E., and Schatz, P. J. A minimal peptide substrate in biotin holoenzyme synthetase-catalyzed biotinylation. *Protein Science*, 8(4):921–929, 1999.

Bellacosa, A., Kumar, C. C., Di Cristofano, A., and Testa, J. R. Activation of AKT kinases in cancer: implications for therapeutic targeting. *Advances in Cancer Research*, 94:29–86, 2005.

Beltrami, A. P., Cesselli, D., and Beltrami, C. A. At the stem of youth and health. *Pharmacology & Therapeutics*, 129(1):3–20, 2011.

Ben-Porath, I. and Weinberg, R. A. The signals and pathways activating cellular senescence. *The International Journal of Biochemistry & Cell Biology*, 37(5): 961–976, 2005.

Bennett, D. C. Ultraviolet wavebands and melanoma initiation. *Pigment Cell and Melanoma Research*, 21(5):520–524, 2008.

Berger, M. F., Hodis, E., Heffernan, T. P., Deribe, Y. L., Lawrence, M. S., Protopopov, A., Ivanova, E., Watson, I. R., Nickerson, E., Ghosh, P., Zhang, H., Zeid, R., Ren, X., Cibulskis, K., Sivachenko, A. Y., Wagle, N., Sucker, A., Sougnez, C., Onofrio, R., Ambrogio, L., Auclair, D., Fennell, T., Carter, S. L., Drier, Y., Stojanov, P., Singer, M. A., Voet, D., Jing, R., Saksena, G., Barretina, J., Ramos, A. H., Pugh, T. J., Stransky, N., Parkin, M., Winckler, W., Mahan, S., Ardlie, K., Baldwin, J., Wargo, J., Schadendorf, D., Meyerson, M., Gabriel, S. B., Golub, T. R., Wagner, S. N., Lander, E. S., Getz, G., Chin, L., and Garraway, L. A. Melanoma genome sequencing reveals frequent PREX2 mutations. *Nature*, 485(7399):502–506, 2012.

Bertoli, C., Skotheim, J. M., and de Bruin, R. A. Control of cell cycle transcription during G1 and S phases. *Nature Reviews. Molecular Cell Biology*, 14(8):518–528, 2013.

Bhatia, S., Tykodi, S. S., and Thompson, J. A. Treatment of metastatic melanoma: an overview. *Oncology (Williston Park)*, 23(6):488–496, 2009.

Bilican, B. and Goding, C. R. Cell cycle regulation of the T-box transcription factor tbx2. *Experimental Cell Research*, 312(12):2358–2366, 2006.

Blasco, M. A. Telomeres and human disease: ageing, cancer and beyond. *Nature Reviews. Genetics*, 6(8):611–622, 2005.

Blobe, G. C., Schiemann, W. P., and Lodish, H. F. Role of Transforming Growth Factor β in Human Disease. *New England Journal of Medicine*, 342(18):1350–1358, 2000.

Bolanos-Garcia, V. M. Aurora kinases. *The International Journal of Biochemistry & Cell Biology*, 37(8):1572–1577, 2005.

Bollag, G., Hirth, P., Tsai, J., Zhang, J., Ibrahim, P. N., Cho, H., Spevak, W., Zhang, C., Zhang, Y., Habets, G., Burton, E. A., Wong, B., Tsang, G., West, B. L., Powell, B., Shellooe, R., Marimuthu, A., Nguyen, H., Zhang, K. Y., Artis, D. R., Schlessinger, J., Su, F., Higgins, B., Iyer, R., D'Andrea, K., Koehler, A., Stumm, M., Lin, P. S., Lee, R. J., Grippo, J., Puzanov, I., Kim, K. B., Ribas, A., McArthur, G. A., Sosman, J. A., Chapman, P. B., Flaherty, K. T., Xu, X., Nathanson, K. L., and Nolop, K. Clinical efficacy of a RAF inhibitor needs broad target blockade in BRAF-mutant melanoma. *Nature*, 467(7315):596–599, 2010.

Bollag, R. J., Siegfried, Z., Cebra-Thomas, J. A., Garvey, N., Davison, E. M., and Silver, L. M. An ancient family of embryonically expressed mouse genes sharing a conserved protein motif with the T locus. *Nature Genetics*, 7(3):383–389, 1994.

Bonnet, D. and Dick, J. E. Human acute myeloid leukemia is organized as a hierarchy that originates from a primitive hematopoietic cell. *Nature Medicine*, 3(7):730–737, 1997.

Bonvin, E., Falletta, P., Shaw, H., Delmas, V., and Goding, C. R. A Phosphatidylinositol 3-Kinase–Pax3 Axis Regulates Brn-2 Expression in Melanoma. *Molecular and Cellular Biology*, 32(22):4674–4683, 2012.

Borycki, A. G., Li, J., Jin, F., Emerson, C. P., and Epstein, J. A. Pax3 functions in cell survival and in pax7 regulation. *Development*, 126(8):1665–1674, 1999.

Bos, J. L. ras oncogenes in human cancer: a review. *Cancer Research*, 49(17): 4682–4689, 1989.

Boucher, P. D., Ostruszka, L. J., Murphy, P. J., and Shewach, D. S. Hydroxyurea significantly enhances tumor growth delay in vivo with herpes simplex virus thymidine kinase/ganciclovir gene therapy. *Gene Therapy*, 9(15):1023–1030, 2002.

Boya, P., Reggiori, F., and Codogno, P. Emerging regulation and functions of autophagy. *Nature Cell Biology*, 15(7):713–720, 2013.

Bruhn, M. A., Pearson, R. B., Hannan, R. D., and Sheppard, K. E. Second AKT: The rise of SGK in cancer signalling. *Growth Factors*, 28(6):394–408, 2010.

Brunet, A., Bonni, A., Zigmond, M. J., Lin, M. Z., Juo, P., Hu, L. S., Anderson, M. J., Arden, K. C., Blenis, J., and Greenberg, M. E. Akt promotes cell survival by phosphorylating and inhibiting a Forkhead transcription factor. *Cell*, 96(6): 857–868, 1999.

Brunet, A., Park, J., Tran, H., Hu, L. S., Hemmings, B. A., and Greenberg, M. E. Protein Kinase SGK Mediates Survival Signals by Phosphorylating the Forkhead Transcription Factor FKHRL1 (FOXO3a). *Molecular and Cellular Biology*, 21 (3):952–965, 2001.

Buchkovich, K., Duffy, L. A., and Harlow, E. The retinoblastoma protein is phosphorylated during specific phases of the cell cycle. *Cell*, 58(6):1097–1105, 1989.

Burke, J. R., Deshong, A. J., Pelton, J. G., and Rubin, S. M. Phosphorylation-induced Conformational Changes in the Retinoblastoma Protein Inhibit E2F Transactivation Domain Binding. *Journal of Biological Chemistry*, 285(21): 16286–16293, 2010.

Burrell, R. A., McGranahan, N., Bartek, J., and Swanton, C. The causes and consequences of genetic heterogeneity in cancer evolution. *Nature*, 501(7467): 338–345, 2013.

Burri, P. H., Hlushchuk, R., and Djonov, V. Intussusceptive angiogenesis: Its emergence, its characteristics, and its significance. *Developmental Dynamics*, 231(3):474–488, 2004.

Cai, C. L., Zhou, W., Yang, L., Bu, L., Qyang, Y., Zhang, X., Li, X., Rosenfeld, M. G., Chen, J., and Evans, S. T-box genes coordinate regional rates of prolif-

eration and regional specification during cardiogenesis. *Development*, 132(10): 2475–2487, 2005.

Campisi, J. The biology of replicative senescence. *European Journal of Cancer*, 33(5):703–709, 1997.

Campisi, J. Senescent cells, tumor suppression, and organismal aging: good citizens, bad neighbors. *Cell*, 120(4):513–522, 2005.

Campisi, J. and d'Adda di Fagagna, F. Cellular senescence: when bad things happen to good cells. *Nature Reviews. Molecular Cell Biology*, 8(9):729–740, 2007.

Cargnello, M. and Roux, P. P. Activation and Function of the MAPKs and Their Substrates, the MAPK-Activated Protein Kinases. *Microbiology and Molecular Biology Reviews*, 75(1):50–83, 2011.

Carlson, H., Ota, S., Campbell, C. E., and Hurlin, P. J. A dominant repression domain in Tbx3 mediates transcriptional repression and cell immortalization: relevance to mutations in Tbx3 that cause ulnar-mammary syndrome. *Human Molecular Genetics*, 10(21):2403–2413, 2001.

Carmeliet, P. and Jain, R. K. Angiogenesis in cancer and other diseases. *Nature*, 407(6801):249–257, 2000.

Carreira, S., Dexter, T. J., Yavuzer, U., Easty, D. J., and Goding, C. R. Brachyury-related transcription factor Tbx2 and repression of the melanocyte-specific TRP-1 promoter. *Molecular and Cellular Biology*, 18(9):5099–5108, 1998.

Carreira, S., Liu, B. G., and Goding, C. R. The gene encoding the T-box factor Tbx2 is a target for the microphthalmia-associated transcription factor in melanocytes. *Journal of Biological Chemistry*, 275(29):21920–21927, 2000.

Carreira, S., Goodall, J., Denat, L., Rodriguez, M., Nuciforo, P., Hoek, K. S., Testori, A., Larue, L., and Goding, C. R. Mitf regulation of Dia1 controls melanoma proliferation and invasiveness. *Genes and Development*, 20(24):3426–3439, 2006.

Castellano, E. and Downward, J. RAS Interaction with PI3K: More Than Just Another Effector Pathway. *Genes & Cancer*, 2(3):261–274, 2011.

Chen, D., Zhang, J., Li, M., Rayburn, E. R., Wang, H., and Zhang, R. RYBP stabilizes p53 by modulating MDM2. *EMBO Reports*, 10(2):166–172, 2009.

Chen, Q. M., Bartholomew, J. C., Campisi, J., Acosta, M., Reagan, J. D., and Ames, B. N. Molecular analysis of H2O2-induced senescent-like growth arrest in normal human fibroblasts: p53 and Rb control G1 arrest but not cell replication. *Biochemical Journal*, 332 (Pt 1):43–50, 1998.

Ciccia, A. and Elledge, S. J. The DNA Damage Response: Making It Safe to Play with Knives. *Molecular Cell*, 40(2):179–204, 2010.

Clark, J., W. H., Elder, D. E., Guerry, D. t., Epstein, M. N., Greene, M. H., and Van Horn, M. A study of tumor progression: the precursor lesions of superficial spreading and nodular melanoma. *Human Pathology*, 15(12):1147–1165, 1984.

Clarke, H. J., Chambers, J. E., Liniker, E., and Marciniak, S. J. Endoplasmic reticulum stress in malignancy. *Cancer Cell*, 25(5):563–573, 2014.

Coll, M., Seidman, J. G., and Müller, C. W. Structure of the DNA-Bound T-Box Domain of Human TBX3, a Transcription Factor Responsible for Ulnar-Mammary Syndrome. *Structure (London, England : 1993)*, 10(3):343–356, 2002.

Collado, M. and Serrano, M. Senescence in tumours: evidence from mice and humans. *Nature Reviews. Cancer*, 10(1):51–57, 2010.

Commisso, C., Davidson, S. M., Soydaner-Azeloglu, R. G., Parker, S. J., Kamphorst, J. J., Hackett, S., Grabocka, E., Nofal, M., Drebin, J. A., Thompson, C. B., Rabinowitz, J. D., Metallo, C. M., Vander Heiden, M. G., and Bar-Sagi, D. Macropinocytosis of protein is an amino acid supply route in Ras-transformed cells. *Nature*, 497(7451):633–637, 2013.

Coppe, J. P., Patil, C. K., Rodier, F., Sun, Y., Munoz, D. P., Goldstein, J., Nelson, P. S., Desprez, P. Y., and Campisi, J. Senescence-associated secretory phenotypes reveal cell-nonautonomous functions of oncogenic RAS and the p53 tumor suppressor. *PLoS Biology*, 6(12):2853–2868, 2008.

Corre, S. and Galibert, M. D. Upstream stimulating factors: highly versatile stress-responsive transcription factors. *Pigment Cell Research*, 18(5):337–348, 2005.

Coulonval, K., Kooken, H., and Roger, P. P. Coupling of T161 and T14 phosphorylations protects cyclin B–CDK1 from premature activation. *Molecular Biology of the Cell*, 22(21):3971–3985, 2011.

Courtois-Cox, S., Jones, S. L., and Cichowski, K. Many roads lead to oncogene-induced senescence. *Oncogene*, 27(20):2801–2809, 2008.

Coussens, L. M. and Werb, Z. Inflammation and cancer. *Nature*, 420(6917):860–867, 2002.

Croce, C. M. Oncogenes and Cancer. *New England Journal of Medicine*, 358(5): 502–511, 2008.

Curtin, J. A., Stark, M. S., Pinkel, D., Hayward, N. K., and Bastian, B. C. PI3-Kinase Subunits Are Infrequent Somatic Targets in Melanoma. *Journal of Investigative Dermatology*, 126(7):1660–1663, 2006.

Dang, C. V. Links between metabolism and cancer. *Genes and Development*, 26 (9):877–890, 2012.

Dankort, D., Curley, D. P., Cartlidge, R. A., Nelson, B., Karnezis, A. N., Damsky, J., W. E., You, M. J., DePinho, R. A., McMahon, M., and Bosenberg, M. Braf(V600E) cooperates with Pten loss to induce metastatic melanoma. *Nature Genetics*, 41(5):544–552, 2009.

Davenport, T. G., Jerome-Majewska, L. A., and Papaioannou, V. E. Mammary gland, limb and yolk sac defects in mice lacking Tbx3, the gene mutated in human ulnar mammary syndrome. *Development*, 130(10):2263–2273, 2003.

Davies, H., Bignell, G. R., Cox, C., Stephens, P., Edkins, S., Clegg, S., Teague, J., Woffendin, H., Garnett, M. J., Bottomley, W., Davis, N., Dicks, E., Ewing, R., Floyd, Y., Gray, K., Hall, S., Hawes, R., Hughes, J., Kosmidou, V., Menzies, A., Mould, C., Parker, A., Stevens, C., Watt, S., Hooper, S., Wilson, R., Jayatilake, H., Gusterson, B. A., Cooper, C., Shipley, J., Hargrave, D., Pritchard-Jones, K., Maitland, N., Chenevix-Trench, G., Riggins, G. J., Bigner, D. D., Palmieri, G.,

Cossu, A., Flanagan, A., Nicholson, A., Ho, J. W., Leung, S. Y., Yuen, S. T., Weber, B. L., Seigler, H. F., Darrow, T. L., Paterson, H., Marais, R., Marshall, C. J., Wooster, R., Stratton, M. R., and Futreal, P. A. Mutations of the BRAF gene in human cancer. *Nature*, 417(6892):949–954, 2002.

De Strooper, B., Annaert, W., Cupers, P., Saftig, P., Craessaerts, K., Mumm, J. S., Schroeter, E. H., Schrijvers, V., Wolfe, M. S., Ray, W. J., Goate, A., and Kopan, R. A presenilin-1-dependent [gamma]-secretase-like protease mediates release of Notch intracellular domain. *Nature*, 398(6727):518–522, 1999.

de Visser, K. E., Eichten, A., and Coussens, L. M. Paradoxical roles of the immune system during cancer development. *Nature Reviews. Cancer*, 6(1):24–37, 2006.

Debacq-Chainiaux, F., Erusalimsky, J. D., Campisi, J., and Toussaint, O. Protocols to detect senescence-associated beta-galactosidase (SA-beta gal) activity, a biomarker of senescent cells in culture and in vivo. *Nature Protocols*, 4(12): 1798–1806, 2009.

Dhillon, A. S., Hagan, S., Rath, O., and Kolch, W. MAP kinase signalling pathways in cancer. *Oncogene*, 26(22):3279–3290, 2007.

Di Micco, R., Fumagalli, M., Cicalese, A., Piccinin, S., Gasparini, P., Luise, C., Schurra, C., Garre, M., Nuciforo, P. G., Bensimon, A., Maestro, R., Pelicci, P. G., and d'Adda di Fagagna, F. Oncogene-induced senescence is a DNA damage response triggered by DNA hyper-replication. *Nature*, 444(7119):638–642, 2006.

Dimri, G. P., Lee, X., Basile, G., Acosta, M., Scott, G., Roskelley, C., Medrano, E. E., Linskens, M., Rubelj, I., and Pereira-Smith, O. A biomarker that identifies

senescent human cells in culture and in aging skin in vivo. *Proceedings of the National Academy of Sciences*, 92(20):9363–9367, 1995.

Dingwall, C., Robbins, J., Dilworth, S. M., Roberts, B., and Richardson, W. D. The nucleoplasmin nuclear location sequence is larger and more complex than that of SV-40 large T antigen. *Journal of Cell Biology*, 107(3):841–849, 1988.

Dittmann, A., Werner, T., Chung, C.-W., Savitski, M. M., Fälth Savitski, M., Grandi, P., Hopf, C., Lindon, M., Neubauer, G., Prinjha, R. K., Bantscheff, M., and Drewes, G. The Commonly Used PI3-Kinase Probe LY294002 Is an Inhibitor of BET Bromodomains. *ACS Chemical Biology*, 9(2):495–502, 2014.

Douglas, N. C. and Papaioannou, V. E. The T-box Transcription Factors TBX2 and TBX3 in Mammary Gland Development and Breast Cancer. *Journal of Mammary Gland Biology and Neoplasia*, 18(2):143–147, 2013.

Draviam, V. M., Orrechia, S., Lowe, M., Pardi, R., and Pines, J. The Localization of Human Cyclins B1 and B2 Determines Cdk1 Substrate Specificity and Neither Enzyme Requires Mek to Disassemble the Golgi Apparatus. *Journal of Cell Biology*, 152(5):945–958, 2001.

Duboc, V. and Logan, M. P. Regulation of limb bud initiation and limb-type morphology. *Developmental Dynamics*, 240(5):1017–1027, 2011.

Dvorak, H. F. Tumors: wounds that do not heal. Similarities between tumor stroma generation and wound healing. *New England Journal of Medicine*, 315 (26):1650–1659, 1986.

Egeblad, M., Nakasone, E. S., and Werb, Z. Tumors as organs: complex tissues that interface with the entire organism. *Developmental Cell*, 18(6):884–901, 2010.

Einhauer, A. and Jungbauer, A. The FLAG™ peptide, a versatile fusion tag for the purification of recombinant proteins. *Journal of Biochemical and Biophysical Methods*, 49(1–3):455–465, 2001.

Elliott, R. L. and Blobe, G. C. Role of Transforming Growth Factor Beta in Human Cancer. *Journal of Clinical Oncology*, 23(9):2078–2093, 2005.

Farley, J., Gray, K., Nycum, L., Prentice, M., Birrer, M. J., and Jakowlew, S. B. Endocervical Cancer Is Associated with an Increase in the Ligands and Receptors for Transforming Growth Factor-β and a Contrasting Decrease in p27Kip1. *Gynecologic Oncology*, 78(2):113–122, 2000.

Fedorenko, I. V., Gibney, G. T., Sondak, V. K., and Smalley, K. S. Beyond BRAF: where next for melanoma therapy? *British Journal of Cancer*, 112(2):217–226, 2015.

Ferlay, J., Shin, H., Bray, F., Forman, D., Mathers, C., and Parkin, D. GLOBOCAN 2008 v2.0, Cancer Incidence and Mortality Worldwide: IARC CancerBase No. 10 [Internet], 29/10/2012 2010.

Fernald, K. and Kurokawa, M. Evading apoptosis in cancer. *Trends in Cell Biology*, 23(12):620–633, 2013.

Fidler, I. J. The pathogenesis of cancer metastasis: the 'seed and soil' hypothesis revisited. *Nature Reviews. Cancer*, 3(6):453–458, 2003.

Field, J., Nikawa, J., Broek, D., MacDonald, B., Rodgers, L., Wilson, I. A., Lerner, R. A., and Wigler, M. Purification of a RAS-responsive adenylyl cyclase complex from Saccharomyces cerevisiae by use of an epitope addition method. *Molecular and Cellular Biology*, 8(5):2159–2165, 1988.

Finn, O. J. Immuno-oncology: understanding the function and dysfunction of the immune system in cancer. *Annals of Oncology*, 23 Suppl 8:viii6–9, 2012.

Firestone, G. L., Giampaolo, J. R., and O'Keeffe, B. A. Stimulus-Dependent Regulation of Serum and Glucocorticoid Inducible Protein Kinase (SGK) Transcription, Subcellular Localization and Enzymatic Activity. *Cellular Physiology and Biochemistry*, 13(1):1–12, 2003.

Flaherty, K. T., Puzanov, I., Kim, K. B., Ribas, A., McArthur, G. A., Sosman, J. A., O'Dwyer, P. J., Lee, R. J., Grippo, J. F., Nolop, K., and Chapman, P. B. Inhibition of mutated, activated BRAF in metastatic melanoma. *New England Journal of Medicine*, 363(9):809–819, 2010.

Flaherty, K. T., Infante, J. R., Daud, A., Gonzalez, R., Kefford, R. F., Sosman, J., Hamid, O., Schuchter, L., Cebon, J., Ibrahim, N., Kudchadkar, R., Burris, H. A., Falchook, G., Algazi, A., Lewis, K., Long, G. V., Puzanov, I., Lebowitz, P., Singh, A., Little, S., Sun, P., Allred, A., Ouellet, D., Kim, K. B., Patel, K., and Weber, J. Combined BRAF and MEK Inhibition in Melanoma with BRAF V600 Mutations. *New England Journal of Medicine*, 367(18):1694–1703, 2012a.

Flaherty, K. T., Robert, C., Hersey, P., Nathan, P., Garbe, C., Milhem, M., Demidov, L. V., Hassel, J. C., Rutkowski, P., Mohr, P., Dummer, R., Trefzer, U., Larkin, J. M., Utikal, J., Dreno, B., Nyakas, M., Middleton, M. R., Becker, J. C.,

Casey, M., Sherman, L. J., Wu, F. S., Ouellet, D., Martin, A. M., Patel, K., Schadendorf, D., and Group, M. S. Improved survival with MEK inhibition in BRAF-mutated melanoma. *New England Journal of Medicine*, 367(2):107–114, 2012b.

Flier, J. S., Mueckler, M. M., Usher, P., and Lodish, H. F. Elevated levels of glucose transport and transporter messenger RNA are induced by ras or src oncogenes. *Science*, 235(4795):1492–1495, 1987.

Fogh, J., Fogh, J. M., and Orfeo, T. One Hundred and Twenty-Seven Cultured Human Tumor Cell Lines Producing Tumors in Nude Mice. *Journal of the National Cancer Institute*, 59(1):221–226, 1977.

Folkes, A. J., Ahmadi, K., Alderton, W. K., Alix, S., Baker, S. J., Box, G., Chuckowree, I. S., Clarke, P. A., Depledge, P., Eccles, S. A., Friedman, L. S., Hayes, A., Hancox, T. C., Kugendradas, A., Lensun, L., Moore, P., Olivero, A. G., Pang, J., Patel, S., Pergl-Wilson, G. H., Raynaud, F. I., Robson, A., Saghir, N., Salphati, L., Sohal, S., Ultsch, M. H., Valenti, M., Wallweber, H. J. A., Wan, N. C., Wiesmann, C., Workman, P., Zhyvoloup, A., Zvelebil, M. J., and Shuttleworth, S. J. The Identification of 2-(1H-Indazol-4-yl)-6-(4-methanesulfonyl-piperazin-1-ylmethyl)-4-morpholin-4-yl-thieno[3,2-d]pyrimidine (GDC-0941) as a Potent, Selective, Orally Bioavailable Inhibitor of Class I PI3 Kinase for the Treatment of Cancer†. *Journal of Medicinal Chemistry*, 51(18):5522–5532, 2008.

Frippiat, C., Chen, Q. M., Remacle, J., and Toussaint, O. Cell cycle regulation in H(2)O(2)-induced premature senescence of human diploid fibroblasts and regu-

latory control exerted by the papilloma virus E6 and E7 proteins. *Experimental Gerontology*, 35(6-7):733–745, 2000.

Fruman, D. A. and Rommel, C. PI3K and cancer: lessons, challenges and opportunities. *Nature Reviews. Drug Discovery*, 13(2):140–156, 2014.

Fu, Y.-M., Zhang, H., Ding, M., Li, Y.-Q., Fu, X., Yu, Z.-X., and Meadows, G. G. Selective amino acid restriction targets mitochondria to induce apoptosis of androgen-independent prostate cancer cells. *Journal of Cellular Physiology*, 209(2):522–534, 2006.

Galibert, M. D., Carreira, S., and Goding, C. R. The Usf-1 transcription factor is a novel target for the stress-responsive p38 kinase and mediates UV-induced Tyrosinase expression. *EMBO Journal*, 20(17):5022–5031, 2001.

Gao, T., Furnari, F., and Newton, A. C. PHLPP: A Phosphatase that Directly Dephosphorylates Akt, Promotes Apoptosis, and Suppresses Tumor Growth. *Molecular Cell*, 18(1):13–24, 2005.

Gharbi, S. I., Zvelebil, M. J., Shuttleworth, S. J., Hancox, T., Saghir, N., Timms, J. F., and Waterfield, M. D. Exploring the specificity of the PI3K family inhibitor LY294002. *Biochemical Journal*, 404(1):15–21, 2007.

Gillies, R. J., Robey, I., and Gatenby, R. A. Causes and consequences of increased glucose metabolism of cancers. *Journal of Nuclear Medicine*, 49 Suppl 2:24S–42S, 2008.

Gómez-Martín, D., Díaz-Zamudio, M., Galindo-Campos, M., and Alcocer-Varela, J. Early growth response transcription factors and the modulation of immune

response: Implications towards autoimmunity. *Autoimmunity Reviews*, 9(6): 454–458, 2010.

Goel, V. K., Ibrahim, N., Jiang, G., Singhal, M., Fee, S., Flotte, T., Westmoreland, S., Haluska, F. S., Hinds, P. W., and Haluska, F. G. Melanocytic nevus-like hyperplasia and melanoma in transgenic BRAFV600E mice. *Oncogene*, 28(23): 2289–2298, 2009.

Goldmann, E. The Growth of Malignant Disease in Man and the Lower Animals. *The Lancet*, 170(4392):1236–1240, 1907.

Hahm, S., Mizuno, T. M., Wu, T. J., Wisor, J. P., Priest, C. A., Kozak, C. A., Boozer, C. N., Peng, B., McEvoy, R. C., Good, P., Kelley, K. A., Takahashi, J. S., Pintar, J. E., Roberts, J. L., Mobbs, C. V., and Salton, S. R. J. Targeted Deletion of the Vgf Gene Indicates that the Encoded Secretory Peptide Precursor Plays a Novel Role in the Regulation of Energy Balance. *Neuron*, 23(3):537–548, 1999.

Hanahan, D. and Weinberg, R. A. The hallmarks of cancer. *Cell*, 100(1):57–70, 2000.

Hanahan, D. and Weinberg, R. A. Hallmarks of cancer: the next generation. *Cell*, 144(5):646–674, 2011.

Hansen, K. H., Bracken, A. P., Pasini, D., Dietrich, N., Gehani, S. S., Monrad, A., Rappsilber, J., Lerdrup, M., and Helin, K. A model for transmission of the H3K27me3 epigenetic mark. *Nature Cell Biology*, 10(11):1291–1300, 2008.

Hardie, D. G., Ross, F. A., and Hawley, S. A. AMPK: a nutrient and energy sensor that maintains energy homeostasis. *Nature Reviews. Molecular Cell Biology*, 13 (4):251–262, 2012.

Harley, C. B., Futcher, A. B., and Greider, C. W. Telomeres shorten during ageing of human fibroblasts. *Nature*, 345(6274):458–460, 1990.

Harrelson, Z., Kelly, R. G., Goldin, S. N., Gibson-Brown, J. J., Bollag, R. J., Silver, L. M., and Papaioannou, V. E. Tbx2 is essential for patterning the atrioventricular canal and for morphogenesis of the outflow tract during heart development. *Development*, 131(20):5041–5052, 2004.

Haugsten, E. M., Wiedlocha, A., Olsnes, S., and Wesche, J. Roles of Fibroblast Growth Factor Receptors in Carcinogenesis. *Molecular Cancer Research*, 8(11): 1439–1452, 2010.

Hayflick, L. The Limited in Vitro Lifetime of Human Diploid Cell Strains. *Exp. Cell. Res.*, 37:614–636., 1965.

Hayward, N. K. Genetics of melanoma predisposition. *Oncogene*, 22(20):3053–3062, 2003.

He, S.-J., Stevens, G., Braithwaite, A. W., and Eccles, M. R. Transfection of melanoma cells with antisense PAX3 oligonucleotides additively complements cisplatin-induced cytotoxicity. *Molecular Cancer Therapeutics*, 4(6):996–1003, 2005.

Heinrich, P. C., Behrmann, I., Haan, S., Hermanns, H. M., Muller-Newen, G.,

and Schaper, F. Principles of interleukin (IL)-6-type cytokine signalling and its regulation. *Biochemical Journal*, 374(Pt 1):1–20, 2003.

Hemmings, B. A. and Restuccia, D. F. PI3K-PKB/Akt Pathway. *Cold Spring Harbor Perspectives in Biology*, 4(9):a011189, 2012.

Hillen, F. and Griffioen, A. W. Tumour vascularization: sprouting angiogenesis and beyond. *Cancer and Metastasis Reviews*, 26(3-4):489–502, 2007.

Hirai, H., Sootome, H., Nakatsuru, Y., Miyama, K., Taguchi, S., Tsujioka, K., Ueno, Y., Hatch, H., Majumder, P. K., Pan, B.-S., and Kotani, H. MK-2206, an Allosteric Akt Inhibitor, Enhances Antitumor Efficacy by Standard Chemotherapeutic Agents or Molecular Targeted Drugs In vitro and In vivo. *Molecular Cancer Therapeutics*, 9(7):1956–1967, 2010.

Hirata, E., Girotti, M. R., Viros, A., Hooper, S., Spencer-Dene, B., Matsuda, M., Larkin, J., Marais, R., and Sahai, E. Intravital Imaging Reveals How BRAF Inhibition Generates Drug-Tolerant Microenvironments with High Integrin beta1/FAK Signaling. *Cancer Cell*, 27(4):574–588, 2015.

Ho, A. and Dowdy, S. F. Regulation of G1 cell-cycle progression by oncogenes and tumor suppressor genes. *Current Opinion in Genetics and Development*, 12(1): 47–52, 2002.

Hoek, K. S. and Goding, C. R. Cancer stem cells versus phenotype-switching in melanoma. *Pigment Cell and Melanoma Research*, 23(6):746–759, 2010.

Hoek, K. S., Schlegel, N. C., Brafford, P., Sucker, A., Ugurel, S., Kumar, R., Weber, B. L., Nathanson, K. L., Phillips, D. J., Herlyn, M., Schadendorf, D.,

and Dummer, R. Metastatic potential of melanomas defined by specific gene expression profiles with no BRAF signature. *Pigment Cell Research*, 19(4):290–302, 2006.

Holderfield, M., Deuker, M. M., McCormick, F., and McMahon, M. Targeting RAF kinases for cancer therapy: BRAF-mutated melanoma and beyond. *Nature Reviews. Cancer*, 14(7):455–467, 2014.

Hollstein, M., Sidransky, D., Vogelstein, B., and Harris, C. C. p53 mutations in human cancers. *Science*, 253(5015):49–53, 1991.

Holmes, K., Roberts, O. L., Thomas, A. M., and Cross, M. J. Vascular endothelial growth factor receptor-2: structure, function, intracellular signalling and therapeutic inhibition. *Cellular Signalling*, 19(10):2003–2012, 2007.

Hoogaars, W. M., Barnett, P., Rodriguez, M., Clout, D. E., Moorman, A. F., Goding, C. R., and Christoffels, V. M. TBX3 and its splice variant TBX3 + exon 2a are functionally similar. *Pigment Cell and Melanoma Research*, 21(3): 379–387, 2008.

Huang, D. W., Sherman, B. T., and Lempicki, R. A. Bioinformatics enrichment tools: paths toward the comprehensive functional analysis of large gene lists. *Nucleic Acids Research*, 37(1):1–13, 2009a.

Huang, D. W., Sherman, B. T., and Lempicki, R. A. Systematic and integrative analysis of large gene lists using DAVID bioinformatics resources. *Nature Protocols*, 4(1):44–57, 2009b.

Huang, J., Dibble, C. C., Matsuzaki, M., and Manning, B. D. The TSC1-TSC2 Complex Is Required for Proper Activation of mTOR Complex 2. *Molecular and Cellular Biology*, 28(12):4104–4115, 2008.

Igney, F. H. and Krammer, P. H. Immune escape of tumors: apoptosis resistance and tumor counterattack. *Journal of Leukocyte Biology*, 71(6):907–920, 2002.

Ikushima, H. and Miyazono, K. TGFβ signalling: a complex web in cancer progression. *Nature Reviews. Cancer*, 10(6):415–424, 2010.

Jacobs, J. J., Keblusek, P., Robanus-Maandag, E., Kristel, P., Lingbeek, M., Nederlof, P. M., van Welsem, T., van de Vijver, M. J., Koh, E. Y., Daley, G. Q., and van Lohuizen, M. Senescence bypass screen identifies TBX2, which represses Cdkn2a (p19(ARF)) and is amplified in a subset of human breast cancers. *Nature Genetics*, 26(3):291–299, 2000.

Jerant, A. F., Johnson, J. T., Sheridan, C. D., and Caffrey, T. J. Early detection and treatment of skin cancer. *American Family Physician*, 62(2):357–368, 375–356, 381–352, 2000.

Jiricny, J. The multifaceted mismatch-repair system. *Nature Reviews. Molecular Cell Biology*, 7(5):335–346, 2006.

Johansson, P., Pavey, S., and Hayward, N. Confirmation of a BRAF mutation-associated gene expression signature in melanoma. *Pigment Cell Research*, 20 (3):216–221, 2007.

Johnson, D. B., Peng, C., and Sosman, J. A. Nivolumab in melanoma: latest

evidence and clinical potential. *Therapeutic Advances in Medical Oncology*, 7 (2):97–106, 2015.

Jonsson, G., Dahl, C., Staaf, J., Sandberg, T., Bendahl, P. O., Ringner, M., Guldberg, P., and Borg, A. Genomic profiling of malignant melanoma using tiling-resolution arrayCGH. *Oncogene*, 26(32):4738–4748, 2007.

Joshi, N. A. and Fass, J. N. Sickle: A sliding-window, adaptive, quality-based trimming tool for FastQ files, 2011.

Kalderon, D., Roberts, B. L., Richardson, W. D., and Smith, A. E. A short amino acid sequence able to specify nuclear location. *Cell*, 39(3, Part 2):499–509, 1984.

Kamaraju, A. K., Bertolotto, C., Chebath, J., and Revel, M. Pax3 Down-regulation and Shut-off of Melanogenesis in Melanoma B16/F10.9 by Interleukin-6 Receptor Signaling. *Journal of Biological Chemistry*, 277(17):15132–15141, 2002.

Kim, B.-j. and Forbes, N. S. Single-cell analysis demonstrates how nutrient deprivation creates apoptotic and quiescent cell populations in tumor cylindroids. *Biotechnology and Bioengineering*, 101(4):797–810, 2008.

King, M., Arnold, J. S., Shanske, A., and Morrow, B. E. T-genes and limb bud development. *American Journal of Medical Genetics. Part A*, 140(13):1407–1413, 2006.

Kispert, A. and Herrmann, B. G. The Brachyury gene encodes a novel DNA-binding protein. *EMBO Journal*, 12:3211–3220, 1993.

Kletsas, D., Stathakos, D., Sorrentino, V., and Philipson, L. The Growth-Inhibitory Block of TGF-β Is Located Close to the G1/S Border in the Cell Cycle. *Experimental Cell Research*, 217(2):477–483, 1995.

Knudson, A. Hereditary cancer: Two hits revisited. *Journal of Cancer Research and Clinical Oncology*, 122(3):135–140, 1996.

Knudson, A. G. Mutation and cancer: statistical study of retinoblastoma. *Proceedings of the National Academy of Sciences of the United States of America*, 68(4):820–823, 1971.

Kobayashi, T. and Cohen, P. Activation of serum- and glucocorticoid-regulated protein kinase by agonists that activate phosphatidylinositide 3-kinase is mediated by 3-phosphoinositide-dependent protein kinase-1 (PDK1) and PDK2. *Biochemical Journal*, 339 (Pt 2):319–328, 1999.

Kobayashi, T., Deak, M., Morrice, N., and Cohen, P. Characterization of the structure and regulation of two novel isoforms of serum- and glucocorticoid-induced protein kinase. *Biochemical Journal*, 344 Pt 1:189–197, 1999.

Kollareddy, M., Zheleva, D., Dzubak, P., Brahmkshatriya, P. S., Lepsik, M., and Hajduch, M. Aurora kinase inhibitors: Progress towards the clinic. *Investigational New Drugs*, 30(6):2411–2432, 2012.

Kong, D., Dan, S., Yamazaki, K., and Yamori, T. Inhibition profiles of phosphatidylinositol 3-kinase inhibitors against PI3K superfamily and human cancer cell line panel JFCR39. *European Journal of Cancer*, 46(6):1111–1121, 2010.

Korc, M., Chandrasekar, B., Yamanaka, Y., Friess, H., Buchier, M., and Beger, H. G. Overexpression of the epidermal growth factor receptor in human pancreatic cancer is associated with concomitant increases in the levels of epidermal growth factor and transforming growth factor alpha. *The Journal of Clinical Investigation*, 90(4):1352–1360, 1992.

Krones-Herzig, A., Mittal, S., Yule, K., Liang, H., English, C., Urcis, R., Soni, T., Adamson, E. D., and Mercola, D. Early Growth Response 1 Acts as a Tumor Suppressor In vivo and In vitro via Regulation of p53. *Cancer Research*, 65(12): 5133–5143, 2005.

Krtolica, A., Parrinello, S., Lockett, S., Desprez, P.-Y., and Campisi, J. Senescent fibroblasts promote epithelial cell growth and tumorigenesis: A link between cancer and aging. *Proceedings of the National Academy of Sciences*, 98(21): 12072–12077, 2001.

Kubic, J. D., Young, K. P., Plummer, R. S., Ludvik, A. E., and Lang, D. Pigmentation PAX-ways: the role of Pax3 in melanogenesis, melanocyte stem cell maintenance, and disease. *Pigment Cell and Melanoma Research*, 21(6):627–645, 2008.

Kuilman, T., Michaloglou, C., Vredeveld, L. C., Douma, S., van Doorn, R., Desmet, C. J., Aarden, L. A., Mooi, W. J., and Peeper, D. S. Oncogene-induced senescence relayed by an interleukin-dependent inflammatory network. *Cell*, 133 (6):1019–1031, 2008.

Kuilman, T., Michaloglou, C., Mooi, W. J., and Peeper, D. S. The essence of senescence. *Genes and Development*, 24(22):2463–2479, 2010.

Kunz, B. A. Mutagenesis and deoxyribonucleotide pool imbalance. *Mutation Research/Fundamental and Molecular Mechanisms of Mutagenesis*, 200(1–2): 133–147, 1988.

Kurz, D. J., Decary, S., Hong, Y., and Erusalimsky, J. D. Senescence-associated (beta)-galactosidase reflects an increase in lysosomal mass during replicative ageing of human endothelial cells. *Journal of Cell Science*, 113(20):3613–3622, 2000.

Labib, K. and Hodgson, B. Replication fork barriers: pausing for a break or stalling for time? *EMBO Reports*, 8(4):346–353, 2007.

Lane, D. P. Cancer. p53, guardian of the genome. *Nature*, 358(6381):15–16, 1992.

Lang, D., Lu, M. M., Huang, L., Engleka, K. A., Zhang, M., Chu, E. Y., Lipner, S., Skoultchi, A., Millar, S. E., and Epstein, J. A. Pax3 functions at a nodal point in melanocyte stem cell differentiation. *Nature*, 433(7028):884–887., 2005.

Langmead, B. and Salzberg, S. L. Fast gapped-read alignment with Bowtie 2. *Nature Methods*, 9(4):357–359, 2012.

Lanigan, F., Geraghty, J. G., and Bracken, A. P. Transcriptional regulation of cellular senescence. *Oncogene*, 30(26):2901–2911, 2011.

Larue, L. and Bellacosa, A. Epithelial-mesenchymal transition in development and cancer: role of phosphatidylinositol 3' kinase/AKT pathways. *Oncogene*, 24(50):7443–7454, 2005.

Lee, C.-C., Putnam, A. J., Miranti, C. K., Gustafson, M., Wang, L.-M., Vande Woude, G. F., and Gao, C.-F. Overexpression of sprouty 2 inhibits

HGF//SF-mediated cell growth, invasion, migration, and cytokinesis. *Oncogene*, 23(30):5193–5202, 2004.

Li, J., Weinberg, M. S., Zerbini, L., and Prince, S. The oncogenic TBX3 is a downstream target and mediator of the TGF-β1 signaling pathway. *Molecular Biology of the Cell*, 24(22):3569–3576, 2013.

Li, J., Ballim, D., Rodriguez, M., Cui, R., Goding, C. R., Teng, H., and Prince, S. The Anti-proliferative Function of the TGF-β1 Signaling Pathway Involves the Repression of the Oncogenic TBX2 by Its Homologue TBX3. *Journal of Biological Chemistry*, 289(51):35633–35643, 2014.

Liebermann, D. A. and Hoffman, B. Myeloid differentiation (MyD)/growth arrest DNA damage (GADD) genes in tumor suppression, immunity and inflammation. *Leukemia*, 16(4):527–541, 2002.

Lieberthal, W., Menza, S. A., and Levine, J. S. Graded ATP depletion can cause necrosis or apoptosis of cultured mouse proximal tubular cells. *American Journal of Physiology - Renal Physiology*, 274(2):F315–F327, 1998.

Lingbeek, M. E., Jacobs, J. J., and van Lohuizen, M. The T-box repressors TBX2 and TBX3 specifically regulate the tumor suppressor gene p14ARF via a variant T-site in the initiator. *Journal of Biological Chemistry*, 277(29):26120–26127, 2002.

Liou, G. Y. and Storz, P. Reactive oxygen species in cancer. *Free Radical Research*, 44(5):479–496, 2010.

Liu, F., Cao, J., Lv, J., Dong, L., Pier, E., Xu, G. X., Wang, R.-a., Xu, Z., Goding, C., and Cui, R. TBX2 expression is regulated by PAX3 in the melanocyte lineage. *Pigment Cell and Melanoma Research*, 26(1):67–77, 2013.

Liu, P., Cheng, H., Roberts, T. M., and Zhao, J. J. Targeting the phosphoinositide 3-kinase pathway in cancer. *Nature Reviews. Drug Discovery*, 8(8):627–644, 2009.

Liu, T., Ortiz, J. A., Taing, L., Meyer, C. A., Lee, B., Zhang, Y., Shin, H., Wong, S. S., Ma, J., Lei, Y., Pape, U. J., Poidinger, M., Chen, Y., Yeung, K., Brown, M., Turpaz, Y., and Liu, X. S. Cistrome: an integrative platform for transcriptional regulation studies. *Genome Biology*, 12(8):R83, 2011.

Livak, K. J. and Schmittgen, T. D. Analysis of relative gene expression data using real-time quantitative PCR and the 2(-Delta Delta C(T)) Method. *Methods*, 25 (4):402–408, 2001.

Loeb, L. A. A mutator phenotype in cancer. *Cancer Research*, 61(8):3230–3239, 2001.

Lokker, N. A., Sullivan, C. M., Hollenbach, S. J., Israel, M. A., and Giese, N. A. Platelet-derived growth factor (PDGF) autocrine signaling regulates survival and mitogenic pathways in glioblastoma cells: Evidence that the novel PDGF-C and PDGF-D ligands may play a role in the development of brain tumors. *Cancer Research*, 62(13):3729–3735, 2002.

Lolas, M., Valenzuela, P. D. T., Tjian, R., and Liu, Z. Charting Brachyury-mediated developmental pathways during early mouse embryogenesis. *Proceedings of the National Academy of Sciences*, 111(12):4478–4483, 2014.

Lu, H., Ouyang, W., and Huang, C. Inflammation, a Key Event in Cancer Development. *Molecular Cancer Research*, 4(4):221–233, 2006.

Lu, J., Li, X. P., Dong, Q., Kung, H. F., and He, M. L. TBX2 and TBX3: The special value for anticancer drug targets. *Biochimica et Biophysica Acta*, 1806: 268–274, 2010.

Luo, Z., Lin, C., and Shilatifard, A. The super elongation complex (SEC) family in transcriptional control. *Nature Reviews. Molecular Cell Biology*, 13(9):543–547, 2012.

Magee, J., Piskounova, E., and Morrison, S. Cancer Stem Cells: Impact, Heterogeneity, and Uncertainty. *Cancer Cell*, 21(3):283–296, 2012.

Maira, M., Couture, C., Le Martelot, G., Pulichino, A.-M., Bilodeau, S., and Drouin, J. The T-box Factor Tpit Recruits SRC/p160 Co-activators and Mediates Hormone Action. *Journal of Biological Chemistry*, 278(47):46523–46532, 2003.

Malumbres, M. and Barbacid, M. Mammalian cyclin-dependent kinases. *Trends in Biochemical Sciences*, 30(11):630–641, 2005.

Malumbres, M. and Barbacid, M. Cell cycle, CDKs and cancer: a changing paradigm. *Nature Reviews. Cancer*, 9(3):153–166, 2009.

Manderfield, L., Engleka, K., Aghajanian, H., Gupta, M., Yang, S., Li, L., Baggs, J., Hogenesch, J., Olson, E., and Epstein, J. Pax3 and Hippo Signaling Coordinate Melanocyte Gene Expression in Neural Crest. *Cell Reports*, 9(5):1885–1895, 2014.

Maniotis, A. J., Folberg, R., Hess, A., Seftor, E. A., Gardner, L. M., Pe'er, J., Trent, J. M., Meltzer, P. S., and Hendrix, M. J. Vascular channel formation by human melanoma cells in vivo and in vitro: vasculogenic mimicry. *American Journal of Pathology*, 155(3):739–752, 1999.

Mannava, S., Moparthy, K. C., Wheeler, L. J., Leonova, K. I., Wawrzyniak, J. A., Bianchi-Smiraglia, A., Berman, A. E., Flanagan, S., Shewach, D. S., Zeitouni, N. C., Gudkov, A. V., Mathews, C. K., and Nikiforov, M. A. Ribonucleotide reductase and thymidylate synthase or exogenous deoxyribonucleosides reduce DNA damage and senescence caused by C-MYC depletion. *Aging*, 4(12):917–922, 2012.

Mannava, S., Moparthy, K. C., Wheeler, L. J., Natarajan, V., Zucker, S. N., Fink, E. E., Im, M., Flanagan, S., Burhans, W. C., Zeitouni, N. C., Shewach, D. S., Mathews, C. K., and Nikiforov, M. A. Depletion of Deoxyribonucleotide Pools Is an Endogenous Source of DNA Damage in Cells Undergoing Oncogene-Induced Senescence. *The American Journal of Pathology*, 182(1):142–151, 2013.

Manning, B. D. and Cantley, L. C. AKT/PKB Signaling: Navigating Downstream. *Cell*, 129(7):1261–1274, 2007.

Margue, C. M., Bernasconi, M., Barr, F. G., and Schafer, B. W. Transcriptional modulation of the anti-apoptotic protein BCL-XL by the paired box transcription factors PAX3 and PAX3/FKHR. *Oncogene*, 19(25):2921–2929, 2000.

Martinet, W., De Meyer, G. R. Y., Herman, A. G., and Kockx, M. M. Amino Acid Deprivation Induces Both Apoptosis and Autophagy in Murine C2C12 Muscle Cells. *Biotechnology Letters*, 27(16):1157–1163, 2005.

Marusyk, A. and Polyak, K. Tumor heterogeneity: causes and consequences. *Biochimica et Biophysica Acta*, 1805(1):105–117, 2010.

McLean, C. Y., Bristor, D., Hiller, M., Clarke, S. L., Schaar, B. T., Lowe, C. B., Wenger, A. M., and Bejerano, G. GREAT improves functional interpretation of cis-regulatory regions. *Nat Biotech*, 28(5):495–501, 2010.

Medic, S. and Ziman, M. PAX3 expression in normal skin melanocytes and melanocytic lesions (naevi and melanomas). *PLoS ONE*, 5(4):e9977, 2010.

Medic, S., Rizos, H., and Ziman, M. Differential PAX3 functions in normal skin melanocytes and melanoma cells. *Biochemical and Biophysical Research Communications*, 411(4):832–837, 2011.

Mendoza, M. C., Er, E. E., and Blenis, J. The Ras-ERK and PI3K-mTOR pathways: cross-talk and compensation. *Trends in Biochemical Sciences*, 36(6): 320–328, 2011.

Menzies, A. M., Long, G. V., and Murali, R. Dabrafenib and its potential for the treatment of metastatic melanoma. *Drug Design, Development and Therapy*, 6: 391–405, 2012.

Meulmeester, E. and ten Dijke, P. The dynamic roles of TGF-β in cancer. *The Journal of Pathology*, 223(2):206–219, 2011.

Meuth, M. The molecular basis of mutations induced by deoxyribonucleoside triphosphate pool imbalances in mammalian cells. *Experimental Cell Research*, 181(2):305–316, 1989.

Michaloglou, C., Vredeveld, L. C., Soengas, M. S., Denoyelle, C., Kuilman, T., van der Horst, C. M., Majoor, D. M., Shay, J. W., Mooi, W. J., and Peeper, D. S. BRAFE600-associated senescence-like cell cycle arrest of human naevi. *Nature*, 436(7051):720–724, 2005.

Mihic-Probst, D., Ikenberg, K., Tinguely, M., Schraml, P., Behnke, S., Seifert, B., Civenni, G., Sommer, L., Moch, H., and Dummer, R. Tumor cell plasticity and angiogenesis in human melanomas. *PLoS ONE*, 7(3):e33571, 2012.

Miller, A. J. and Mihm, M. C. Melanoma. *New England Journal of Medicine*, 355 (1):51–65, 2006.

Mizuno, H. and Nishida, E. The ERK MAP kinase pathway mediates induction of SGK (serum- and glucocorticoid-inducible kinase) by growth factors. *Genes to Cells*, 6(3):261–268, 2001.

Müller, C. W. and Herrmann, B. G. Crystallographic structure of the T domain-DNA complex of the Brachyury transcription factor. *Nature*, 389:884–889, 1997.

Mo, J.-S., Park, H. W., and Guan, K.-L. The Hippo signaling pathway in stem cell biology and cancer. *EMBO Reports*, 15(6):642–656, 2014.

Mocellin, S. and Nitti, D. CTLA-4 blockade and the renaissance of cancer immunotherapy. *Biochimica et Biophysica Acta*, 1836(2):187–196, 2013.

Momand, J., Zambetti, G. P., Olson, D. C., George, D., and Levine, A. J. The mdm-2 oncogene product forms a complex with the p53 protein and inhibits p53-mediated transactivation. *Cell*, 69(7):1237–1245, 1992.

Morey, L. and Helin, K. Polycomb group protein-mediated repression of transcription. *Trends in Biochemical Sciences*, 35(6):323–332, 2010.

Morgan, D. O. Principles of CDK regulation. *Nature*, 374(6518):131–134, 1995.

Moullan, N., Mouchiroud, L., Wang, X., Ryu, D., Williams, E., Mottis, A., Jovaisaite, V., Frochaux, M., Quiros, P., Deplancke, B., Houtkooper, R., and Auwerx, J. Tetracyclines Disturb Mitochondrial Function across Eukaryotic Models: A Call for Caution in Biomedical Research. *Cell Reports*, 10(10):1681–1691, 2015.

Mukherjee, P., Winter, S. L., and Alexandrow, M. G. Cell Cycle Arrest by Transforming Growth Factor β1 near G1/S Is Mediated by Acute Abrogation of Prereplication Complex Activation Involving an Rb-MCM Interaction. *Molecular and Cellular Biology*, 30(3):845–856, 2010.

Muñoz-Espín, D. and Serrano, M. Cellular senescence: from physiology to pathology. *Nature Reviews. Molecular Cell Biology*, 15(7):482–496, 2014.

Muñoz-Espín, D., Cañamero, M., Maraver, A., Gómez-López, G., Contreras, J., Murillo-Cuesta, S., Rodríguez-Baeza, A., Varela-Nieto, I., Ruberte, J., Collado, M., and Serrano, M. Programmed Cell Senescence during Mammalian Embryonic Development. *Cell*, 155(5):1104–1118, 2013.

Murguía, J. R. and Serrano, R. New functions of protein kinase Gcn2 in yeast and mammals. *IUBMB Life*, 64(12):971–974, 2012.

Naiche, L. A., Harrelson, Z., Kelly, R. G., and Papaioannou, V. E. T-box genes in vertebrate development. *Annual Review of Genetics*, 39(1):219–239, 2005.

Nakayama, K., Qi, J., and Ronai, Z. e. The Ubiquitin Ligase Siah2 and the Hypoxia Response. *Molecular Cancer Research*, 7(4):443–451, 2009.

Nazarian, R., Shi, H., Wang, Q., Kong, X., Koya, R. C., Lee, H., Chen, Z., Lee, M. K., Attar, N., Sazegar, H., Chodon, T., Nelson, S. F., McArthur, G., Sosman, J. A., Ribas, A., and Lo, R. S. Melanomas acquire resistance to B-RAF(V600E) inhibition by RTK or N-RAS upregulation. *Nature*, 468(7326):973–977, 2010.

Negrini, S., Gorgoulis, V. G., and Halazonetis, T. D. Genomic instability - an evolving hallmark of cancer. *Nature Reviews. Molecular Cell Biology*, 11(3): 220–228, 2010.

Nelson, A. C., Pillay, N., Henderson, S., Presneau, N., Tirabosco, R., Halai, D., Berisha, F., Flicek, P., Stemple, D. L., Stern, C. D., Wardle, F. C., and Flanagan, A. M. An integrated functional genomics approach identifies the regulatory network directed by brachyury (T) in chordoma. *The Journal of Pathology*, 228(3):274–285, 2012.

Nogueira, C., Kim, K. H., Sung, H., Paraiso, K. H., Dannenberg, J. H., Bosenberg, M., Chin, L., and Kim, M. Cooperative interactions of PTEN deficiency and RAS activation in melanoma metastasis. *Oncogene*, 29(47):6222–6232, 2010.

Nowak, M. A., Komarova, N. L., Sengupta, A., Jallepalli, P. V., Shih, I.-M., Vogelstein, B., and Lengauer, C. The role of chromosomal instability in tumor initiation. *Proceedings of the National Academy of Sciences*, 99(25):16226–16231, 2002.

Nurse, P. A Long Twentieth Century of the Cell Cycle and Beyond. *Cell*, 100(1): 71–78, 2000.

Nyga, A., Cheema, U., and Loizidou, M. 3D tumour models: novel in vitro approaches to cancer studies. *Journal of Cell Communication and Signaling*, 5 (3):239–248, 2011.

Oikawa, T. and Yamada, T. Molecular biology of the Ets family of transcription factors. *Gene*, 303:11–34, 2003.

Okochi, M., Steiner, H., Fukumori, A., Tanii, H., Tomita, T., Tanaka, T., Iwatsubo, T., Kudo, T., Takeda, M., and Haass, C. Presenilins mediate a dual intramembranous gamma-secretase cleavage of Notch-1. *EMBO Journal*, 21(20): 5408–5416, 2002.

O'Konek, J. J., Boucher, P. D., Iacco, A. A., Wilson, T. E., and Shewach, D. S. MLH1 deficiency enhances tumor cell sensitivity to ganciclovir. *Cancer Gene Therapy*, 16(9):683–692, 2009.

Oliner, J. D., Kinzler, K. W., Meltzer, P. S., George, D. L., and Vogelstein, B. Amplification of a gene encoding a p53-associated protein in human sarcomas. *Nature*, 358(6381):80–83, 1992.

Olivier, M., Hollstein, M., and Hainaut, P. TP53 mutations in human cancers: origins, consequences, and clinical use. *Cold Spring Harbor Perspectives in Biology*, 2(1):a001008, 2010.

Omholt, K., Krockel, D., Ringborg, U., and Hansson, J. Mutations of PIK3CA are rare in cutaneous melanoma. *Melanoma Research*, 16(2):197–200, 2006.

O'Sullivan, R. J. and Karlseder, J. Telomeres: protecting chromosomes against

genome instability. *Nature Reviews. Molecular Cell Biology*, 11(3):171–181, 2010.

Packham, E. A. and Brook, J. D. T-box genes in human disorders. *Human Molecular Genetics*, 12(Suppl. 1):R37–44, 2003.

Papaioannou, V. E. The T-box gene family: emerging roles in development, stem cells and cancer. *Development*, 141(20):3819–3833, 2014.

Papapetrou, C., Edwards, Y. H., and Sowden, J. C. The T transcription factor functions as a dimer and exhibits a common human polymorphism Gly-177-Asp in the conserved DNA-binding domain. *FEBS Letters*, 409(2):201–206, 1997.

Park, J., Leong, M. L., Buse, P., Maiyar, A. C., Firestone, G. L., and Hemmings, B. A. Serum and glucocorticoid-inducible kinase (SGK) is a target of the PI 3-kinase-stimulated signaling pathway. *EMBO Journal*, 18(11):3024–3033, 1999.

Parry, R. V., Chemnitz, J. M., Frauwirth, K. A., Lanfranco, A. R., Braunstein, I., Kobayashi, S. V., Linsley, P. S., Thompson, C. B., and Riley, J. L. CTLA-4 and PD-1 Receptors Inhibit T-Cell Activation by Distinct Mechanisms. *Molecular and Cellular Biology*, 25(21):9543–9553, 2005.

Patel, J. H., Loboda, A. P., Showe, M. K., Showe, L. C., and McMahon, S. B. Analysis of genomic targets reveals complex functions of MYC. *Nature Reviews. Cancer*, 4(7):562–568, 2004.

Paxton, C., Zhao, H., Chin, Y., Langner, K., and Reecy, J. Murine Tbx2 contains domains that activate and repress gene transcription. *Gene*, 283(1-2):117–124., 2002.

Peinado, H., Ballestar, E., Esteller, M., and Cano, A. Snail mediates E-cadherin repression by the recruitment of the Sin3A/histone deacetylase 1 (HDAC1)/HDAC2 complex. *Molecular and Cellular Biology*, 24(1):306–319, 2004.

Peinado, H., Olmeda, D., and Cano, A. Snail, Zeb and bHLH factors in tumour progression: an alliance against the epithelial phenotype? *Nature Reviews. Cancer*, 7(6):415–428, 2007.

Peres, J., Davis, E., Mowla, S., Bennett, D. C., Li, J. A., Wansleben, S., and Prince, S. The Highly Homologous T-Box Transcription Factors, TBX2 and TBX3, Have Distinct Roles in the Oncogenic Process. *Genes & Cancer*, 1(3): 272–282, 2010.

Plummer, R. S., Shea, C. R., Nelson, M., Powell, S. K., Freeman, D. M., Dan, C. P., and Lang, D. PAX3 expression in primary melanomas and nevi. *Modern Pathology*, 21(5):525–530, 2008.

Pollock, P. M., Harper, U. L., Hansen, K. S., Yudt, L. M., Stark, M., Robbins, C. M., Moses, T. Y., Hostetter, G., Wagner, U., Kakareka, J., Salem, G., Pohida, T., Heenan, P., Duray, P., Kallioniemi, O., Hayward, N. K., Trent, J. M., and Meltzer, P. S. High frequency of BRAF mutations in nevi. *Nature Genetics*, 33 (1):19–20, 2003.

Poulikakos, P. I., Persaud, Y., Janakiraman, M., Kong, X. J., Ng, C., Moriceau, G., Shi, H. B., Atefi, M., Titz, B., Gabay, M. T., Salton, M., Dahlman, K. B., Tadi, M., Wargo, J. A., Flaherty, K. T., Kelley, M. C., Misteli, T., Chapman, P. B., Sosman, J. A., Graeber, T. G., Ribas, A., Lo, R. S., Rosen, N., and Solit,

D. B. RAF inhibitor resistance is mediated by dimerization of aberrantly spliced BRAF(V600E). *Nature*, 480(7377):387–U144, 2011.

Prince, S., Carreira, S., Vance, K. W., Abrahams, A., and Goding, C. R. Tbx2 Directly Represses the Expression of the p21(WAF1) Cyclin-Dependent Kinase Inhibitor. *Cancer Research*, 64(5):1669–1674, 2004.

Pylayeva-Gupta, Y., Grabocka, E., and Bar-Sagi, D. RAS oncogenes: weaving a tumorigenic web. *Nature Reviews. Cancer*, 11(11):761–774, 2011.

Quezada, S. A. and Peggs, K. S. Exploiting CTLA-4, PD-1 and PD-L1 to reactivate the host immune response against cancer. *British Journal of Cancer*, 108(8): 1560–1565, 2013.

Quinlan, A. R. and Hall, I. M. BEDTools: a flexible suite of utilities for comparing genomic features. *Bioinformatics*, 26(6):841–842, 2010.

Reya, T., Morrison, S. J., Clarke, M. F., and Weissman, I. L. Stem cells, cancer, and cancer stem cells. *Nature*, 414(6859):105–111, 2001.

Rheault, T. R., Stellwagen, J. C., Adjabeng, G. M., Hornberger, K. R., Petrov, K. G., Waterson, A. G., Dickerson, S. H., Mook, J., R. A., Laquerre, S. G., King, A. J., Rossanese, O. W., Arnone, M. R., Smitheman, K. N., Kane-Carson, L. S., Han, C., Moorthy, G. S., Moss, K. G., and Uehling, D. E. Discovery of Dabrafenib: A Selective Inhibitor of Raf Kinases with Antitumor Activity against B-Raf-Driven Tumors. *ACS Med Chem Lett*, 4(3):358–362, 2013.

Ribas, A. Tumor immunotherapy directed at PD-1. *New England Journal of Medicine*, 366(26):2517–2519, 2012.

Ritchie, M. E., Phipson, B., Wu, D., Hu, Y., Law, C. W., Shi, W., and Smyth, G. K. limma powers differential expression analyses for RNA-sequencing and microarray studies. *Nucleic Acids Research*, 43(7):e47, 2015.

Rodier, F. and Campisi, J. Four faces of cellular senescence. *Journal of Cell Biology*, 192(4):547–556, 2011.

Rodier, F., Coppe, J. P., Patil, C. K., Hoeijmakers, W. A., Munoz, D. P., Raza, S. R., Freund, A., Campeau, E., Davalos, A. R., and Campisi, J. Persistent DNA damage signalling triggers senescence-associated inflammatory cytokine secretion. *Nature Cell Biology*, 11(8):973–979, 2009.

Rodriguez, M., Aladowicz, E., Lanfrancone, L., and Goding, C. R. Tbx3 represses E-cadherin expression and enhances melanoma invasiveness. *Cancer Research*, 68(19):7872–7881, 2008.

Rowley, M., Grothey, E., and Couch, F. J. The Role of Tbx2 and Tbx3 in Mammary Development and Tumorigenesis. *Journal of Mammary Gland Biology and Neoplasia*, 9(2):109–118, 2004.

Rufini, A., Tucci, P., Celardo, I., and Melino, G. Senescence and aging: the critical roles of p53. *Oncogene*, 32(43):5129–5143, 2013.

Russ, A. P., Wattler, S., Colledge, W. H., Aparicio, S. A., Carlton, M. B., Pearce, J. J., Barton, S. C., Surani, M. A., Ryan, K., Nehls, M. C., Wilson, V., and Evans, M. J. Eomesodermin is required for mouse trophoblast development and mesoderm formation. *Nature*, 404(6773):95–99, 2000.

Ryazanov, A. G. and Spirin, A. S. Phosphorylation of elongation factor 2: a key mechanism regulating gene expression in vertebrates. *New Biologist*, 2(10): 843–850, 1990.

Sakagami, H., Satoh, M., Yokote, Y., Takano, H., Takahama, M., Kochi, M., and Akahane, K. Amino acid utilization during cell growth and apoptosis induction. *Anticancer Research*, 18(6A):4303–4306, 1998.

Sakoda, H., Gotoh, Y., Katagiri, H., Kurokawa, M., Ono, H., Onishi, Y., Anai, M., Ogihara, T., Fujishiro, M., Fukushima, Y., Abe, M., Shojima, N., Kikuchi, M., Oka, Y., Hirai, H., and Asano, T. Differing Roles of Akt and Serum- and Glucocorticoid-regulated Kinase in Glucose Metabolism, DNA Synthesis, and Oncogenic Activity. *Journal of Biological Chemistry*, 278(28):25802–25807, 2003.

Saucedo, L. J. and Edgar, B. A. Filling out the Hippo pathway. *Nature Reviews. Molecular Cell Biology*, 8(8):613–621, 2007.

Schatz, P. J. Use of peptide libraries to map the substrate specificity of a peptide-modifying enzyme: a 13 residue consensus peptide specifies biotinylation in Escherichia coli. *Bio/Technology*, 11(10):1138–1143, 1993.

Scheller, J., Chalaris, A., Schmidt-Arras, D., and Rose-John, S. The pro- and anti-inflammatory properties of the cytokine interleukin-6. *Biochimica et Biophysica Acta (BBA) - Molecular Cell Research*, 1813(5):878–888, 2011.

Schlisio, S., Halperin, T., Vidal, M., and Nevins, J. R. Interaction of YY1 with E2Fs, mediated by RYBP, provides a mechanism for specificity of E2F function. *EMBO Journal*, 21(21):5775–5786, 2002.

Scholl, F. A., Kamarashev, J., Murmann, O. V., Geertsen, R., Dummer, R., and Schäfer, B. W. PAX3 Is Expressed in Human Melanomas and Contributes to Tumor Cell Survival. *Cancer Research*, 61(3):823–826, 2001.

Searl, T. J. and Silinsky, E. M. LY 294002 inhibits adenosine receptor activation by a mechanism independent of effects on PI-3 kinase or casein kinase II. *Purinergic Signalling*, 1(4):389–394, 2005.

Sebé-Pedrós, A., Ariza-Cosano, A., Weirauch, M. T., Leininger, S., Yang, A., Torruella, G., Adamski, M., Adamska, M., Hughes, T. R., Gómez-Skarmeta, J. L., and Ruiz-Trillo, I. Early evolution of the T-box transcription factor family. *Proceedings of the National Academy of Sciences*, 110(40):16050–16055, 2013.

Seftor, R. E., Hess, A. R., Seftor, E. A., Kirschmann, D. A., Hardy, K. M., Margaryan, N. V., and Hendrix, M. J. Tumor cell vasculogenic mimicry: from controversy to therapeutic promise. *American Journal of Pathology*, 181(4): 1115–1125, 2012.

Serrano, M. SHP2: a new target for pro-senescence cancer therapies. *EMBO Journal*, 34(11):1439–1441, 2015.

Serrano, M., Lin, A. W., McCurrach, M. E., Beach, D., and Lowe, S. W. Oncogenic ras provokes premature cell senescence associated with accumulation of p53 and p16INK4a. *Cell*, 88(5):593–602, 1997.

Sharrocks, A. D. The ETS-domain transcription factor family. *Nature Reviews. Molecular Cell Biology*, 2(11):827–837, 2001.

Sherk, A. B., Frigo, D. E., Schnackenberg, C. G., Bray, J. D., Laping, N. J., Trizna, W., Hammond, M., Patterson, J. R., Thompson, S. K., Kazmin, D., Norris, J. D., and McDonnell, D. P. Development of a Small-Molecule Serum- and Glucocorticoid-Regulated Kinase-1 Antagonist and Its Evaluation as a Prostate Cancer Therapeutic. *Cancer Research*, 68(18):7475–7483, 2008.

Sherr, C. J. Principles of Tumor Suppression. *Cell*, 116(2):235–246, 2004.

Sherr, C. J. and McCormick, F. The RB and p53 pathways in cancer. *Cancer Cell*, 2(2):103–112, 2002.

Shull, A. Y., Latham-Schwark, A., Ramasamy, P., Leskoske, K., Oroian, D., Birtwistle, M. R., and Buckhaults, P. J. Novel Somatic Mutations to PI3K Pathway Genes in Metastatic Melanoma. *PLoS ONE*, 7(8):e43369, 2012.

Siegel, P. M. and Massague, J. Cytostatic and apoptotic actions of TGF-[beta] in homeostasis and cancer. *Nature Reviews. Cancer*, 3(11):807–820, 2003.

Slamon, D. J., Clark, G. M., Wong, S. G., Levin, W. J., Ullrich, A., and McGuire, W. L. Human breast cancer: correlation of relapse and survival with amplification of the HER-2/neu oncogene. *Science*, 235(4785):177–182, 1987.

Solit, D. B., Garraway, L. A., Pratilas, C. A., Sawai, A., Getz, G., Basso, A., Ye, Q., Lobo, J. M., She, Y., Osman, I., Golub, T. R., Sebolt-Leopold, J., Sellers, W. R., and Rosen, N. BRAF mutation predicts sensitivity to MEK inhibition. *Nature*, 439(7074):358–362, 2006.

Sosman, J. A., Kim, K. B., Schuchter, L., Gonzalez, R., Pavlick, A. C., Weber, J. S., McArthur, G. A., Hutson, T. E., Moschos, S. J., Flaherty, K. T., Hersey,

P., Kefford, R., Lawrence, D., Puzanov, I., Lewis, K. D., Amaravadi, R. K., Chmielowski, B., Lawrence, H. J., Shyr, Y., Ye, F., Li, J., Nolop, K. B., Lee, R. J., Joe, A. K., and Ribas, A. Survival in BRAF V600-mutant advanced melanoma treated with vemurafenib. *New England Journal of Medicine*, 366(8): 707–714, 2012.

Soufir, N., Avril, M.-F., Chompret, A., Demenais, F., Bombled, J., Spatz, A., Stoppa-Lyonnet, D., Bénard, J., and Bressac-de Paillerets, B. Prevalence of p16 and CDK4 Germline Mutations in 48 Melanoma-Prone Families in France. *Human Molecular Genetics*, 7(2):209–216, 1998.

Steeg, P. S. Tumor metastasis: mechanistic insights and clinical challenges. *Nature Medicine*, 12(8):895–904, 2006.

Stennard, F. A. and Harvey, R. P. T-box transcription factors and their roles in regulatory hierarchies in the developing heart. *Development*, 132(22):4897–4910, 2005.

Storer, M., Mas, A., Robert-Moreno, A., Pecoraro, M., Ortells, M. C., Di Giacomo, V., Yosef, R., Pilpel, N., Krizhanovsky, V., Sharpe, J., and Keyes, W. M. Senescence Is a Developmental Mechanism that Contributes to Embryonic Growth and Patterning. *Cell*, 155(5):1119–1130, 2013.

Suzuki, T., Takeuchi, J., Koshiba-Takeuchi, K., and Ogura, T. Tbx Genes Specify Posterior Digit Identity through Shh and BMP Signaling. *Developmental Cell*, 6(1):43–53, 2004.

Talmadge, J. E. and Fidler, I. J. AACR centennial series: the biology of cancer metastasis: historical perspective. *Cancer Research*, 70(14):5649–5669, 2010.

Tanner, K. and Gottesman, M. M. Beyond 3D culture models of cancer. *Science Translational Medicine*, 7(283):283ps289, 2015.

Tessier, M. and Woodgett, J. R. Serum and glucocorticoid-regulated protein kinases: Variations on a theme. *Journal of Cellular Biochemistry*, 98(6):1391–1407, 2006.

Tomlinson, I. P., Roylance, R., and Houlston, R. S. Two hits revisited again. *Journal of Medical Genetics*, 38(2):81–85, 2001.

Topalian, S. L., Hodi, F. S., Brahmer, J. R., Gettinger, S. N., Smith, D. C., McDermott, D. F., Powderly, J. D., Carvajal, R. D., Sosman, J. A., Atkins, M. B., Leming, P. D., Spigel, D. R., Antonia, S. J., Horn, L., Drake, C. G., Pardoll, D. M., Chen, L., Sharfman, W. H., Anders, R. A., Taube, J. M., McMiller, T. L., Xu, H., Korman, A. J., Jure-Kunkel, M., Agrawal, S., McDonald, D., Kollia, G. D., Gupta, A., Wigginton, J. M., and Sznol, M. Safety, Activity, and Immune Correlates of Anti–PD-1 Antibody in Cancer. *New England Journal of Medicine*, 366(26):2443–2454, 2012.

Tran, T. T., Schulman, J., and Fisher, D. E. UV and pigmentation: molecular mechanisms and social controversies. *Pigment Cell and Melanoma Research*, 21 (5):509–516, 2008.

Tsai, J., Lee, J. T., Wang, W., Zhang, J., Cho, H., Mamo, S., Bremer, R., Gillette, S., Kong, J., Haass, N. K., Sproesser, K., Li, L., Smalley, K. S., Fong, D., Zhu, Y. L., Marimuthu, A., Nguyen, H., Lam, B., Liu, J., Cheung, I., Rice, J., Suzuki, Y., Luu, C., Settachatgul, C., Shellooe, R., Cantwell, J., Kim, S. H., Schlessinger, J., Zhang, K. Y., West, B. L., Powell, B., Habets, G., Zhang, C.,

Ibrahim, P. N., Hirth, P., Artis, D. R., Herlyn, M., and Bollag, G. Discovery of a selective inhibitor of oncogenic B-Raf kinase with potent antimelanoma activity. *Proceedings of the National Academy of Sciences of the United States of America*, 105(8):3041–3046, 2008.

Tsao, H., Zhang, X., Benoit, E., and Haluska, F. G. Identification of PTEN/MMAC1 alterations in uncultured melanomas and melanoma cell lines. *Oncogene*, 16(26):3397–3402, 1998.

Tsao, H., Mihm Jr, M. C., and Sheehan, C. PTEN expression in normal skin, acquired melanocytic nevi, and cutaneous melanoma. *Journal of the American Academy of Dermatology*, 49(5):865–872, 2003.

Tsao, H., Chin, L., Garraway, L. A., and Fisher, D. E. Melanoma: from mutations to medicine. *Genes and Development*, 26(11):1131–1155, 2012.

Ugi, S., Imamura, T., Maegawa, H., Egawa, K., Yoshizaki, T., Shi, K., Obata, T., Ebina, Y., Kashiwagi, A., and Olefsky, J. M. Protein Phosphatase 2A Negatively Regulates Insulin's Metabolic Signaling Pathway by Inhibiting Akt (Protein Kinase B) Activity in 3T3-L1 Adipocytes. *Molecular and Cellular Biology*, 24(19):8778–8789, 2004.

Urso, C., Bondi, R., Balzi, M., Scubla, E., Mauri, P., Becciolini, A., Tarocchi, C. Vallecchi, S., and Vallecchi, C. Cell Kinetics of Melanocytes in Common and Dysplastic Nevi and in Primary and Metastatic Cutaneous Melanoma. *Pathology, Research and Practice*, 188(3):323–329, 1992.

van der Schaft, D. W., Hillen, F., Pauwels, P., Kirschmann, D. A., Castermans, K., Egbrink, M. G., Tran, M. G., Sciot, R., Hauben, E., Hogendoorn, P. C.,

Delattre, O., Maxwell, P. H., Hendrix, M. J., and Griffioen, A. W. Tumor cell plasticity in Ewing sarcoma, an alternative circulatory system stimulated by hypoxia. *Cancer Research*, 65(24):11520–11528, 2005.

Vance, K. W., Carreira, S., Brosch, G., and Goding, C. R. Tbx2 is overexpressed and plays an important role in maintaining proliferation and suppression of senescence in melanomas. *Cancer Research*, 65(6):2260–2268, 2005.

Vance, K. W., Shaw, H. M., Rodriguez, M., Ott, S., and Goding, C. R. The retinoblastoma protein modulates Tbx2 functional specificity. *Molecular Biology of the Cell*, 21(15):2770–2779, 2010.

Vander Heiden, M. G., Cantley, L. C., and Thompson, C. B. Understanding the Warburg effect: the metabolic requirements of cell proliferation. *Science*, 324 (5930):1029–1033, 2009.

Vanhaesebroeck, B., Stephens, L., and Hawkins, P. PI3K signalling: the path to discovery and understanding. *Nature Reviews. Molecular Cell Biology*, 13(3): 195–203, 2012.

Vermeulen, K., Van Bockstaele, D. R., and Berneman, Z. N. The cell cycle: a review of regulation, deregulation and therapeutic targets in cancer. *Cell Proliferation*, 36(3):131–149, 2003.

Villanueva, J., Vultur, A., Lee, J. T., Somasundaram, R., Fukunaga-Kalabis, M., Cipolla, A. K., Wubbenhorst, B., Xu, X., Gimotty, P. A., Kee, D., Santiago-Walker, A. E., Letrero, R., D'Andrea, K., Pushparajan, A., Hayden, J. E., Brown, K. D., Laquerre, S., McArthur, G. A., Sosman, J. A., Nathanson, K. L.,

and Herlyn, M. Acquired resistance to BRAF inhibitors mediated by a RAF kinase switch in melanoma can be overcome by cotargeting MEK and IGF-1R/PI3K. *Cancer Cell*, 18(6):683–695, 2010.

Visvader, J. and Lindeman, G. Cancer Stem Cells: Current Status and Evolving Complexities. *Cell Stem Cell*, 10(6):717–728, 2012.

Vivanco, I. and Sawyers, C. L. The phosphatidylinositol 3-Kinase-AKT pathway in human cancer. *Nature Reviews. Cancer*, 2(7):489–501, 2002.

Vlahos, C. J., Matter, W. F., Hui, K. Y., and Brown, R. F. A specific inhibitor of phosphatidylinositol 3-kinase, 2-(4-morpholinyl)-8-phenyl-4H-1-benzopyran-4-one (LY294002). *Journal of Biological Chemistry*, 269(7):5241–5248, 1994.

Vodermaier, H. C. APC/C and SCF: Controlling Each Other and the Cell Cycle. *Current Biology*, 14(18):R787–R796, 2004.

Vredeveld, L. C. W., Possik, P. A., Smit, M. A., Meissl, K., Michaloglou, C., Horlings, H. M., Ajouaou, A., Kortman, P. C., Dankort, D., McMahon, M., Mooi, W. J., and Peeper, D. S. Abrogation of BRAFV600E-induced senescence by PI3K pathway activation contributes to melanomagenesis. *Genes and Development*, 26(10):1055–1069, 2012.

Wagle, N., Emery, C., Berger, M. F., Davis, M. J., Sawyer, A., Pochanard, P., Kehoe, S. M., Johannessen, C. M., MacConaill, L. E., Hahn, W. C., Meyerson, M., and Garraway, L. A. Dissecting Therapeutic Resistance to RAF Inhibition in Melanoma by Tumor Genomic Profiling. *Journal of Clinical Oncology*, 2011.

Wallberg, A. E., Pedersen, K., Lendahl, U., and Roeder, R. G. p300 and PCAF Act Cooperatively To Mediate Transcriptional Activation from Chromatin Templates by Notch Intracellular Domains In Vitro. *Molecular and Cellular Biology*, 22(22):7812–7819, 2002.

Walunas, T. L., Lenschow, D. J., Bakker, C. Y., Linsley, P. S., Freeman, G. J., Green, J. M., Thompson, C. B., and Bluestone, J. A. CTLA-4 can function as a negative regulator of T cell activation. *Immunity*, 1(5):405–413, 1994.

Walunas, T. L., Bakker, C. Y., and Bluestone, J. A. CTLA-4 ligation blocks CD28-dependent T cell activation. *Journal of Experimental Medicine*, 183(6): 2541–2550, 1996.

Wang, G.-S., Hong, C.-J., Yen, T.-Y., Huang, H.-Y., Ou, Y., Huang, T.-N., Jung, W.-G., Kuo, T.-Y., Sheng, M., Wang, T.-F., and Hsueh, Y.-P. Transcriptional Modification by a CASK-Interacting Nucleosome Assembly Protein. *Neuron*, 42 (1):113–128, 2004.

Wang, S., Sun, H., Ma, J., Zang, C., Wang, C., Wang, J., Tang, Q., Meyer, C. A., Zhang, Y., and Liu, X. S. Target analysis by integration of transcriptome and ChIP-seq data with BETA. *Nature Protocols*, 8(12):2502–2515, 2013.

Warburg, O., Wind, F., and Negelein, E. Über den Stoffwechsel von Tumoren im Körper. *Klinische Wochenschrift*, 5(19):829–832, 1926.

Weber, J. S., D'Angelo, S. P., Minor, D., Hodi, F. S., Gutzmer, R., Neyns, B., Hoeller, C., Khushalani, N. I., Miller Jr, W. H., Lao, C. D., Linette, G. P., Thomas, L., Lorigan, P., Grossmann, K. F., Hassel, J. C., Maio, M., Sznol, M.,

Ascierto, P. A., Mohr, P., Chmielowski, B., Bryce, A., Svane, I. M., Grob, J.-J., Krackhardt, A. M., Horak, C., Lambert, A., Yang, A. S., and Larkin, J. Nivolumab versus chemotherapy in patients with advanced melanoma who progressed after anti-CTLA-4 treatment (CheckMate 037): a randomised, controlled, open-label, phase 3 trial. *The Lancet Oncology*, 16(4):375–384, 2015.

Wei, S., Wei, W., and Sedivy, J. M. Expression of Catalytically Active Telomerase Does Not Prevent Premature Senescence Caused by Overexpression of Oncogenic Ha-Ras in Normal Human Fibroblasts. *Cancer Research*, 59(7):1539–1543, 1999.

Weinberg, R. A. The retinoblastoma protein and cell cycle control. *Cell*, 81(3): 323–330, 1995.

Wellbrock, C., Karasarides, M., and Marais, R. The RAF proteins take centre stage. *Nature Reviews. Molecular Cell Biology*, 5(11):875–885, 2004a.

Wellbrock, C., Ogilvie, L., Hedley, D., Karasarides, M., Martin, J., Niculescu-Duvaz, D., Springer, C. J., and Marais, R. V599EB-RAF is an oncogene in melanocytes. *Cancer Research*, 64(7):2338–2342, 2004b.

White, E. Exploiting the bad eating habits of Ras-driven cancers. *Genes and Development*, 27(19):2065–2071, 2013.

Wilson, V. and Conlon, F. L. The T-box family. *Genome Biology*, 3(6): REVIEWS3008, 2002.

Woo, S.-R., Corrales, L., and Gajewski, T. F. Innate Immune Recognition of Cancer. *Annual Review of Immunology*, 33(1):445–474, 2015.

Xie, H., Lee, M.-H., Zhu, F., Reddy, K., Peng, C., Li, Y., Lim, D. Y., Kim, D. J., Li, X., Kang, S., Li, H., Ma, W., Lubet, R. A., Ding, J., Bode, A. M., and Dong, Z. Identification of an Aurora kinase inhibitor specific for the Aurora B isoform. *Cancer Research*, 73(2):716–724, 2013.

Yancovitz, M., Litterman, A., Yoon, J., Ng, E., Shapiro, R. L., Berman, R. S., Pavlick, A. C., Darvishian, F., Christos, P., Mazumdar, M., Osman, I., and Polsky, D. Intra- and inter-tumor heterogeneity of BRAF(V600E))mutations in primary and metastatic melanoma. *PLoS ONE*, 7(1):e29336, 2012.

Yang, G., Rosen, D. G., Zhang, Z., Bast, J., R. C., Mills, G. B., Colacino, J. A., Mercado-Uribe, I., and Liu, J. The chemokine growth-regulated oncogene 1 (Gro-1) links RAS signaling to the senescence of stromal fibroblasts and ovarian tumorigenesis. *Proceedings of the National Academy of Sciences of the United States of America*, 103(44):16472–16477, 2006.

Yang, L., Dan, H. C., Sun, M., Liu, Q., Sun, X.-m., Feldman, R. I., Hamilton, A. D., Polokoff, M., Nicosia, S. V., Herlyn, M., Sebti, S. M., and Cheng, J. Q. Akt/Protein Kinase B Signaling Inhibitor-2, a Selective Small Molecule Inhibitor of Akt Signaling with Antitumor Activity in Cancer Cells Overexpressing Akt. *Cancer Research*, 64(13):4394–4399, 2004.

Ying, H., Kimmelman, A., Lyssiotis, C., Hua, S., Chu, G., Fletcher-Sananikone, E., Locasale, J., Son, J., Zhang, H., Coloff, J., Yan, H., Wang, W., Chen, S., Viale, A., Zheng, H., Paik, J.-h., Lim, C., Guimaraes, A., Martin, E., Chang, J., Hezel, A., Perry, S., Hu, J., Gan, B., Xiao, Y., Asara, J., Weissleder, R., Wang, Y. A., Chin, L., Cantley, L., and DePinho, R. Oncogenic Kras Maintains

Pancreatic Tumors through Regulation of Anabolic Glucose Metabolism. *Cell*, 149(3):656–670, 2012.

Zhang, B.-H., Tang, E. D., Zhu, T., Greenberg, M. E., Vojtek, A. B., and Guan, K.-L. Serum- and Glucocorticoid-inducible Kinase SGK Phosphorylates and Negatively Regulates B-Raf. *Journal of Biological Chemistry*, 276(34):31620–31626, 2001.

Zhang, Y. and Yang, J.-M. The impact of cellular senescence in cancer therapy: is it true or not? *Acta Pharmacologica Sinica*, 32(10):1199–1207, 2011.

Zhang, Y., Liu, T., Meyer, C. A., Eeckhoute, J., Johnson, D. S., Bernstein, B. E., Nusbaum, C., Myers, R. M., Brown, M., Li, W., and Liu, X. S. Model-based analysis of ChIP-Seq (MACS). *Genome Biology*, 9(9):R137, 2008.

Zilfou, J. T. and Lowe, S. W. Tumor Suppressive Functions of p53. *Cold Spring Harbor Perspectives in Biology*, 1(5):a001883, 2009.

Zuo, L., Weger, J., Yang, Q., Goldstein, A. M., Tucker, M. A., Walker, G. J., Hayward, N., and Dracopoli, N. C. Germline mutations in the p16INK4a binding domain of CDK4 in familial melanoma. *Nature Genetics*, 12(1):97–99, 1996.